THÈSE

En vue de l'obtention du

DOCTORAT DE L'UNIVERSITÉ DE TOULOUSE

Délivré par *l'Université Toulouse III - Paul Sabatier (UT3Paul Sabatier)*
Discipline ou spécialité : *Génie Civil*

Présentée et soutenue par *: Maria Eleni Mitzithra*
Le *21 Octobre 2013*

Titre : *Detection of corrosion of reinforced concrete on cooling towers of energy production sites*

JURY

Jean-Paul BALAYSSAC Examinateur Université de Toulouse III
Thierry CHAUSSADENT Rapporteur IFSTTAR (HDR)
Fabrice DEBY Examinateur Université de Toulouse III
Didier DEFER Examinateur Université d'Artois
Jean-François LATASTE Examinateur Université Bordeaux I
Jean SALIN Examinateur EDF R&D
Frédéric SKOCZYLAS Rapporteur Ecole Centrale de Lille
Pierre STEPHAN Examinateur EDF R&D

Ecole doctorale : *Mécanique, Energétique, Génie civil et Procédés (MeGeP)*
Unité de recherche : *Laboratoire Matériaux et Durabilité des Constructions (LMDC)*
Directeur(s) de Thèse : *Jean-Paul BALAYSSAC*
Co-directeur: Fabrice DEBY
Rapporteurs :

Université de Toulouse

THESE

En vue de l'obtention du

DOCTORAT DE L'UNIVERSITE DE TOULOUSE

Délivré par l'Université Toulouse III-Paul Sabatier

Discipline ou Spécialité: Génie Civil

Présentée et soutenue par Maria Eleni Mitzithra

le 21 Octobre 2013

Titre: Detection of corrosion of reinforced concrete on cooling towers of energy production sites

---

JURY

Jean-Paul BALAYSSAC	**Examinateur**	**Université de Toulouse III**
Thierry CHAUSSADENT	**Rapporteur**	**IFSTTAR (HDR)**
Fabrice DEBY	**Examinateur**	**Université de Toulouse III**
Didier DEFER	**Examinateur**	**Université d'Artois**
Jean-François LATASTE	**Examinateur**	**Université Bordeaux I**
Jean SALIN	**Examinateur**	**EDF R&D**
Frédéric SKOCZYLAS	**Rapporteur**	**Ecole Centrale de Lille**
Pierre STEPHAN	**Examinateur**	**EDF R&D**

Ecole doctorale: *Mécanique, Energétique, Génie civil et Procédés (MeGeP)*
Unité de recherche: *Laboratoire Matériaux et Durabilité des Constructions (LMDC)*
Directeur de thèse: *Jean-Paul BALAYSSAC*
Co-directeur: *Fabrice DEBY*

Université de Toulouse

THESE

En vue de l'obtention du

DOCTORAT DE L'UNIVERSITE DE TOULOUSE

Délivré par l'Université Toulouse III-Paul Sabatier

Discipline ou Spécialité: Génie Civil

Présentée et soutenue par Maria Eleni Mitzithra

le 21 Octobre 2013

Titre: Detection of corrosion of reinforced concrete on cooling towers of energy production sites

---

JURY

Jean-Paul BALAYSSAC	**Examinateur**	**Université de Toulouse III**
Thierry CHAUSSADENT	**Rapporteur**	**IFSTTAR (HDR)**
Fabrice DEBY	**Examinateur**	**Université de Toulouse III**
Didier DEFER	**Examinateur**	**Université d'Artois**
Jean-François LATASTE	**Examinateur**	**Université Bordeaux I**
Jean SALIN	**Examinateur**	**EDF R&D**
Frédéric SKOCZYLAS	**Rapporteur**	**Ecole Centrale de Lille**
Pierre STEPHAN	**Examinateur**	**EDF R&D**

Ecole doctorale: *Mécanique, Energétique, Génie civil et Procédés (MeGeP)*
Unité de recherche: *Laboratoire Matériaux et Durabilité des Constructions (LMDC)*
Directeur de thèse: *Jean-Paul BALAYSSAC*
Co-directeur: *Fabrice DEBY*

Université de Toulouse

Abstract

The current thesis is the result of a study funded by Electricité de France –Research and Development (EDF R&D). It aims to develop an original methodology for a better estimation of the state of corrosion of steel reinforced concrete of cooling towers, due to atmospheric carbonation, based on a double approach: the Ground Penetrating Radar (GPR) and the electrochemical measurement of polarization resistance[1].

GPR can be used for detecting zones with a high risk of corrosion (detection of contrasts of permittivity). In addition, GPR is used for the location of steel rebars and the estimation of concrete cover thickness.

On the zones identified by GPR with high risk of corrosion, it is proposed to use the polarization resistance measurement to define quantitatively the corrosion activity. This study proposes an original simple operative measurement mode, adapted only for this particular context. After a critical analysis of the existing devices of the polarization resistance measurement, a novel probe is proposed. A numerical model of this probe is developed. Based on the results of the model, abacuses are built in order to gather the real electrochemical proprieties of the steel reinforcement (potential and current) from those values measured on the concrete surface. The role of the influencing factors i.e. physical (injected current, resistivity), geometric (concrete cover, probe's position) and electrochemical (state of the reinforcement), are fully investigated. The proposed model is applied in a laboratory environment, by reproducing the real site conditions[2]. The experimental work proves its feasibility, efficiency and effectiveness (within certain limits) by confirming its theoretical principles and indicating some uncertainties during its application. Finally, a primary operational protocol for the on site utilization of the technique is proposed.

Keywords: cooling towers, corrosion, carbonation, GPR, polarization resistance, concrete resistivity, concrete cover, feasibility

1.M.E.Mitzithra, F. Deby, S; Laurens, J. Salin, P. Stephan, D; François, JP Balayssac, ***Use of an electrochemical method coupled with ground penetrating radar for the detection of reinforced concrete on cooling towers***, *6th International Symposium on Cooling Towers, Cologne, Germany, June 20-23 2012 , pp 529-537*

2 M.E.Mitzithra, F. Deby, S; Laurens, J. Salin, P. Stephan, D; François, JP Balayssac, ***Numerical Simulations of a operative measurement mode of polarization resistance adapted for evaluating the corrosion of reinforced concrete on cooling towers***, *EUROCORR 2012, Istanbul, Turkey, 8-13 September 2012. (CD-ROM).*

Université
de Toulouse

Résumé

Cette thèse a été financée par Electricité de France-Recherche et Développement (EDF R&D). L'objectif est le développement d'une méthodologie pour une meilleure estimation de l'état de corrosion des armatures du béton des aéroréfrigérants, soumis à la carbonatation atmosphérique, sur la base d'une double approche: le radar géophysique (GPR) et la mesure de la résistance de polarisation[1].

Le GPR peut être utilisé pour la détection rapide des zones présentant un risque élevé de corrosion (détection des contrastes de permittivité). En plus, le GPR est utilisé pour la localisation des armatures d'acier et l'estimation de l'épaisseur d'enrobage. Cette dernière application est très importante pour cette étude.

Dans les zones identifiées comme potentiellement corrodées par le GPR, il est proposé d'utiliser la mesure de la résistance de polarisation pour quantifier l'activité de corrosion. Cette étude propose une méthode opérationnelle et originale, adaptée seulement à cette problématique. Après une analyse critique des dispositifs existants pour la mesure sur site de la résistance de polarisation, un nouveau dispositif est proposé. Un modèle numérique de ce dispositif est développé. Sur la base des résultats du modèle, des abaques sont construites afin de remonter aux propriétés électrochimiques de l'acier (potentiel et courant) à partir des valeurs qui sont mesurées à la surface du béton. Le rôle des paramètres influents, physiques (courant injecté, résistivité), géométriques (enrobage, position de la sonde) et électrochimiques (état de l'acier), est examiné en détail. Ensuite, la méthode d'inversion proposée est testée en laboratoire, sur des corps d'épreuve reproduisant les conditions du site[2]. La fiabilité et l'efficacité du modèle dans son domaine de définition sont démontrées. Les limites et l'incertitude du protocole de mesure sont également abordées. Enfin, un premier protocole opérationnel pour l'utilisation sur site de la technique est proposé.

Mots clés: aéroréfrigérants, corrosion, carbonatation, GPR, résistance de polarisation, résistivité, enrobage, fiabilité

---

1. M.E.Mitzithra, F. Deby, S; Laurens, J. Salin, P. Stephan, D; François, JP Balayssac, ***Use of an electrochemical method coupled with ground penetrating radar for the detection of reinforced concrete on cooling towers****, 6th International Symposium on Cooling Towers, Cologne, Germany, June 20-23 2012 , pp 529-537*

2. M.E.Mitzithra, F. Deby, S; Laurens, J. Salin, P. Stephan, D; François, JP Balayssac, ***Numerical Simulations of a operative measurement mode of polarization resistance adapted for evaluating the corrosion of reinforced concrete on cooling towers****, EUROCORR 2012, Istanbul, Turkey, 8-13 September 2012. (CD-ROM).*

Acknowledgments

The current PhD thesis which consists part of the national project ANR-Ville Durable-EVADEOS was financed by EDF R&D, in the frame of a contract CIFRE and was carried out in LMDC, INSA-Toulouse, during the period of October 2010 – October 2013. The objective of the thesis was the detection of corrosion of reinforced concrete on cooling towers of energy production stations.

From this position I would like to thank:

- Prof. Jean-Paul BALAYSSAC and Dr. Fabrice DEBY (Université de Toulouse III), thesis supervisors, for their substantial support, precious guidance and huge patience during these three years.
- Jean SALIN and Pierre STEPHAN (EDF R&D-STEP) for their precious guidance and co-operation during this project.
- The Exam Committee, formed by: Prof. Dider DEFER (Université d'Artois) as President of the committee, Prof. Fréderic SKOCZYLAS (Ecole Centrale de Lille), Dr. Thierry CHAUSSADENT (IFSTTAR) and Dr. Jean François LATASTE (Université Bordeaux I).

Special thanks to:

- Erwan GALENNE (EDF R&D- CIWAP), for giving me the opportunity to work on this project.
- Dr. Stephan LAURENS (INSA Toulouse), for his scientific contribution to the *"kick off"* the current thesis.
- Pierre-Louis FILLIOT, Antoine De CHILLAZ, Alexandre GIRARD (EDF R&D-STEP) and Prof. Jerôme MARS (ENSE3-Grenoble INP), for their substantial help on the *GPR and Signal Processing* part of the thesis.
- Daniel FRANÇOIS (EDF R&D-STEP), for his scientific contribution during this project.

I woud also like to thank the technical staff of the laboratory for their contribution to the experimental part of the thesis (Sylvain, Bernard, Yann, Carole, Moah...) and the laboratory's secretariat (Ghislaine, Fabienne..) for their assistance to all administrative matters.

Last but not least, I would like to thank my PhD colleagues, among all: office colleagues (Thomas M., Thomas V., An, Angel, Manh…), Elsa for her substantial support and the always nice conversations we had, Thierry L., Pierre S., Hugo M. and

Cédric B. for all the pleasant moments inside and outside the lab during the last hard year of the thesis.

Finally I would like to express my deep gratitude to my family, all my Greek and international friends for their psychological support, comprehension and help during these three years, without them the current PhD thesis would be much more difficult.

Toulouse, January 2014

Contents

List of figures

List of tables

List of symbols

α Charge transfer coefficient for the redox reaction

α_a Charge transfer coefficient for the anodic reaction

α_c Charge transfer coefficient for the cathodic reaction

β_a Anodic Tafel constant [V/dec]

β_c Cathodic Tafel constant [V/dec]

ΔE Potential drift or polarization along Butller-Volmer curve[V]

ΔE_a Total potential drop [V]

ΔE_p Polarisation on the steel surface [V]

ΔE_Ω Ohmic drop between steel reinforcement and the counter electrode [V]

Δi *or*

Δj Current density shift along Butler-Volmer curve [A/m^2]

Δt Duration of corrosion process (sec)

Δt_R Time difference between negative peak of the direct wave and positive peak of the reflected wave [sec]

ΔV Tension between two internal electrodes [V]

Δx Distance between two GPR receivers [cm]

ε Dielectric permittivity [F/m]

ε_0 Air permittivity [= 8.854×10^{-12} F/m]

ε_e Complex effective permittivity

ε_r Complex relative permittivity

ε_r' Dielectric constant

ε_r'' Loss factor

η Activation polarisation [V]

η_a Anodic polarisation [V]

η_c Cathodic polarisation [V]

θ Temperature (^oC)

μ_o free space magnetic permeability [=$4\pi \times 10^{-7}$ H/m]

v Direct wave speed [cm/sec]

ρ Concrete resistivity [Ohm.m]

σ Electric conductivity

φ	Phase angle
ω	Pulsation of the electric field [r/sec]
A,a	Proposed coefficients for the polarization resistance model
a	the electrode spacing [m]
B,b	Proposed coefficients for the polarization resistance model
B	Stern-Geary constant [26mV for active steel and 52mV for passive steel]
C	Double layer capacitance
c	Light speed in free space [=3.10^8 m/sec]
D/L	Depth of defect for ultrasonic testing
E	Redox potential after polarisation of the electrode [V vs. Ref]
E_0	Equilibrium redox potential [V vs. Ref]
E_A	Anodic electrode potential of steel [V]
E_{Ao}	Standard electrode potential of steel [V],
E_a	Anodic overpotential [V]
E_{ar}	Potential at the "point of interest" on the surface of the steel reinforcement [V]
E_C	Cathodic electrode potential of steel [V]
E_c	Cathodic overpotential [V]
E_{corr}	Corrosion potential [V]
E_{RE}	Potential measured by the reference electrode [V]
$E_p(t)$	Potential response as a function of time in Randles circuit [V]
E_Ω	Instant potential response due to ohmic resistance of concrete [V]
e	Concrete cover [cm]
F	Faraday's constant [96485 C mol^{-1}],
f	Frequency of the electric field [Hz]
h	Concrete cover in Pythagora's law [cm]
I	Current intensity flowing between two external electrodes [A]
I_{CE}	Current intensity injected from the counter electrode [µA]
I'_{CE}	Assumed current intensity injected from the counter electrode [µA]
I_{GE}	Current intensity injected from the guard ring electrode [µA]
i_{CE}	Current density injected from the counter electrode [A/m^2]
J or	
J_0	Apparent current intensity [A]
J_m	Macrocell current intensity [A]

J_{corr} Corrosion current intensity [A]

J_p Net current density after polarisation [Am^{-2}]

j_0 Exchange current density of the redox reaction [Am^{-2}]

j_a Anodic net current density [Am^{-2}]

$j_{a,c}$ Exchange current density of the cathodic reaction [Am^{-2}]

$j_{a,o}$ Exchange current density of the anodic reaction [Am^{-2}]

j_{ar} Current density at the "point of interest" on the surface of the steel reinforcement [Am^{-2}]

j_c Cathodic net current density [Am^{-2}]

j_{corr} Corrosion current density [Am^{-2}]

k Proposed coefficient for the polarisation resistance model

L Signal's path during the ultrasonic testing [cm]

L_o Distance between the GPR emitter and GPR receiver [cm]

L_{CE} Confinement length on the steel reinforcement surface of the injected current from the counter electrode [cm]

L'_{CE} Assumed confinement length on the steel reinforcement surface of the injected current from the counter electrode [cm]

L_t Trajectory of the reflected signal: emitter-reinforcement and GPR-receiver [cm]

M Molecular weight of metal [M =55.85g/mol for Fe]

m Mass loss of steel due to corrosion process [g]

Q Total electric charge passed through the steel rebar [A.sec]

R Ohmic resistance of concrete between active and passive steel bars (Ohm)

R^2 Coefficient of determination

R_{gas} Universal gas constant [8.314 J $mol^{-1}K^{-1}$],

R_p Polarisation resistance of steel [$Ohm.m^2$]

R_Ω Ohmic resistance of concrete between the concrete surface and the steel reinforcement (Ohm)

S_{CE} Surface of the counter electrode [m^2]

s_r Surface of the steel reinforcement [m^2]

T Absolute temperature [K]

t (%) Student Test value

t time (sec)

U Electromotive force of the reinforcement corrosion

x_j^a or

x_{aj}	Quantity or property corresponding to an active state of steel reinforcement
x_j^p *or*	
x_{pj}	Quantity or property corresponding to a passive state of steel reinforcement
Z	Impedance
Z’	Real component of impedance
Z”	Imaginary component of impedance
|Z|	Magnitude of impedance
z	Number of electrons taking part in the redox reaction
z_a	Number of electrons taking part in the anodic reaction
z_c	Number of electrons taking part in the cathodic reaction
$\nabla\varphi$	Potential gradient [V]

Abbreviations

ACDC	**A**nalyse et **C**apitalisation pour le **D**iagnostic des **C**onstructions
ANR	**A**gence **N**ationale de la **R**echerche
APPLET	**A**pproche **P**redictive **P**erformantielle et **P**robabiliste
ASTM	**A**merican **S**ociety for **T**esting and **M**aterials
C	**C**arbonated
CCC	**C**entral subs**C**ribed **C**omposite
CE	**C**ounter **E**lectrode
CIFRE	**C**onventions **I**ndustrielles de **F**ormation par la **R**echerche
CMP	**C**ommon **M**iddle **P**oint
DOE	**D**esign **O**f **E**xperiments
EDF R&D	**E**lectricité **D**e **F**rance –**R**esearch **& D**evelopment
EECs	**E**lectric **E**quivalent **C**ircuit**s**
EIS	**E**lectrchemical **I**mpedance **S**pectroscopy
EVADEOS	**EVA**luation non destructive pour la prédiction de la **DE**gradation des ouvrages et l'**O**ptimisation de leur **S**uivi
FO	**F**ixed **O**ffset
FEM	**F**inite **E**lement **M**ethod
GPR	**G**round **P**enetrating **R**adar
GR	**G**uard **R**ing Electrode
IR	**I**nfra **R**ed
ICR	**I**ndex **C**orrosion **R**adar
LMDC	**L**aboratoire de **M**atériaux et **D**urabilité des **C**onstructions
NC	**N**on **C**arbonated
OC	**O**pen **C**ircuit
OPC	**O**rdinary **P**ortlant **C**ement
RE	**R**eference **E**lectrode
RH	**R**elative **H**umidity
RILEM	**R**éunion **I**nternationale des **L**aboratoires d'**E**ssais et de **R**echerches sur les **M**atériaux
RSM	**R**esponse **S**urface **M**ethodology

SCE	**S**aturated **C**alomel **E**lectrode
SHE	**S**aturated **H**ydrogen **E**lectrode
SHM	**S**tructural **H**ealth **M**onitoring
SVD	**S**ingular **V**alue **D**ecomposition
UPV	**U**ltrasonic **P**ulse **V**elocity
WARR	**W**ide **A**ngle **R**eflexion **R**efraction
WE	**W**orking **E**lectrode

INTRODUCTION

1. CONTEXT OF THE STUDY

The continuous monitoring of the state of civil engineering structures is of crucial importance for EDF (Electricité de France, French Electricity Board) in order to assure the competiveness and the high level functionality of their energy production installations. According to EDF (I. Petre-Lazar ,October 2007), the maintenance cost associated to civil engineering, for the period 2000-2004, reached 45MEuro and it will continue increasing as the state of the structures will downgrade.

EDF possesses different types of concrete structures, such as cooling towers, reactor buildings and dams whose degradation may be due to their construction materials' ageing or different kinds of pathologies. More particularly, EDF has enlisted the following main mechanisms of degradation of their concrete constructions:

- Corrosion of steel rebars embedded in concrete, for all the structures, i.e. cooling towers, built at a proximity from the sea or big rivers,, leading to cracking and loss of initial mechanical properties of the concrete. The economical aspect associated to this particular mechanism of degradation is very high, taking into consideration that the maintenance cost of the installations suffering from corrosion consists of 30% or 50% of the initial value of the installation (I. Petre-Lazar, 2007).
- Chemical degradation of concrete. More particularly, it refers to concrete swelling and leaching due to direct contact of the structures with the water.
- Cracking of concrete, as a result of continuous hydro-and thermal cycles (case of cooling towers).

For that reason, EDF, being in charge of monitoring of the state of their structures, invests and carries out several studies, having as main objective the amelioration of Non Destructive Techniques, allowing a better and faster:

- Characterisation of the degradation mechanisms of their large surface structures
- Application of innovative operative modes for their control and inspection
- Techno-economical optimisation of the different means of reparation.

In that frame, EDF R&D, instead of a general study for any type of structure, prefers to focus on a specific case, the cooling towers. EDF R&D has a good knowledge of the degradation of cooling towers: atmospheric corrosion of steel rebars seems to be the main type of their deterioration. In an effort to reduce all the influencing parameters on the issue, this particular dissertation aims to determine a methodology

permitting a fast and more reliable estimation of the state of reinforcement corrosion of cooling towers, in order to allow preventive actions to avoid the ruin of this structure.

In the following paragraphs, a more thorough description of the problem raised for cooling towers will be presented. Then, the objectives and the strategy development of this project will be explained and finally the outline of the current thesis will be given.

2. EDF's COOLING TOWERS

Cooling towers (figure 1) are reinforced concrete structures, necessary in the thermodynamic cycle of the nuclear power stations, used in closed cycle water systems. Their role is to ensure the cooling down by air of the water that is heated up traversing the condenser loop. They are composed of: a tower (shell, piles and foundations), hydraulic infrastructures (hot water as input, cool water as output) and infrastructure supports. The natural circulation down-up of the air takes place via the chimney's shape of the shell of the cooling tower (F. Coppel, 2009).

Figure 0. 1: Cooling towers (shell, piles and foundations) of nuclear power stations.

The lifetime of cooling towers is estimated more or less 30 years old, for functioning 200 000 hours. The height of the tower and the foundations can reach 165m and 28m respectively. As it has been already mentioned, they are reinforced concrete structures (figure 2), with a compact double layer reinforcement network. The network consists of vertical and horizontal steel rebars with a maximum spacing of 25cm and 20cm respectively. The steel rebars may have a minimum diameter of 8mm. The minimum concrete cover of the steel rebars is 2.5cm (F. Coppel, 2009).

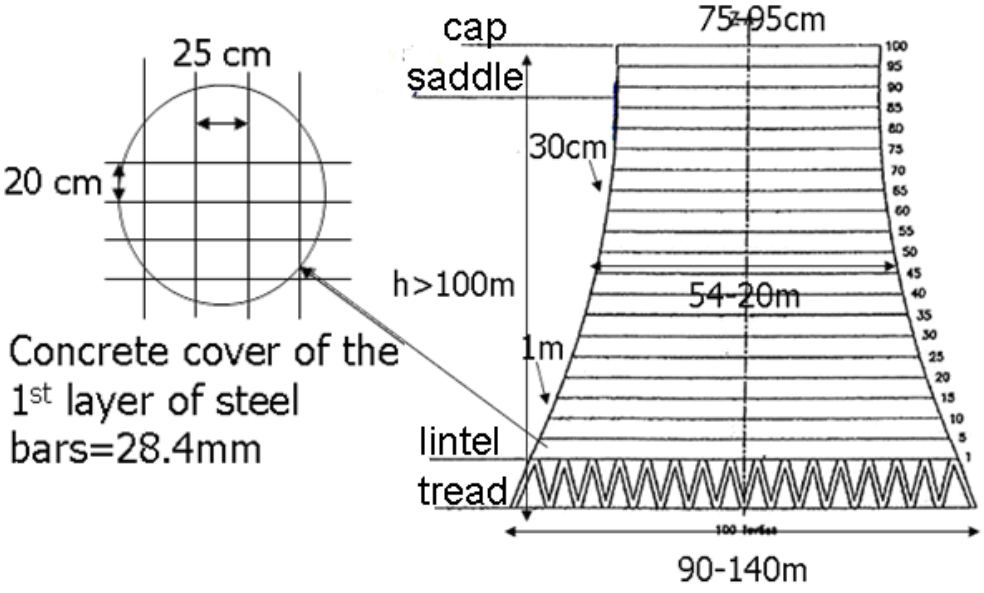

Figure 0. 2: Schematic illustration of cooling towers (F. Coppel, 2009).. Moving from the top and downwards: cap, saddle, lintel and tread. The shell consists of a compact double layer reinforcement network embedded in concrete. The average concrete cover of steel rebar, whether extrados or intrados is around 3cm (Eiffage, 2009).

In France, during the period 1950-1970, more than 20 cooling towers as those illustrated in figure 2, were constructed and started to function in fossil power plants (125-250 MW). Once the development of nuclear energy technology took off in late 70s, the nuclear power plants were also equipped with same type of cooling towers (figure 2). In 1991, a cooling tower with a height of 172m was launched into service for a pressurised water reactor of 1400 MW (R.Witasse, 2000).

As it can be understood, a large number of reinforced concrete cooling towers, are at an advanced stage of their service life and they start exhibiting some signs of structural deterioration. Since they are exposed to water containing chloride, sulphate and carbonic gases, they severely risk experiencing steel reinforcement corrosion. In its turn, the degraded reinforcing steel may lead to cracking, spalling and surface

deterioration of the concrete. There are some reports (NEA - CSNI, 2002), (P.C. Bamu, 2005), (F. Toutlemonde, 2008), (J.Wall,2009) (X.Chen, 2010) which state an already visible oxidation of the rebar, indicating corrosion.

As it is already known, the carbonic gases favour significantly the corrosion of steel rebars of the external part of cooling towers shells. Apart from its dissolved form in water, the atmospheric carbon dioxide can also penetrate directly, in gaseous form, inside the non saturated concrete pores and react with the cement hydrates. This process, known as carbonation, may lead to a neutralisation of concrete cover, by diminishing the pH of the interstitial solution and initiating corrosion process.

EDF R&D is aware that atmospheric carbonation is the principal reason of cooling towers' steel corrosion. More particularly, an average carbonation depth between 18mm and 30mm has been measured on different EDF's cooling towers, emphasizing that the deeper carbonated zones were located at the external face of the shell (,C. Toulemonde, 2010). In addition, it has been noted that the different environmental effects (i.e. rain, sun drying) may play an important role to the observed variations in the carbonation depth on different parts of cooling towers.

Thus, cooling towers are submitted to degradation due to steel reinforcement corrosion, **induced, on the external part of their shell, only by atmospheric carbonation**. More particularly**, carbonation depth has already surpassed the 1st layer of steel rebars in most of the cases of cooling towers, developing uniform conditions of corrosion.** EDF R&D (Y.Le Pape, 2010), (Roure, 2010) has clearly shown the role of corrosion on the mechanical durability of the cooling towers. For that reason, the necessity for an accurate evaluation of the corrosion state of the steel rebars of cooling towers is underlined.

The estimation of the corrosion rate is carried out by **local** non destructive electrochemical techniques .A big obstacle for their application is posed by the large surfaces of the specific structures, since it would demand an extreme effort and long time to inspect, locate and evaluate the corroded zones: For that reason, it is highly important the use of, firstly; a **global** dynamic technique for isolating the in risk of corrosion zones and then a more precise electrochemical technique in order to quantify corrosion.

However, the existing electrochemical techniques (i.e. GECOR, Galvapuse) for characterising corrosion of reinforcing steel suffer from a reliability deficiency. For that reason, the suggestion of an original operative methodology is imperative, in

order to evaluate effectively and accurately the state of reinforcement corrosion of EDF's cooling towers.

Thus, the current dissertation proposes a methodology which will allow a better estimation of the corrosion state of the steel rebars of the cooling towers, based on a double non destructive approach: a global technique such as the Ground Penetrating Radar (GPR) for the detection of zones with a high risk of corrosion and a local, electrochemical technique, such as the measurement of polarisation resistance of steel rebar, for the exact estimation of the corrosion rate of the steel rebars. The precise objectives and the strategy development of the proposed techniques are thoroughly explained in the following paragraph.

3. OBJECTIVES AND STRATEGY DEVELOPMENT

As it has been mentioned, the current study is related to the evaluation of the service lifetime of cooling towers of the electrical power stations. The cooling towers are large surface reinforced concrete structures, initially planned for a service life time of 30 years, however, their usefulness could be prolonged up to 60 years and in that purpose, EDF, in its agenda of sustainable management, requires the improvement of their structural state monitoring.

The main goal of the current thesis is to propose a methodology, allowing a better estimation of the state of steel reinforcement corrosion of cooling towers, based on a double approach:

- In order to inspect their very large surfaces, the use of a global, rapid and dynamic tool such as the Ground Penetrating Radar, (GPR), for the delimitation of those showing a high risk of corrosion. In the aid of this technique, a mapping of the inspected zones with significant contrasts of electromagnetic properties will allow to distinguish the areas with high potential risk of corrosion.
- On that zones the aim is to propose the use of a local technique for the exact evaluation of steel corrosion. More particularly, it consists of introducing a novel method and protocol of interpretation for the evaluation of the corrosion kinetics of the steel rebars.

3.1. Use of a global technique for the localisation of zones exhibiting a potential risk of corrosion

LMDC (**L**aboratoire de **M**atériaux et **D**urabilité des **C**onstructions) possesses about 15 years experience on the utilisation of the radar technique for the physical and geometrical characterisation of reinforced concrete, following different approaches. Several studies (J.P. Balayssac, 2005, 2007), (S.Laurens, 2005) have demonstrated that the radar signal processing allowed the detection of zones with a great potential of corrosion. The main advantage of this technique lies in its rapidity, and thus GPR consists of a very dynamic tool for the inspection of structures. The operator of GPR can identify the zones in risk of corrosion and then investigate them more thoroughly by techniques, used for the electrochemical characterisation of the steel rebars.
In this study the GPR signals will be then processed for:

- the development of a measurement and processing methodology, in order to evaluate the velocity and the attenuation (related strongly to the presence of water content in concrete, one of the major favouring parameter of corrosion) of the GPR signals. The objective is a quasi real time mapping of the inspected surfaces, allowing the determination of the corroded zones.
- The estimation of the dimensions of concrete cover of the steel rebars (3D localisation of reinforcement), via a more advanced signal processing. The 3D positioning of the steel rebars is indispensable for a complete diagnostic of the state of the structure, as far as the evaluation of the corrosion state of the steel rebars is concerned.

3.2. Proposal of an original operative local electrochemical technique for the evaluation for the evaluation of corrosion kinetics of the steel rebars embedded in concrete

The actual non destructive techniques for the characterisation of steel corrosion in concrete suffer from a lack of reliability. The reasons of their deficiency lie precisely on the theoretical principles of these techniques. The linear polarisation resistance measurement, which consists the basic tool for the estimation of corrosion kinetics, is considered to be the most remarkable example of this lack of reliability. The error sources are directly related to the interpretation protocol defined by the RILEM

committees (C. Andrade). For example, the protocol assumes that the current imposed from the instrument on the concrete surface to the surface of the steel rebars, is distributed uniformly around the steel rebar. On the contrary, numerical simulations carried out by LMDC, in the frame of the ANR (**A**gence **N**ationale de la **R**echerche) APPLET (Durée de vie des ouvrages: **A**pproche **P**redictive **P**erformantielle et **P**robabiliste) project, have shown that the most of the injected current is gathered on the steel rebar, right under the measurement point (or area) on the concrete surface. Thus, the wrong assumption of a uniform distribution of the injected current around the steel rebar leads to the over estimation of the polarisation resistance and thus the under estimation of the corrosion current density.

In addition, other sources of error, influencing significantly the quality of the measurement are: the way the ohmic drop is compensated, the incertitude on the determination of the steel rebar surface assumed to be polarised, the use of the confinement technique of the injected current, the uncertainty on the Stern-Geary constant. Furthermore, the quasi-systematic over polarisation imposed by the classical devices on the steel rebar may drive to an under estimation of the polarisation resistance. This effect adds to the complexity of the problem. Finally, questions are asked on the real polarisation induced by the existing techniques on the electrochemical system, since the steel rebar may be polarised up to hundreds of milivolts, causing probably irreversible alterations of the electrochemical system.

All the previous, illustrate the need for developing a more reliable approach of characterising the corrosion of reinforced concrete. The second part of the thesis is focused on the proposal of an innovative operation mode of measuring linear polarisation resistance, by eliminating or reducing the impact of the different error sources as they were briefly previously identified. This part of the study will be essentially carried out by numerical simulations of the proposed measurement technique and will be validated on lab scale.

These two parts of the thesis aim to develop procedures of data processing of Non Destructive Techniques for the characterisation of such a major pathology, the corrosion of reinforced concrete, on real site structures. More particularly, the current study proposes a global assessment methodology based on two complementary techniques, since a very local method such as that of the polarisation resistance is difficult to implement on large surfaces without *a priori* determination of zones

exhibiting a potential risk of corrosion. This determination will be carried out by a global technique, which in its turn is unable to provide with all information necessary for the precise "diagnosis" of the corrosion of the steel reinforcement. The diagnosis is possible only via the polarisation resistance measurement, already applied on an industrial scale, but its interpretation protocol needs to be improved. The following last paragraph presents the outline of the thesis.

4. OUTLINE OF THE THESIS

The current thesis which consists part of the national project ANR-Ville Durable-EVADEOS (**EVA**luation non destructive pour la prédiction de la **DE**gradation des ouvrages et l'**O**ptimisation de leur **S**uivi), is financed by EDF R&D, in the frame of a contract CIFRE (**C**onventions **I**ndustrielles de **F**ormation par la **R**echerche) and is carried out in LMDC, INSA-Toulouse. This thesis is entitled as: "Detection of corrosion of reinforced concrete on cooling towers of energy production stations" and is divided in two parts, A and B.

Part A is focused on the description of the corrosion of reinforced concrete as electrochemical process and its characterisation by Non Destructive Techniques. More particularly it consists of three chapters:

Chapter I presents the phenomenon of steel corrosion, as one of the major pathologies of reinforced concrete structures. Firstly, the mechanism and the kinetics laws of corrosion are explained. Then, the main types of corrosion due to different aggressive environments (atmospheric carbonation, chloride ions) are described.

Chapter II mentions extensively the different Non Destructive Techniques already used for the characterisation of reinforced concrete corrosion of real site structures. Firstly, the usual conventional techniques (proposed by RILEM recommendations) are described. Then, a reference to the alternative techniques (ultrasounds, impact echo, Rayleigh waves, infrared thermography) used for the characterisation of the degradation of structures, induced by concrete corrosion, is made. Their main advantages and disadvantages versus the estimation of steel corrosion are enlisted.

Part A ends with Chapter III, where the use of an alternative dynamic tool, the Ground Penetrating Radar (GPR), is proposed for the delimitation of zones with a high potential risk of corrosion. More particularly, the use of GPR in Civil

Engineering is presented, describing the basic principle of its application for the inspection of reinforced concrete structures and the influence of humidity, one of the major favouring factors of corrosion, on the electromagnetic properties of concrete and the propagation of the GPR signals (amplitude, direct wave speed). Then the different techniques for measuring the velocity of propagation of the direct signal are presented. This chapter mainly focuses on the aptitude of GPR for the location of zones with a potential risk of corrosion. The development of peak to peak amplitude mapping of the inspected zones for the determination of corroded zones, based on significant contrasts is proposed. However, as it will be explained, the dense reinforcement network consists of an obstacle for the processing and the interpretation of the signals. For that reason, in the frame of the study, different techniques for signal processing will be presented in collaboration with GIPSA Lab, Grenoble (Prof. J. Mars) and EDF R&D –STEP (P.L. Filiot)

Part B of the current dissertation focuses on the work carried out for the development and validation of a proposed novel operative measurement mode of polarisation resistance, for the accurate and reliable evaluation of steel reinforcement corrosion in concrete. It also consists of three chapters:

In chapter IV, a brief overview of experimental and numerical studies, focusing on the main problems of the polarisation resistance measurement and interpretation is given. Then, chapter V describes the proposal of a novel and effective operative measurement of polarisation resistance. Firstly, the theoretical background of the suggested methodology is presented. Afterwards, the novel model is demonstrated via numerical simulations and a procedure for calculating the real value of polarisation resistance is developed; in this way, new relationships, correction laws and abacuses are established. Finally, by means of experimental design, the model's sensibility to different parameters and their possible combinations are studied.

Chapter VI consists of the experimental demonstration and validation of the proposed measurement mode of polarisation resistance on lab scale. Firstly, the complete experimental program is given, including both the preparation and conditioning of the concrete specimen, the different materials' characterisation techniques and the several series of polarisation resistance measurements. The results obtained from all these measurements are fully discussed and explained, allowing the development of protocol for the on site measurement and interpretation of polarisation resistance.

This dissertation ends with the conclusions and the perspectives of the effectuated work on both parts of the current study.

PART A: CORROSION OF REINFORCED CONCRETE: PHENOMENOLOGY AND CHARACTERISATION VIA NON DESTRUCTIVE TECHNIQUES

I. Corrosion of reinforced concrete: Process and influencing factors

II. Conventional and alternative techniques for the characterisation of corrosion of reinforced concrete

III. Ground Penetrating Radar for the location of zones with a high risk of corrosion: Potential of the technique and proposed ameliorations

I. Corrosion of reinforced concrete: Process and influencing factors

I.1. INTRODUCTION

Reinforcement corrosion is the major threat to the durability of reinforced concrete structures. In the past, concrete was considered as the barrier against to the aggressive species from the outside environment (due to the high alkalinity of its pore solution), the reinforcement has been believed to be “non corrodible”; or in other words, the corrosion rate has been believed to be too slow to be of concern (G. Song, A. Shayan, 1998). In general, the majority of the reinforced structures perform very well under normal conditions. However, it was found that various structures, such as bridges and buildings, exhibit over time, concrete degradation associated with the ingress of aggressive corrosive species from the environment.

In addition, due to their big height and large surface, different parts of a structure could be exposed to different environments, so the same steel rebar in a structure may be subjected to different types of corrosion attacks and various extents of corrosion damage. More specifically, contrary to mechanical charges (i.e. wind), the influences from the environment may be complicated. Generally, environmental actions (i.e. humidity, temperature cycling during the day and night, variation of temperature) are irreversible and interact strongly with each other. This drives aggressive substances to build up over the years (i.e. chloride ions) and thus to changes in the corrosion behaviour of the reinforcement in structure (C.Andrade, 1995), (R.Polder, 2000).

The damage attributed to corrosion, due to lack of efficient design and correct estimation of the severity of the environmental activities has also a great economical impact. According to a study commissioned by the Federal Highway Administration, it was sated that the cost of corrosion in the USA reached about $286 billion in 2009 (R.Arndt, F. Jalinoos, 2009). Consequently, this underlines the need for rapid corrosion inspection methods that could lead to cost savings of billions of dollars worldwide by the detection of corroded reinforcement in concrete at an early stage. Damaged areas could then be targeted for strengthening or repair at the appropriate stage of the lifecycle of the investigated structure.

However, before that, it is necessary to obtain an understanding of steel corrosion on reinforced concrete structures. The current chapter covers the most important issues on that field; in the following paragraphs, the mechanism of steel corrosion is described and the laws that determine the kinetics of the phenomena are given; the

two main types of steel corrosion attacking the reinforced concrete structures are then explained.

I.2. STEEL CORROSION OF REINFORCED CONCRETE

Structures of reinforced concrete suffer very often from damage due to corrosion. Corrosion, in general, may be attributed, either to structure's flaws (i.e. poor quality of concrete, insufficient concrete cover of steel rebars) or to insufficient maintenance of the structure. In the majority of the industrial countries, the repair of the reinforced concrete structures damaged from corrosion is as important as the construction of new structures. However, the extreme environmental conditions make the corrosion control difficult, contributing to an even more serious degradation of the structures (R.Revie, 2011).

I.2.1. Mechanism of steel corrosion

Metal corrosion in an aqueous environment is a fundamental electrochemical process, related to the attempt of all metals to revert back to their natural thermodynamic or state. Steel exposed to a moist environment will corrode due to electrical potential differences created on its surface. These areas form anodes and cathodes, electrically connected through the body of steel, which permit an electric current flow from the first to the second ones. The steel becomes a "mixed electrode", allowing coupled anodic and cathodic reactions to take place on the metal-electrolyte interface. Figure I.1 shows the corrosion process of steel into a basic environment (pH>7).

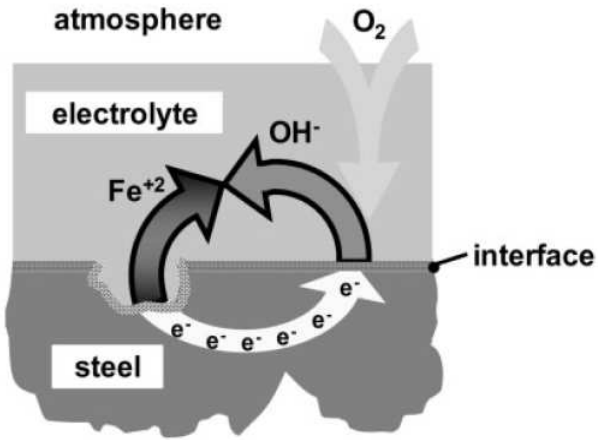

Figure I. 1: Schematic representation of steel corrosion process in the basic environment (Gulikers, 2005).

On the anodic sites, iron atoms are oxidized into Fe^{2+} ions, passing into the electrolyte, according to the reaction:

$$Fe \rightarrow Fe^{2+} + 2e^{-} \qquad \text{(eq.1)}$$

On the cathodic sites, the free electrons on steel are consumed, in order to reduce the oxygen, into OH^- ions:

$$2H_2O + O_2 + 4e^{-} \rightarrow 4OH^{-} \quad \text{(eq.2)}$$

The above schematic representation (Figure I.1) can also describe the corrosion process of steel reinforcing bars embedded in concrete: the complete reinforcement mesh acts as an electrode system whereas pore solution provides the common electrolyte.

The creation of anodes and cathodes is developed due to heterogeneities in the corrosion system, either in the concrete electrolyte phase or in the steel electrode phase. When the corrosion cell is established, the net anodic current is equal to the net cathodic current in order to maintain an electrical charge balance (conservation of charge). More particularly, the anodic current corresponds to the production rate of negatively charged electrons resulting from anodic dissolution of the steel, whereas the cathodic current corresponds to the consumption rate of electrons in the reduction of dissolved oxygen. Once corrosion has initiated, ionic currents are induced in the pore solution of the concrete material surrounding the steel (Gulikers, 2005).

Referring to the anodic reaction (eq.1), the anodic electrode potential, $E_{A,}$ can be expressed by the Nernst equation as:

$$E_A = E_{Ao} + \frac{RT}{zF} \ln \frac{[Fe^{2+}]}{[Fe]} \qquad \text{(eq.3),}$$

where:

E_{Ao} is the standard electrode potential of steel (V),

R_{gas} is the universal gas constant (8.314 J $mol^{-1}K^{-1}$),

F is Faraday's constant (96485 C mol^{-1}),

T is the absolute temperature (K) and

z is the number of electrons taking part in the reaction.

Similarly, referring to the cathodic reaction (eq.2), the cathodic electrode potential, Ec, can be expressed by the Nernst equation as:

$$Ec = E_{CO} + \frac{RcT}{zF} \ln \frac{[O_2][H_2O]^2}{[OH^-]^4} \qquad \text{(eq.4)},$$

Where: $[O_2]$, is the oxygen concentration (mol l^{-1}).

The electromotive force, U, of the reinforcement corrosion cell, involving a couple of anodic and cathodic reactions, can be derived as a difference of E_C and E_A

$$U=E_c-E_A \qquad \text{(eq.5)}$$

It's U, which drives the corrosion current through the electrolyte from anode to cathode. In general, the corrosion current (or the corrosion rate) is affected by the following factors:

- The pH of the electrolyte in concrete (affected by the presence of aggressive substances).
- The availability of oxygen and capillary water

I.2.2. Kinetics laws of steel corrosion

For a redox couple, if the potential deviates from the equilibrium potential (polarisation), then, either the anodic or the cathodic reaction dominates. The relation between the resulted current and the reaction potential of the electrode is non linear. If the rate-determining step in the electrode reaction is controlled by the activation energy required for the electron transfer to take place for both the anodic and cathodic reaction, then the net current density can be described by the so called Butler-Volmer equation. The Butler Volmer equation is the sum of the cathodic and anodic current of the redox reaction, (S.Ahmad, 2003), (G.Ji, 2006), (A.E. Pursaee, 2007).

The net current density can be described as follows:

$$j = j_o \cdot [\exp(\frac{\alpha \cdot z \cdot F}{RT} \cdot \eta) - \exp(\frac{-(1-\alpha) \cdot z \cdot F}{RT} \cdot \eta)] \qquad \text{(eq.6)},$$

Where:

j_o: the exchange current density of the reaction [Am^{-2}]

α: the charge transfer coefficient

η: the activation overpotential, (V) defined as:

$$\eta = E - E_0 , \qquad \text{(eq.7)}$$

where:

E: the redox potential after polarisation of the electrode [V vs. Ref]

E_0: the equilibrium redox potential [V vs. Ref].

Thus, net current density, j; represents the net transfer of electrical charge.

In the case of anodic polarisation η_a, the overpotential and so the net current density, noted as E_a and j_a, respectively are positive, while in the case of cathodic polarisation η_c, the same quantities, noted as E_c and j_c, are negative.

At the equilibrium potential, E_0, the rate of the anodic reaction equals the rate of the cathodic reaction, and as a result, no net current flows.

$$j_a + j_c = 0 \qquad \text{(eq.8)}.$$

The anodic and cathodic current densities will then equal the exchange current density, j_o.

Eq. 6 can be simplified when the electrode potential moves far from the equilibrium potential and so one of the current contributions becomes negligible. As a result, in the case of a strong anodic polarisation, the net current density is evaluated according to:

$$j = j_a = j_{a,o} \cdot \exp(\frac{\log(10)}{\beta_a} \cdot \eta) \text{ (eq.9) where: } \beta_a = \frac{\log(10) \cdot RT}{\alpha_a \cdot z_a \cdot F} \qquad \text{(eq.10)}$$

Similarly, after a strong cathodic polarisation, the net current density is calculated according to:

$$j = j_c = j_{c,o} \cdot \exp(\frac{\log(10)}{\beta_c} \cdot \eta) \text{ (eq.11), where: } \beta_c = \frac{\log(10) \cdot RT}{\alpha_c \cdot z_c \cdot F} \qquad \text{(eq.12)}.$$

The electrochemical constants β_α and β_c, are referred to the anodic and cathodic Tafel slopes, respectively. Examination of the Tafel equations in the form of (eq.10) and (eq.11) reveals that a graph of η against *log (j)* for both electrode processes gives a straight line with a slope equal to the respective β-constant (Figure I.2).

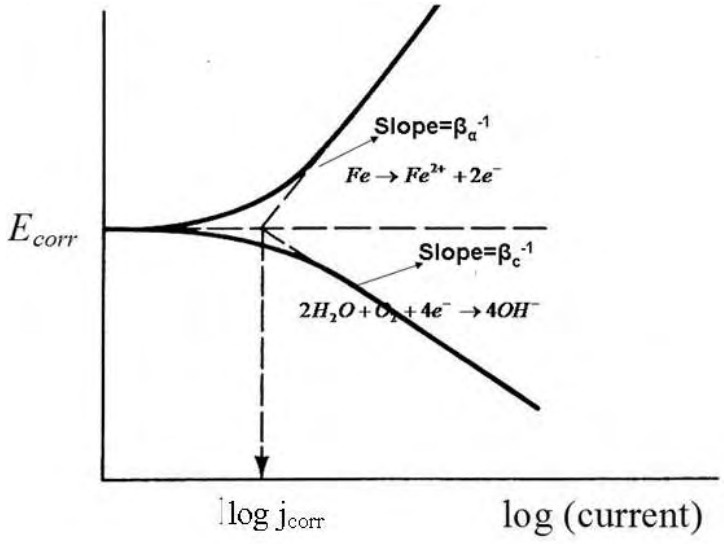

Figure I. 2: Graph of η against log(j) for both electrode processes during corrosion. Straight lines are traced with a slope equal to the respective β-constant. The intersection defines the system's equilibrium (no current flow): the corrosion potential, E_{corr}, and the corrosion current density, j_{corr}.

I.3. TYPES OF STEEL CORROSION OF REINFORCED CONCRETE

Concrete itself is a porous compound material consisting of mineral aggregates and the cement matrix that form a durable structure. The porosity of the concrete renders possible movement and retention of water and other substances. Concrete generally protects steel reinforcements from corrosion. The protection is due to the high alkalinity of the pore solution that causes passivation of the steel, in other words, the build up of an extremely thin inert layer on the steel's surface. However, this passive protection layer may be seriously compromised when the chemical composition of the pore solution is altered by carbonation or chloride contamination of the concrete cover. As a consequence, corrosion begins, resulting in a reduction in steel cross-sectional area, cracking and spalling as well as loss in bond between steel and concrete (C.Andrade, 1995), (A.Steffens, 2002), (A.Saetta, 2004), (L.Dao, 2010), (J. Ozbolt, 2011).

I.3.1. Uniform corrosion: phenomenon of carbonation

During hydration, the anhydrous calcium oxide of the cement, CaO, forms calcium silicate hydrate, mCaO SiO_2 nH_2O, denoted by C-S-H, and calcium hydroxide, $Ca(OH)_2$. Whereas C-S-H is insoluble, the alkaline $Ca(OH)_2$ may dissolve in the pore liquid. Additional alkalis are supplied in form of sodium and potassium oxides of the cement. They dissolve in the pore liquid during hydration, forming sodium, potassium and hydroxyl ions respectively. As these ions do not take part in the formation of the major cement hydration products, they accumulate in the pore solution and thus make calcium very insoluble. The pH of such pore fluids may well be greater than 12,4. The CO_2 that penetrates into concrete reacts with the alkaline hydration products of the cement paste. The reaction is called **carbonation** (A.Steffens,2002).

After hydration, sodium hydroxide and potassium hydroxide are completely dissolved in the pore liquid and therefore react readily with penetrating CO_2 that dissolves in the pore liquid. Unstable sodium and potassium carbonates are formed, while calcium hydroxide ($Ca(OH)_2$) dissolves in the pore solution to restore the chemical equilibrium. In its turn, dissolved $Ca(OH)_2$ reacts with CO_2 and the almost insoluble calcium carbonate is stored into the concrete pores. It is only when the soluble $Ca(OH)_2$ is completely bound in $CaCO_3$ that the sodium and potassium carbonates become stable. So the concentration of soluble $Ca(OH)_2$ in the cement paste is far greater than those of sodium hydroxide and potassium hydroxide. That is why the governing factor for the alkalinity of the pore liquid is the concentration of soluble $Ca(OH)_2$. Thus carbonation may be described only by the reaction of $Ca(OH)_2$, neglecting the minor alkalis:

$$Ca(OH)_2 + CO_2 \xrightarrow{H_2O} CaCO_3 + H_2O. \qquad \text{(eq.15)}.$$

The chemical reaction results in structural changes of the cement paste. Moreover, the volume of the reaction products may change with respect to the initial volume of the reactants. In addition, it has been observed that carbonation leads to a decrease in total porosity and pore volume of OPC (Ordinary Portland Cement) concrete (J.Kropp, 1995), (W.P.S. Dias, 2000).

Carbonation reduces the pH of the pore solution of concrete. The change in pH due to carbonation is very abrupt and therefore appears as “carbonation front” (Figure I.3). It usually comprises a very narrow zone separating two sides, one towards the exposed

concrete surface exhibiting pH values near 8 and the other towards the concrete bulk with pH values higher than 12.

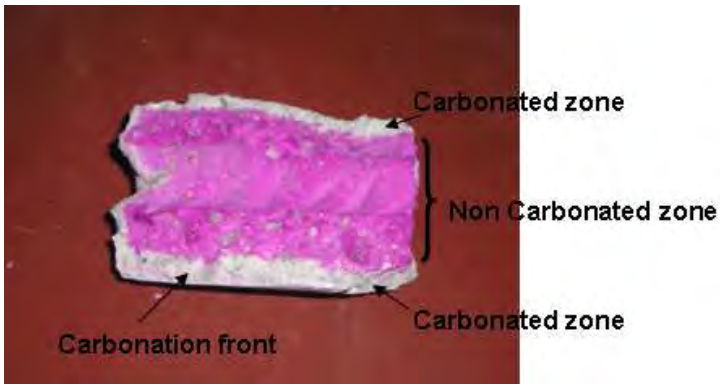

Figure I. 3 : Carbonation front via the phenolphthalein technique. The transparent sides are attributed to the carbonation (ME Mitzithra, 2008).

When the carbonation front reaches the level of the steel reinforcement, the passive film is no longer stable and active corrosion initiates. The ensuing corrosion process is uniformly distributed. Over the long term, the corrosion process leads to a reduction in the cross-sectional area of the steel bar and a significant amount of oxides which may crack the cover or diffuse through the pores to the surface of the concrete (A.Steffens, 2002), (A.Saetta, R.Vitaliani 2004), (A.Saetta, R.Vitaliani 2005).

Uniform or "microcell" corrosion, the anodic and cathodic surface areas are on a molecular scale and located directly next to each other. Their position is not fixed and can change with time (J.Warkus, 2006).

Due to carbonation, the corrosion current density, $j_{corr,}$, increases, accompanied by a change in corrosion potential, E_{corr}, towards to more electronegative values. However, the passivation is reinforced by the presence of humidity in the pores.

In order to explain the electrochemical behaviour of the reinforced concrete suffering from uniform corrosion due to carbonation, two steel bars are depicted in figure I.4, one considered to be active, the other passive, as two independent electrochemical systems (no electrical connection) (A. Nasser, 2010). For uniform condition, the polarization behaviour of such electrochemical systems may be described by the Butler-Volmer equation either for active steel:

$$j^{a} = j^{a}_{corr}[\exp(\frac{\ln(10)}{\beta^{a}_{a}}(E - E^{a}_{corr})) - \exp(\frac{-\ln(10)}{\beta^{a}_{c}}(E - E^{a}_{corr}) \quad \text{(eq.16)}$$

Or passive steel:

$$j^p = j^p_{corr}[\exp(\frac{\ln(10)}{\beta^p_a}(E - E^p_{corr})) - \exp(\frac{-\ln(10)}{\beta^p_c}(E - E^p_{corr}) \quad \text{(eq.17)}$$

where:

j^a and j^p are the net current densities flowing through the electrochemical interface for active and passive states respectively;

j^a_{corr} and j^p_{corr} are the corrosion current densities occurring in active and passive steel bars respectively ($j^a_{corr} > j^p_{corr}$, *figure.I.4*);

E^a_{corr} and E^p_{corr} are the free corrosion potentials of active and passive steel bars respectively ($E^a_{corr} < E^p_{corr}$ *figure.I.4*);

β^a_a and β^p_a are the anodic Tafel constants of active and passive steel bars respectively ($\beta^a_a < \beta^p_a$);

β^a_c and β^p_c are the cathodic Tafel constants of active and passive steel bars respectively $\beta^a_c \approx \beta^p_c$; (A.Nasser, 2010).

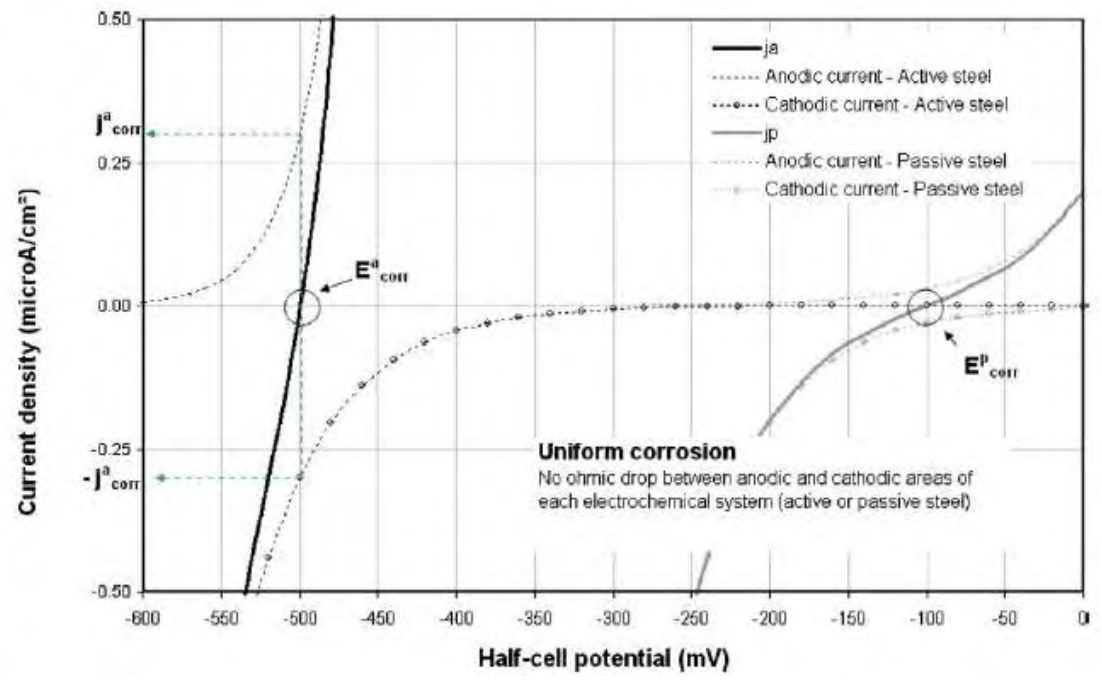

Figure* I. 4.*:Electrochemical behaviour of active and passive steel bars acting as independent electrochemical systems. (A.Nasser, 2010).

According to Figure I.4, for each case of state of the steel bar, the equilibrium potential *(E_{corr})* corresponds to the value for which the anodic current density (j^a_{corr}

for active steel and j_{corr}^{p} for passive steel) compensates the cathodic current density (- j_{corr}^{a} for active steel and - j_{corr}^{p} for passive steel). Therefore, at this point, even if corrosion may occur (especially for active steel), there is no net corrosion current density flowing through the electrochemical interface (see also Figure I.2.). For each system, anodic and cathodic areas can be spatially distinguished. Therefore, there is no ohmic drop (eq.18) between anodic, E_a and cathodic, E_c potential which are identical to E_{corr}. This is referred to as uniform corrosion (A.Nasser,2010).

$$E_a - E_c = 0 \qquad \text{(eq.18)}$$

I.3.2. Penetration of chloride ions

When anodically and cathodically acting surface areas are locally separated from each other, macro elements are formed. In other words, when there is a net distinction between the corroded (anodes) and the no corroded (cathodes) regions, localised corrosion is developed. This type of corrosion is attributed to the presence of chloride ions (pitting corrosion) and, generally, in that case, the anodic (corroded) area is smaller than the passive (non corroded) area of the steel bar (C. Andrade, 1995) (B.Elsener, 2002).

In order to understand the general principle of localised corrosion, an electrical connexion is established between the two steel bars, active and passive, mentioned in the previous paragraph. Figure I.5. exhibits the electrochemical behaviour of the connected system:

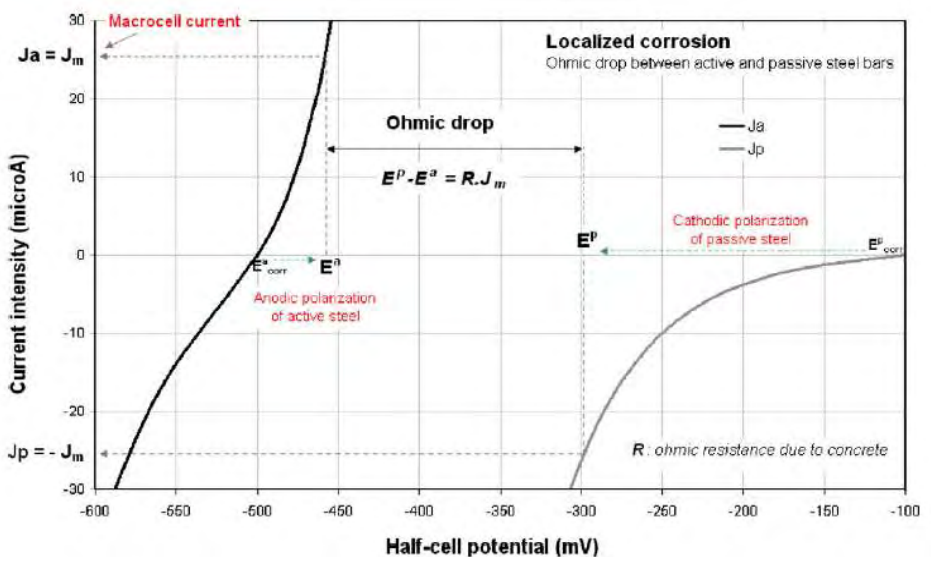

Figure I. 5: Electrochemical behaviour of active and passive steel bars after electrical connection (coupled electrochemical system) (A.Nasser, 2010).

It has to be underlined that current intensities are used, instead of current densities, in order to take account of the passive to active surface ratio which may exist in real structures.

After electrical connection, active steel potential, E^a, is attracted towards higher potential values, while passive steel potential, E^p, is attracted towards lower values. The active steel is anodically polarised (from E^a_{corr} to E^a) resulting in an apparent positive current intensity (J_a) flowing through the active steel-concrete interface. The passive steel is cathodically polarised (from E^p_{corr} to E^p) resulting in an apparent negative current intensity (J_p) flowing through the passive steel-concrete interface. Due to the distance between active and passive steel areas and due to concrete resistivity, E^p remains higher than E^a and the difference E^p- E^a is the ohmic drop existing in the case of a localised corrosion. The equilibrium of such a coupled electrochemical system corresponds to active and passive potential values (E^p, E^a), satisfying the two following conditions:

$$J_a = -J_p = J_m \qquad \text{(eq.19)}$$

$$E^p - E^a = R \cdot J_m \qquad \text{(eq.20),}$$

Where J_m is the macrocell current of the coupled electrochemical system and R is the ohmic resistance of concrete between active and passive steel bars (A.Nasser,2010).

I.4. CONCLUSION

Corrosion of reinforced concrete is a world wide problem. It is causing high economical losses through repair and maintenance needed to keep the facilities functional. This chapter presented the basic principles (mechanism, kinetics) of corrosion and described the main two types that can attack the reinforced concrete structures.

The potential risks of corrosion in a structure are quite unpredictable. As it can be understood, monitoring, predicting, preventing and rehabilitating the corrosion damage of steel in concrete structures is of high importance and thus it has become a vast area of research interest. A great deal of research work has been done on these

aspects the past two decades and much progress has been made in the field of monitoring and prevention.

In the following chapter, a state-of-the-art review of Non Destructive Techniques for the detection of corrosion is realised. The main purpose of that review is to summarize the latest knowledge on the existing techniques, conventional and alternative, to present their advantages and disadvantages and to prepare for the suggestion of a methodology that will allow the efficient detection of corroded reinforcement in concrete at early stage and thus any further degradation will be prevented.

II. Conventional and alternative techniques for the characterisation of corrosion of reinforced concrete

II.1. INTRODUCTION

As it is already mentioned above, corrosion of steel reinforcement is the main cause of damage and early failure of reinforced concrete structures in civil engineering. This leads to enormous costs for inspection, maintenance, restoration and replacement of the infrastructure worldwide. To ensure a sound decision on the type of repair work, it is essential to realise a thorough assessment of the condition of the structure, including the evaluation of:

- Cause of damage or loss of protection,
- Degree and amount of damage,
- Expected progress of damage with time,
- Effect of damage on structural behaviour ad serviceability.

Visual inspection is the most common method: it allows the description and the quantification of the damage. However, it is highly dependent on the expertise of the operator and by definition cannot detect hidden corrosion. In addition, it requires sampling from the structures, which cannot be always possible, especially, in the nuclear domain (R.Andt, 2009), (RILEM, 2003).

Conventional methods of Structural Health Monitoring (SHM) for detecting corrosion are based on electrochemical techniques:

- Measurement of concrete resistivity
- Half –cell potential measurement
- Linear polarisation resistance measurement
- Electrochemical Impedance Spectroscopy measurement D.E. John, (1981), (C.Andrade, 1995)

In addition, as it is already mentioned the steel rebar corrosion is directly related to the quantity of moisture in the concrete. In order to improve the diagnostic, it is necessary to estimate the spatial distribution of that property in the structure. Among the techniques the most used, are those based on the propagation of acoustic signals in the structures or even Infra Red (IR) thermography. It has to be noted that these alternative techniques may enlighten **indirectly** on the corrosion of the steel rebars, since they detect only the effect of corrosion on the structure (i.e. cracking, delaminating).

Thus, in this chapter, both the electrochemical and alternative techniques are presented, describing their basic principles, their advantages and drawbacks, during their use for the detection and estimation of corrosion of reinforced concrete.

II.2. CONVENTIONAL TECHNIQUES FOR DETECTING STEEL CORROSION OF REINFORCED CONCRETE STRUCTURES

II.2.1. Electrical resistivity of concrete

Resistivity (applied voltage/resulting current) is a specific geometry-independent material property and describes the electrical resistance of a unit cell. Its unit is Ohm.m. Resistivity measurements can be performed on all parts of concrete structures that are exposed to air. They are useful for the following purposes:

-estimation of risk of corrosion in the case of active corroding conditions

-location of zones of the structures with high exposure to water (detection of cracks, (J.F. Lataste, 2003), (C.Larsen, 2007)) and dissolved aggressive species

-enhancement of design systems for cathodic protection and other protective electrochemical treatments.

On site, resistivity can be measured using a probe with four equally spaced point electrodes that are pressed onto the concrete surface (Wenner or 4 point method). The two outer electrodes induce the current and the two inner electrodes measure the potential drop (fig.8)

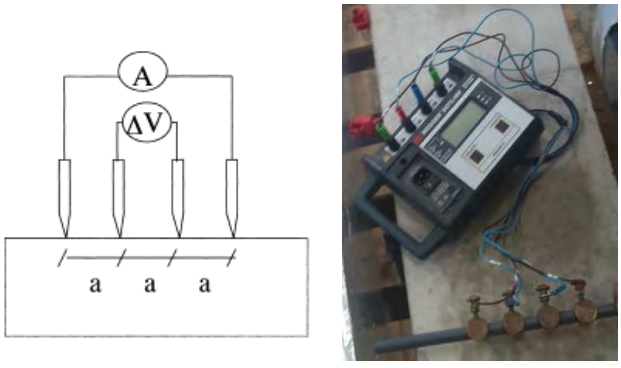

Figure II. 1: Set up of four electrodes measurement of concrete resistivity (R.Polder, 2001).

The current flows through a volume of concrete with a depth approximately equal to the electrode distance a. A resistance value is measured which depends on the

geometry of the electrodes and which is converted to the resistivity, ρ, via the equation:

$$\rho = 2 \cdot \pi \cdot \mathrm{a} \cdot R_{\Omega} \qquad \text{(eq. 21)}$$

Where: a: the electrode spacing

$$R_{\Omega} = \frac{\Delta V}{I}(Ohm) \qquad \text{(eq. 22)}$$

Where:

I: the current intensity flowing between the two external electrodes (A)

ΔV: the tension measured between the internal electrodes (V)

Current flow in concrete in the above measurement can be influenced by several factors. So the obtained values of resistivity can deviate from the real ones. As it is known, concrete is not a homogeneous conductor, since it consists of aggregates which are by nature inert bodies. This may lead to a non homogeneous current flow, which then can be decreased by placing the electrodes far apart. Another source of local disturbances in the current flow can be the presence of steel bars (excellent conductors). If one or more electrodes are placed above or near the steel bars, current flow will be disturbed and erroneous estimation of the real concrete resistivity is produced. With the usual rebar spacing, the measuring electrodes should be placed quite close, but this conflicts with the need to have them far apart to avoid non-homogeneity due to aggregates. (R.B. Polder, 2001).

However, eq. (21) applies only for homogeneous semi-infinite volumes of concrete and infinitely small electrode points. Thus, due to the no-homogeneity of the concrete, as discussed above, and the finite size of the electrodes, the result is not the true resistivity. According to literature, the correlation was studied between 4-point resistivity and values from cast in electrodes over a wide range of values. The true resistivity was obtained within an error of 25% (R.Weydert,1999), (Z.Bazant, 1979). A practical compromise appears to be an electrode spacing of 30-50mm (R.B. Polder, 2001). Some factors which have important effect on concrete resistivity are:

- Temperature for a constant relative humidity,
- Surface layer of different resistivity,
- Depth of carbonation,
- Contact between electrodes and concrete

Concrete resistivity is a function of porosity, the chemical composition of the solution in the pores and the number and distribution of pores filled with solution as a result of the interaction with the environment; it may vary between 10 and 10^5 Ohm m (R. Polder, 2001). Electrical current is carried by ions dissolved in the pore liquid. A wet or highly porous concrete exhibits lower values of resistivity. The resistivity of concrete increases when the concrete:

- Has a lower water to cement (w/c) ratio,
- Dries out after long curing times,
- Carbonates (the amount of ions available for carrying the current is decreased and the concrete becomes more compact)
- Is enriched with reactive minerals such as blast furnace slag, fly ash ad silica fume.

From the electrochemical nature of the corrosion process, a relationship is expected between the resistivity of concrete and the corrosion rate of reinforcement after depassivation. Bazant (Bazant, 1979) has shown that corrosion rate is inversely proportional to the resistivity. Later, it has been demonstrated that this relationship may be different for different concrete compositions (L.Bertolini, 1997). More recent studies have focused on the establishment of relationships between the electrical resistivity and its influencing factors, i.e. moisture, diffusion of aggressive species in concrete (A.A. Ramezanianpour, 2011).

So the relationship between concrete resistivity and corrosion rate is still subjected to study. However, table II.1, gives some suggestions for interpreting the resistivity values with regard to risk of corrosion. Generally, in any case, within a given structure, areas with low resistivity will have a higher corrosion rate than areas with high resistivity.

Table II- 1: Concrete resistivity and risk of reinforcement corrosion at 20°C for OPC concrete (R.B. Polder, 2001)

Concrete resistivity, $\rho_{concrete}$ (Ohm.m)	**Risk of corrosion**
<100	High
100-500	Moderate
500-1000	Low
>1000	Negligible

II.2.2. "Half cell" potential measurements

In that type of measurement, the corrosion potential, E_{corr}, (half cell rebar/concrete) is measured as potential difference against a reference electrode (half cell). Its principle and main components are depicted in figure II.2:

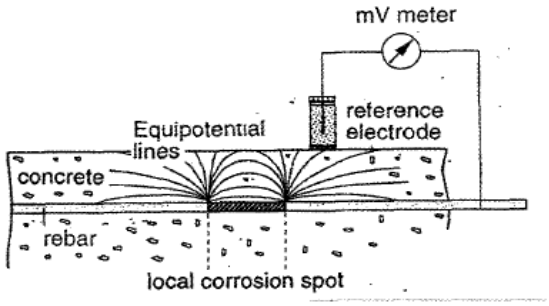

Figure II. 2: Principle and main components of half cell potential measurements: Reference electrode, high impedance voltmeter, connection to the rebar (R.B. Polder, 2001)

As it is shown above, the measurement takes place on the concrete surface, above the embedded steel bar; an electrical connection to the rebar is required. Then, the reference electrode is connected to the negative terminal and the reinforcing steel to the positive terminal of the voltmeter. In general, the current applied does not exceed 10pA. Electrical conduction between the reference electrode and the concrete is established by the transport of ions, by placing a conductive bridge between the reference electrode and the concrete (C.Andrade, 2004).

Potential measurements give the thermodynamics of the corrosion, not the rate of corrosion. It gives only an indication of the risk of steel corrosion. Corrosion potentials can be misleading, since its interpretation is mostly based on empirical observation and they are based on several factors, other than that of corrosion conditions. These factors can be:

- Electrical continuity between steel rebars in concrete,
- Electrical continuity between voltmeter and steel rebar,
- Concrete cover thickness,
- Concrete resistivity (moisture content),
- Influence of pH (carbonation front),
- Contact with buried or submerged parts of reinforced concrete structures,
- Junction potentials (J.P.Broomfield, 1997).

The primary goal of potential measurements on the reinforced concrete structures is to locate areas indicating a high risk of steel corrosion. In order to achieve this on large surfaces (bridge decks, walls, parking decks etc), potential mapping is usually performed with a multiple wheel arrangement and a small grid size of 0.15m. With a single or multiple electrode instruments several $100m^2$ per hour can be measured and about 30-50 single measurements are taken per square meter of concrete surface. In a half-cell potential map, each data is represented by a coloured square of adequate size on a suitably scaled plan view. The colour is related to the potential interval. Apart from colour plots, 3D and equipotential contour (lines of constant potential plotted through of equal values) plots can also be used for data representation (figure II.3).

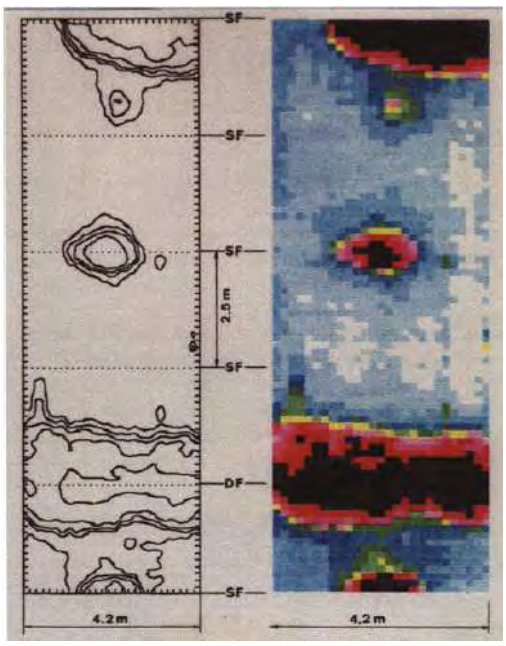

Figure II. 3: Examples of half-cell potential maps (Riding dick in the Tunnel San Berardino) in a colour plot (right) and equicontour line plot (left) (C.Andrade,, 2004).

When it comes to the criteria which associate the potential values to the risk of corrosion, RILEM committee doesn't recommend typical range of potentials of normal steel in concrete for different environments. On the other hand, ASTM (American Society for Testing and Materials), quotes values of potential (V. vs. E_{SCE} (**S**aturated **C**alomel **E**lectrode) presented in the following table (table II.2), related more directly to the risk of corrosion. In this dissertation, the ASTM criteria are used for the results of half cell measurements:

TableII- 2: Corrosion potential and risk of reinforcement corrosion at 20°C for OPC concrete (J.P.Broomfield, 1997)), (Cox, 1997)

E_{corr} (vs. E_{SCE}) (V)	Risk de corrosion
>-0,126	Low (<10% risk of corrosion)
-0,276 - -0,126	Intermediate corrosion risk
<-0,276	High (>90% risk of corrosion)
<-0,426	Severe Corrosion

II.2.3. Linear Polarisation Resistance Measurement

II.2.3.1. Definition

Corrosion rate is often expressed in terms of corrosion current density, (or intensity) j_{corr}, (or J_{corr}) or mass loss of steel rebar (Luping, 2002). Faraday relates corrosion current density to the mass loss according to the equation:

$$m = \left(\frac{J_{corr} \cdot \Delta t}{F} \right) \left(\frac{M}{z} \right) \quad \text{(eq. 23)}$$

Where:

m is the mass loss of steel due to corrosion process (g),

Δt is the duration of corrosion process (sec),

F is Faraday's constant (96485 C mol^{-1}),

M is the molecular weight of metal (M=55.85g/mol for Fe),

z is the number of free electrons (z=2 for Fe)

Stern and Geary (M.Stern, A.L.Geary, 1957) first presented the relationship between corrosion current density and polarisation resistance R_p as follows:

$$j_{corr} = \frac{B}{R_p} \qquad \text{(eq. 24),}$$

Where

B: is a constant (mV)

Let's consider the polarisation ΔE_p $(=E-E_{corr})$ of the electrochemical system steel rebar/concrete, being under conditions of uniform corrosion. This perturbation leads to the apparition of the apparent current density Δj_p on that interface, which is

expressed by the Butler-Volmer equation (see also *§I.3.1*). B is then theoretically derived from the first order development of Butler Volmer equation for $E=E_{corr}$ (eq.25):

$$\Delta j_p = j_{corr}\left[\exp\left(\frac{\log(10)}{\beta_a}\Delta E\right)-\exp\left(\frac{-\log(10)}{\beta_c}\Delta E\right)\right] \text{ (eq. 25)}$$

$$\Delta j_p = j_{corr}\frac{\log(10)(\beta_a+\beta_c)}{\beta_a\beta_c}\Delta \mathrm{E} = \frac{j_{corr}\cdot\Delta \mathrm{E}}{R_p} \qquad \text{(eq.26) (S.Laurens,2010)}$$

However, due to practical difficulties (i.e. obtaining a part of the reinforcement from the structure), the on site values of Tafel constants, β_a and β_c, can be hardly attained. For theat reason, it has been agreed that *B* is taken equal to 26mV for active steel rebars and to 52mV for passive steel rebars (Luping, 2002).

Linear polarisation resistance is defined as the slope of the linear part of the polarisation curve at E_{corr} (figure II.4). Now if eq. 24 is combined with eq.26, polarisation resistance is described by the equation (eq.27):

$$Rp = \left.\frac{\Delta E}{\Delta j_p}\right|_{E=Ecorr} = \frac{B}{j_{corr}} = \frac{\beta_a\beta_c}{j_{corr}\cdot\log(10)(\beta_a+\beta_c)} \qquad \text{(eq.27)}$$

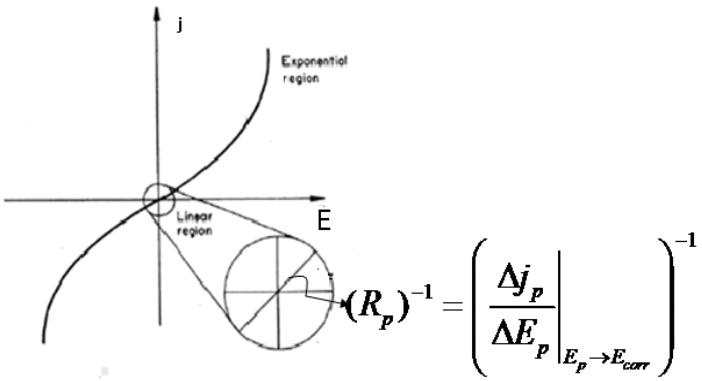

Figure II. 4.: Polarisation curve describing the Butler-Volmer model. The linear part of the curve corresponds to the target zone of the polarisation resistance, R_p, measurement. The slope corresponds to Rp^{-1}. (Luping, 2002).

Different techniques can be used for measuring linear polarisation resistance. In all cases, linearity between potential drift and the current density is an essential requirement (eq.27).

There are two ways in order to measure R_p:

- Potentiostatic way: applying a constant external potential ΔE_a and measuring the response current J_p.

- Galvanostatic way: applying a constant external current J_p and measuring the potential response, ΔE_a

ΔE_a is the total potential drop, which is a sum of ΔE_p and ΔE_Ω; the latter is the "ohmic drop" attributed to the ohmic resistance R_Ω between the steel reinforcement and the counter electrode. So, according to the equation (eq.28):

$$\Delta E_p = \Delta E_a - \Delta E_\Omega = \Delta E_a - J_p \cdot R_\Omega \qquad \text{(eq.28)}$$

Therefore, it is important to know the actual value of R_Ω in order to quantify correctly the polarisation resistance, R_p (Luping, 2002), (A. Poursaee, 2011).

II.2.3.2. Measurement instruments of linear polarisation resistance

In the market, there are two types of instrument for the onsite measurement of Rp: GECOR 6 and Galvapulse, which both of them function in a galvanostatic way but with certain differences (given in table II.3).

GECOR 6

Figure II.5 depicts the instrument GECOR 6 Corrosion Rate Meter developed in Spain:

Figure II. 5: The GECOR 6 corrosion Rate Meter developed in Spain (D.Macdonald,2009).

The electrode assembly consists of two circular, stainless steel electrode rings with outer/inner diameter of 70/11 mm and 180/140 mm, respectively. The inner electrode works as a counter electrode and the outer electrode serves as a guard rig. A

$Cu/CuSO_4$ reference electrode is positioned in the centre for recording steel rebar's reinforcement's potential. Two additional auxiliary reference electrodes, of the same type, are used for controlling the guard ring and they are positioned between the counter electrode and the guard ring. A constant current I_{CE} (in the form of pulse) is injected from the counter electrode, polarising the reinforcement in the cathodic direction. The potential response is then measured by the reference electrode. The instrument assumes a steel rebar length of 105mm to be polarised by the applied I_{CE}, which is less than 10μA. During the measurement, a secondary current is applied from the guard ring, I_{GE}, maintaining the polarisation with the length of the steel bar determined to be polarised. The injected current from the guard ring is such so as to maintain the potential difference between the two auxiliary reference electrodes at the initial level. ΔE_a is recorded after a polarisation of 100 sec. The ohmic drop is calculated before the start of the polarisation, when a very short current pulse is applied from the counter electrode and ΔE_Ω is recorded from the reference electrode. Then, ΔE_p is calculated via eq. 28. Figures II.6 and II.7 illustrate the configuration of GECOR 6 and the polarisation realised according to this instrument:

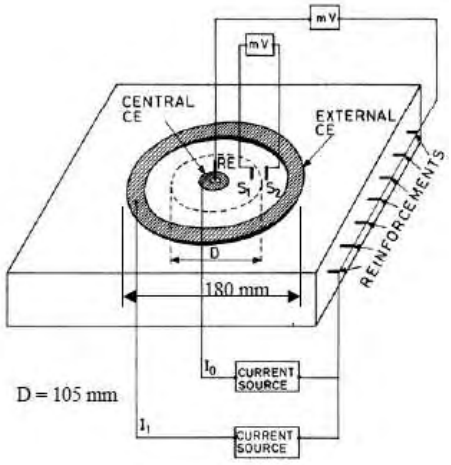

Figure II. 6: GECOR 6 electrodes' configuration (Nygaard, 2009).

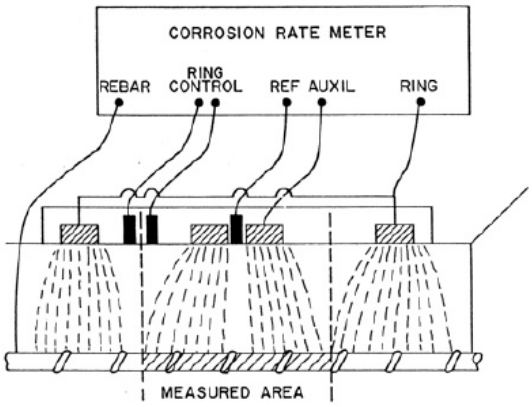

Figure II. 7: Polarisation of reinforcement according to GECOR 6.(Nygaard,2009).

Galvapulse

The Galvapulse fabricated from Force Technology (Denmark) (figure.I.13) is based on a transient technique for measuring R_p. A short galvanostatic pulse, I_{CE}, is applied to the reinforcement and the response is defined as the evolution of potential in time, $E_p(t)$.

Figure II. 8: The Galvapulse instrument from FORCE Technology (Denmark) (Nygaard,2009)

The transient technique assumes that the value of R_p is obtained by the adjustment of Randles circuit (figure II.9) to the potential response $E_p(t)$, according to the equation:

$$E_p(t) = J_o\left(\left(R_\Omega + R_p\right) - R_p \cdot e^{-t/R_pC}\right) \quad \text{(eq. 29)}$$

Where: C: the double layer capacitance.

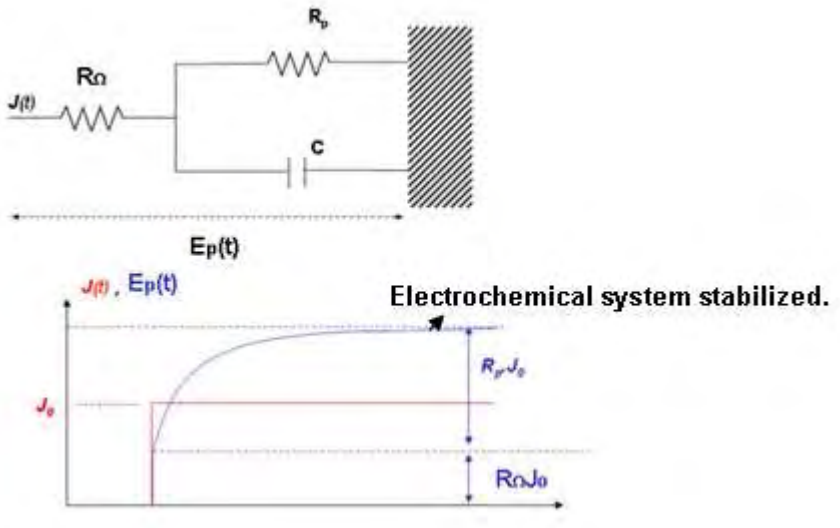

Figure II. 9: Randles circuit and the response to a short galvanostatic pulse (S.Laurens, 2010)

The polarisation lasts only 10 sec, and as a result the measurement is interrupted before the stabilisation of the electrochemical system (reinforcement/concrete). According to figure II.9, it seems that the instant response of the system corresponds to the ohmic drop. The deferred response that follows depends on the capacitance of the interface reinforcement/concrete and the polarisation resistance. If the measurement lasts more than 10 sec, then, the capacitance is charged and the potential is stabilised at $(R_p + R_\Omega)J_o$ (S.Laurens,2010).

As in the case of GECOR 6, Galvapulse also uses a guard ring electrode in order to limit the polarisation within that length of the reinforcement, which is supposed to be polarised (70mm). It injects a current between 20 and 100µA and it uses an Ag/AgCl reference electrode. The Galvapulse configuration is shown in figure II.10:

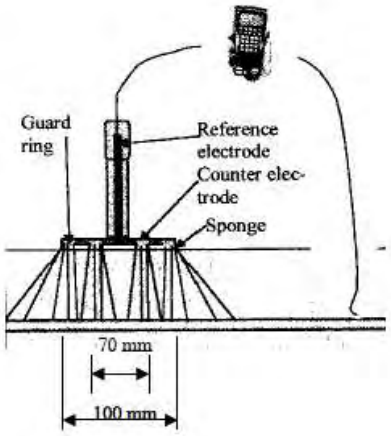

Figure II. 10: Galvapulse electrodes configuration (Nygaard, 2009)

Table II.3 mentions all the principal characteristics of these two commercial instruments for the on site measurement of R*p*:

Table II- 3: Characteristics of GECOR 6 and Galvapulse

	GECOR6	**Galvapulse**
Reference electrode	$Cu/CuSO_4$	Ag/AgCl
Contact between electrodes' configuration/concrete	Saturated wet sponge	Saturated wet sponge
Electrical continuity between instrument/reinforcement	Access and electrical connexion to the steel rebar	Access and electrical connexion to the steel bar
Type of measurement	Galvanostatic	Galvanostatic
State of measurement	Stationary $\Delta E_p = \Delta E_a - \Delta E_\Omega = \Delta E_a - J_p \cdot R_\Omega$	Transitory $E_p(t) = J_o\left(\left(R_\Omega + R_p\right) - R_p \cdot e^{-t/R_p C}\right)$
Type of confinement of polarisation	Guard ring electrode (ø180mm) + 2 auxiliary reference electrodes	Guard ring electrode (ø99mm)
Injected current from the counter electrode, I_{CE} (µA)	10	20-100
Injected current from the guard ring electrode, I_{GE} (µA)	Controlled by the potential difference between the 2 auxiliary reference electrodes: $\Delta E_{aux.ref}$=0.	Controlled by the potential of the counter electrode, E_{CE}
Polarisation duration (sec)	100	10
Reinforcement length assumed to be polarised (mm)	105	70

Once R_p is calculated, the estimation of the corrosion rate of the reinforcement can be calculated (either as corrosion current density (eq.24) or as steel mass loss (eq.23)). The table II.4 presents the criteria which relate the values of the corrosion rate to the different levels of corrosion. Any decisions about maintenance, intervention or repairing of the structures are principally based on these criteria (table II.4).

Table II- 4: Correlation between corrosion classification and corrosion current density (D.W. Law, 2004)

j_{corr}(µAcm^{-2})	Corrosion classification
0,1-0,2	Very low or passive
0,2-0,5	Low to moderate
0,5-1	Moderate to high
>1	High

II.2.4. Electrochemical Impedance Spectroscopy-EIS

Electrochemical Impedance Spectroscopy is now well established as a powerful tool (D. Macdonald, 2009) for investigating the mechanisms of electrochemical reactions, for measuring the dielectric and transport properties of materials, for exploring the properties of porous electrodes and the processes carried out on them, and for investigating passive surfaces and complex interfaces. This method studies the system response to the application of a periodic small amplitude AC-signal. The measurements are carried out at different AC frequencies. Analysis of the system response contains information about the interface, its structure, and the reactions taking place there (C. Andrade, 1995) (B.E. Conway,1999), (Fédération internationale du béton, 2003).

In this technique impedance is expressed as a complex number

$$Z(j\omega)= Z'-jZ'' \qquad \text{(eq. 30)},$$

where Z' is the real component and

Z'' the imaginary component of impedance.

The impedance may be expressed in an alternative form as

$$Z(j\omega)=|Z|e^{-j\varphi} \qquad \text{(eq. 31)},$$

where $|Z|$ is the magnitude of the impedance and

φ is the phase angle.

These two equations form the basis of the two common methods of presenting impedance data; Z'' vs. Z' (Nyquist diagram) and $log|Z|$ vs. $log(\omega)$ (Bode plane) (A.A. Sagues, 1990), (B.E.Coway,1999).

The measurement of electrochemical impedance is largely used in the evaluation of the state of corrosion of the steel rebar/concrete system. On a practical level, a potentiostat and a spectrum analyzer are required. Firstly, the open circuit potential of the system is measured and then a sinusoidal potential is applied (between 10 and 20 mV) on the system within a large range of frequencies. A sinusoidal response with a phase shift is recorded.

The major advantage of this technique consists of the physical interpretation of the process, provided the correct interpretation of the impedance spectrum (S. Feliu, 1985), (J.P.Broomfield,1997), (Luping, 2002).

The impedances of common passive circuit elements are the resistor R, the capacitor $1/j\omega C$ and the inductor $j\omega L$. In addition to these elements, the Warburg impedance is also important; it represents the impedance due to diffusion, of an electroactive species to an electrode surface, (D.D. MacDonald, 1987), (B.E.Coway, 1999).

EIS data are often interpreted in terms of Electrical Equivalent Circuits (EECs), which are analogs and not models, and hence the information they can deliver on physico-electrochemical processes involved are very limited. The Ershler-Randles equivalent circuit provides a surprisingly effective simulation of the impedance characteristics (figure II.11).

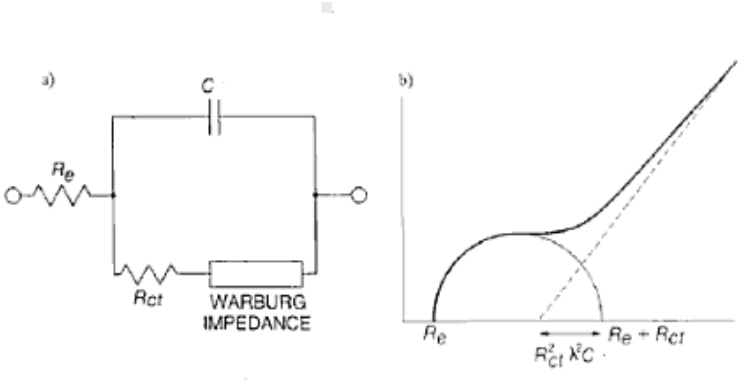

Figure II. 11: Ershler-Randles equivalent circuit for a charge transfer reaction at an electrode surface. R_e is the resistance in the solution between the electrode surface and the reference electrode, R_{ct} the charge transfer resistance and C the double layer capacitance (B.E.Conway,1999).

II.2.5. Synthesis

The evaluation of corrosion in reinforced concrete can be realised with destructive or non destructive techniques. The Destructive techniques allow a precise estimation of the corrosion rate, based on the measurement of the mass or section loss of the corroded reinforcement. However, as their name reveals, they require the destruction of the specimen, found in corroded state, after certain time and it cannot give information on the intermediary steps of evolution of the corrosion process. On the other hand, the Non Destructive Techniques, according to RILEM recommendations, include visual inspection, measurements of resistivity of concrete, half cell potential and polarisation resistance and Electrochemical Impedance Spectroscopy. The visual inspection allows a first verification of imperfections, defects or damages on the structure surface. In addition, a primary estimation of the concrete deterioration is possible. However, via this technique, corrosion damage can be detected only in an advanced level.

The four electrodes resistivity measurement is a very fast technique, which actually locate areas exposed to very aggressive conditions and may exhibit a high risk of corrosion. On the other hand, the resistivity results are highly sensitive to a certain number of environmental, technical and structural factors (i.e. moisture, concrete cover, spacing of electrodes). The half cell potential measurement can be applied in all cases of thickness of concrete cover and reinforcement dimensions, at any climate condition (θ>2°C). This rapid method doesn't provide quantitative information on the corrosion rate of the steel rebars and doesn't locate precisely the corroded zones of the reinforcement. On the contrary, the evaluation of the corrosion rate can be carried out via the measurement of linear polarisation resistance. On the market, there are two types of equipment for measuring polarisation resistance on site: GECOR and Galvapulse. Finally, the Electrochemical Impedance Spectroscopy is a quite powerful tool, because it allows the physical interpretation of the corrosion process and the transfer properties of the interfaces. However, the complexity of this technique lies into practical problems for its on site application (i.e. long duration) and the difficulties faced for the interpretation of the results. Table II.5, resumes the advantages and drawbacks of each method:

Table II- 5: Advantages and Disadvantages of the conventional techniques used for the evaluation of the reinforcement corrosion

Technique	Advantages	Drawbacks
Destructive	Estimation of corrosion rate (mass or section loss)	-Subtraction of specimen from the structures: possible damage of the structures -Destruction of specimen -No information about the evolution of corrosion
Non Destructive		
Visual Inspection	Detection of damage due to corrosion	-Detection of corrosion at a very advanced stage: intervention for repairing may be impossible -Parts of civil structures cannot be visible
Resistivity measurement (Wenner method)	-Location of zones exposed to aggressive species -Estimation of risk of corrosion, -A very rapid technique (~sec), -No connection to the steel rebar	Apparent values due to -the size and spacing of electrodes, -the presence of steel rebars, -coarse aggregates, -temperature, -moisture, -carbonation depth etc.
Half cell potential measurement	- Location of zones exposed to aggressive species -Rapid Potential mapping ($100m^2/h$, 30-50 pts/m^2), -Applicable throughout the structure's life at any climate condition (θ>2°C)	-Indication of the risk of corrosion -it may be influenced by the presence of moisture and carbonation depth: -It requires connection the steel bar

Linear Polarisation Resistance measurement (commercial instruments)	--Detection of the corroded zones -Estimation of the corrosion rate -Relatively rapid (5-15min) - Applicable throughout the structure's life at any climate condition (θ=2-50°C)	-Influenced by: - the type of corrosion, -concrete cover thickness, -moisture, -carbonation depth etc; -It requires connection the steel bar; -Different values may be obtained according to the different instruments (see Chapter IV)
Electrochemical Impedance Spectroscopy	-Information on the electrochemical reactions, dielectric and transfer properties of the interfaces -Interpretation of the physics of the processes	-On site measurements: non feasible. Mostly used on lab scale -Long measurement (> 12 hours) -It requires connection to the steel rebar -Complicated and difficult interpretation of results

II.3. ALTERNATIVE TECHNIQUES FOR THE CHARACTERISATION OF CORROSION OF REINFORCED CONCRETE STRUCTURES

II.3.1. Acoustic methods

The acoustic methods are based on the sensitivity of the mechanical waves to any damage of the concrete. They are adapted for detecting damages such as delaminating, micro cracking or any possible change in the mechanical properties of concrete. An acoustic technique cannot detect the corrosion or even its products, but mostly, the damages due to these products (A. Lamber, 1994), (W.Yeih,1998).

The general principle of acoustic auscultation consists of producing an echo in the material due to a mechanical impact on a material's surface. The acoustic wave can be propagated via the three following ways:

- a pressure wave (P wave), propagated parallel to the source's impact direction,
- a shear wave (S wave), perpendicular to the source's impact direction,
- a surface wave (Rayleigh wave) which propagates on the material's surface.

The signal's shape depends on the characteristics of the signal's source. Acoustic methods' sensitivity to imperfections or discontinuities of their propagation medium depends on the frequencies these signals are generated. It is generally accepted that the defect must be smaller than the wavelength, in order that the wave is propagated without any perturbation. In concrete, it's preferable to use low frequencies (0.02-0.5MHz), so that the signal's attenuation, due to the interface (discontinuity) mortar/aggregate, is limited. However, defects with strong irregularities in shape or very small dimensions make their detection via the acoustic techniques highly difficult (S. Laurens, 2001).

Among these techniques, Ultrasonic Pulse Velocity (UPV) is often used in order to test the quality of the concrete of a structure. In this technique, very short ultrasonic pulse-waves with centre frequencies (for all kinds of materials) ranging from 0.1-15MHz and occasionally up to 50MHz are launched into materials and echoes are registered. Via this technique, voids can be detected after calculating the propagation velocity of the acoustic signals. Caution, however, is required during the signal processing, since UPV can register echoes from interfaces that are not located right under the impact's source (*BS* EN 583-2:2001). The principle of the technique is illustrated in figure II.12:

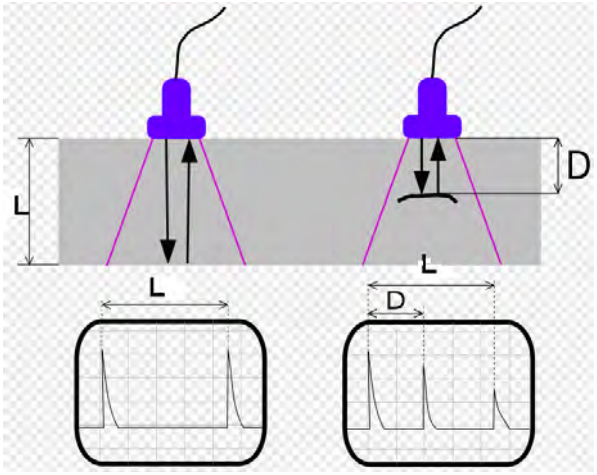

Figure II. 12: Principle of ultrasonic testing. A probe sends a sound wave into a test material. An echo is produced due to the back wall. L is the signal's path from the probe to the back wall and backwards (left). A defect creates another echo which reduces the amplitude of the back wall echo. D is the signal's path from the probe to the defect and backwards (right).The depth of the defect is determined by the ratioD /L (BS EN 583-2:2001).

The impact echo method can be used to provide thickness measurements of concrete slabs with accuracy better than 3%, and it can locate voids beneath slabs and pavements. It is based on the use of transient waves generated by elastic impact. The method's principle is shown in Figure II.13. A short-duration mechanical impact, is used to generate low-frequency sounds that propagate into the structure and are reflected by flaws and/or external surfaces. Surface displacements caused by reflections of these waves are recorded by a transducer, located adjacent to the impact. Multiple reflections of stress waves between the impact surface, flaws, and/or other external surfaces give rise to transient resonances, which can be identified in the spectrum, and used to evaluate the integrity of the structure or to determine the location of flaws (Telford, 1990), (Sansalone, 1998).

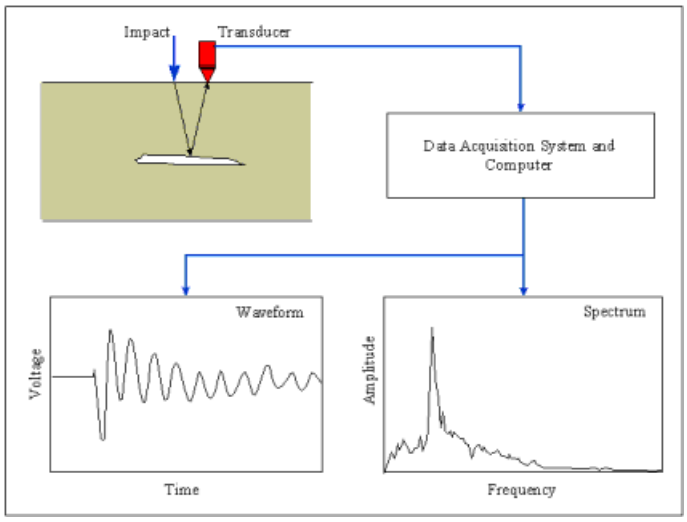

Figure II. 13: Schematic simplified representation of the impact echo method (Sansalone, 1998).

Rayleigh waves include both longitudinal and transverse motions whose attenuation increases exponentially as the distance from the surface increases. There is a phase difference between these component motions. In concrete, Rayleigh waves are widely used for detecting cracking, and the related shear modulus. The Rayleigh waves used for this purpose are in the ultrasonic frequency range. (0.1-15MHz) They are used at different length scales because they are easily generated and detected on the free surface of the structure under testing. Since they are confined in the vicinity of the free surface within a depth linked to the frequency of the wave, different frequencies can be used for characterization at different length scales (W.M.Telford, 1990), (Y.He, 1996), (D.O.Thompson, 1997).

The mapping of the acoustic wave velocity within a medium at various sections, known as acoustic or sonic tomography may give important information with regard to the structure and condition of the medium. The velocity determination is accomplished by measuring the time intervals taken by acoustic waves to travel from various sources to receivers placed on the surface of the medium. An acoustic ray is defined by each pair of source-receiver and its calculated velocity is just an average of the particular velocities along its trajectory path. For this kind of method, a large number of sources and receivers is used. The set of measurements is processed by specialized inversions analysis, solving the particular problem. Apart from velocity, tomography can also describe the attenuation factor. In this kind of tomography the measurements are related to the amplitudes of the acoustic waves. The sources and the

receivers can be located either in faced positions (crosshole tomography) or at the same surface (one-sided acoustic tomography) (V.K. Karastathis,2002).

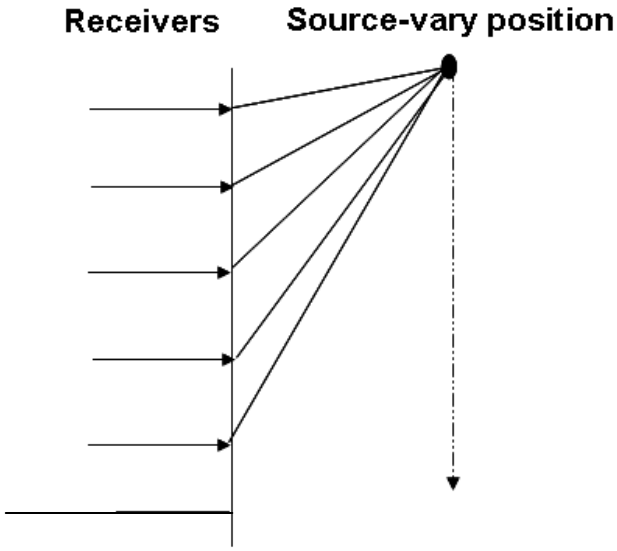

FigureII. 14: Schematic representation of tomographic transmission measurements

II.3.2. Infra Red thermography

Infrared (IR) thermography is based on the principle that defects within a material will alter the way heat flow is dissipated at the surface of that material. These changes in surface temperature can be measured and so it is possible to locate and determine the quantity of subsurface defects. Heat flow will occur when the temperature of the material differs from the temperature of its surroundings. Steel concrete structures which involve large areas, natural sources of heat (i.e. the sun) perform infrared thermography. However, this form of passive heating tends to reduce the ability to resolve the dimension of specific defects, since radiation from the sun is not very strong and thus it takes significant amount of time to provide enough heat to flow through a large structure. Several factors may influence the accuracy of infra red thermography including surface texture, wind speed and surface moisture.

Apart from natural heating, IR cameras can be used. They are mainly distinguished by the detector types which are characterised by their spectral change, spatial resolution long term stability and size of observation area (D. Breysse,2012). The principle of infra red thermography is depicted in the figure II.15:

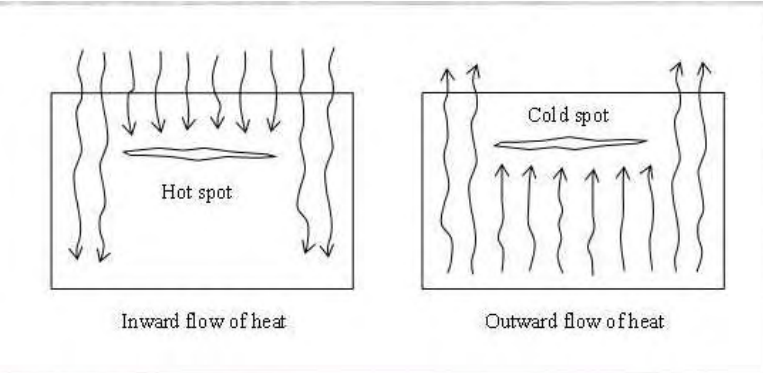

Figure II. 15: Principle of infra red thermography

II.3.3. Synthesis

In the previous paragraphs, alternative techniques that can be used for the characterisation of corrosion of reinforced concrete structures were presented. More specifically, these techniques deliver important information on the degradation of concrete due to corrosion. The acoustic techniques consist of the Ultrasonic Pulse Velocity (UPV), Impact echo, Rayleigh waves and acoustic tomography. UPV is used for the quality control of the concrete, but echoes from non-target interfaces can also be registered along with the targeted ones, due to the form of the propagated wave. The impact echo method is used for thickness measurements and location of voids in the concrete structures, while the method of Rayleigh waves can detect structural defects and damages, only at a very close distance from the structure's surface. A general and fast inspection of the condition of the structure can be provided by acoustic velocity or amplitude tomography. Finally, another alternative technique is the IR thermography which can be realised with the aid of the sun and it determines the quantity of the subsurface defects. However, the natural heating is a long time procedure. So IR cameras can also be preferred. Table II. 6 summarizes the positive and negative aspects of each technique:

Table II- 6: Advantages and Drawbacks of the alternative techniques used for the general evaluation of the condition of a structure

Methods	Advantages	Drawbacks
Ultrasonic Pulse Velocity	-Low frequency method, -Quality control of concrete, detection of voids of certain size	-Tiny subsurface defects undetectable -Registered echoes from interfaces that are not under the impact's source
Impact echo	-Low frequency method, -Transient resonance facilitating the location of flaws	-Complex instrumentation -Delicate calibration of the instrument -Propagation medium has to be under continuous stress
Rayleigh waves	-Easy production at different length scales, -Detection of cracking	-Propagation depth limited -Detection of flaws only on the free surfaces of the structures
Acoustic tomography	Amplitude and Velocity Mapping of large surfaces, -Detection of damaged zones	Specialised inversion analysis
Infrared Thermography (natural heating)	-Auscultation of large surfaces -Low cost technique	-Accuracy is influenced by -surface texture, - wind speed, -moisture etc, -Long time procedure, -Reduced resolution of defects

II.4. CONCLUSION

In order to be able to detect corrosion at early stages, Health Structural Monitoring proposes several techniques in order to intervene in time and extend the structure's life time.

Firstly, this chapter gave a full description of the usual conventional non-destructive techniques (also mentioned by RILEM recommendations), such as the electrical resistivity, the half cell potential the linear polarisation resistance measurement. As it was seen, these techniques perform a diagnostic on the state of corrosion, however it is rather difficult to use for the auscultation of large surfaces. These electrochemical techniques are mostly used for applications of small scale, such as concrete beams; thus, they consist of local approaches, which can be used, for the accurate evaluation of corrosion of reinforced concrete. Towards that direction, in part B of this thesis, a novel model of polarisation resistance measurement will be proposed and a methodology will be developed, taking into account all the influencing factors.

Next, the advantages and drawbacks of alternative techniques, such as acoustic methods and the infra red thermography, were presented. As it was mentioned, these techniques are mainly used for a global inspection of the structures and they can detect only the damages due to corrosion process. As a result, the information they provide, cannot be used for any acts of prevention and maintenance.

Thus, it is underlined the need for a global technique, which, contrary to the ones previously mentioned, during its application for the inspection of large surfaces, will be directly linked to the characterisation of corrosion of steel rebars. Ground Penetrating Radar (GPR) seems to have a very strong potential, due to its dynamic character, for the indication of zones with a high risk of corrosion. The correct delimitation of zones in risk of corrosion, will allow the use of a reliable local (electrochemical) technique for the exact detection and estimation of the corrosion at such a stage, so that any possible damage will be prevented.

In chapter III, the use of GPR in civil is described and some examples of its application for the research of zones with high potential of risk of corrosion are presented. Last but not least, the problems faced during the on site GPR application are discussed. In the frame of the current study, some signal processing techniques to overcome those problems are proposed.

III. Ground Penetrating Radar for the location of zones with a high risk of corrosion: Potential of the technique and proposed ameliorations

III.1. INTRODUCTION

During the last decade, progress has been made on the technology of geophysical radars (Ground Penetrating Radar-GPR), allowing their adaptation for the auscultation of the reinforced concrete structures (Non destructive technique). The utilisation of such a tool is based on the fact that the propagation of the electromagnetic waves in concrete is highly disturbed by the presence of chlorides and water. Compared to the techniques presented in the previous chapter, the radar possesses a great advantage: it's a dynamic tool that allows large scale auscultation and thus it could rapidly detect those zones with a potential risk of corrosion (presence of water).

The most frequent application of GPR consists of the detection of steel reinforcement. In addition the determination of the 3D positioning (estimation of concrete cover) of the steel rebars in reinforced concrete is a very important application in the domain of Civil Engineering ,(X.Derobert, 2001), (G.Klysz, 2004) (J.P. Balayssac (2006, 2007,) (C.W. Chang, 2009). In this study, the precise estimation of concrete cover is of high importance, since, it consists one of the major influencing parameters and entries for the local electrochemical technique of corrosion estimation that will be proposed and developed in chapters V and VI.

Since concrete cover thickness is a crucial information, improvements are needed to be made, in order to improve the precision of the steel reinforcement localisation (thus, estimation of concrete cover), which signifies that a very accurate estimation of the velocity of the electromagnetic wave propagation in the concrete is required. **This in its turn acquires a very good knowledge of the electromagnetic properties of concrete**.

In the current thesis, Ground Penetrating Radar (GPR) will be used for

- the delimitation of those zones (contrasts of permittivity-peak to peak amplitude mapping) on cooling towers which exhibit a potential risk of corrosion.
- the localization of the steel rebars and the exact estimation of their concrete cover thickness

Thus, in this chapter, the basic principle of using GPR for the characterisation of concrete's quality will be described, mentioning its main advantages and disadvantages. Then, the influence of the water content in concrete on both attenuation and radar wave velocity will be analysed and a quick reference to the different techniques of estimating the propagation velocity, presented in literature, will be made. Then, different examples of the application of GPR for the determination of those zones, exhibiting a high potential of risk of corrosion will

be given. This chapter will end with listing those problems that were encountered, after its on site application, and they are strongly related to the evaluation of the wave velocity and so the concrete cover of the steel rebars.

III.2. USE OF GPR IN CIVIL ENGINEERING

III.2.1. Basic Principle of GPR for the auscultation of reinforced concrete structures

As it has been already mentioned, among the various non destructive evaluation techniques, radar has become an interesting instrument for the rapid evaluation of reinforced concrete structures since it makes it possible to detect and locate sub surface features in them in a completely non-destructive way. More particularly, the 3D localisation of steel rebars or prestressing cables is an important application in Civil Engineering. GPR consists of a dynamic non destructive tool, easy and rapid to apply for the auscultation of large surfaces of structures. The principle of radar for civil engineering structures is based on the propagation of electromagnetic pulses, via an antenna, in the structures. The essential features are a source antenna (transmitter (T)) placed on the material surface, radiating energy both upward into the air and downward into the material, and an antenna receiving the signal transmitted by the source (receiver (R)) (X.Dérobert,2001), (G.Klysz,2004), (Z.M.Sbartai, 2009) .Figure III.1 presents the principle of a radar measurement on a structure of reinforced concrete.

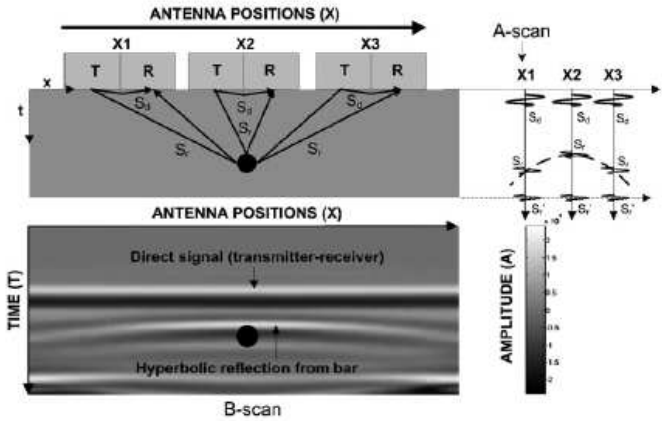

Figure III. 1: Principle of radar measurement in reinforced concrete (K.Viriyametanont, 2008)

The receiver measures the amplitude of the electric field (A) as a function of time (t) (A-scan). The part of the energy transmitted directly, via the interface “concrete-air”, from the

transmitter (T) to the receiver (R) is the direct wave (S_d). The other part of the energy is reflected by the interface "reinforcement-concrete" (S_r). The juxtaposition of the temporal signals recorded during the displacement of the radar antennas on the surface of the structure, leads to the in-depth representation of the structure (B-scan). The hyperbolic form corresponds to the presence of the armature. The transmission of an electromagnetic pulse is related to the simultaneous propagation of waves over a wide range of frequencies. The wavelength of the emitted pulse corresponds physically to the central frequency, at which the radiated energy reaches its peak. The commercial GPR antennas are distinguished by the centre frequency, for example, the GSSI antenna of 1.5 GHz, uses frequencies between 400MHz and 3GHz (S.Laurens 2001), (K.Viriyametanont, 2008).

III.2.2. Electromagnetic properties of concrete

During the propagation in the concrete, the electromagnetic waves are modified according to the electromagnetic properties of the material. Concrete is a non magnetic material ($\mu = \mu_o = 4\pi$ x 10^{-7} H/m, where μ_o is the free space magnetic permeability). As a result, its properties are limited to the electrical conductivity, σ, and the dielectric permittivity,ε, expressed via the equations 33 and 34:

$$\sigma(\omega) = \sigma'(\omega) + j\sigma''(\omega) \qquad \text{(eq. 33)}$$

$$\varepsilon(\omega) = \varepsilon'(\omega) - j\varepsilon''(\omega) \qquad \text{(eq. 34)}$$

$$\omega = 2\pi f \qquad \text{(eq.35)}$$

$$j^2 = -1 \qquad \text{(eq.36)}$$

where, ω (r/sec) is the pulsation and f (Hz) the frequency of the electric field. As it can be seen via the above equations, the electromagnetic properties are complex properties. In the frequency range of radar, the electromagnetic waves are influenced by these two properties, making it impossible to distinguish their effects. For that reason, the complex effective permittivity, ε_e, is defined, combining the conductivity and dielectric permittivity effects. Now, if ε_e is divided by the air permittivity, ε_o = 8.854 x 10^{-12} F/m, the complex relative permittivity, ε_r, of the material is determined (Eq.37):

$$\varepsilon_r = \frac{\varepsilon_e}{\varepsilon_o} = \frac{\varepsilon_e - j\varepsilon''}{\varepsilon_o} = \varepsilon'_r - j\varepsilon''_r \qquad \text{(eq.37)}$$

The real part ε_r' of the relative permittivity is the dielectric constant and represents the amount of electromagnetic energy stored in concrete and the imaginary part, ε_r'' (loss factor), represents the losses of energy, due to absorption or attenuation of the propagated waves. In the case of concrete, whose energy losses are low, the direct wave velocity propagation depends only on the dielectric constant (c is the light speed in free space) (Eq.38).

$$v(\omega) = \frac{c}{\sqrt{\varepsilon'_r(\omega)}} \qquad \text{(eq. 38)}$$

III.2.3. Influence of humidity on the electromagnetic concrete properties and the propagation of GPR waves

III.2.3.1. Influence of humidity of the effective permittivity of concrete

It has been shown (S.Laurens, 2001) that such a global technique allows the delimitation of areas which exhibit a potential risk of corrosion by detecting strong contrasts on the electromagnetic permittivity of concrete on those areas. In literature, several examples link the variation of the electromagnetic permittivity of concrete to different contents of water in it, consisting of one of the most important factors of corrosion of reinforced concrete. Several authors have shown that the water content in concrete influences the effective permittivity. More particularly, it has been reported that an increase in the water content of concrete leads to an augmentation of the dielectric constant (Soutsos, 2001), (R.L.Du Plooy, 2013).

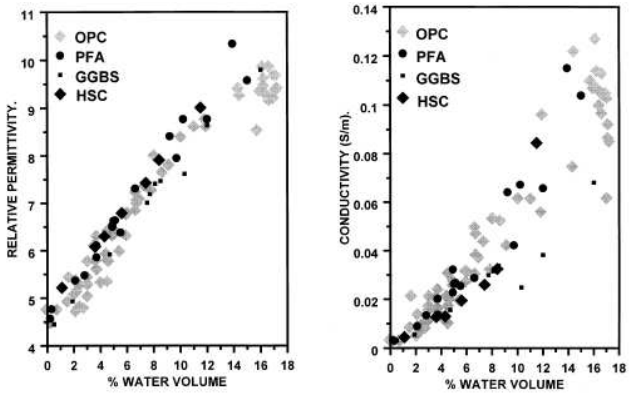

Figure III. 2: Effect of water volume (%) on the relative permittivity and conductivity of concrete for a frequency of 500 MHz (Soutsos et al, 2001)

It has also been demonstrated that while porosity has no important effect on the behaviour of the dielectric constant, mineralogical nature of the aggregates plays a significant role (G. Klysz, 2007, Viriyametanont et al, 2008).

III.2.3.2. Influence of humidity on the amplitude and the speed of GPR direct wave

There are several studies in literature, showing that the properties of concrete may modify the propagation of the GPR waves in it. More particularly, it has been stated that the peak to peak amplitude of the direct wave varies as a function of the water content of concrete (K. Viriyametanont et al, 2008). The peak to peak amplitude refers to the difference between the first positive peak and the first negative peak of the direct wave (figure III.3.a). Figure III.3.b demonstrates that the peak to peak amplitude of the direct wave diminishes linearly when the water content of concrete increases:

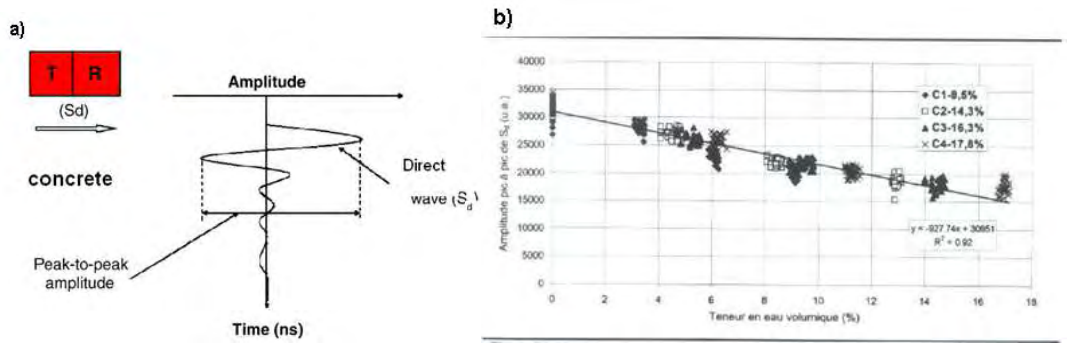

Figure III. 3.: a) Direct wave of GPR antenna in concrete (Z.M.Sbartai, 2007) b) Relation between the peak to peak amplitude of the direct wave and the water volume (%) in different concretes (K.Viriyametanont, 2008)

Still, the augmentation of the dielectric constant due to the increased water content leads consequently to a significant linear decrease in the propagation velocity of the radar direct wave (G. Klysz,2007), (figure III.4):

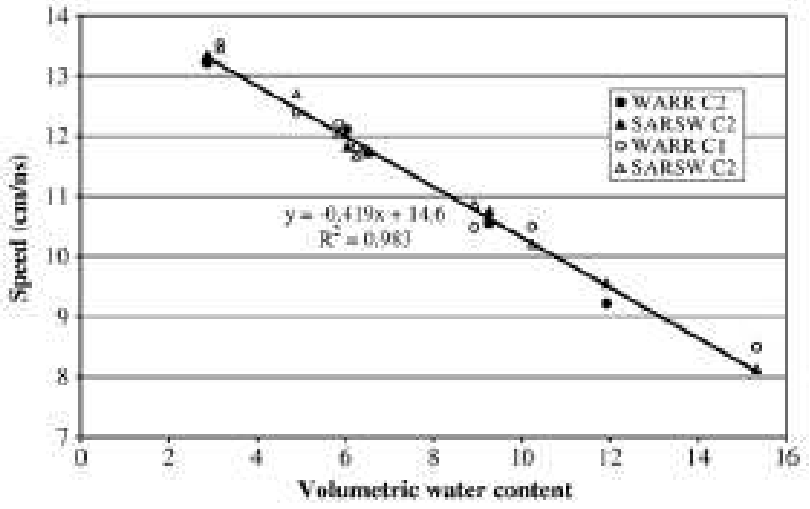

Figure III. 4. Variation of the direct wave velocity as a function of the water content in concrete (G.Klysz, 2007)

III.2.4. Methods for measuring the propagation velocity of the GPR waves

In order to measure the propagation velocity of both direct and reflected waves, three techniques are mentioned in literature (L.W. Galagedara, 2003, 2005):

1. Wide Angle Reflection and Refraction (WARR)
2. Common Middle Point (CMP)
3. Fixed Offset (FO)

These three methods are used in order to estimate the direct wave velocity that can be related to the water content.

III.2.4.1. WARR and CMP methods

According to WARR, the receiver of the GPR stays put and the transmitter is moved away from the receiver by successive fixed steps. The CMP technique consists of fixing a point between the transmitter and the receiver, and displacing them at the same time and to opposite directions at fixed successive steps, using as a reference that fixed point. These two techniques may estimate indirectly the water content in concrete, but they suffer from a low spatial resolution and long measurement durations at each position of the antennas. Knowing the arrival time of the different signal as a function of the distance between the receiver and

the transmitter allows finding the propagation velocity, v, of the different signals (G.Klysz, 2004):

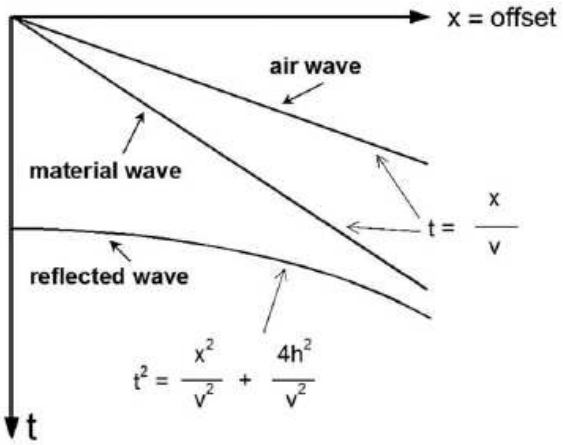

Figure III. 5: Arrival time of the direct and reflected wave as a function of the distance between transmitter-receiver (G.Klysz, 2004)

III.2.4.2. FO method

During the FO method, the transmitter and receiver move towards the same direction, keeping their between distance fixed along the measurement profile. Compared to WARR and CMP, FO is a faster technique and its spatial resolution is relatively high. However, its precision in estimating the wave velocity depends largely on the correct evaluation of the transmission and arrival time of the direct wave. Normally, the transmission time of the signal can be estimated with the aid of the velocity of the wave, propagated in the air. Although the short fixed distance between the transmitter-receiver offers a high spatial resolution, it is rather difficult to separate and distinguish the direct wave from the other signals (i.e. reflected waves due to the presence of steel rebars) (L.W. Galagedara, 2003,2005).

Figure III.6 depicts the different methods used for measuring the propagation speed of GPR signals (L.W. Galagedara, 2003):

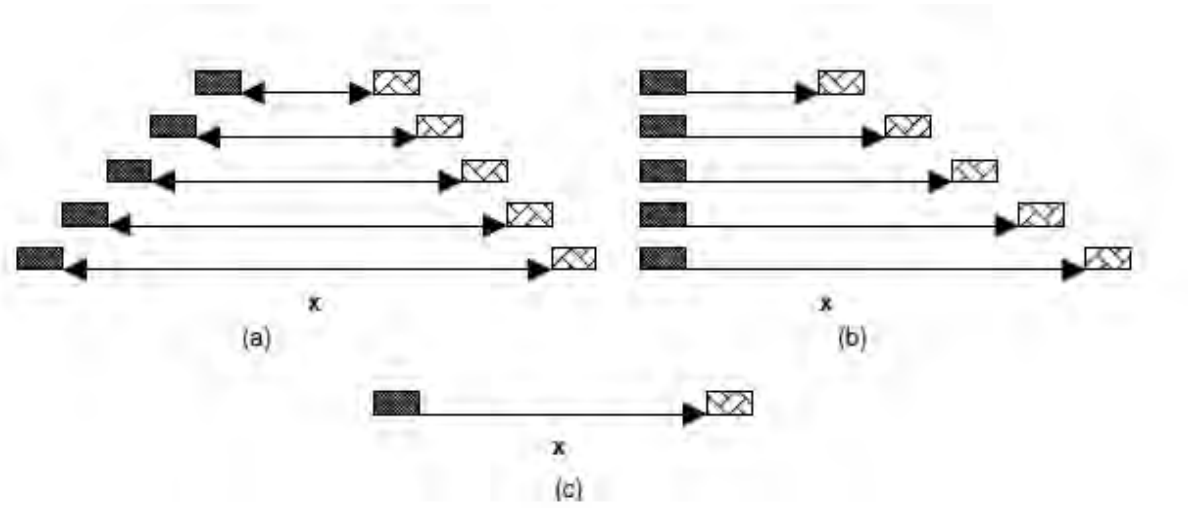

Figure III. 6: Schematic illustration of the different methods used for measuring the propagation velocity of GPR signals: a) CMP b) WARR c) FO. ■ is the GPR transmitter and ▨ is the GPR receiver.

III.2.5. Synthesis

In the previous paragraphs, the basic principle of using GPR in the auscultation of reinforced concrete structures has been thoroughly described. As it has been presented, the propagation of the electromagnetic signals can be disturbed by the presence of humidity in concrete. The latter, consists of one of the main factors of concrete degradation. More particularly, it has been shown that an augmentation in water content leads to an increase of the dielectric constant. In addition, the propagation velocity of direct wave and so the peak-to peak amplitude (the difference between the first positive peak and the first negative peak of the direct wave) decrease linearly when the water content of concrete augments. Apart from that, it has been also stated that the mineralogical nature of aggregates has also a significant influence on the propagation velocity of the direct signal, while the cement type, content and porosity play a less important role on the electromagnetic properties of concrete. Table III.1 resumes the influence of humidity on the electromagnetic properties of concrete and characteristics of direct wave:

Table III- 1: Influence of humidity on the electromagnetic properties of concrete and characteristics of direct wave

Influence of humidity of concrete on:	*Increase in water content leads to:*
Permittivity	Increase in dielectric constant
Peak to peak amplitude of the direct wave	Linear decrease
Propagation velocity of direct wave	Linear decrease

Finally, three different methods, found in literature for measuring the propagation velocity of the direct wave, were presented. The methods WARR and CMP are slow and are characterised by a weak spatial resolution. On the other hand, FO is faster and its spatial resolution higher. However, it requires the separation of the direct wave from the other signals and thus the exact transmission and arrival time of the signals. Table III.2 summarizes the three methods with their advantages and disadvantages:

Table III- 2: Advantages and disadvantages of the methods for measuring the propagation velocity of direct wave of GPR. E: is the emitter and R is receiver of the electromagnetic signal

Methods	*Procedure*	*Advantages*	*Disadvantages*
WARR/CMP	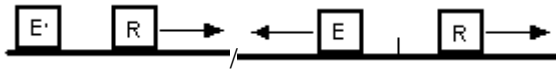	Indirect estimation of the water content of concrete	-Low spatial resolution -Long duration measurement
FO		-High spatial resolution -Faster than WARR and CMP	-Demands the precise emission and arrival time of the electromagnetic waves for the correct evaluation of the propagation velocity of the direct wave

III.3. EXAMPLES OF THE TECHNIQUE RADAR FOR THE RESEARCH OF ZONES WITH HIGH POTENTIAL OF RISK OF CORROSION

III.3.1. General Principle of evaluating the risk of corrosion via radar

As it has been mentioned earlier, the radar technique has shown a great potential for indicating those zones on reinforced concrete structures, with a high risk of corrosion. Its main principle consists of putting in evidence contrasts of permittivity on the concrete surface of the structures. This can be realised, after data processing, via a peak to peak amplitude or direct wave velocity mapping of those zones inspected by GPR.

As it has been described in the previous paragraph, the electromagnetic properties are strongly influenced by the water content of concrete. More particularly, as it has been demonstrated, an increase in the humidity of concrete leads to an increase of the dielectric constant of concrete. In their turn, the behaviour of the electromagnetic properties towards the water content of concrete, will affect the amplitude and the propagation velocity of the direct signal, leading consequently to a linear decrease of these two properties of the direct signal.

In addition, it is already known by the previous chapters that humidity, expressed by means of resistivity, plays a high significant role in the evolution of corrosion. Resistivity and GPR signals react similarly to the variations of water content in concrete. Thus, the (peak-to-peak) amplitude or propagation velocity of the direct wave mapping allows the indirect electrochemical evaluation of the state of the reinforced concrete. Concrete surface zones of strong permittivity (low peak-to-peak amplitude and wave velocity) due to high water content suggest an elevated risk of corrosion while zones of low permittivity (high peak-to-peak amplitude and wave speed) due to low water content suggest a low probability of corrosion. In the following paragraphs, some case studies of applying ground penetrating radar for the indication of zones with high moisture content and thus an elevated risk of corrosion will be presented.

III.3.2. Examples of GPR application for the location of zones in risk of corrosion

In literature, several studies have confirmed the GPR's effectiveness and reliability for the identification of zones with high penetration of moisture. Figure III.7 illustrates a zone with an in depth signal attenuation for a GPR scanning of the Forth Road Bridge, near Edinburgh in Scotland (A. Alani et al., 2013):

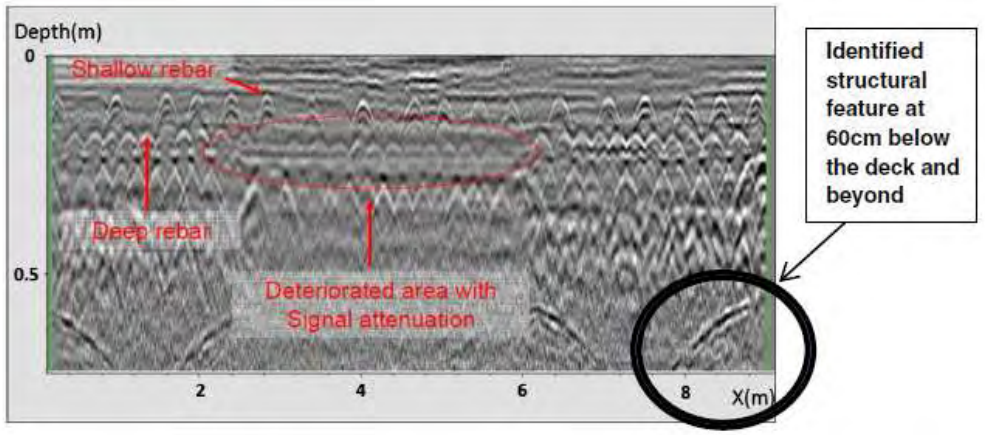

Figure III. 7: GPR scanned area of Forth Road Bridge detecting different rebar layers on a longitudinal section (depth against distance) (A.Alani et al, 2013)

The above image indicated a deteriorated area, suggesting as a cause of the signal's attenuation, the possibility of moisture penetration. Indeed, during the study, that area was excavated and the presence of moisture was confirmed. After data processing, A. Alani managed to locate those zones with high moisture penetration and illustrate them in the aid of AUTOCAD:

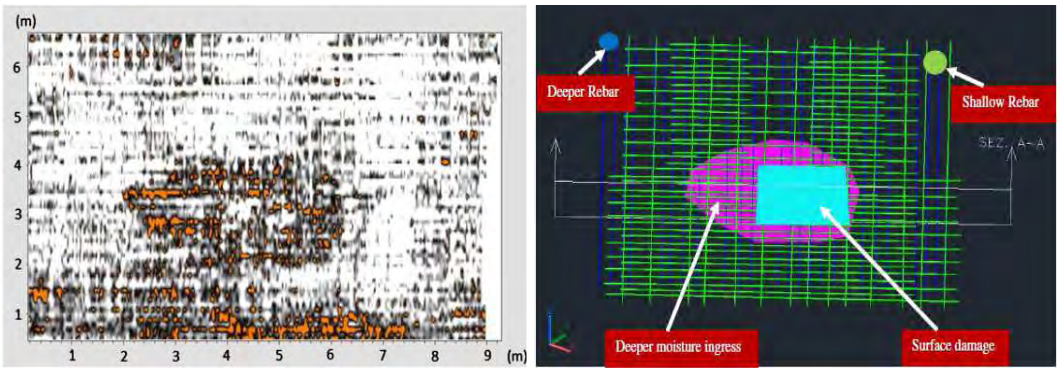

Figure III. 8: Area with increased attenuation (left) and schematic 3D drawing with AutoCAD indicating the zones of high moisture penetration (right) of the Forth Road Bridge, Edinburgh, Scotland (A .Alani et al, 2013).

The study carried out by A. Alani, consists of a proof that via GPR data, the location and illustration of the zones with high moisture content on structures is feasible. However, it doesn't provide with any quantitative information neither on the electromagnetic properties of the reinforced concrete nor on the characteristics of the GPR signals. Thus an accurate evaluation of the state of the reinforced concrete structure vis-à-vis the corrosion process cannot be effectuated.

On the other hand, S. Laurens, (2001) established the Index Corrosion Radar (ICR), a coefficient based on the ratio of the amplitude of the reflected signal to the amplitude of the direct signal. The contrasts in the values of ICR along a concrete surface suggest contrasts of moisture content in concrete, and thus indicate indirectly contrasts of probability of corrosion of the reinforcement. He then compared the radar results with the results of the corrosion potential measurement technique (see also §II.2.2), since both these techniques are influenced by the same concrete properties (moisture content, electrical resistivity). More specifically, he realised ICR and corrosion potential mappings and showed that these two techniques can lead to the delimitation of the same zones with high risk of corrosion. As it is depicted in figure III.9, a relative colour scale was used (red for a strong probability of corrosion and blue for a low probability of corrosion):

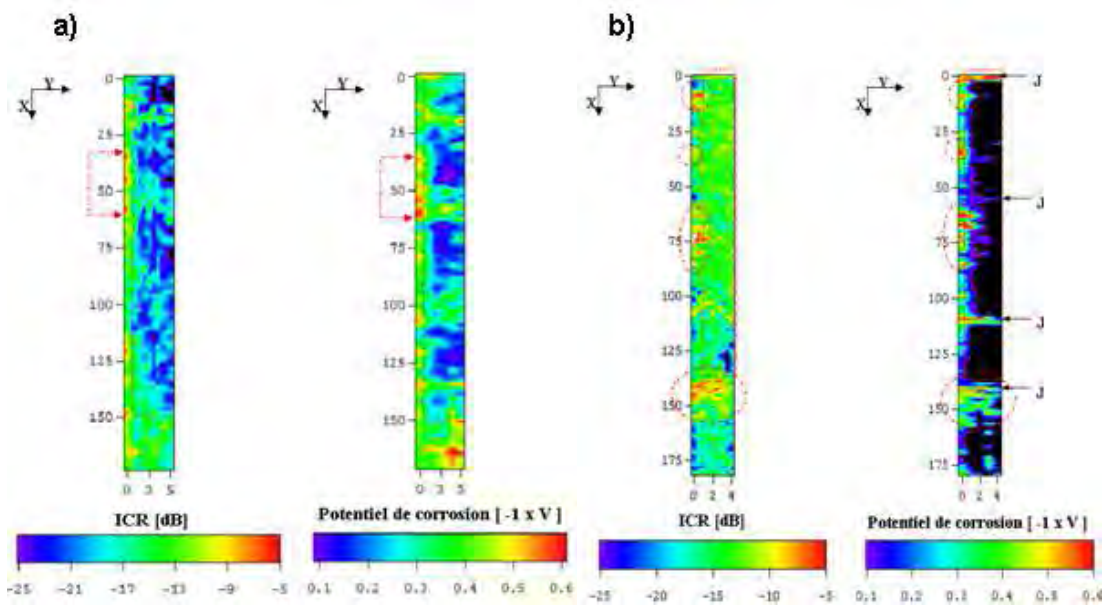

Figure III. 9: Examples of ICR and corrosion potential mappings for two different a) and b) concrete bridge decks. The red dotted fleshes for surface a) and the red dotted circles for surface b) indicate the zones with the higher risk of corrosion. Radar and corrosion potential measurements indicated the same zones for each surface. (S. Laurens, 2001)

According to S. Laurens' work, the zones that indicated a high risk of corrosion were the ones severely assaulted by humidity. However, in order to simplify the interpretation of the data and avoid the calculation of ICR, the peak-to-peak amplitude mapping of the inspected concrete surface can also be used for the delimitation of the zones with an high risk of corrosion.

For that purpose, in the frame of this study, GPR scans were carried out on an EDF reinforced concrete beam (EPR model), equipped with optical fibre sensors for tests of deformation, temperature and hygrometry. The dimensions of the beam were 5000x250x250mm while the steel rebars had a diameter of 32mm and 12mm. The scans were realised with a GSSI 5100 model of 2.6GHz and a SIR-20 central unit. One transmitter and two receivers were used and profiles were effectuated along three sides of the reinforced concrete beam according to the FO method. Figure III.10 demonstrates an example of radar scanning on one of the sides of the reinforced concrete beam:

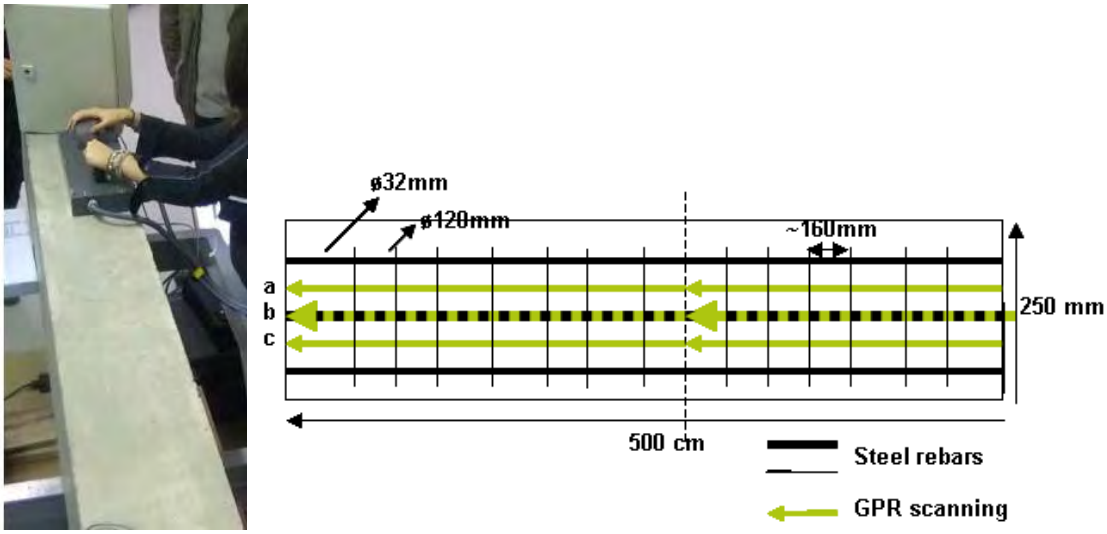

Figure III. 10: GPR scanning along the reinforced concrete beam. Three scannings were realised on each side. In the case depicted, the left side of the concrete beam is under investigation.

As it can be seen from the above graph, three B-scans were obtained for each side. Figure III.11 depicts the peak-to-peak amplitude mapping of the direct signal for the side depicted in Figure III.11. The MATLAB code was developed by P.L. Filiot, EDF-R&D, STEP.

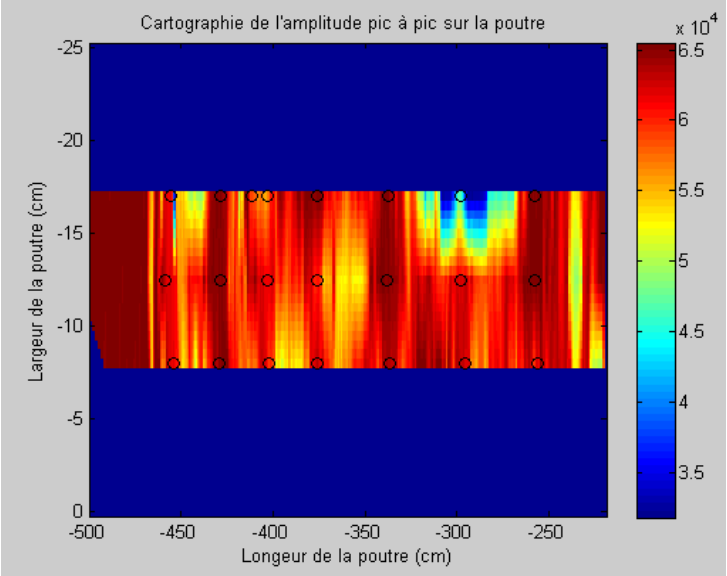

Figure III. 11: Peak to peak amplitude mapping of the GPR direct signal of one of the sides of the reinforced concrete beam. The dimensions of the concrete beam are (-1)x cm. o indicates the position of the vertical detectable steel rebars in the beam. A relative colour scale is used (red for strong amplitude and blue for low amplitude).

According to the figure above very strong peak to peak amplitude is obtained throughout the whole reinforced concrete beam. Apparently, the strong presence of steel rebars disturbs the propagation of the direct signal. As it is already known, the wavelength λ, of the electromagnetic signals, propagating in concrete, remains superior to 10cm. Thus, it has been stated in literature, that during their propagation, the different GPR signals can be distinctive only for steel rebars, having a distance from each other and a concrete cover larger than 20cm and 4cm respectively. In the case of the peak to peak amplitude mapping, depicted in figure III.11, the direct signal is highly mixed with the reflected signal from the reinforcement (spacing=16cm, concrete cover=2cm). The problem of mixed signals becomes even more intense, due to the reflection of the steel rebars that were in parallel with the GPR scanning (scanning b).

As a result, in figure III.11, the direct signal cannot be distinguished and no accurate or reliable information can be extracted for the properties of the inspected concrete surface. Apart from that, the calculation of the propagation velocity of the signals could be highly problematic and hence the exact 3D positioning of the steel rebars can be difficult. In addition, the use of high frequency antennas can be very helpful in the case of a depth - investigation, however, for this particular study, where the detection of only the first layer of reinforcement is of interest, the use of lower frequency antennas could be more convenient.

As it can be understood, the mixture of the signals consists one of the major problems of real reinforced concrete structures' inspection with GPR. Unfortunately, due to logistics (i.e.

equipment transportation) and time schedule (i.e. period of non functioning of the tower) difficulties, it was impossible to register radar profiles on cooling towers (structure under test for the current thesis).

However, taking into consideration the steel rebar configuration of the cooling towers, as it was presented in the Introduction of the thesis (§2) and using as a reference radar signals profiles obtained on a wall of EDF's power plant at Le Havre (wall I (1965), side N for ACDC project), the main cause of mixed signals is considered to be the low concrete cover thickness *(e≤3cm)* of the embedded steel rebars (mixture between the direct and reflected signal). In their turn, the mixed signals produces difficulties in the precise estimation of the concrete cover thickness of the steel rebars, a quantity which, in the current study, is one of the most important influencing parameters of the electrochemical model that will be described in chapters V and VI.

Thus, this important obstacle must overcome for the acquisition of appropriate signals, the accurate 3D location of the steel rebars and the reliable diagnosis of the state of the structure. The following paragraph describes the proposals of LMDC, Toulouse (R. Hamrouche, 2011) GIPSA, Grenoble (Prof. J. Mars) and EDF R&D, STEP (.P.L. Filiot, A. De Chillaz).

III.3.3 Synthesis

In the previous paragraph, the aptitude of GPR for the delimitation of zones with a potential of risk of corrosion was demonstrated. As it was demonstrated, resistivity and GPR signals vary according to the variations of water content, one of the major favoring parameters of corrosion of the steel rebars. The basic principle of this application of GPR, consists of relative contrasts of permittivity on the concrete surface of the structures: zones of strong permittivity (or low peak to peak amplitude of the direct wave) indicate a zone of high risk of corrosion and zones with low permittivity (or elevated peak to peak amplitude of the direct wave) indicate zones with high permittivity. Table III.3 exhibits some examples of this application of GPR:

Table III- 3: Overview of examples of GPR applied for the research of zones with a potential of risk of corrosion

Examples	Advantages	Disadvantages
Indication of zones with increased attenuation (length of profile vs. depth of investigation) (Alani et al, 2013)	3D illustration of zones with high moisture penetration (AutoCAD)	-No quantitative information on the electromagnetic properties of the inspected surface -Inefficient evaluation vis-à-vis the corrosion process
Index Corrosion Radar (ICR) mapping vs. Corrosion potential mapping (S. Laurens,2001)	Both techniques lead to the delimitation of the same zones with high risk of corrosion	-Calculation of ICR is required
Peak to peak amplitude mapping	Relative quantitative information on the properties (water content) of the concrete and the characteristics of the signal.	An indication of mixed signals may be possible; The use of tools for the separation of the signals is required.

III.4 SIGNAL PROCESSING FOR SOLVING THE PROBLEMS ENCOUNTERED DURING THE ON SITE APPLICATION OF RADAR

As it was previously mentioned, GPR can be used for the 3D positioning of the steel rebars in the reinforced concrete structures and for the delimitation of zones with great potential of risk of corrosion via the direct signals' peak-to-peak amplitude mapping. The latter application requires the acquisition of appropriate GPR signals, whose composites can be easily distinctive. However, the low concrete cover thickness of the steel rebars of real structures (concrete cover of 2-4cm) consists of a major obstacle for the accurate location of the steel rebars. The reflected signals due to the reinforcement are highly mixed with the direct signals and no information can be obtained.

Figure III.12a shows an example of a GPR signal (A-scan) in concrete where the direct and reflected waves are appropriate and thus clearly distinctive while figure III.12b shows a signal (A-scan), where the direct and reflected wave are mixed:

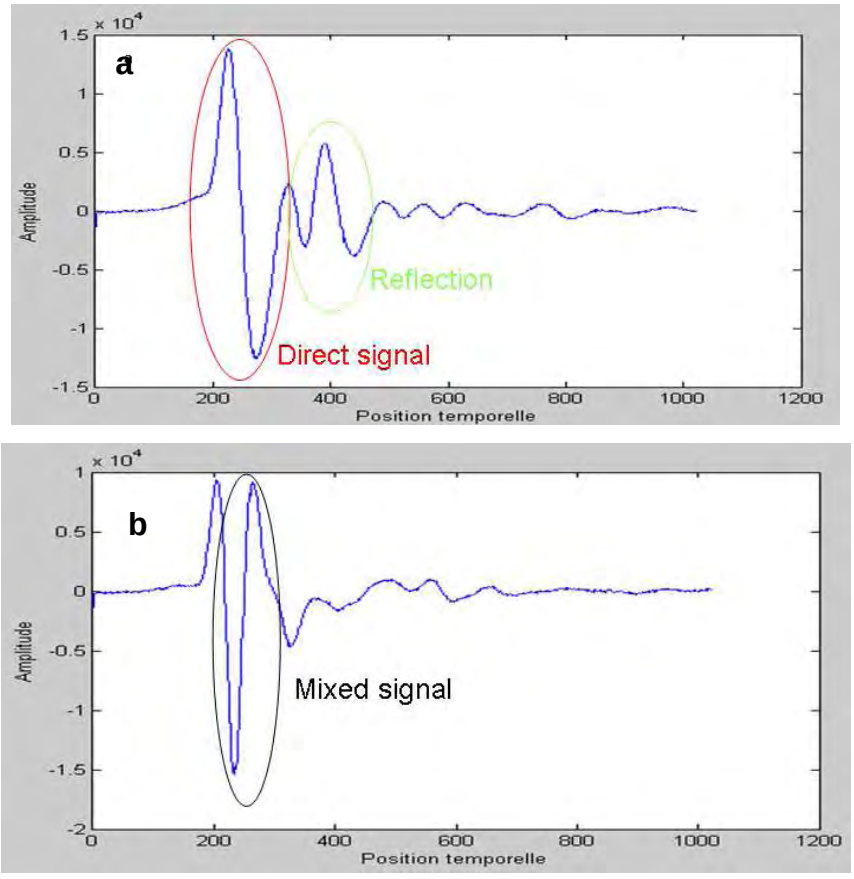

Figure III. 12: A-scan of GPR signal propagated in concrete structure with steel rebars embedded at a) >5cm and b) <3cm.

Several suggestions have been made in order to overcome this problem. One of them consists of reducing the duration of the transmitted pulses, in order to improve the resolution of the radar signals (X. Derobert, 2001). Some works focus on the use of techniques of signal processing, such as de-convolution (G.Turner, 1994, S.Malagodi, 1996), migration (E. Fisher, 1992) or inversion (C.Maierhofer, 1996) techniques. Other researchers use complementary techniques of inspection such as the pachometer (F.N. Kong, 1998) in order to validate the results of GPR. The following paragraphs present some signal processing techniques for the separation of the GPR signals, proposed in the frame of the current dissertation, in collaboration with Prof. J. Mars from GIPSA Lab, Grenoble and P.L. Filiot & A.De Chillaz, from EDF R&D-STEP.

III.4.1. Wiener and Median Filter (GIPSA Lab)

Wiener filter is a linear filter, used to produce an estimation of a desired random signal by linear-time invariant filtering of an observed noisy signal, assuming known stationary signal (reference) and noise spectra. It is based on a statistical approach and its main goal is to minimize the mean square error between the estimated random and the actually desired signal. Median filter is a non linear filtering technique, also used to remove noise. The main idea is to run through the entire GPR B-scan, A-scan by A-scan, and replace each A-scan with the median of the neighbouring A-scans. The pattern of neighbours is called the "window", which slides, A-scan by A-scan. Both kinds of filters are fast and used in the digital image processing (J-L. Mari, 2001), (W. Galagedara, 2005), (J. Mars, 2011). The median filter is more efficient than the Wiener filter, however it may distort the amplitudes of the signals. The above techniques were tested on radar profiles obtained according to the FO technique, on a dry sand box of 1x1x0.3m, where two smooth rounded steel rebars (ø 16mm) were embedded at 2.2cm (figure III.13).

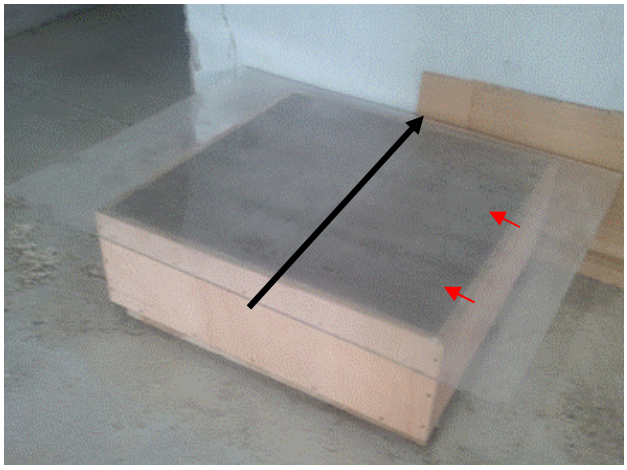

Figure III. 13: Dry sand box of 1x 1 x 0.3m, where smooth rounded steel rebars (ø 16mm)-indicated by the red arrow were embedded at 2.2 cm. The black arrow indicates the position and the direction of the radar antennas. The bottom and the sides of the sand box were covered by Al foil in order to assure the perfect reflection of the signals. A plastic cover was also used in order to facilitate the radar scanning, by providing with a smooth surface.

The radar scanning took place for a steel rebar spacing of 20cm and 40cm. Two antennas (1 transmitter-2 receivers) of 1.5GHz were used. The signal processing with the filters was realised via Matlab codes, provided by J. Mars.

Figure III.14 depicts the radar zones for the steel rebars with spacing of 20cm, for the two receivers, where the direct wave was highly mixed with the reflection of the steel rebars:

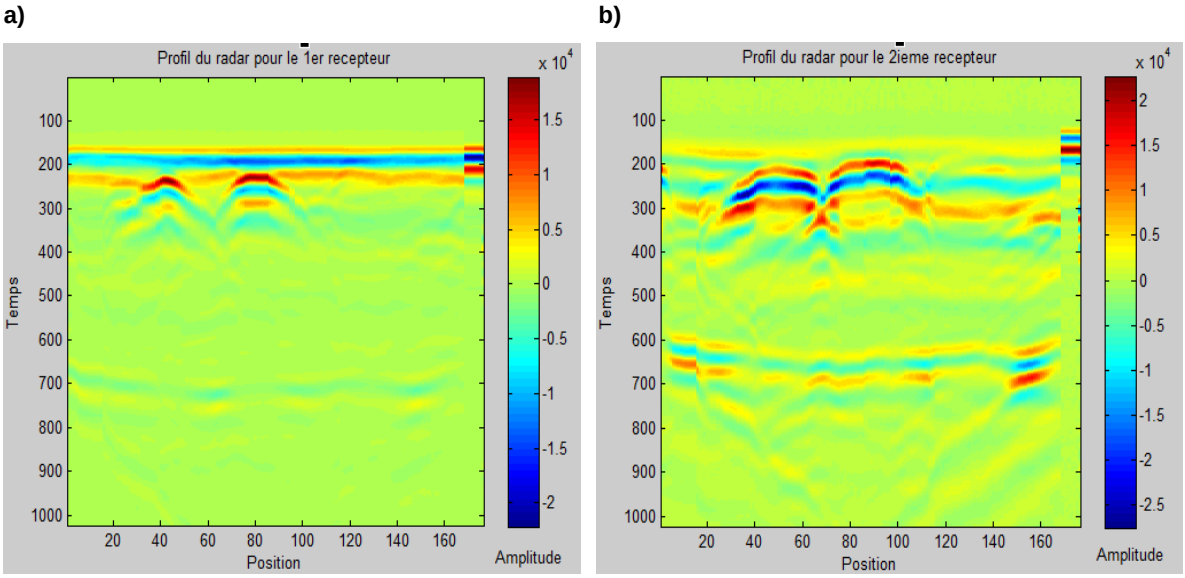

Figure III. 14: Radar profiles with highly mixed signals (direct wave and reflection of the steel rebars embedded in the dry sand at 2.2cm and with a spacing of 20cm for a) 1st and b) 2nd receiver of GPR.

The direct and reflected from the reinforcement signals separated after Wiener filtering, for both receivers, are demonstrated below, in figures III.15 and III.16:

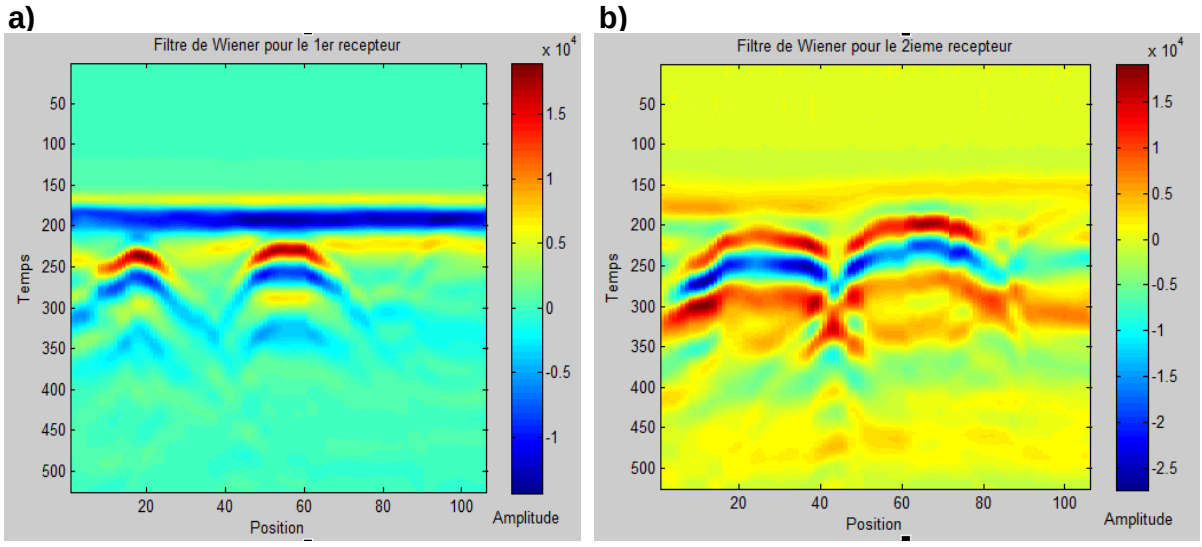

Figure III. 15: Direct signal after the application of Wiener filter for the steel rebars embedded in the dry sand at 2.2cm and with a spacing of 20cm for a) 1st and b) 2nd receiver of GPR

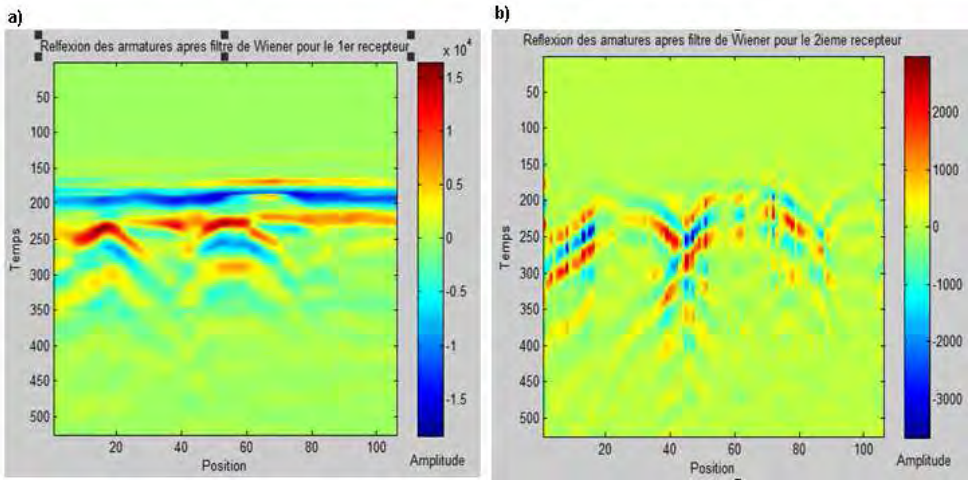

Figure III. 16: Reflected signal from the steel rebars after the application of Wiener filter for the steel rebars embedded in the dry sand at 2.2cm and with a spacing of 20cm for a) 1st and b) 2nd receiver of GPR

As it can be seen from the above figures, it seems that the Wiener filter is not efficient for the separation of the signals, in the case of a spacing of 20cm between the steel rebars. Apparently, the filtrated zone around the reinforcement indicates always a significant disturbance of the direct wave from the reflected one. Similar images were obtained after the application of the median filter.

Figure III.17 demonstrates the profiles radar for the two receivers, obtained for the steel rebars with a spacing of 40cm:

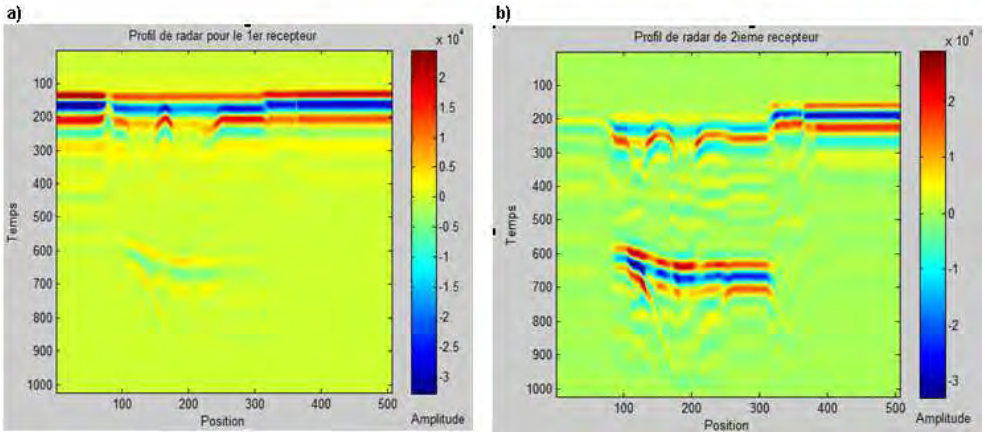

Figure III. 17: Radar profiles (B-scans) for the steel rebars with a spacing at 40cm, embedded at 2.2cm in the dry sand, for the a) 1st and b) the 2nd receiver. The first two lines of the up part of the B-scans represent the direct wave transmitter-receiver. The hyperboles correspond to the presence of steel rebars, while their summits indicate the exact position of the steel rebars in the sand. The right part of the B-scans (from position 313) corresponds to the signal registered in the air, which serves for the adjustment of the temporal scale of the 2nd receiver while at the low part of the profile, the signals reflected from the bottom of the box are registered. 1 position = 0.5cm.

The Wiener and median filtering was applied for the zone of the first hyperbole, where the direct and reflected signals' mixture is due to the low concrete cover of the steel rebar.

Figures III.18 and III.19 show the separated signals after Wiener filtering while figures III.20 and III.21 show the direct and reflected signal after the application of median filter:

a) **b)**

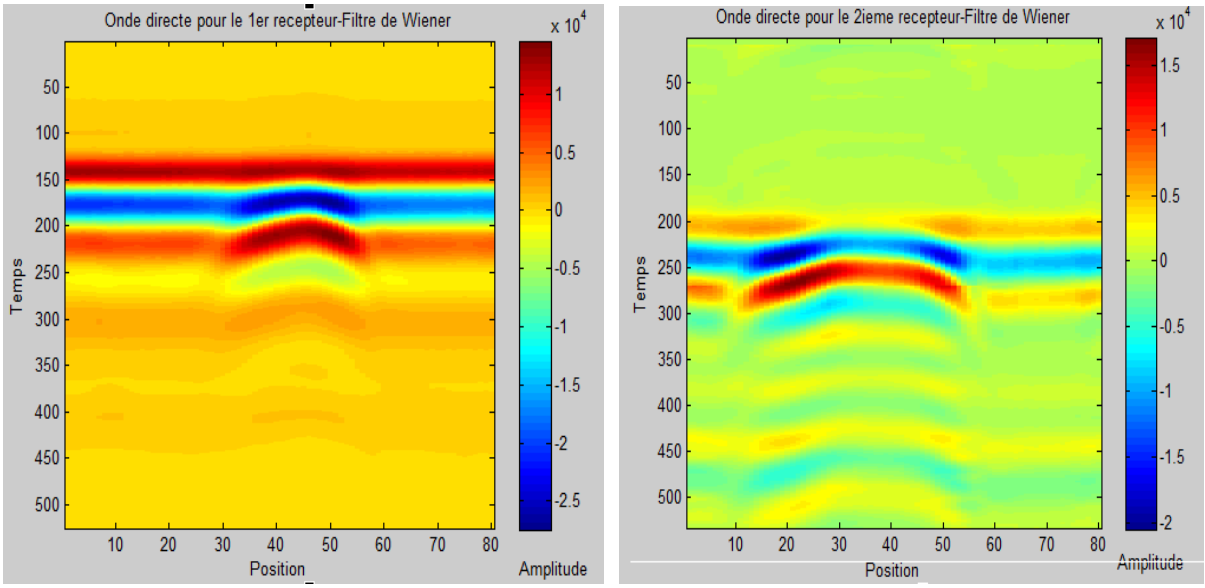

Figure III. 18: Direct signal after the application of Wiener filter for the steel rebar embedded in the dry sand at 2.2cm with a spacing of 40cm for a) 1st and b) 2nd receiver of GPR

a) **b)**

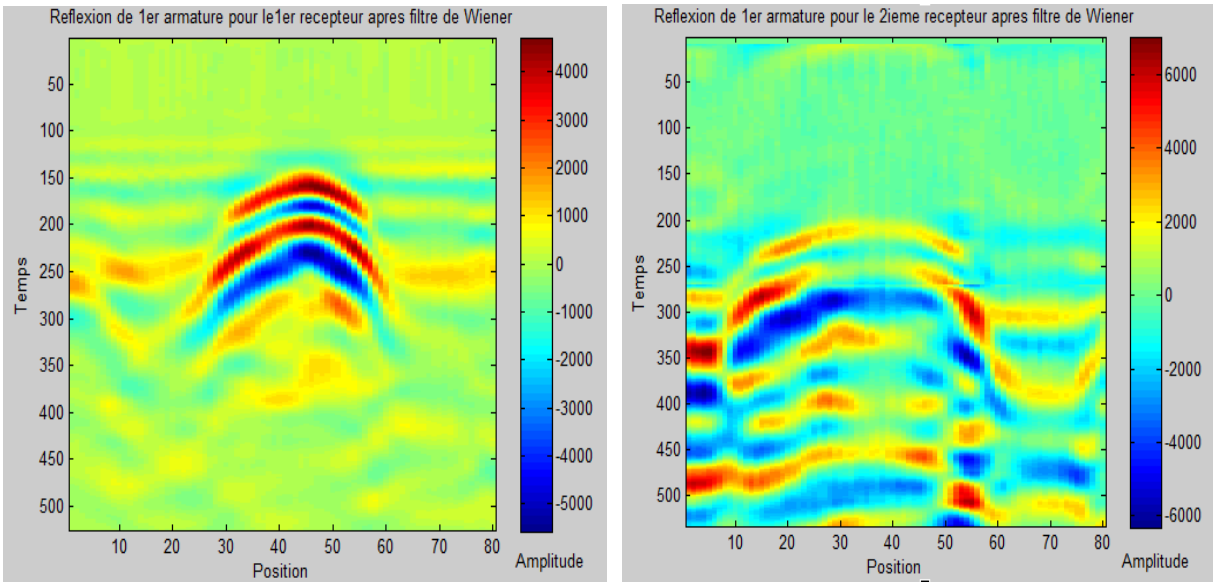

Figure III. 19: Reflected signal from the steel rebars after the application of Wiener filter for the steel rebar embedded in the dry sand at 2.2cm with a spacing of 40cm for a) 1st and b) 2nd receiver of GPR

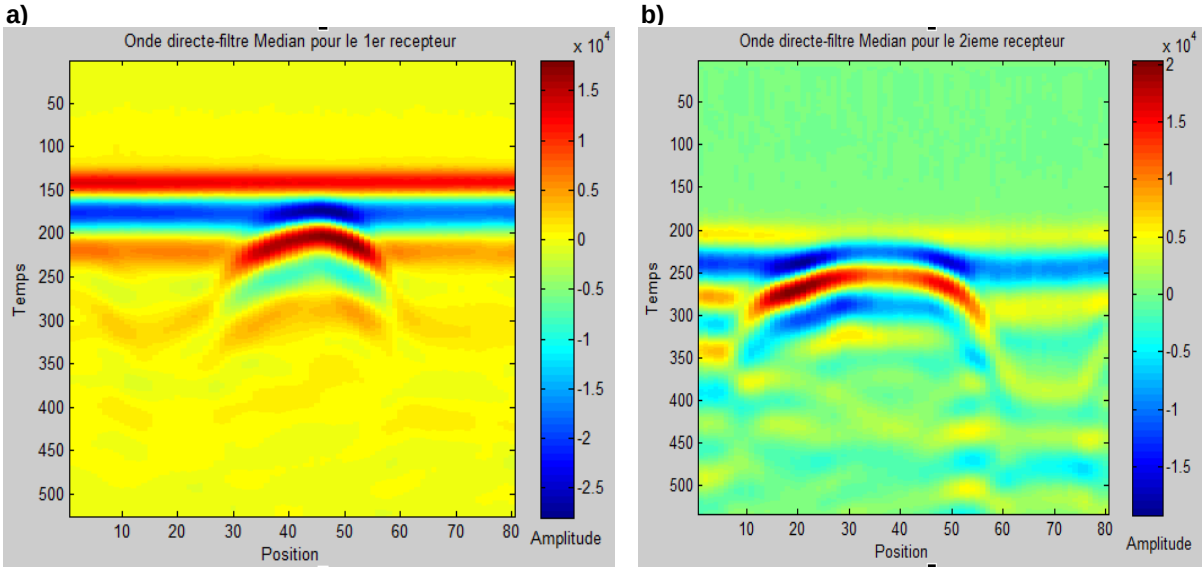

Figure III. 20: Direct signal after the application of Median filter for the steel rebar embedded in the dry sand at 2.2cm with a spacing of 40cm for a) 1st and b) 2nd receiver of GPR

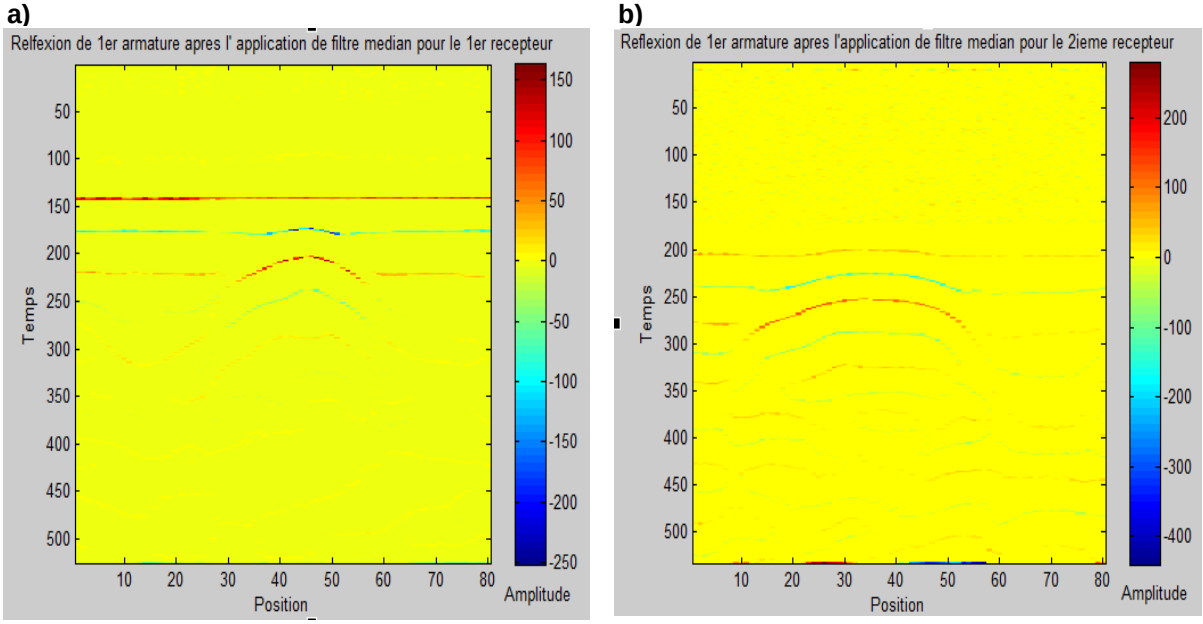

Figure III. 21: Reflected signal from the steel rebars after the application of Wiener filter for the steel rebar embedded in the dry sand at 2.2cm with a spacing of 40cm for a) 1st and b) 2nd receiver of GPR

As it can be understood from the figures above, in the case of a spacing of 40cm, the separation can be considered more or less satisfactory, and thus, the calculation of the direct wave speed and the 3D localisation of the steel rebars may be done. However, while the tested configuration is regarded as rather simple, in the case of a real and complex reinforced structure, (i.e. cooling towers) the use of these filtering techniques would not allow a reliable and satisfactory separation of the directed wave from the reflected one. For that reason, LMDC (R. Hamrouche, 2011) and EDF R&D-STEP (P.L. Filiot, A. De Chillaz) proposed two

other techniques. The results of these two techniques are presented in the following paragraph.

III.4.2. Subtraction of the direct signal from the mixed signal (LMDC) and Singular Value Decomposition (SVD) (EDF R&D-STEP)

The technique proposed by LMDC consists of a subtraction of the direct signal from the mixed one. It is based on the fact that the direct signal is the same throughout the radar profile. As a result, a more proper (less disturbed from the presence of the reinforcement) signal between the steel rebars can be isolated and then subtracted from the zones with the mixed signals (zones of hyperboles). The Singular Value Decomposition (SVD) is widely used in signal processing and statistics. It is a factorization of a real or complex matrix , in the form of:

$$M = SUV^* \qquad \text{(eq. 39)}$$

Where U is a [m x m] real or complex unitary matrix, S is a [m x n] rectangular diagonal matrix with non negative real numbers on the diagonal and V* is a [n x n] real or complex unitary matrix. The diagonal entries of S are the singular values of M. Compared to other techniques (i.e. Wiener and Median filter) SVD has been "accused" for considerable distortions of the amplitude of the signal and long duration (J. Mars, 2011).

These techniques have been tested on radar profiles obtained on:

- a wall of EDF's power plant at Le Havre (wall I (1965), side N for ACDC (**A**nalyse et **C**apitalisation pour le **D**iagnostic des **C**onstructions project) and EvaDéOS
- on the II-NC reinforced concrete slab, fabricated in LMDC (see also §VI.2.1 and §VI.2.3).

The FO technique was applied in the aid of 1.5GHz antennas, having one transmitter and two receivers. Once these techniques applied, the velocity of propagation of the direct signal was calculated (MATLAB code developed by EDF R&D STEP-P.L. Filiot) and the value of the concrete cover was estimated and validated.

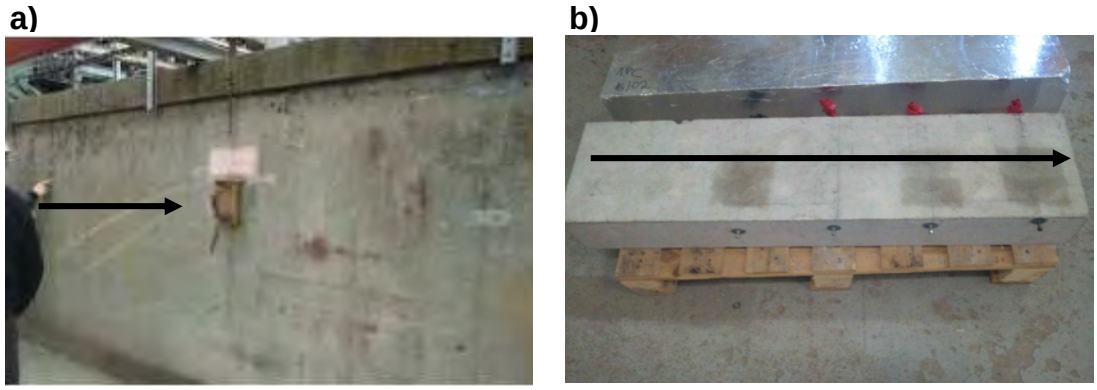

Figure III. 22: a) Wall I-N (EDF power plant, Le Havre). b) II-NC reinforced concrete slab casted in LMDC (see also §VI.2.1. and §VI.2.3). The black arrow indicates the direction of the GPR scanning. In the case of the LMDC slab the antennas were placed in the middle of the slab.

Figure III.23.a illustrates a radar profile obtained on the wall I-N for the 1st receiver. SVD was applied to the A-scan corresponding to the exact position of the fourth steel rebar along the radar profile. Figure III.23.b depicts the separated signals for that position, after the application of SVD:

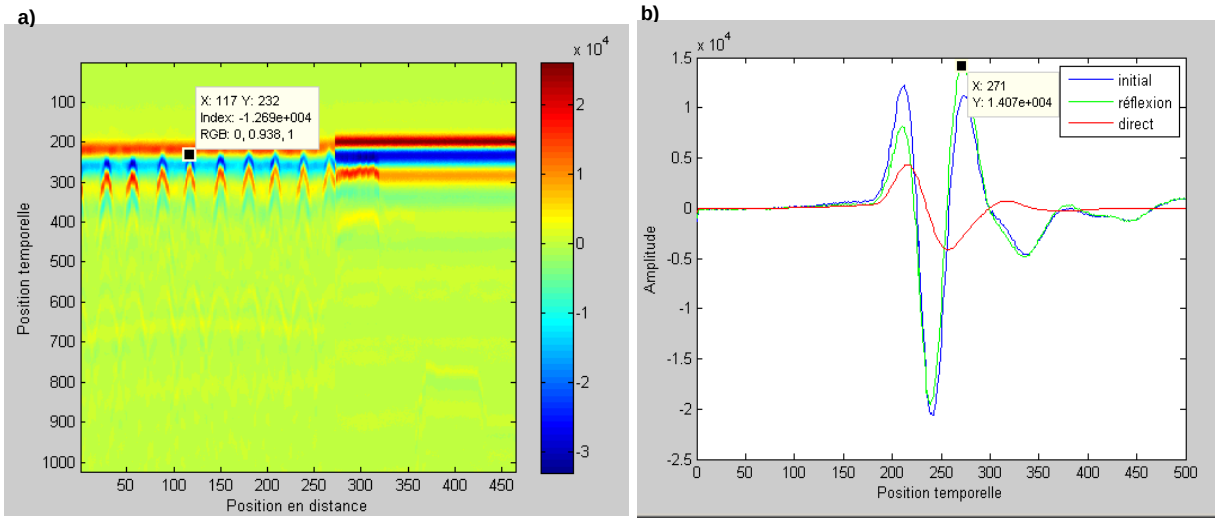

Figure III. 23: a) GPR profile along the wall I-N (EDF power plant, le Havre) for the 1st receiver. The hyperboles correspond to the presence of steel rebars, while their summits indicate the exact position of the steel rebars in the sand. The right part of the B-scans (from position 280) corresponds to the signal registered in the air. 1 position = 0.5cm. The mixed signal zones are those of the hyperboles, due to the low concrete cover of the steel rebars (e~2cm, on site measurement). The dark rectangle on the profile indicates the hyperbole for which SVD is applied. b) Signals before and after SVD, for the hyperbole indicated in III.23.a). Blue curve: mixed signal, red curve: direct signal after SVD, green curve: reflected signal from the steel rebar after SVD.

For the same mixed zone (hyperbole), on the same B-scan (figure III.23.a), the LMDC method was then used. The direct signal between the 4th and 5th hyperbole was used as a

reference and thus subtracted from that zone under test. Figure III.24 and III.25 exhibit the results after the subtraction of the direct signal:

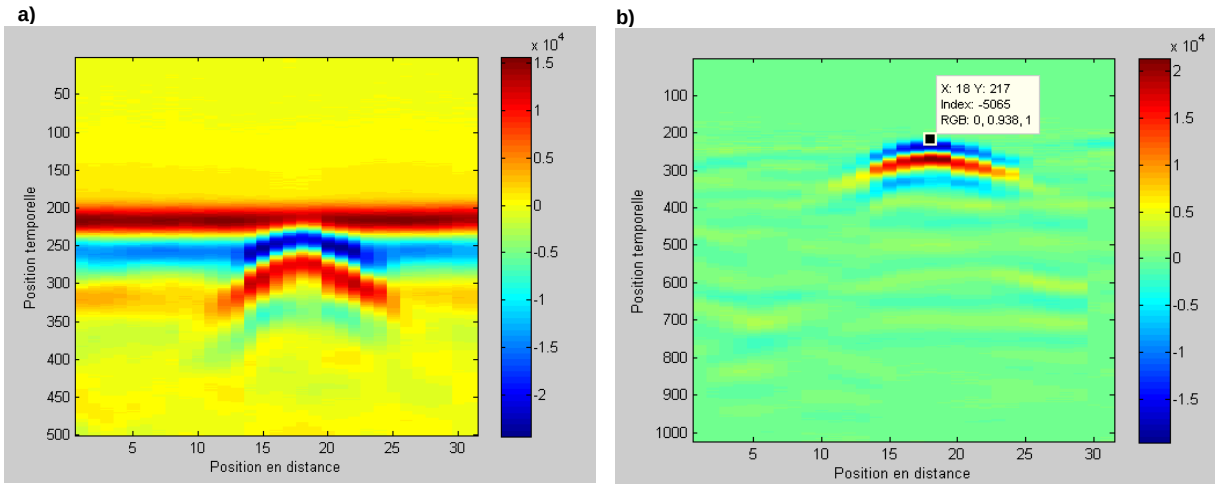

Figure III. 24: a) Hyperbolic zone (see also figure III.23) with mixed signal b) Reflected signal of the steel rebar after the subtraction of the direct signal. As a reference, the direct signal between the under test and its neighbour hyperbole was used. The summit of the reflected zone corresponds to the exact location of the steel rebar.

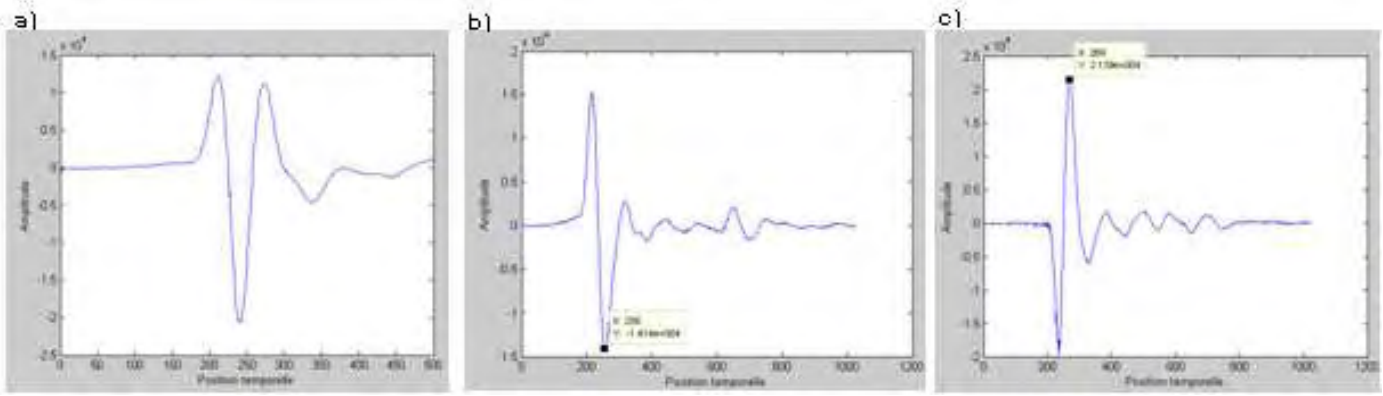

Figure III. 25: Signals for the summit (exact position f the steel rebar) of the hyperbole a) mixed signal b) direct signal after the subtraction c) reflected signal from the steel rebar after the subtraction

At a first sight, it seems that both techniques separate sufficiently the mixed signals for the zone of the armatures with small concrete cover, allowing the calculation of the direct wave speed and the estimation of concrete cover. However, as it is expected, SVD filtering decreases the amplitude of the separated signals, compared to the technique of the subtraction of the direct signal. Due to the fact that, in this study, the interest is focused on being able to distinguish the exact arrival time of the direct and reflected signal from the steel rebar (perfect reflector), the effect of SVD on the amplitude of the signals, observed in figure III.25, could be *a priori* accepted. However, it would be wise to determine a specific tolerance in the

change of the waves' amplitude to avoid a complete distortion of the registered signals on reinforced concrete structures.

III.4.3. Example of calculation of concrete cover thickness after signal processing with subtraction of the direct signal or SVD

In order to calculate the wave velocity of the direct wave, firstly the adjustment of the temporal scale of the 2nd receiver takes place, using as a reference the signal registered in the air. Then, the direct wave velocity for the same position of the two receivers is calculated according to:

$$v(cm/\sec) = \frac{\Delta x}{\Delta t} \qquad \text{(eq. 40)}$$

Where Δx the fixed distance between the two receivers (6cm) and Δt the difference between the arrival times of the negative peak of the direct wave at the two receivers, passing from the same position. The MATLAB code for the calculation of the direct wave speed was developed by P.L. Filiot, EDF R&D STEP.

Once the speed is calculated the concrete cover is then estimated in the aid of Pythagora's law and equations (41) and (42) (figure III.26):

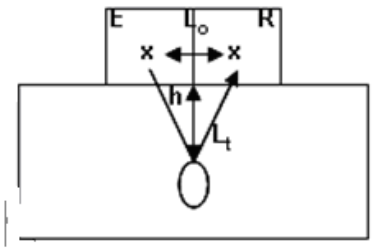

$$v = \frac{L_t - L_o}{\Delta t_R} \longrightarrow \text{(eq.41)}$$

$$\left(\frac{L_t}{2}\right)^2 = h^2 + \left(\frac{L_o}{2}\right)^2 \longrightarrow \text{(eq.42)}$$

Figure III. 26: Estimation of concrete cover, h(cm), according to Pythagora's law and equations (eq. 41) and (eq. 42), where: v (cm/sec) the wave speed calculated via (eq. 40), L_o (cm) the distance between the emitter and the receiver (L_o=6cm), L_t (cm) the trajectory of the reflected signal: emitter-reinforcement-receiver and Δt_R (sec) the difference between the arrival times of the negative peak of the direct wave and the positive peak of the reflected wave at the receiver at a specific position.

Based on the above, the concrete cover of the steel rebar, indicated in figure III.23.a, was estimated after the application of SVD filtering at 2.32cm, while after the subtraction of the direct signal, the concrete cover was evaluated at 2.14cm. Compared to the value measured on site, the concrete cover was estimated with an error of 17% for the use of the LMDC

technique, while using SVD, the error on the calculation of concrete cover reaches 21,7%. As it will be depicted in chapter V, concrete cover consists of an important entry for the application of the proposed electrochemical model for the evaluation of corrosion of the steel rebars and its exact knowledge affects the reliability and the precision of the estimation of corrosion current density (§V.3 and §V.4). For that reason, a tolerance of ±15% on the estimation of the correct value of concrete of steel rebars is regarded as acceptable.

As it was previously mentioned, the LMDC technique and SVD were also applied for radar profiles obtained on the II-NC reinforced concrete slab (figure III.25b, see also §VI.2.1. and §VI.2.2). In this concrete slab, the different concrete covers of the steel rebars are already known. Figure III.27 depicts a radar profile and the separation of the signals for the last hyperbolic zone, after the application of SVD filtering:

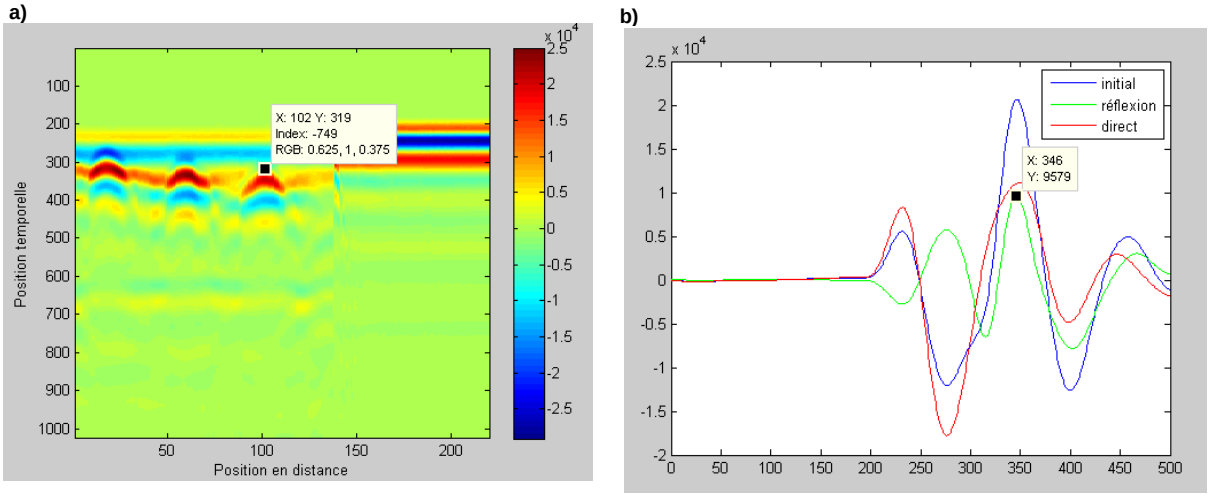

Figure III. 27: a) Radar profiles on the II-NC reinforced concrete slab, fabricated in LMDC. The steel rebar under test is indicated by the dark square. Its concrete cover is known at 5.2cm. b) Separation of signals after SVD for the summit of the hyperbole indicated at figure III.26. Blue curve: mixed signal, red curve: direct signal, green curve: reflected signal from the steel rebar.

As it can be seen from the figure above, the signal for steel rebars with low concrete cover is more proper and thus filtering is even more effective. Similar results were obtained after the subtraction of the direct signal for the same zone. As far as the estimation of concrete cover is concerned, both techniques led to the estimation of concrete cover at 4.93cm. Thus, for high concrete covers, both techniques drive to similar or identical values of concrete cover. Generally, it has been observed, that for concrete covers higher than 3cm (e>3cm), the error on the real and exact 3D positioning of the steel rebars varies for SVD between 3.2% and 5.2% and for the subtraction of the direct signal lies with 3.8 and 5.2%. Apparently, for both

techniques, the error diminishes significantly when it comes to steel rebars with high concrete covers.

Table III.4 summarizes the results obtained for the tests with these two techniques:

Table III- 4: Errors of the techniques SVD and subtraction of the direct signal on the estimation of concrete cover

	Error (%) for concrete cover:	
Method of signal processing	**e≤3cm**	**3cm <e <5cm**
SVD	~17	3.2-5.2
Subtraction of the direct signal	~20	3.8-5.2

III.4.4. Synthesis

This paragraph proposed different techniques of signal processing in order to encounter the problems that appear during the application of GPR on real reinforced concrete structures. The signals received are highly mixed (direct and reflected signal) and thus no reliable and precise information can be obtained as far as the peak to peak amplitude, the velocity of the direct signal and the 3D location of the steel rebars are concerned. In the frame of the current study, some suggestions have been made in order to overcome this problem: the Wiener and Median filter in collaboration with Prof. J. Mars from GIPSA Lab, Grenoble and SVD by P.L. Filiot from EDF R&D-STEP. LMDC proposed the subtraction of the direct signal from the mixed signal zone. It was shown that Wiener and median filtering are fast techniques, widely used in image processing and quite efficient and effective in the case of structures with simple configurations, where the spacing between the steel rebars is high (40cm). As a result, this raises several questions concerning their reliability during their application on real complex reinforced concrete structures (i.e. cooling towers). Then, the subtraction of the direct signal (LMDC) and SVD (EDF R&D-STEP) were tested on real site and lab scale configurations. It was shown that SVD may leads to a deviation up to 21,7% for the real 3D location of steel rebars with small concrete cover (e≤3cm) while the subtraction of direct signal indicates an error of 17%. On the contrary, when the concrete cover of the steel rebars increases, the error of both techniques diminishes significantly (3.1-5.8%). Furthermore, via SVD, the amplitude of the signals was severely distorted. Since the concrete cover consists one of the major

entries in the novel electrochemical model of measuring polarisation resistance, proposed in chapters V and VI, its precise knowledge is highly necessary. **A tolerance of ±15% in the precise estimation of concrete cover can be regarded as acceptable**. For that reason, more research should be performed on signal's separation in order to improve the proposed developments and increase GPR's reliability on the 3D positioning of steel rebars and the limitation of potentially corroded zones on real reinforced concrete structures. The following table III.5 summarizes the techniques previously presented:

Table III- 5: Techniques tested in the frame of the current study for the separation of mixed signals (direct and reflected wave) due to the dense reinforcement network of real reinforced concrete structures

Techniques of signal processing	Effect on signals' separation
Wiener and Median filters (GIPSA Lab)	-Fast, - widely used in image processing, -Efficient for simple configurations and large spacing in steel rebars
Singular Value Decomposition (SVD) (EDF R&D STEP)	-Long duration, -Possible distortion of amplitude, -21.7% (e≤3cm) and 3.2-5.2% (e>3cm) of error on the precision of 3D location of steel rebars
Subtraction of direct signal (LMDC)	-Simple, -17% (e≤3cm) and 3.8-5.2% (e>3cm) of error on the precision of 3D location of steel rebars

III.5. CONCLUSION

In this thesis, the main reasons for using GPR are the delimitate those zones on real reinforced concrete structures with a high risk of corrosion, the detection of the embedded steel rebars in concrete and the estimation of their concrete cover thickness. Especially, the latter is highly important, since concrete cover thickness influences significantly the efficiency of electrochemical proposed technique in part B of the current dissertation and thus a high precision in its estimation is required.

Firstly, the basic principle of the radar for the auscultation of reinforced concrete structures was described. As it was presented, the electromagnetic signals are modified according to the electromagnetic properties of concrete. Among the most significant, the relative permittivity (or dielectric constant) of concrete, the peak to peak amplitude and the velocity of propagation of the direct GPR signal vary as a function of the different water contents present in the concrete structure.

Then, a short reference to the three different methods (WARR, CMP, FO), found in literature, for measuring the direct wave velocity, was made. Due to its main advantages (high spatial resolution, short duration), the current study used the FO technique.

Furthermore, the aptitude of GPR for the delimitation of zones with a great potential of risk of corrosion was demonstrated. Based on relative contrasts of permittivity on the concrete surface of structures, this dissertation proposes peak to peak amplitude mapping of the inspected real site zones. Due to logistics and time schedule difficulties, it was impossible to carry out radar profiles, and thus peak to peak amplitude mapping of a cooling tower surface.

In addition, as it has been already mentioned, GPR is also used for the 3D positioning of the steel rebars. However, radar signals registered on other real sites surfaces (EDF's thermal power plant, Le Havre) have indicated that due to low concrete cover thickness of the steel rebar reinforcement ($e \leq 3cm$), mixed signals (direct mixed with reflected signal) were registered. This prevents to estimate the concrete cover thickness with high precision.

Thus, in order to overcome this severe problem, for the current dissertation, some tools of signal processing were applied in order to separate the signals for the zones where they were higly mixed (zones with steel rebars): Wiener and Median filters (GIPSA Lab), SVD (EDF R&D) and Subtraction of the direct signal (LMDC). As far as the first two are concerned, their effectiveness is limited only for simple reinforcement configurations, while in the case of SVD and the LMDC technique seem to be more efficient in all configurations than Wiener and Median filtering.

From the above, it is clearly indicated that the signal separations consists a quite complicated-to- solve problem. Once a reliable separation of signals is obtained, the precise estimation of concrete cover of the steel rebars will be achieved. In the methodology presented in this dissertation, the precise evaluation of concrete cover is of major importance, since it consists one of the main entries of the proposed polarisation resistance measurement model, for the exact quantitative estimation of the corrosion of the reinforced concrete structures. This will

be even clearer, in chapter V and VI, where the role of the concrete cover-among other parameters-will be analysed during the development of the novel polarisation resistance measurement model and its validation on lab scale.

Finally, it is highly important to accomplish GPR signals' registration on cooling towers' surfaces in order to obtain a clear view of the state (presence of humidity) and the reinforcement configuration of the structure. This would also permit the realisation of peak to peak amplitude mapping of cooling towers and the testing of the efficiency of the suggested tools for the separation of the mixed (if any) signals.

PART B: DEVELOPMENT AND VALIDATION OF A PROTOCOL FOR THE POLARISATION RESISTANCE MEASUREMENT

IV. Problems of the polarisation resistance measurement: State of the art

IV.1 INTRODUCTION

As it has been already mentioned, the evaluation of the corrosion rate of a reinforced concrete structure is of major importance, before any acts of prevention or maintenance are taken. Chapter II presented the main electrochemical techniques used for this purpose. Polarisation resistance measurement provides quite quantitative information about the state of the reinforcement. However, throughout literature, the efficiency and precision of the current apparatus used for the polarisation resistance measurement, has been put into question. Several works (Luping, 2002), Nygaard (2009), (Wojtas, 2004), (S.Laurens (2010), (A.Clement, 2012) (Andrade, 2010). have been carried out in order to locate the problem source, either qualitatively or quantitatively. At the same time, the RILEM protocol used for the polarisation resistance interpretation presents several "blanks", and as a result, a misleading evaluation of the state of the structure may take place. In this chapter, a brief overview of experimental and numerical studies focusing on the main problems of the polarisation resistance measurement is given.

IV.2 STATE OF THE ART

As it has been already mentioned (§II.2.3.2.) the current apparatus used for the measurement of polarisation resistance on large surface structures works in the following way: current is injected from the counter electrode on the structure's surface to the surface of the steel rebar and a potential response is received by the reference electrode (figure 14, figure 17). A guard-ring electrode in both devices injects a secondary current and contributes to restrain the polarisation within the supposing surface of the steel rebar, which is determined to be polarised.

However, literature states differences between the values obtained with GECOR6 and those with Galvapulse. These differences can often be greater than one or two magnitude orders. In addition, it has been reported that the corrosion rate given by the commercial instruments may not correspond to the real corrosion rate (Wojtas, 2004), (S.Laurens, 2010). In other words, an erroneous interpretation of the polarisation resistance results may lead to inconsistent conclusions about the true conditions of the reinforced structure. Several authors have questioned the reliability, the effectiveness and the efficiency of these two apparatus for the

measurement of polarisation resistance. Experimental and numerical studies have been carried out to locate the source of the measurement uncertainties and the difficulty in the interpretation of the results.

Luping (2002), via experimental work, has attributed the instruments' deviations to **the lack of calibration method for these two techniques**. He investigated the influence of the technical characteristics of these methods, i.e. **polarisation duration** and injected current from the counter electrode, showing that Galvapulse is more prompt to give erroneous estimation on the corrosion state of the reinforcement due to the rapid polarisation it induces. On the other hand, his studies have demonstrated that the value of the injected current is insignificant, as long as a linear polarisation takes place. However, his approach has been based on the false comparisons between the instant values obtained by GECOR 6 and Galvapulse and the values defined by destructive techniques, realised only once, in the end of the measurement period. Taking also into account the fact that his work is limited on a lab scale his research doesn't provide with sufficient information about the origin of the measurement problems.

A qualitative analysis has been carried out by Nygaard, (2009), according to which the problem lies into the **confinement techniques** used in GECOR6 and Galvapulse. He observed that during the polarisation of reinforcement at a uniform state (either passive or active), the injected current can be distributed on a larger steel rebar surface than that the instruments assume to polarise. This is the case of an **under-confinement** of the injected current, as depicted in the following figure, leading to an under estimation of the polarisation resistance and thus to an over estimation of the corrosion rate. GECOR6 over estimates the corrosion rate by a factor of 10 while Galvapulse by a factor of 100:

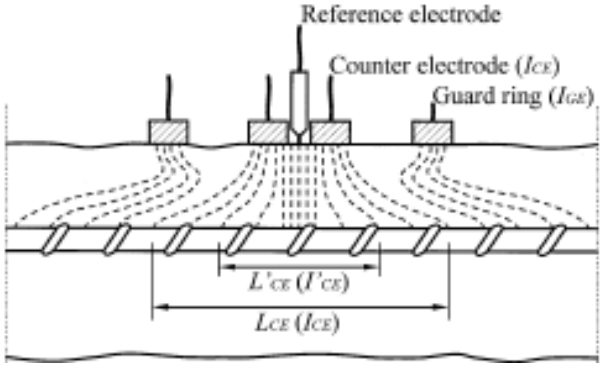

Figure IV. 1. Schematic illustration of the current, I'_{CE}, flowing to the reinforcement over the assumed confinement length, L'_{CE}, and the length L_{CE} over which the applied counter electrode current, I_{CE}, is distributed. A current I_{GE} is applied from the guard ring for confining the counter electrode current, I_{CE}. (Nygaard, 2009)

In the case of polarisation of reinforcement corroded on a local level, Nygaard (2009) stated the over or self confinement of the injected current (figure IV.2) into the active surface area of the steel rebar, since the current will follow the less resistive path towards the reinforcement. Both instruments polarise only the active part of the steel rebar, making the detection of a corroded spot over a large passive area, impossible. As a result, the polarised surface is less than the one assumed to be polarised. Thus, polarisation resistance is over estimated and corrosion rate is under estimated. In the case of a local corrosion, GECOR6 under estimates corrosion rate by a factor of 10 while Galvapluse by a factor of 2:

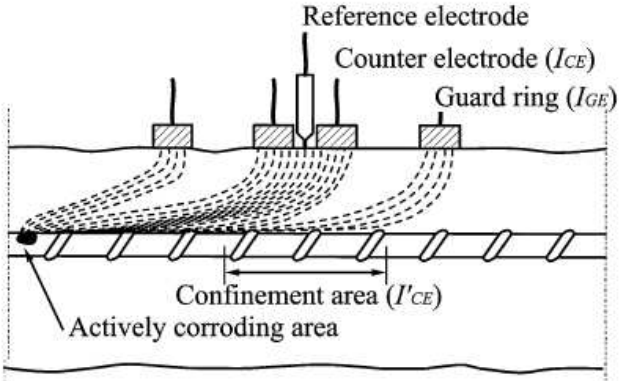

Figure IV. 2: Schematic illustration of self confinement. The current applied from the counter electrode, I_{CE}, and the guard ring, I_{GE}, flows into the reinforcement bar at the actively corroding area irrespective of the position of the electrode assembly on the concrete surface (Nygaard, 2009).

Apart from the instruments' incapability to confine effectively the injected current within the surface assumed to be polarised, **Nygaard (2009) questioned for the first time, the linearity of the measurement, claimed to be so, for GECOR6 and Galvapulse**. However, his experimental work doesn't provide with a physical explanation of the phenomena observed, neither proposes any possible ways to eliminate the errors made during the estimation of corrosion rate.

On the other hand, numerical simulations of the polarisation resistance measurement permit an insight to the way, according to which, GECOR6 and Galvapulse function. Some years earlier than Nygaard, Wojtas (2004), simulated a 2D GECOR6 polarisation measurement (PSpice) on a steel rebar uniformly and locally corroded. He proved that trying to determine a certain steel rebar area as the surface to be polarised leads to erroneous calculation of polarisation resistance, no matter how intensive or not the corrosive activity is. In the case, of the uniform corrosion, he underlined the importance of the use of a guard ring electrode which adapts the confinement of the injected current according to the measurement

conditions. Figure IV.3 depicts the GECOR6 measurement for a uniformly corroded steel rebar.

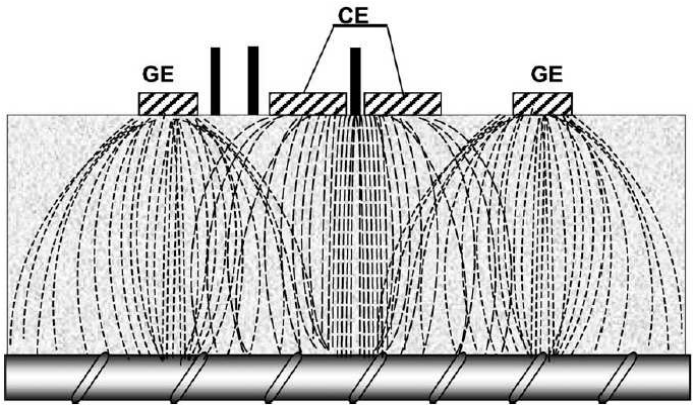

Figure IV. 3: Illustration of the «overconfining» occurring at high corrosion activity of rebar during measurements with the modulated GE. Current from the GE partially suppresses CE current (Wojtas, 2004)

In the case of local corrosion, Wojtas's (2004) and Nygaard's (2009) results coincide. More particularly, he has shown that the under estimation of the corrosion rate depends on the ratio between the dimensions of the counter electrode and the corroded spot. In addition the orientation of the auxiliary reference electrodes of GECOR6, may also influence the estimation of corrosion rate. However, his study cannot be considered as a complete one, since his simulations were carried out in 2D; non classical electrical models are used and thus significant influences of other parameters could be neglected.

S. Laurens (2010) evaluated the influence of several parameters on the linear polarisation measurement and quantified the errors made on the calculation of the corrosion rate. He realised 3D numerical simulations (Comsol Multiphysics) of GECOR6 and Galvapulse, on a uniformly corroded reinforcement As in the case of the previous studies, he also stated problems of over or under confinement of the injected current within the steel rebar surface, supposed to be polarised. **He attributed these problems to the wrong hypothesis of a homogeneous distribution of the injected current** along the steel surface assumed to be polarised. In addition, he has demonstrated that the systematic errors made on the calculation of polarisation resistance are **due to the use of an average current density**, as it was proposed by RILEM in the eq. 26 (§ II.2.3.1). In the following figure, he proved that the current density maximises right under the centre of the counter electrode, where the potential response of the system is measured, and from that point and after, the current density decreases:

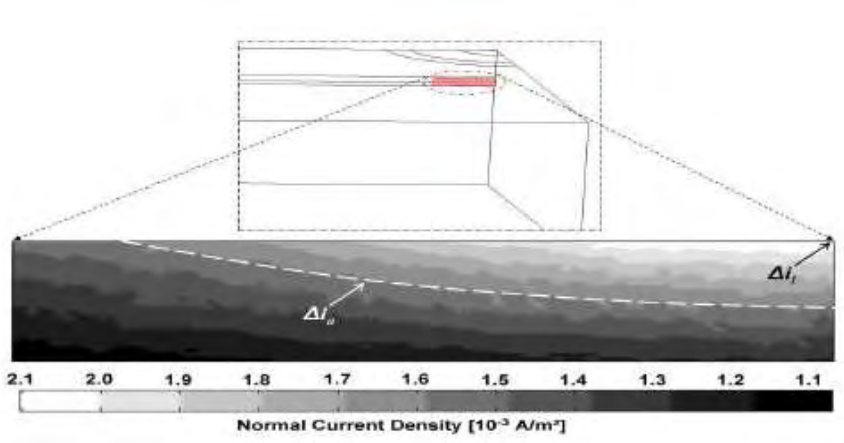

Figure IV. 4: Current density mapping of the steel area assumed to be polarised according to RILEM recommendations. Δi_l (noted in black) corresponds to the current density under the centre of the counter electrode, where the potential response measurement takes place. Δi_a (noted in white) corresponds to the average current density used for the calculation of polarization resistance.(S. Laurens, 2010).

Furthermore, the figure above demonstrates that the upper part of the reinforcement is more polarized than the rest steel rebar. It seems also that the average current density proposed by RILEM committee, doesn't correspond to the current density which polarizes effectively that steel bar zone, where the potential response measurement takes place.

As far as the influence of different parameters on the polarization resistance measurement is concerned, Laurens carried out numerical experiments taking into account **geometric characteristics of the instruments** (different orientations of auxiliary reference electrodes for GECOR6), different values of concrete resistivity and concrete cover of steel rebar. The following figure illustrates the effects of these different parameters during a GECOR6 measurement:

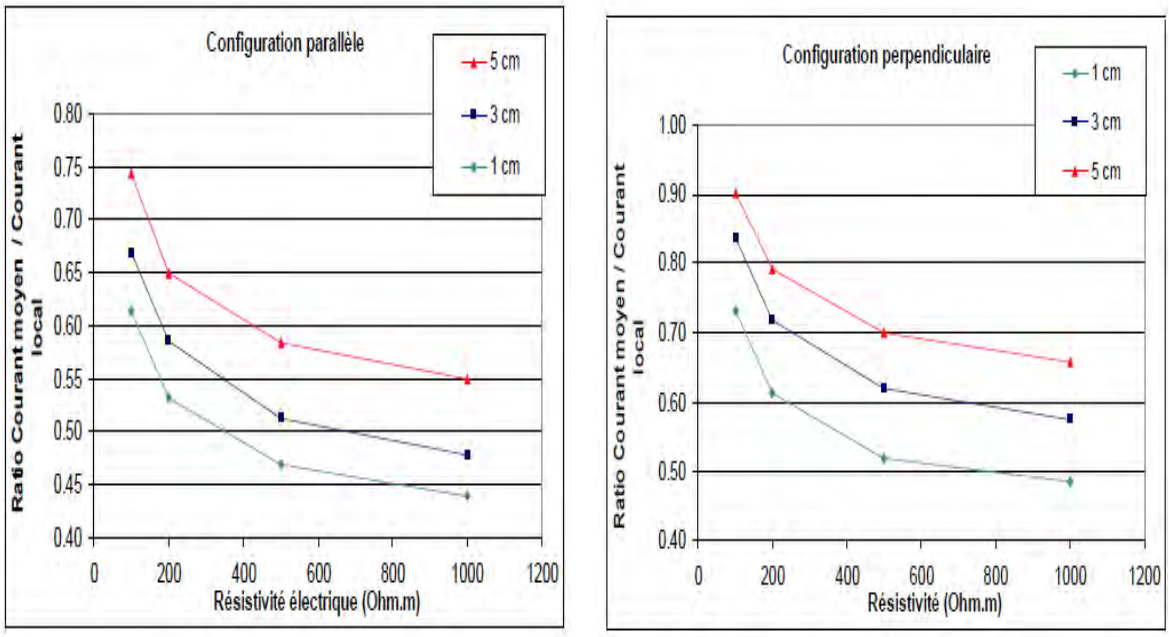

Figure IV. 5: Numerical simulations of GECOR6 measurement: The effect of concrete resistivity and concrete cover (1,3,5 cm) of the steel rebar on the ratio between the average current density and the local current density right under the counter electrode. On the left: auxiliary reference electrodes parallel to the axe of the steel rebar. On the right: auxiliary reference electrodes perpendicular to the axe of the steel rebar (S.Laurens, 2010).

According to the above results, the hypothesis of an average current density becomes even more erroneous, when the concrete cover decreases and the resistivity increases. In addition, it seems that the errors are minimized (greater current ratios), when the auxiliary reference electrodes are placed perpendicularly to the steel rebars. Thus, Laurens precised the importance of applying the right corrections on the calculation of the corrosion rate, as a function of the different geometrical and physical parameters.

As far as Galvapulse is concerned, Laurens realized numerical simulations of polarization resistance measurements on reinforced concrete slab, corroded due to different environmental aggressive conditions. He then presented the different values of the Randles circuit elements (§II.2.3.2.) obtained for each aggressive environment, proving that the combination of these information can be very useful for the identification of the type of corrosion, when it comes to the sounding of a structure, whose state is unknown.

Although Laurens (2010) underlined the need to improve the interpretation protocol of polarization resistance measurement and approached the problem more quantitatively than the previously mentioned works, his study didn't confirm neither refuse that GECOR6 and Galvapulse measurements carried out within the linear part of the Butler-Volmer curve (§II.2.3.1), as they are theoretically considered to be.

Last but not least, C. Andrade (2010) has launched numerical simulations, similar to those of S. Laurens (2010). She also proved that the upper part of the reinforcement is more polarized than its lower part. However, during her study, she didn't take into account the influencing geometrical and physical parameters, neither she quantify nor explained adequately the problem's source. According to C. Andrade (2010), the presence of auxiliary reference electrodes assures the correct estimation of the polarization resistance, proposing at the same time the introduction of a coefficient which will describe a secondary polarization effect, attributed to corrosion. However, this doesn't provide with any perspective for making the polarization resistance measurement more reliable and its results easier to interpret.

IV.3. SYNTHESIS

The current apparatus used for the measurement of polarisation resistance on large surface structures function in a similar way. This paragraph summarized several studies which have demonstrated the high complexity of the polarisation resistance measurement on large surface structures at a practical level via the current apparatus. Moreover, the presence of the guard ring electrode during the polarisation of the reinforcement can modify the polarisation of the steel. Phenomena of over or under-polarisation are indeed observed leading to inconsistent results and to an erroneous interpretation of the polarisation resistance. It is insisted that the assumption of a homogeneous distribution of the current density on the supposing polarised surface of the reinforcement is false and the use of an average current density in the calculation of R_p may drive to a misleading estimation of the state of corrosion of reinforced concrete. Table 12 summarizes the objectives, conclusions and drawbacks of the studies presented in this chapter.

Table IV- 1: Review: On-site polarisation resistance measurement with GECOR6 and Galvapulse

	EXPERIMENTAL STUDIES			***NUMERICAL STUDIES***	
	Luping (2002)	**Nygaard (2009)**	**Wojtas (2004)**	**Laurens,(2010) Clement (2012)**	**Andrade (2010)**
Objective	Comparison between GECOR6/Galvapuse/SP/ASTM G1	Qualitative evaluation of the confinement techniques of GECOR6/Galvapulse	Estimation of polarisation resistance via GECOR6	Quantitative analysis of the parameters that influence the Rp measurement and a primary proposition of corrections	Comparison between GECOR6/Galvapuse
Measurements of:	Corrosion rate of reinforced concrete due to the presence of chloride ions	Corrosion rate of reinforced concrete: -uniformly corroded -locally corroded	-	-	-
Numerical simulations of:	-	-	GECOR6 (2D-PSpice)	Galvapulse, GECO6, Laboratory potentiostat (3D-Comsol Multiphysics)	Galvapulse, GECOR6 (3D-Comsol Multiphysics)

Conclusions	Influence of instrument's calibration and polarisation duration: important The value of injected current: insignificant	Differences in the values obtained with the two apparatus due to the presence of the guard ring electrode. Uniform corrosion: Overestimation of corrosion rate Local corrosion: Underestimation of corrosion rate Linearity criteria of measurement in question	Uniform corrosion: Adaptation of a modulated guard ring electrode according to the experimental conditions Local corrosion: in accordance with Nygaard's results- influence of: auxiliary reference electrodes' orientation and ratio between the dimensions of counter electrode and corroded spot	Non-homogeneous distribution of the injected current along and width wise the reinforcement Strong polarisation of the steel area right under the counter electrode Estimation of corrosion rate as a function of physical parameters GECOR6: important influence of: auxiliary reference electrodes' orientation Galvapulse: precise identification of the corrosion type (Randles model)	CECOR6 outclasses Galvapulse Non-homogeneous distribution of the injected current along and width wise the reinforcement A secondary polarisation of the steel bar due to corrosion may not be negligible

Drawbacks	Lab scale study Calibration of the instruments based on destructive techniques	Lack of quantitative analysis -on the guard ring electrode efficiency. -on the errors made during the corrosion rate estimation	2D simulation: the perpendicular current distribution of the injected current around the steel bar is neglected. Only qualitative analysis of some influencing parameters	Linear condition of the measurement not studied Incomplete study – no improvement proposed in the interpretation protocol of polarisation resistance	Influence of physical or geometrical parameters not studied. Lack of quantitative analysis and insufficient explication of the problem origin

IV.4. CONCLUSION

In this chapter, it has been demonstrated that the existing electrochemical devices for characterising corrosion of reinforcing steel suffer from a reliability deficiency. As it has been explained, due to their electrodes' assembly and the hypothesis on which the polarisation resistance measurement is based, phenomena of over-or under- polarisation are indeed observed leading to inconsistent results and to an erroneous interpretation of the polarisation resistance. This may lead to a misleading estimation of the state of corrosion of reinforced concrete. For all these reasons, a measurement model which will correctly estimate the value of polarisation resistance and will effectively inform on the real state of the structure is highly needed. In the following chapter, an original operative measurement mode of polarisation resistance is proposed, adapted for cooling towers submitted to corrosion due to carbonation (as it was defined in the objectives in the Introduction of this study). The novel model will be thoroughly demonstrated via numerical simulations and a procedure for calculating the real value of polarisation resistance will be developed, based on the establishment of new relationships, correction laws and abacuses.

Finally, by means of numerical experimental design, the model's sensibility to different parameters and their possible combinations will be studied.

V. Proposal of a novel operative measurement mode of polarisation resistance

V.1. INTRODUCTION

The previous chapter has presented a number of numerical and experimental studies that have proven the complexity of measuring linear polarisation resistance with the existing commercial devices. It has been insisted that practical problems and erroneous theoretical assumptions lead to a misleading polarisation of the steel rebars and a false interpretation of the polarisation resistance measurement.

In an effort, to overcome all these problems and obtain solid information on the real state of the steel rebars, this chapter focuses on **the presentation of a novel operative measurement mode of polarisation resistance, adapted for cooling towers submitted to uniform corrosion**.

Firstly, the theoretical background for the proposal of an original operative methodology of measurement and interpretation of polarisation resistance is presented. Secondly, the novel model is thoroughly demonstrated via numerical simulations, taking into account those physical (i.e. concrete cover, resistivity) and geometrical parameters (i.e. injected current from the probe, steel rebar configuration) that have a direct influence on its efficiency. Then, in the aid of the results of the numerical experiments, a procedure for calculating the real value of polarisation resistance is developed, as new relationships, correction laws and abacuses are established. Last but not least, numerical experimental design will be launched in order to study the model's sensitivity to the different parameters and their possible combinations.

V.2. PROPOSAL OF AN ALTERNATIVE METHODOLOGY FOR THE POLARISATION RESISTANCE MEASUREMENT

As it has been already mentioned in §IV.1, the existing electrochemical techniques for on site characterising the steel reinforcement corrosion suffer from a reliability deficiency. For that reason, the proposal of a novel operative mode of polarisation resistance measurement, which will provide reliable and accurate information on the real state of the reinforced structure, can be considered as fully relevant.

As described in the introduction of the thesis, the current study aims to contribute towards a better estimation of the real state of the reinforcement corrosion of cooling towers of energy

production units, suffering from carbonation. As it was explained in §I.3.1., carbonation may lead to uniform corrosion. In this particular case, it is assumed that **the carbonation front has already passed the first layer of the steel rebars,** inducing a uniform corrosion on the reinforcement of the structures. Thus, the methodology that is proposed in the following paragraphs focuses on the accurate and efficient estimation of state of the reinforcement of cooling towers, submitted to uniform corrosion, via the polarisation resistance measurement. In order to achieve this, the following actions should be taken for a more reliable and operative measurement mode:

- Simplify the electrode assembly
- Avoid the errors during the evaluation of current density distribution along the steel rebar
- Taking into account the influencing physical parameters of the measurement
- Assure the linear condition of the measurement
- Indicate an alternative protocol for the interpretation of polarisation resistance.

More specifically:

a) **Simplify the electrode assembly.** As it has been reported, the additional use of large guard ring electrodes and auxiliary reference electrodes increases the complexity of the measurement on a practical level and consequently leads to confusion about the phenomena occurring during the polarisation. For this reason, this study proposes the removal of the guard ring electrode and the auxiliary reference electrodes. As a result, **the measurement probe consists of only a counter electrode, which excites the system, by injecting current, and a reference electrode, in the middle of the counter electrode, which measures the system's response to the excitation, in potential**. In the absence of any confinement technique, the distribution of the injected current along the reinforcement will be easier to evaluate.

b) **Avoid the errors during the evaluation of current density distribution along the steel rebar**. Throughout the literature, the use of the confinement technique has been regarded as one of the main reasons of the over or under estimation of the corrosion rate, since it can influence the current density distribution along the steel bar, in a way contrary to the expected one. The elimination of the guard ring electrode, as this study solicits, signifies at the same time, the **abolishment of the concept of "the steel rebar surface assumed to be polarised."** In addition, it has been demonstrated that the use of an average current density for the calculation of polarisation resistance can be misleading, since the reinforcement is not polarised homogeneously; in fact, it has

been clearly indicated that the upper layer of the reinforcement part, located right under the measurement apparatus on the concrete surface, exhibits the strongest polarisation. Based on these observations, this new methodology **focuses on the polarisation phenomena** occurring only in the zone of the measurement response: **the steel rebar surface right under the reference electrode surface**. In other words, this measurement can be referred as **a single point measurement, taking place on the concrete surface of the structure**. Furthermore, in order to be able to evaluate the current density distribution with **higher precision**, this study avoids the use of a large counter electrode. On the contrary, it proposes **a smaller counter electrode** (a ring with an external diameter of 2cm and an internal diameter of 8mm)**,** compared to the ones the commercial apparatus use, in order to "canalize" as much injected current as possible, at a small proximity from the measurement point of the system's response.

c) Calculate the real value of polarisation resistance, taking into account the influencing physical or geometrical parameters of the measurement. Many authors have reported a disagreement between the values obtained from GECOR6 and Galvapulse. In addition, they have stated that important physical or geometrical parameters that influence the measurement are neglected. This may induce a considerable uncertainty on the estimation of the real corrosion rate of the reinforced structure. Therefore, the main originality of this method lies into the fact that the influence of these parameters on the polarisation measurement is studied and thus, **reinforcement's concrete cover, concrete cover's resistivity and injected current from the counter electrode are directly integrated in the estimation of the real polarisation resistance**. More specifically**, these parameters allow a transition from the single measurement point on the concrete surface to the point on the reinforcement surface, right under the reference electrode**. The latter, can be achieved via **numerical simulations**. Information about the real state of the reinforcement is gathered and a reliable evaluation of the corrosion rate is attained.

d) Assure the linear condition of the measurement. GECOR6 and Galvapulse are theoretically considered to perform a linear polarisation resistance measurement. However, only a few researches have been carried out in order to confirm, whether indeed these commercial devices function within the linear part of the polarisation curve. On the contrary, the current study develops an original operative technique, **which respects the basic theoretical principle of linear polarisation resistance**

measurement. This linearity will be demonstrated and confirmed through the experimental work fully described in chapter VI.

e) **Indicate an alternative interpretation protocol of polarisation resistance**. It has been remarked by some researchers, that no significant improvement has been ever recommended as far as the interpretation protocol of polarisation resistance is concerned. In this study, a different approach is presented: by means of numerical simulations, relationships are established, allowing **to pass from measurement point on the concrete surface to the steel bar** surface while **abacuses and correction laws** are built up, involving rebar's concrete cover, concrete cover resistivity and injected current from the probe. The new established relationships will provide **all the real information**, of the reinforcement's reaction to the polarization, **necessary for the calculation of the polarization resistance**.

Figure V.1 illustrates qualitatively the electrodes' configuration of the proposed measurement polarization technique:

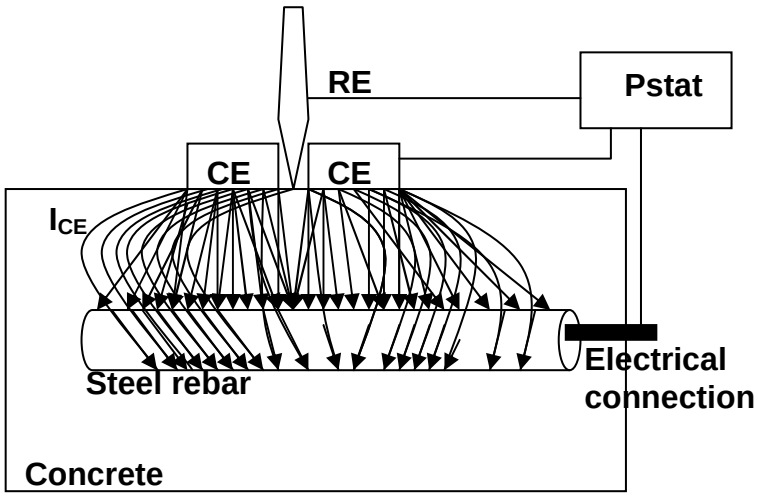

Figure V. 1: Qualitative schematic representation of the proposed measurement polarization technique. The counter electrode (CE) injects current (I_{CE}) from the concrete surface towards the reinforcement. A reference electrode (RE) measures the system's response in potential on the concrete surface. An electrical connexion to the reinforcement is required. A wet sponge is used for the electrical continuity between the reinforcement and the probe. The measurements are carried out with a potentiostat (Pstat).

V.1.1. Synthesis

The difficulties faced during the on site polarization resistance measurement make imperative the proposal of an improved measurement and interpretation model. This study proposes a three electrodes configuration, carrying out a single point measurement on the surface of the concrete structure. The probe consists only of a small counter electrode, which injects current to the reinforcement and a reference electrode, in the middle of the counter electrode, which measures the system's response in potential. Similarly to GECOR6 and Galvapulse, it requires an electrical connection to the reinforcing steel rebar. However, its simplicity allows a better and a more precise evaluation of the current distribution on the reinforcement. In addition, this methodology proposes a certain procedure in order to gather the real information about the polarization phenomena taking place on the steel bar's surface and so to calculate the real value of polarization resistance. In order to achieve this, the important parameters that influence the measurement such as concrete cover, concrete cover's resistivity and injected current from the counter electrode are taken into account. More specifically thanks to numerical simulations of the proposed measurement model, the polarization phenomena are studied under the influence of these parameters, allowing to pass from the single point measurement point on the concrete surface to the point on the reinforcement surface, right under the reference electrode. Abacus and correction laws are built for this purpose while new established relationships will provide those quantities necessary for the calculation of the real polarization resistance of the reinforcement. Finally, this proposed model is created with respect to the basic theoretical principle of linear polarization resistance measurement. This will be studied and validated in chapter VI of the dissertation.

Table V.1 consists of a quick primary comparison between the suggested measurement model of polarization resistance and the existing ones:

Table V- 1: A primary comparison between GECOR6, Galvapulse and the proposed Rp measurement model

	GECOR6	**Galvapulse**	**LMDC procedure**
Electrodes' configuration	CE + RE + GR+ auxiliary reference electrodes	CE+RE+GR	CE+RE
Electrical connection to the reinforcement	Yes	Yes	Yes
Contact between electrodes/concrete	Saturated wet sponge	Saturated wet sponge	Saturated wet sponge
Type of measurement	Galvanostatic	Galvanostatic	Galvanostatic
State of measurement	Stationary	Transitory	Stationary
Current density distribution	Average current density along a steel surface assumed to be polarized	Average current density along a steel surface assumed to be polarized	Current density on a single point right under the RE
Rp calculation	Use of ohmic drop	Randles circuit elements	Relationships, abacus and correction laws as a function of concrete cover, concrete cover resistivity and injected current from the probe

V.3. NUMERICAL SIMULATIONS OF THE NOVEL PROBE PROPOSED FOR THE POLARIZATION RESISTANCE MEASUREMENT

In the previous paragraph, the background for a novel probe of measuring polarization resistance was given. Numerical simulations of the measurement with the proposed technique were launched in order to obtain a better insight in the occurring polarization phenomena on the reinforcement and to develop the procedure, according to which, the polarization resistance will be calculated. These numerical simulations were carried out, using the module "DC conductive media" of the commercial Finite Element Method (FEM) software Comsol Multiphysics®.

In the following paragraphs, a thorough description of the numerical experimentation is given (geometries, volume properties, boundary conditions, electro-kinetics equations, parameters) Then, the obtained results of the simulations, current density and potential distribution along the reinforcement, are qualitatively and quantitatively presented and the influence of the parameters below is thoroughly discussed:

-resistivity, concrete cover (combined with the influence of the size of the counter electrode) and injected current,

-reinforcement state,

-reinforcement configuration and

-probe's position.

V.3.1. Geometry definition

As it has been already mentioned in the previous paragraph, the novel probe consists of only a counter electrode and a reference electrode, placed in the middle of the counter electrode. This new counter electrode, responsible for polarizing the steel bar, is represented by a ring of smaller dimensions compared to the counter electrode used by the commercial devices. More particularly, the ring has an external diameter D=20mm and an internal diameter d=8mm. In the middle, the central hole corresponds to the reference electrode which measures the potential response. Figure V.2 depicts the simulated probe along with that used by GECOR6 and Galvapulse:

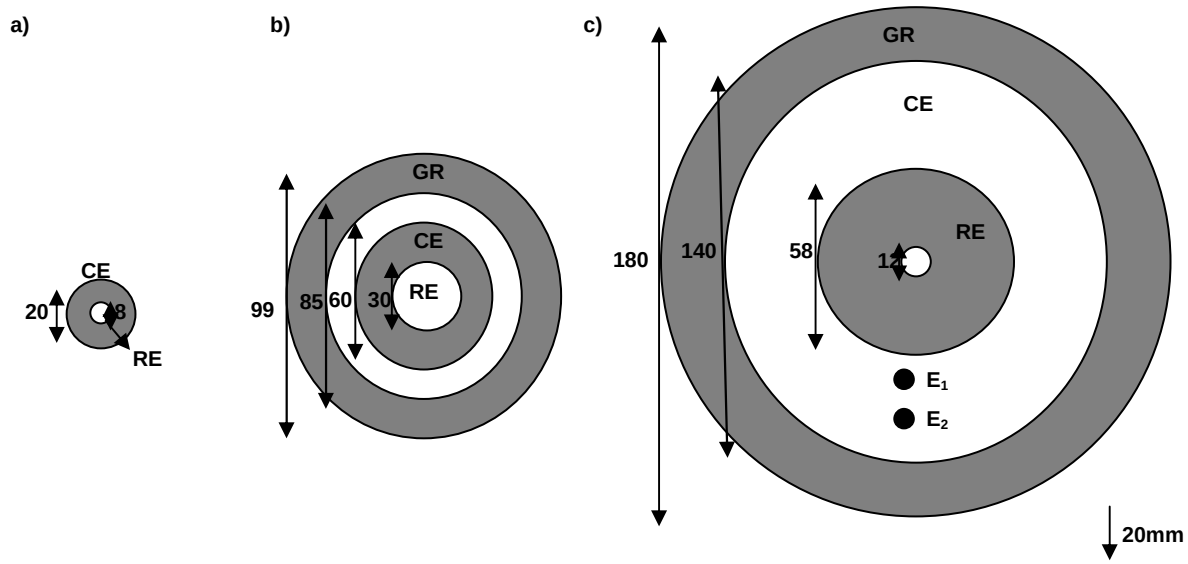

Figure V. 2: Schematic illustration of probes for: a) LMDC simulated model; b) Galvapuse (Laurens, 2010);c) Gecor6 (Laurens, 2010). Dimensions in mm.

As it is already known, this probe is adapted for the measurement of polarization resistance, on the reinforced concrete structure of cooling towers. In this numerical study, the tested geometries are representative of those of cooling towers.

So to begin with, for these numerical experimentations, prismatic concrete specimens were simulated with dimensions of 1m x 1m x 30cm. Three different configurations of reinforcement network, embedded in the specimens, were put under test:

- One single rebar placed horizontally in the middle of the specimen.
- Two steel rebars crossed, having a single point of contact
- A network of four steel bars forming two-by-two layers: For each layer the steel rebars are parallel, (with a distance in between of 20cm for the first layer and 25cm for the second layer respectively), and crossed two by two (i.e. one from the first layer crossed with one from the second layer), with one single point of contact at each crossing.

The diameter of the embedded steel rebars (ø 12mm), and all the above information, were determined, according to EDF's specifications for the construction of cooling towers (Note d'étude, EDF 2009).

At the same time, two different positions of the probe on the top surface of the concrete specimens were tested:

- In the middle, right above the crossing of the two crossed steel rebars
- For the same configuration, at a distance of 11.9cm from the axis of the upper rebar and 9.4 cm from the axis of lower rebar, right on the concrete specimen's surface

Due to the symmetries created, only ¼ of the specimen was simulated. There are two planes of symmetry: one perpendicular to the surface, passing by the axis of resolution of the rebar and the other perpendicular to the previous one.

Thus, the geometry of the physical problem allows to use two symmetries and so to calculate the different fields within a volume that corresponds to the ¼ of the global geometry. The figures V.3 and V.4 depict one example for each of the simulated geometries, previously described:

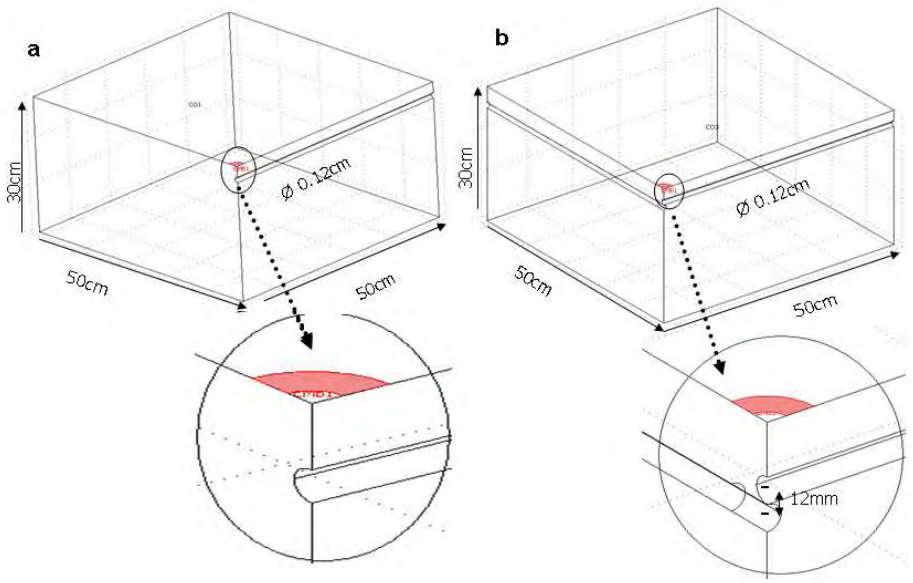

Figure V. 3: Geometry of the simulated reinforced concrete specimens with: a) a single steel rebar embedded at 6cm and the probe placed above the middle of the single bar b) two crossed rebars-the top embedded at 6cm and the probe placed above the crossing of the rebars.

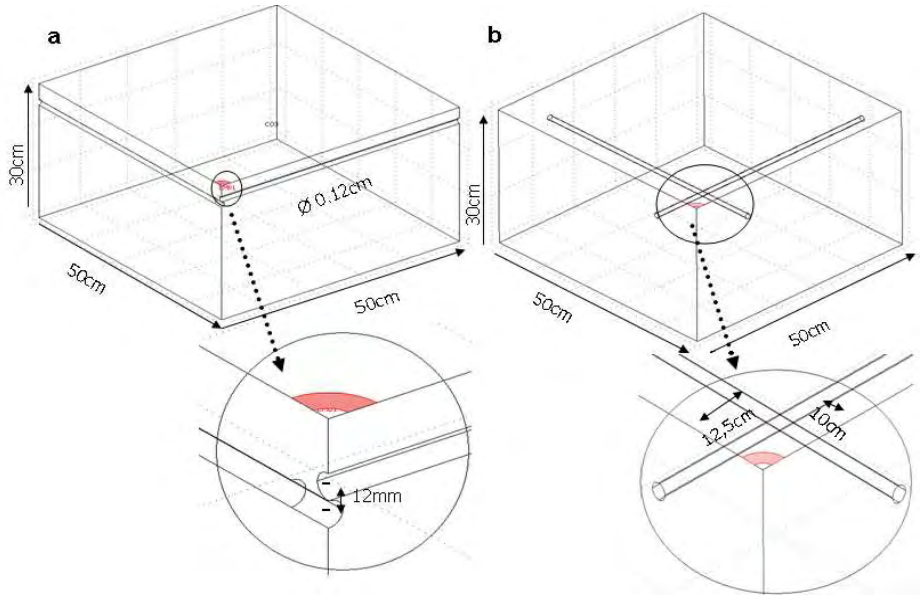

Figure V. 4: Geometry of the simulated reinforced concrete specimens with: a)) two crossed rebars-the top embedded at 6cm and the probe above the crossing of the rebars b) the same reinforcement configuration and the probe placed above the middle of the reinforcement mesh

V.3.2. General properties, electro-kinetics equations and boundary conditions of the model

In the current study, concrete specimens are assumed to be homogeneous media, with a uniform electric resistivity; the moisture gradients throughout their volumes are neglected. In the concrete volume, the equations governing electrical phenomena are Ohm's law, linking the local current density *j* and the potential gradient $\nabla\varphi$ Eq. (43) and charge conservation Eq. (44):

$$j = -\frac{1}{\rho}\nabla\phi \qquad \text{(eq. 43)}$$

$$\nabla \cdot j = 0 \qquad \text{(eq. 44)}$$

In each simulation, a current density is applied and injected from the counter electrode boundary, while the boundaries that define the concrete domain were under electrical isolation conditions. In all configurations, the steel reinforcement is completely either at a passive or an active state. Thus, the steel–concrete boundaries were modelled according to the Butler–Volmer nonlinear equation implemented in the code.

Taking into consideration the numerical work done by Nasser (2010) and the experimental work carried out in the frame of the current thesis for the definition of electrochemical parameters (see also §VI.3.2.), table V.2 exhibits the Butler Volmer simulation parameters used in this study:

Table V- 2: The Butler- Volmer parameters implemented in the model

Active state		**Passive state**	
β_{aa} ***(V/dec)***	0.3	β_{pa} ***(V/dec)***	0.4
β_{ac} ***(V/dec)***	0.125	β_{pc} ***(V/dec)***	0.125
j_{acorr} ***(A/m^2)***	0.005	j_{pcorr} ***(A/m^2)***	4e-5
E_{acorr} ***(V)***	-0.419	E_{pcorr} ***(V)***	-0.102

The simulations of all above configurations are carried out for all possible combinations of the values of the following parameters:

• Injected current from the counter electrode: I_{CE}=1, 5, 10, 20 30 and 50 μA

• Concrete cover (the top steel rebar(s) is (are) used as a reference): e=1, 2, 3, 4, 5, 6 cm

• Resistivity: ρ=50, 150, 300, 600, 1000, 2000 Ohm .m.

As it is depicted in the figure V.5, in order to solve the highly non linear problem a very fine mesh was used on the counter electrode and steel-concrete boundaries for precision reasons. In addition a coarse mesh in the concrete volume for reasons of numeric convergence:

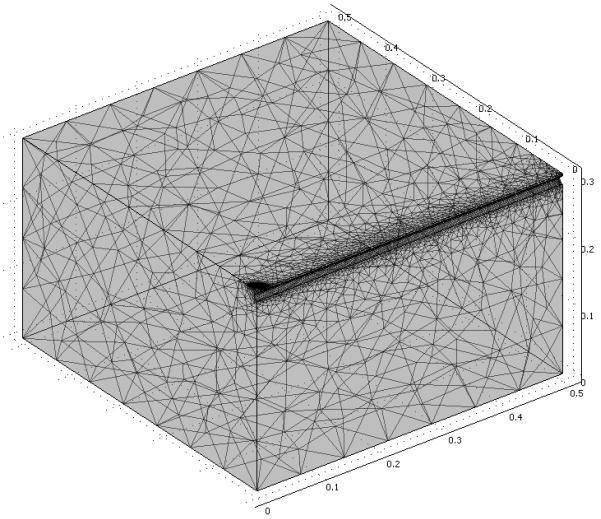

Figure V. 5: Coarse mesh applied on the concrete volume with a single steel rebar embedded at 1cm. A very fine mesh is used on the counter electrode and the steel-concrete boundary. The total number of triangular elements is 265488 and the element volume ratio is $3.18*10^{-7}$. The number of degrees of freedom (ddl) is 382931.

V.3.3. Distribution of the injected current lines in the simulated geometries

Figures V.6 to V.9 depict the current density lines, resulting from the simulation of the proposed model of polarisation resistance measurement, tested for the different geometries and different states of the reinforcement. The start point coordinates and the magnitude of the current lines (maximum and minimum distance) are automatically defined by Comsol Multiphysics®. For the qualitative illustration of the injected current distribution; a number of 10 injected current lines were selected.

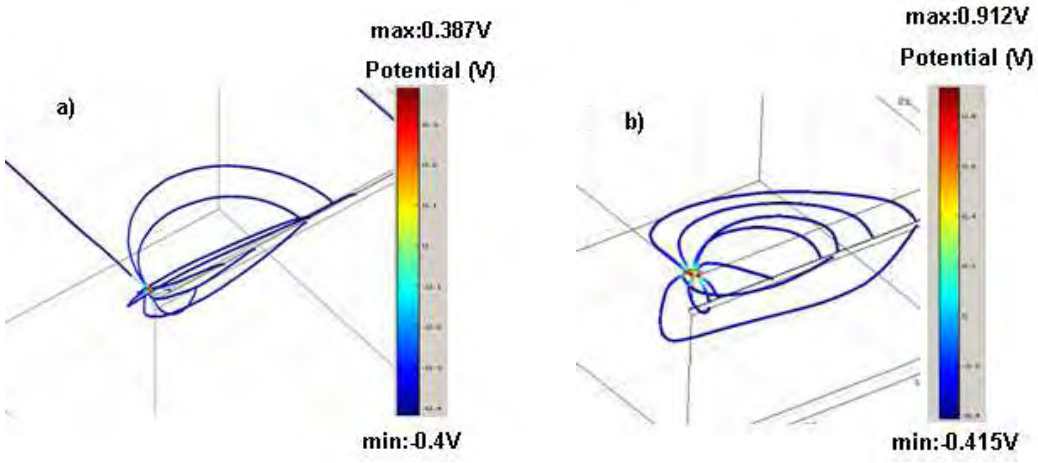

Figure V. 6: Injected current density lines (I_{CE}=50µA) for the geometry with one single bar at active state, for concrete resistivity of 2000 Ohm m, embedded at a)1cm and at b)6cm and the probe placed above the middle of the single bar. The colour bar gives the potential range (V).

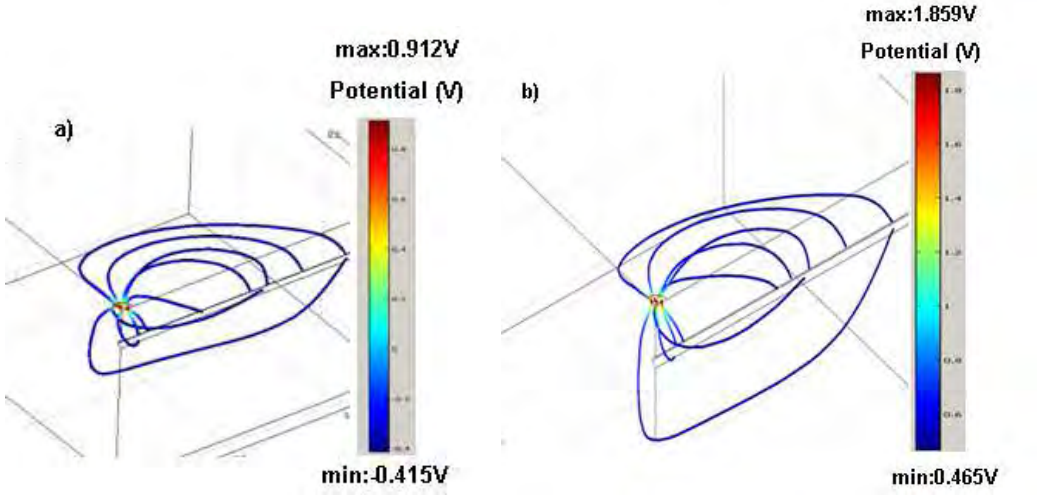

Figure V. 7: Injected current density lines (I_{CE}=50µA) for the geometry with one single bar embedded at 6cm at a) active state) and b) at passive state for concrete resistivity of 2000 Ohm m and the probe placed above the middle of the single bar. The colour bar gives the potential range (V).

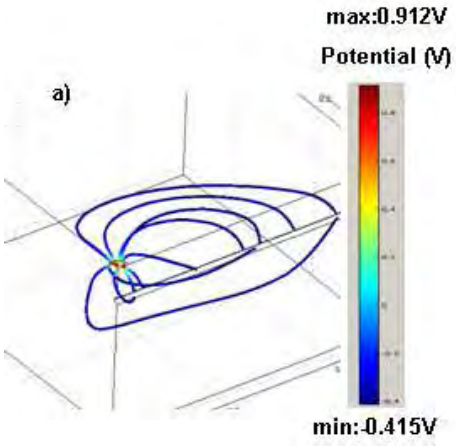

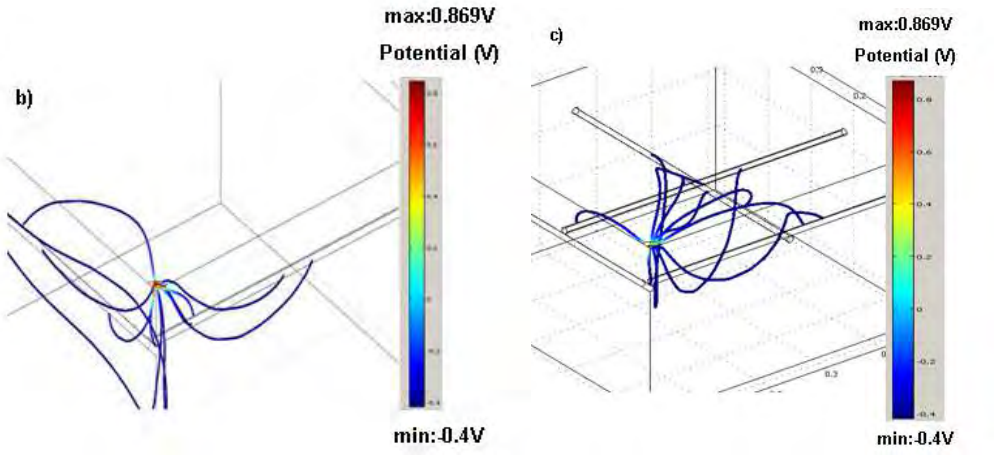

Figure V. 8: Injected current density lines (I_{CE}=50μA) for the geometry with a) a single steel rebar at active state embedded at 6cm and the probe placed above the middle of the single bar ,b) two crossed rebars at active state-the top embedded at 6cm and the probe placed above the crossing of the rebars c) a network of 4 rebars at active state–the top ones embedded at 6cm- and the probe above one of the crossing of the rebars. The concrete resistivity is 2000 Ohm m. The colour bar gives the potential range (V).

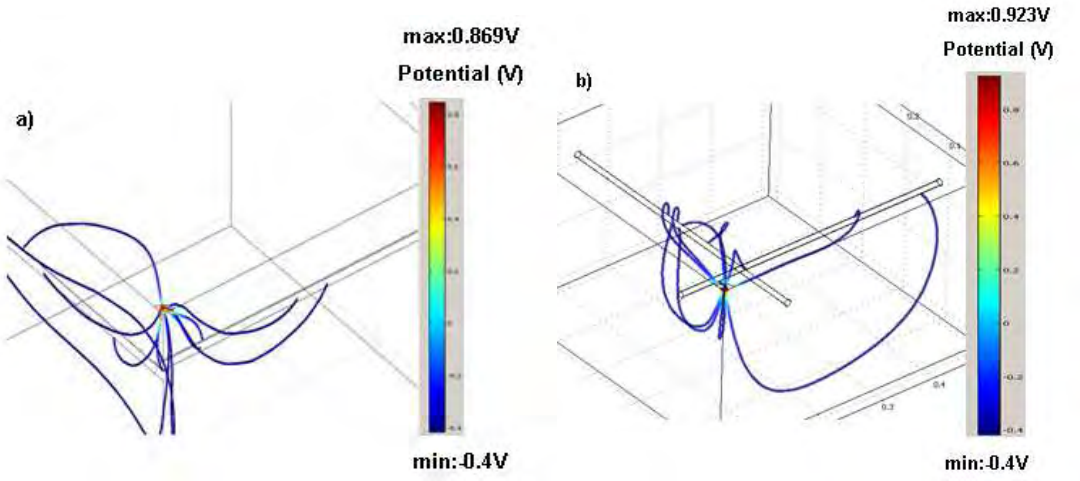

Figure V. 9: Injected current density lines (I_{CE}=50μA) for the geometry with two crossed rebars at active state-the top embedded at 6cm and the probe placed a) above the crossing of the rebars, b) at a distance of 11.9cm from the upper rebar and 9.4 cm from the lower rebar, right on the concrete specimen's surface. The concrete resistivity is 2000 Ohm m. The colour bar gives the potential range (V).

The above figures are some examples of the realized numerical simulations and illustrate the injected current density dispersion in the concrete volume during the polarisation resistance measurement. This qualitative representation of the measurement consists only of an indication of the way the injected current is distributed along the steel rebar and the way the "point of interest" is polarised. It has to be reminded, that the "point of interest" is that point of the upper layer of the reinforcement right under the measurement point on the concrete surface (see also figure V.11). In addition, when it comes to the two and four rebar

configuration, the reinforcement that is under study and is used as a reference for the concrete cover, is only the top steel rebar, right under the measurement zone.

Influence of the concrete cover of the steel rebar.

Figure V.6 shows the current density distribution during polarisation for the active single bar configuration with a concrete cover at 1 and 6 cm. At a first sight, it seems that **for a concrete cover of 1cm the "point of interest"** on the steel rebar, right under the reference electrode surface **is less polarised than for a concrete cover of 6cm**. In fact, as it can be seen, it appears that for a really small concrete cover such as 1cm, the injected current tends to polarise more that area of the reinforcement which is found at a small proximity from the measurement zone. The opposite phenomenon can be observed for the concrete cover of 6cm. As it will be thoroughly described in §V.3.4.1 and figure 67, the size of the counter electrode combined with the depth at which the steel rebar is embedded justify the phenomena observed in figure V.6.

Influence of the electrochemical state of the steel rebar

Figure V.7 depicts the current density distribution for a single bar configuration, when the reinforcement is found at an active and a passive state. It can be suggested that **the way the inject current is distributed along the reinforcement is similar for both electrochemical states** of the rebar. This can be considered logical since the conditions imposed from Butler Volmer equations are uniform. The active state corresponds to uniformly corroded rebar while the passive one to a completely non corroded rebar. The latter can be primary indicated in that figure by the potential range measured during the polarisation.

Influence of the steel rebar configuration

Furthermore, figure V.8 illustrates the influence of the presence of one more or of a network of steel rebars on the polarisation of that point of the upper steel rebar right under the measurement point on the concrete surface. As it can be expected, the neighbour reinforcement is also polarised, affecting the quantity of current received on that "point of interest". In order to assess precisely how much current is "lost" from that specific point on the upper reinforcement, a quantitative analysis will be carried out in the following paragraphs.

Influence of the position of the probe on the reinforced concrete specimen

Last but not least, as far as the probe's position is concerned, figure V.9 demonstrates at a first level, that a more effective polarisation of the studied reinforcement is achieved when the probe is placed right above the reinforcement. In other words, when the probe is placed above the steel rebar most of the injected current is focused on that steel rebar, carrying out a more reliable polarisation measurement of the "point of interest". In the other case, when the probe is placed at a distance from the reinforcement, a large current dispersion is observed in the concrete volume.

All the above, they have clearly indicated that parameters such as the concrete cover, the geometry and the probe's position influence the polarisation measurement, carried out by the proposed model. The following paragraphs describe quantitatively the influence of the geometric and physical parameters on the current density and potential distribution along the rebar after the polarisation.

V.3.4. Current density and potential distribution along the reinforcement of the simulated geometries

As it has been already mentioned, S. Laurens (2010) has proven that the upper layer of the steel rebar is more strongly polarised compared to the rest of its body. Based on this ascertainment, this study demonstrates the polarisation along the upper fibre of the steel rebar for the single bar configuration and of the top armature of the two and four bar configuration (figure V.10), under the influence of the geometric and physical parameters:

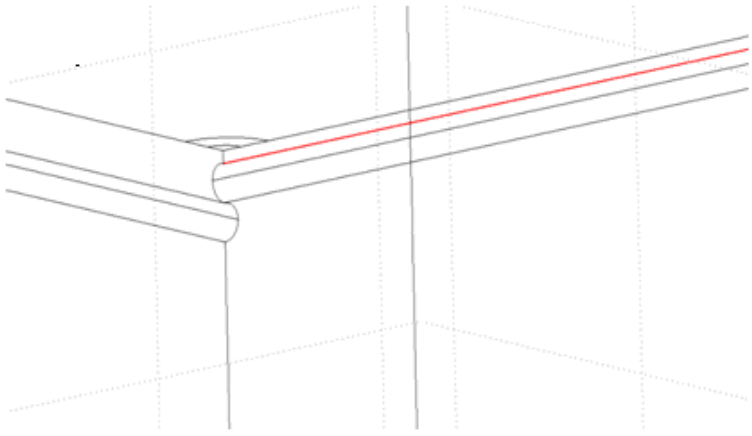

Figure V. 10: Indication (in red) of the fibre under investigation towards polarisation for two bars configuration.

In addition, S. Laurens (2010) has shown that along that fibre, the point that is found right under the reference electrode provides the real information measured on the concrete surface and thus a correct evaluation of the polarisation resistance of the steel rebar. As a result, in this study, the response of that particular point towards the steel rebar's perturbation will be investigated (figure V.11):

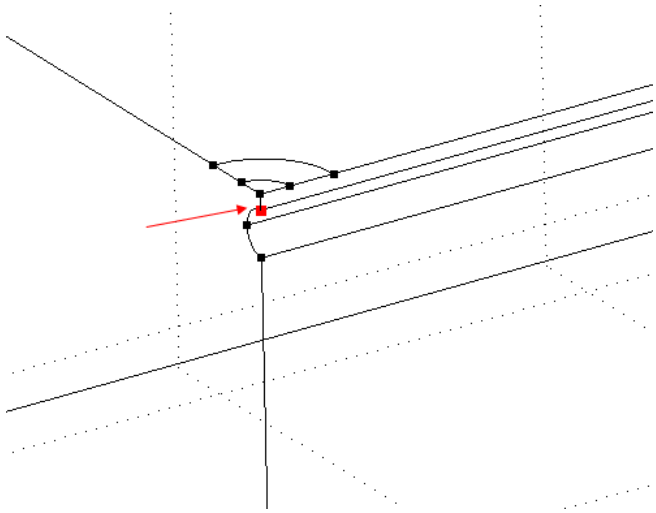

Figure V. 11: Indication (in red) of the "point of interest" on the steel rebar right under the measurement point on the surface of the concrete specimen.

V.3.4.1. Influence of resistivity, concrete cover, size of the counter electrode and injected current on the current density and potential distribution

As a result of all these simulations, a huge data base was built. In this paragraph only the results for the extreme values of the studied parameters will be given. More particularly, the following figure illustrates the current density distribution along the reinforcement, for the one single bar configuration, in active state, with the steel rebar embedded at 1cm and a concrete resistivity of 50 Ohm m and 2000 Ohm m:

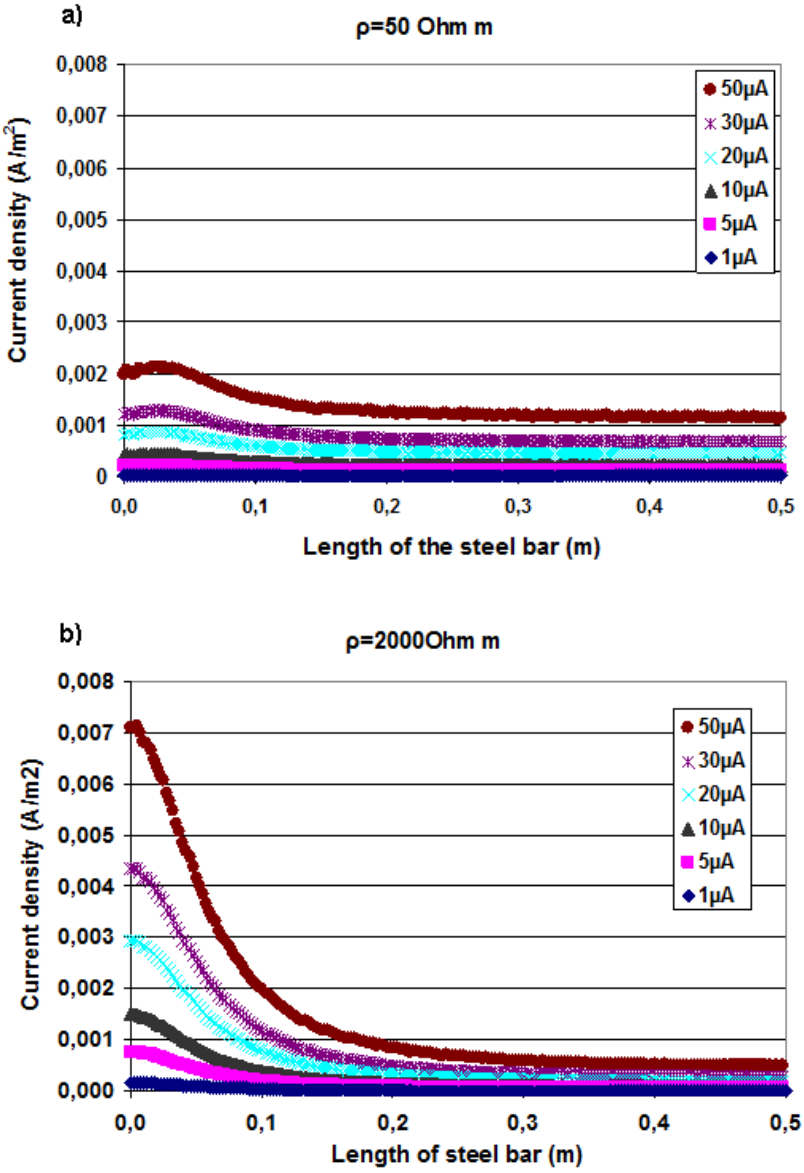

Figure V. 12: Current density distribution along the steel bar for the single bar configuration in active state for every value of injected current from the probe with e=6 cm and a) ρ=50 Ohm m and b) ρ=2000 Ohm m.

In the figure V.12, and as well in the figures that follow, the starting point on x-axis corresponds to that point on the steel rebar's surface right under the measurement point on the surface of the structure which provides the information on the real state of the reinforcement. Firstly, as it can be seen, the current density distribution decreases along the steel rebar. In other words, as the distance increases from the measurement point, the polarisation is less strong. Apparently, this observation comes into agreement with the results of S. Laurens (2010). Indeed, the point that exhibits the stronger polarisation along the rebar is the point right under the reference electrode. In addition, it is observed that the higher the injected current is, the more that particular point on the steel bar is polarised. The same tendency is

noted for an increase in concrete resistivity. The attenuation of the injected current along the rebar seems to be faster and becomes even more remarkable for a resistivity of 2000 Ohm m. **The high resistivity of concrete becomes an obstacle for the spreading of the current around the reinforcement**. In other words, the injected current polarises a limited zone around the "point of interest" due to the high resistivity, as if straight current lines arrive on the reinforcement.

The injected current distribution, as presented above, led to the potential distribution along the rebar embedded at 6cm, for a resistivity of 50 and 2000 Ohm.m and for each value of injected current, shown in figure V.13:

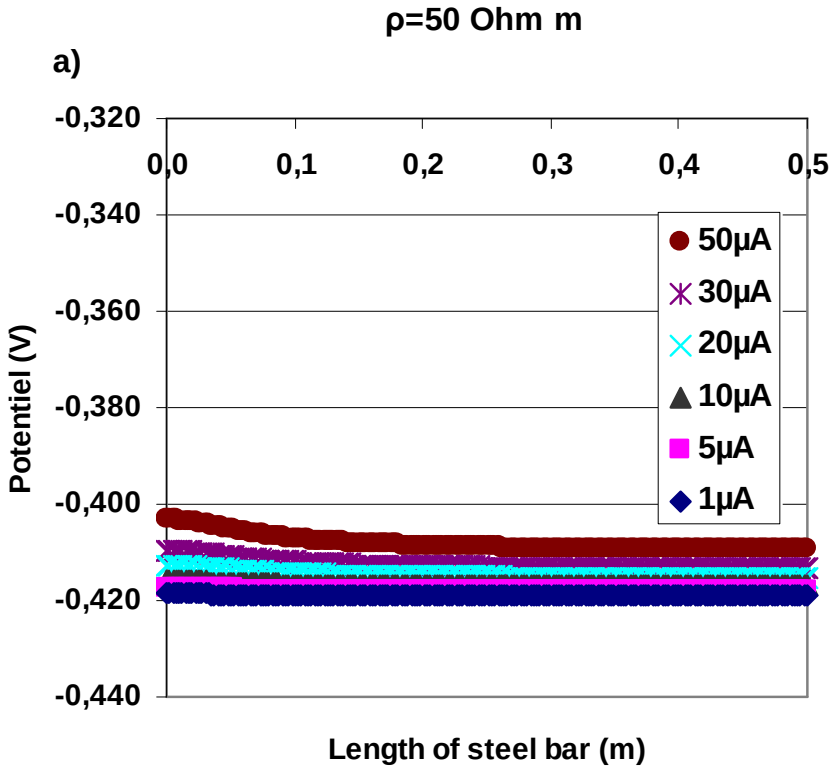

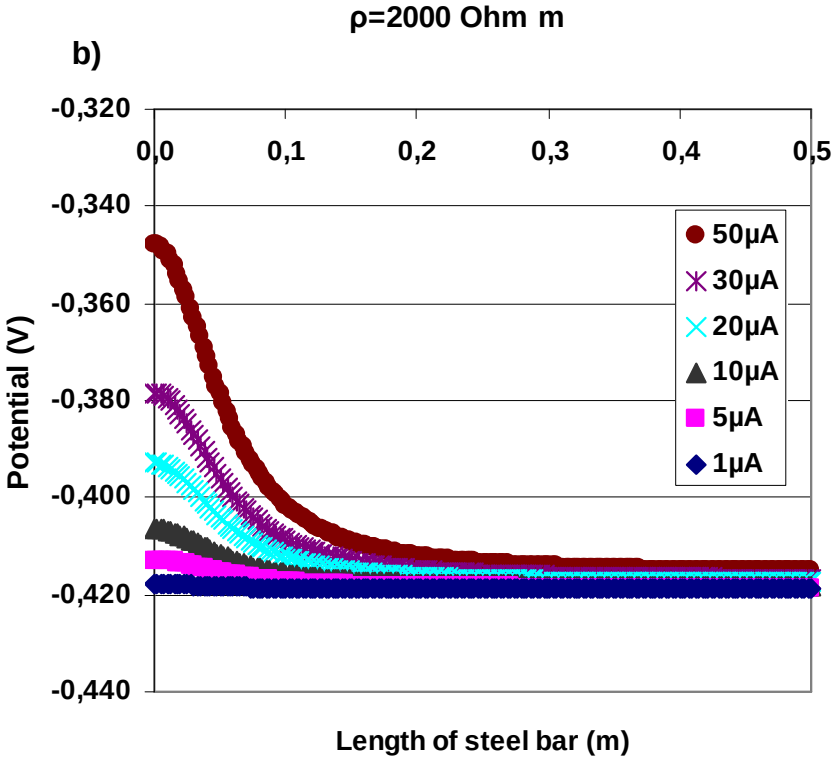

Figure V. 13: Potential distribution along the steel bar for the single bar configuration, in active state, for every value of injected current from the probe with e=6 cm and a) ρ=50 Ohm.m and b) ρ=2000 Ohm.m.

In the figures V.14 and V.15 the influence of the concrete cover is presented on the current density distribution along the rebar. Figure V.14 illustrates the current density distribution along the rebar at active state, for two different concrete covers:

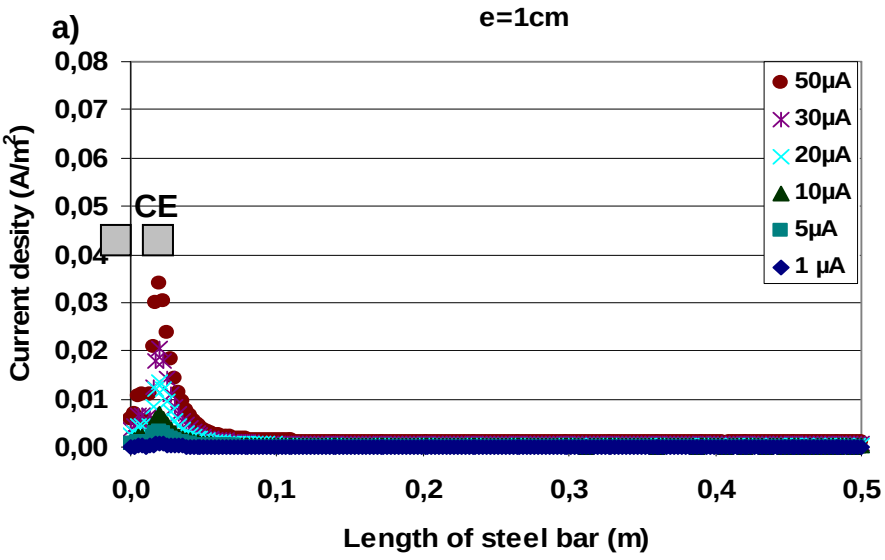

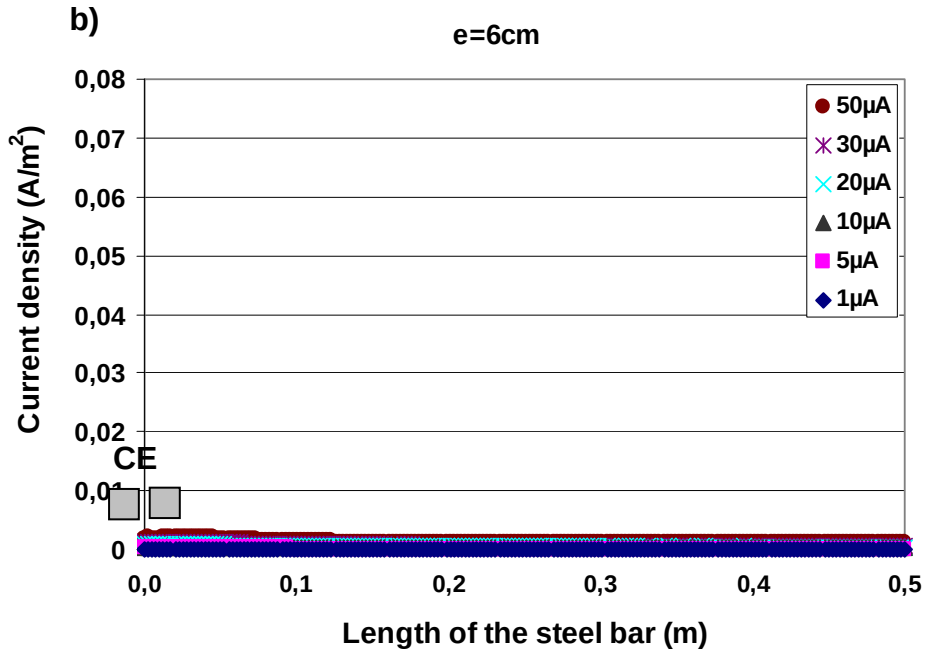

FigureV. 14: Current density distribution along the steel bar for the single bar configuration in active state, for every value of injected current from the probe with ρ=50 Ohm.m, a) e=1 cm and b) e=6 cm. The probe's position along the steel rebar (x-axis) is also indicated.

As it can be seen from the previous graphs, the concrete cover influences the current received on the steel rebar. **The greater the distance of the steel rebar from the concrete surface, the less the steel rebar is polarised** (figure V.14). In addition, it is obvious that the starting point on the x-axis doesn't receive the most of the current, as it is expected to be. Instead, at a few centimetres further than that particular point, the curve of the current density distribution exhibits its maximum (figure V.14a). This maximum is observed at the same position for all values of injected current. However, the peak becomes even more distinctive when a high value of current is applied from the probe (I_{CE}=50μA). The phenomenon can be attributed to the geometric effect, **due to the ratio between the counter electrode's dimensions and concrete cover (influence of the size of the counter electrode)**. Obviously, the concrete cover of 1cm is smaller than the diameter of the counter electrode (2cm). As a result, the distance is not big enough for the current lines injected from the probe to arrive at that point of the steel rebar, right under the measurement point on the concrete surface. Instead, the surface of the steel rebar right under the polarising ring receives more current than the point under the reference electrode. The phenomenon becomes less intense as the concrete cover increases (figure V.15).

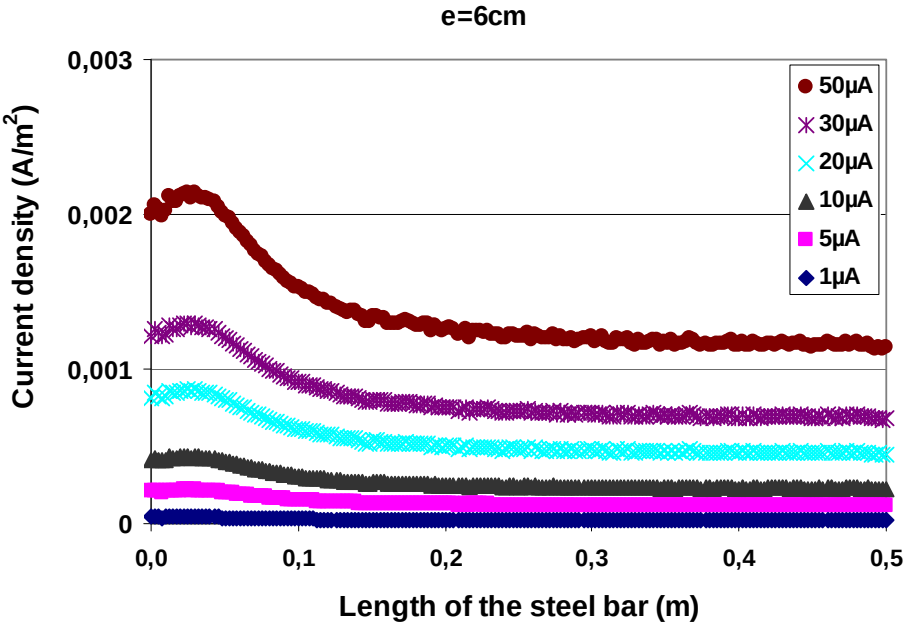

Figure V. 15: Current density distribution along the steel bar for the single bar configuration in active state, for every value of injected current from the probe with ρ=50 Ohm.m and e=6 cm.

The current density distribution as depicted in the figure V.14, leads to the following potential distribution respectively:

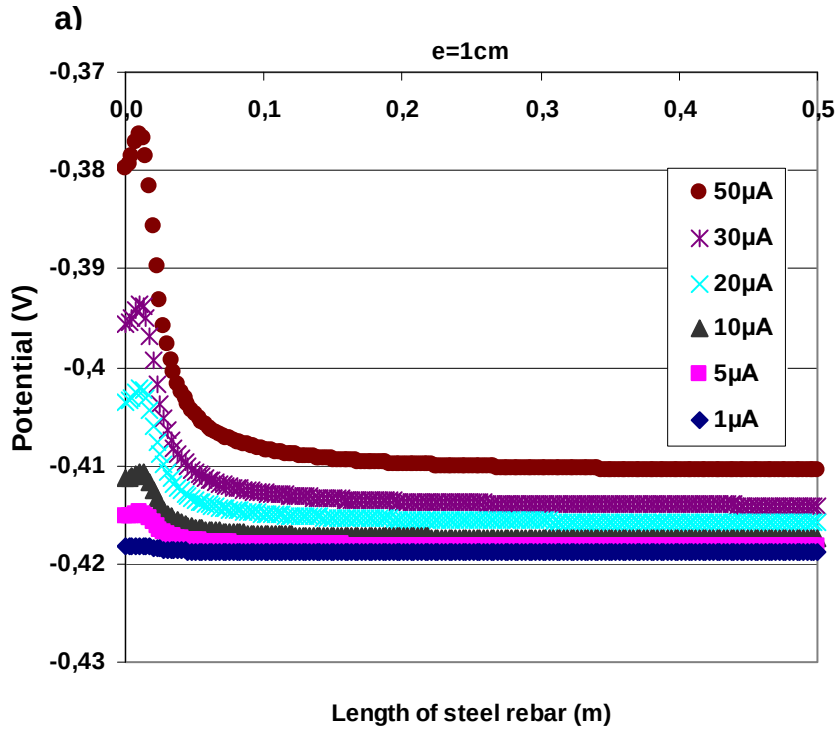

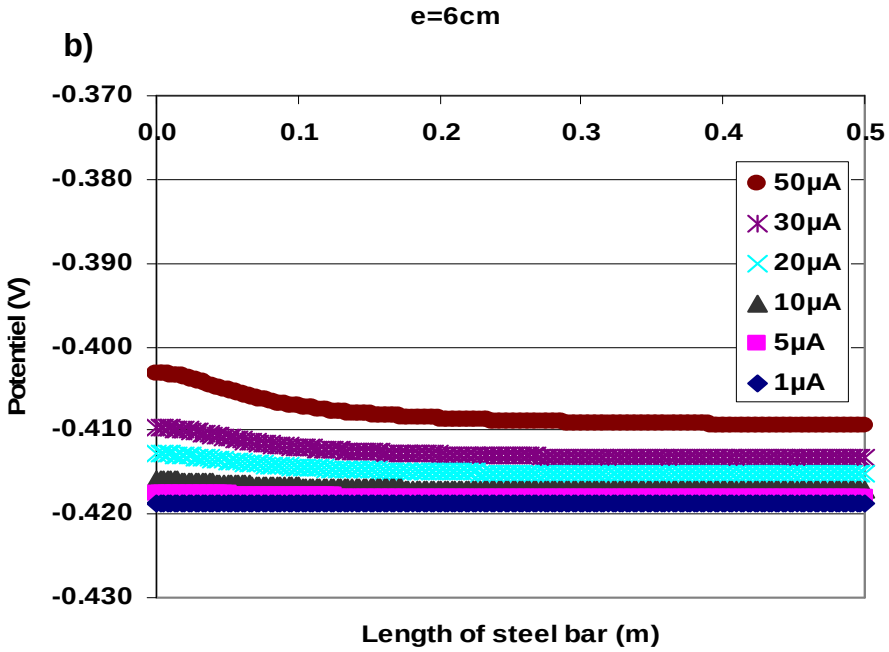

Figure V. 16: Potential distribution along the steel bar for the single bar configuration, in active state, for every value of injected current from the probe with ρ=50 Ohm.m, a) e=1cm and b) e=6cm (under).

Last but not least, the figures V.13 and V.16 indicate that an anodic polarisation is carried out during the simulated polarisation resistance measurement, since the potential values moves towards more electropositive values than the corrosion potential.

V.3.4.2. Influence of the reinforcement state on the current density and potential distribution

In figure V.17, the current density distribution is presented for the two different states of the steel rebars, modelled according to the Butler Volmer equations (eq.16 and eq.17):

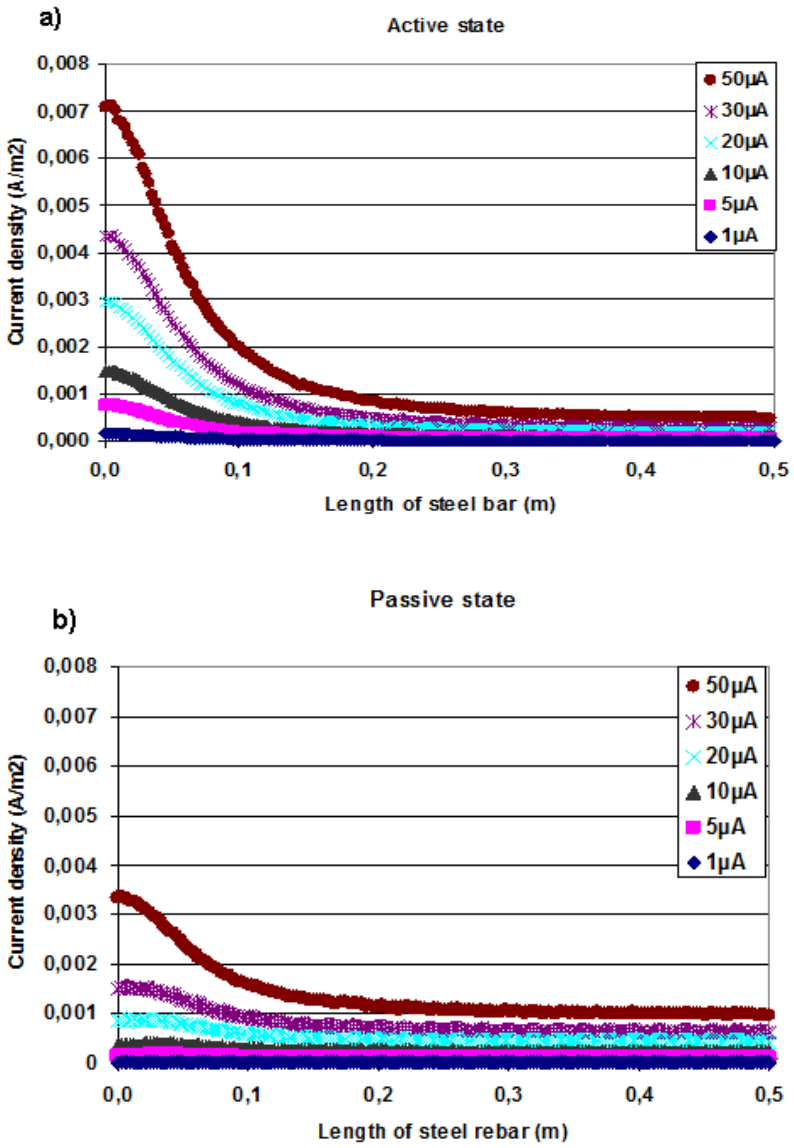

Figure V. 17: Current density distribution along the steel bar for the single bar configuration for every value of injected current from the probe with ρ=2000 Ohm.m and e=6 cm in a) active and b) passive state.

As it is expected, in all cases of injected current, **the point right under the reference electrode receives much more current when the reinforcement is in active state** rather than in passive state. However, **the attenuation of the current density along the passive steel rebar occurs quite smoothly** compared to that along the active steel rebar. Figure V.18 demonstrates the potential distribution along the steel rebar for both states of the reinforcement:

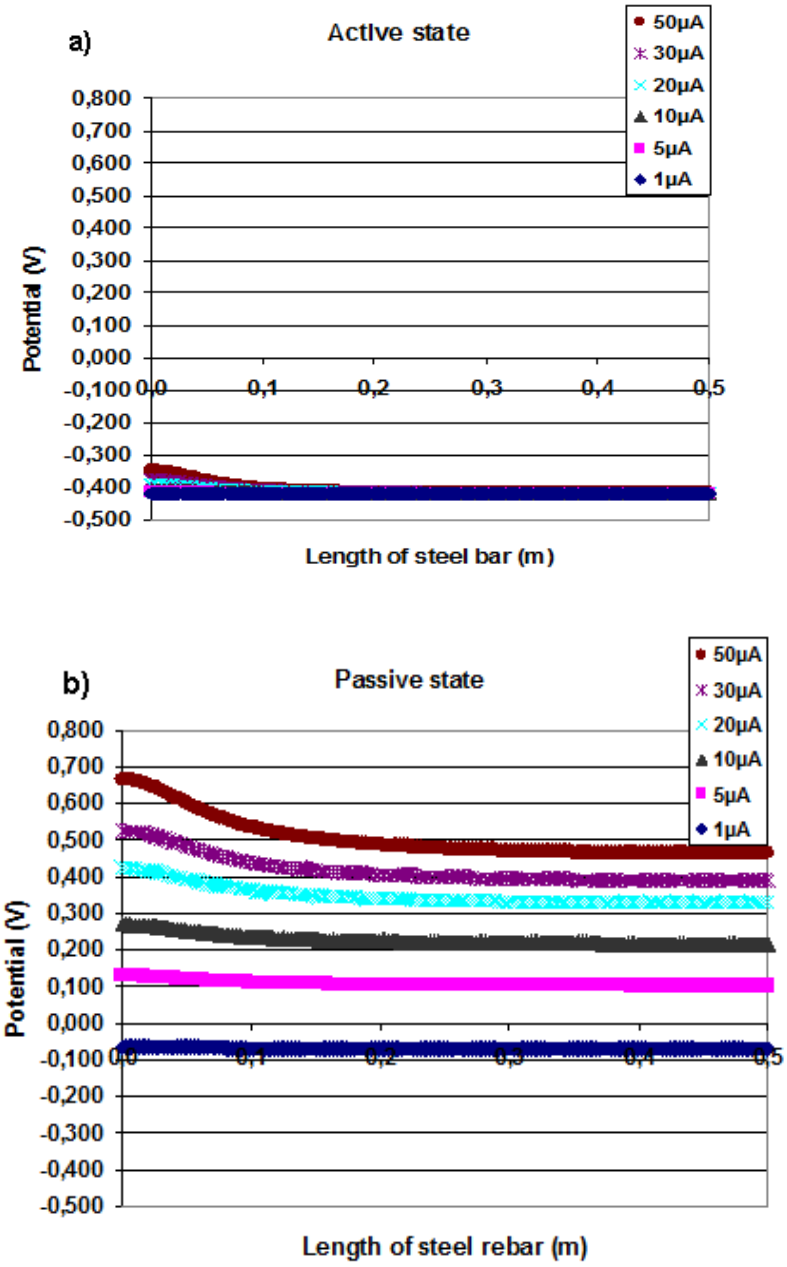

Figure V. 18: Potential distribution along the steel bar for the single bar configuration, for every value of injected current from the probe with ρ=2000 Ohm.m, e=6cm, in a) active state and b) passive state.

According to figure V.18, **the polarisation seems to be stronger for the passive bar than for the active one**. This can be explained by the Butler-Volmer curves that describe each state of the reinforcement. According to the curve for the passive rebar, characterised by a big plateau around E_{corr}, the injection of a very small current, may lead to a strong potential drift. On the other hand, for a steel rebar at active state, a strong polarisation (high potential drift) will be only achieved by the injection of a very strong current (figure V.19).

For the case studied, for example, an injection of 10μA may lead to a potential drift on the steel rebar of only 6mV for a active bar while for the same injected current, the potential drift on a passive bar would be more than 150mV. Still, the influence of each Butler-Volmer parameter on the proposed mode of polarisation measurement will be studied more thoroughly in a following paragraph of the chapter.

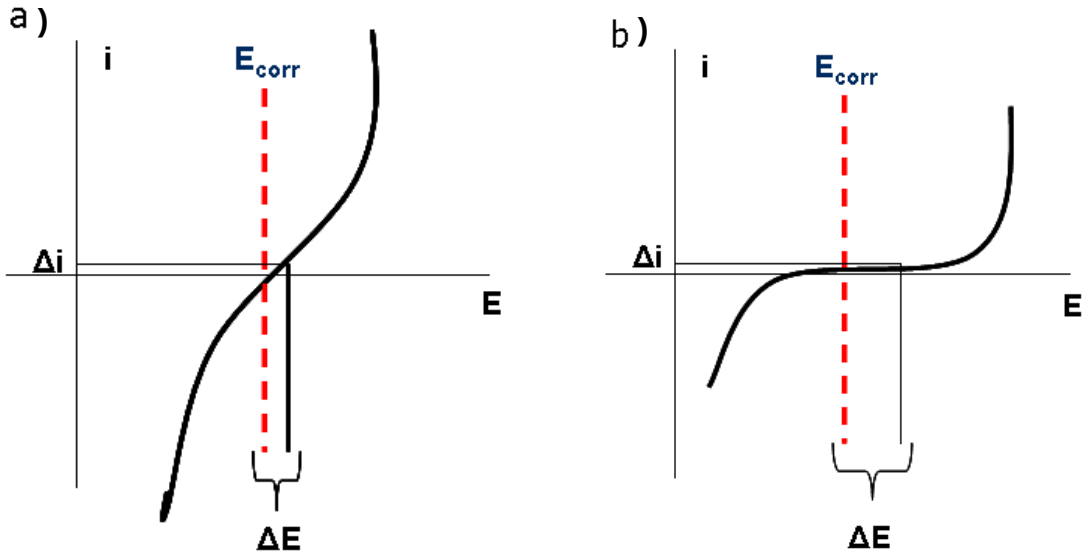

Figure V. 19: Polarisation measurement: Qualitative representation of potential shift, ΔE, due to current shift, Δi, along the Butler Volmer curves for: a) active steel rebar b) passive steel rebar

The question that may be now raised concerns the linear "character" of the potential drift, imposed by the injected current. In figure V.20, the current density collected on that "point of interest" is plotted against the potential drift *(= E_{ar}-E_{corr})* induced by every injected current, for the same steel rebars depicted in figure V.18.

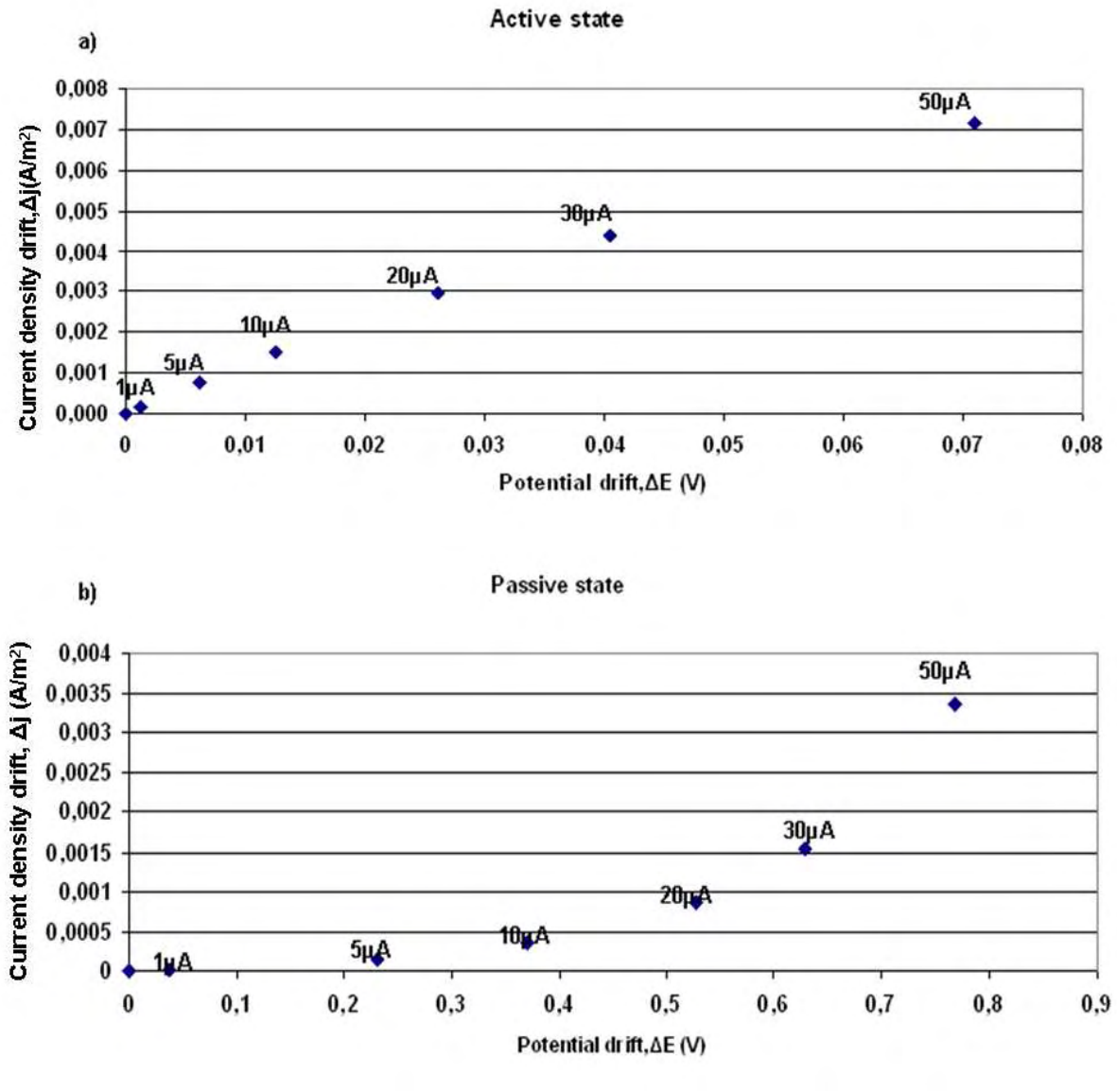

Figure V. 20: Anodic polarisation curve for the steel bar (on the "point of interest") for the single bar configuration, for every value of injected current from the probe with ρ=2000 Ohm.m, e=6cm, in a) active state and b) passive state.

Figure V.20 consists of **a first confirmation of the linearity of the proposed polarisation resistance measurement model**: In the case of the active steel rebar, the linear condition seems to be valid for every injected current. On the other hand, more cautiousness is required in the case of the passive steel rebar, since when a very strong injected current (20 –50µA) the system presents a non linear polarisation behaviour. The topic of the linearity of the proposed polarisation resistance measurement will be thoroughly described in chapter VI.

V.3.4.3. Influence of the different reinforcement configurations on the current density distribution

Another parameter investigated in this study was the influence of the different reinforcement configurations on the polarisation resistance measurement. As it has been already presented in figure V.8, the presence of neighbouring steel rebars, influences the current density distribution and the polarisation of the rebar on which the measurement is carried out. The figures V.21 demonstrate the current density distribution along the rebar for a single and two bars configuration:

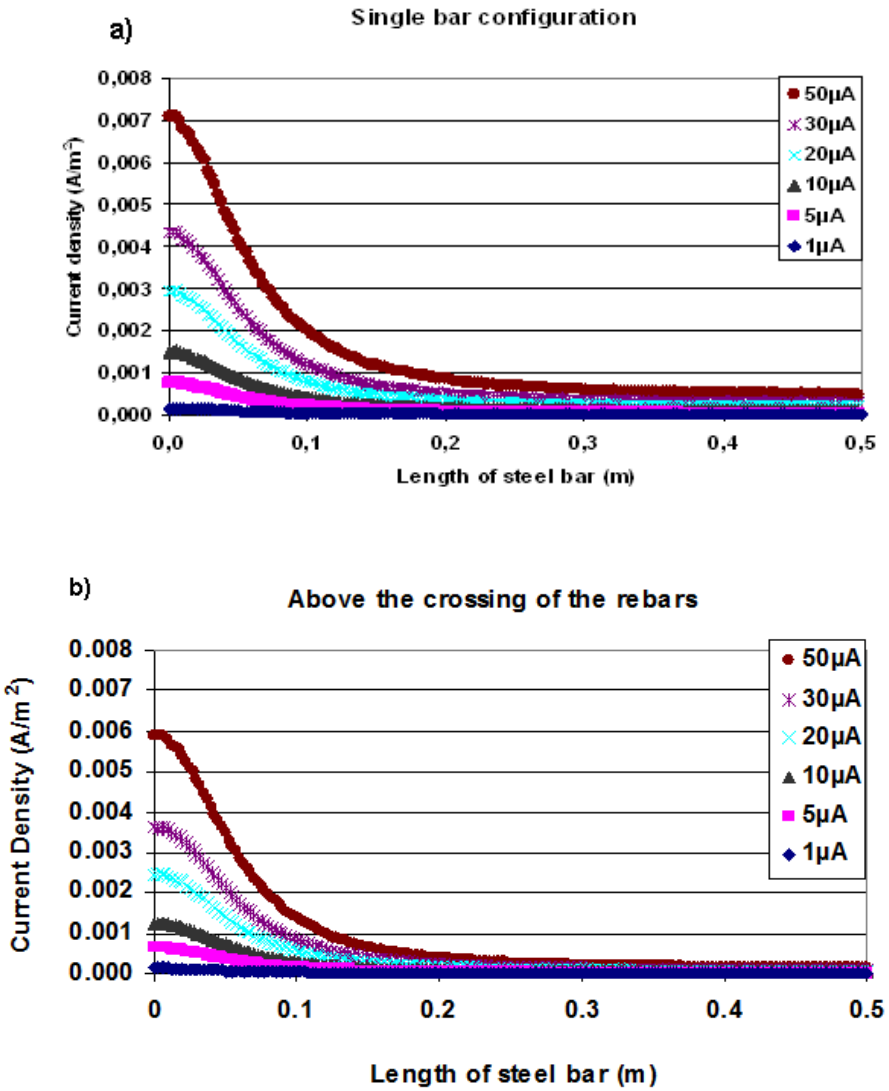

Figure V. 21: Current density distribution along the active steel bar for every value of injected current from the probe with ρ=2000 Ohm.m and e=6 cm for a) a single bar and b) two crossing rebars configuration.

In figure V.21, it is quite obvious that the presence of a second bar diminishes the quantity of current received by the "point of interest" on the upper steel rebar, compared to the current received on the same point but in the two rebars configuration. Figure V.22 demonstrate the current losses between these two types of configuration for concrete cover of 1 and 6cm:

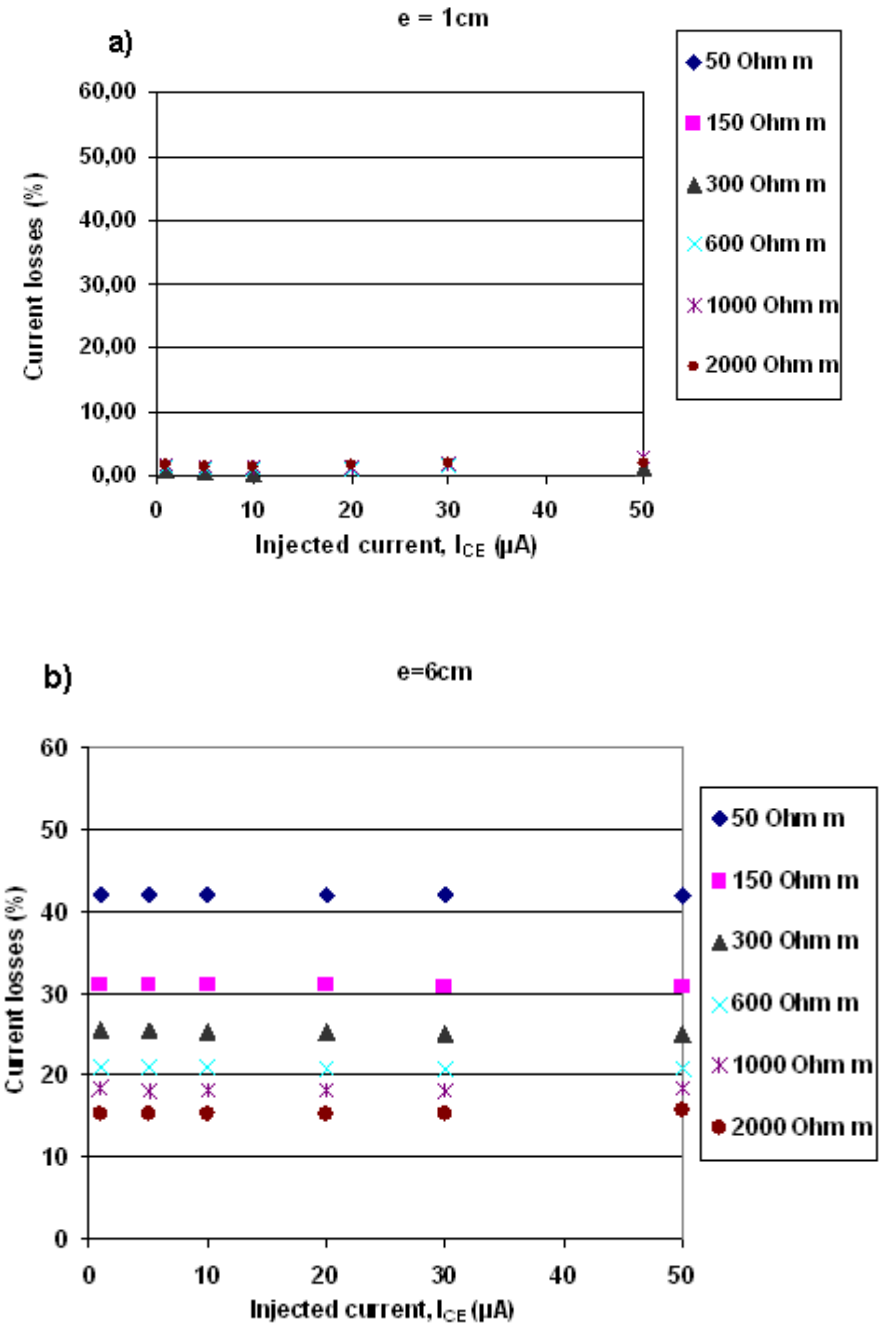

Figure V. 22: Current density losses (%) on the active steel rebar, right under the measurement point on the concrete surface, between the single and two bars configuration for every injected current and resistivity, for a) e=1cm and b) e=6cm.

According to figure V.22, the injected current seems to have a very little- almost no influence on the current losses between the single and the two bar configuration. For a small concrete cover, the current losses may slightly increase as the resistivity augments, but still they remain much less significant (<5%) than those for high concrete cover. Now, when the concrete cover becomes higher, the current losses become less for a high concrete resistivity. It seems that the geometrical effect, observed for the small values of concrete cover, influence in the same way, whether the polarisation measurement takes place on a single or a two rebars configuration. The current losses between the single and the four rebar configuration for a concrete cover of 1 and 6 cm are depicted in the figure V.23:

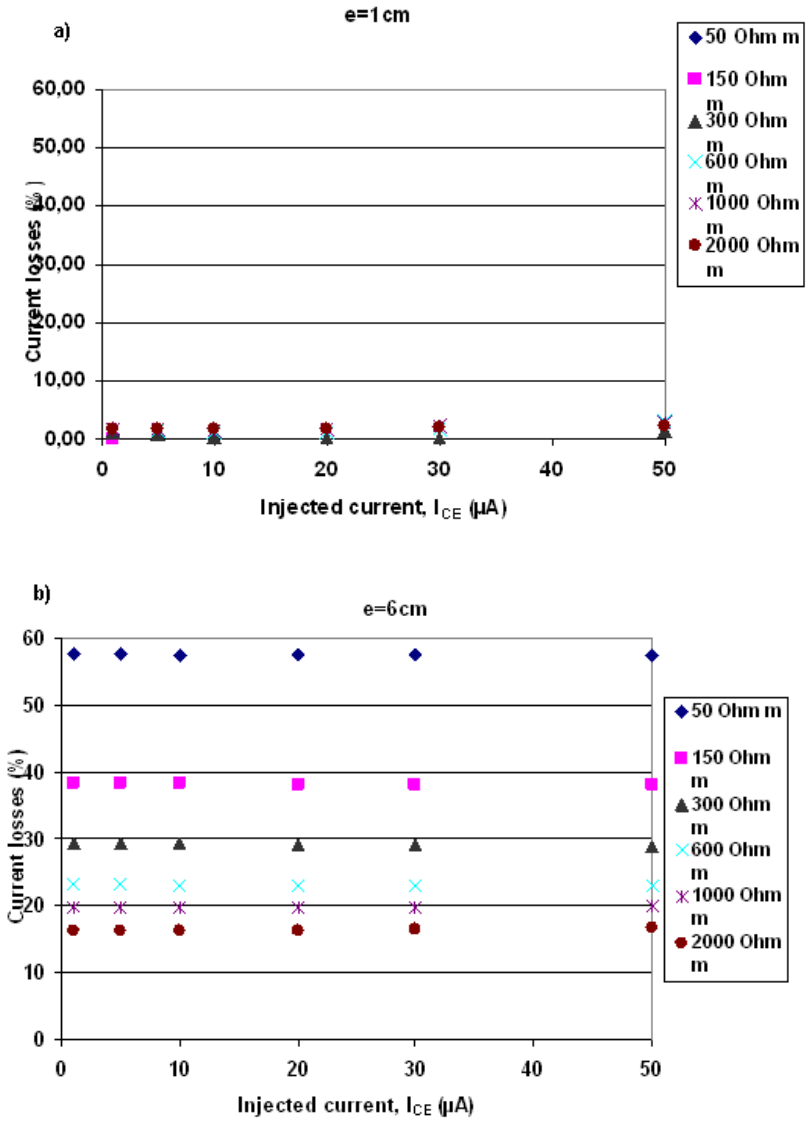

Figure V. 23: Current density losses (%) on the active steel rebar, right under the measurement point on the concrete surface, between the single and four bars configuration for every injected current and resistivity, for a) e=1cm and b) e=6cm.

According to figure V.23, the losses between the single bar and four bar configuration are in the same order of magnitude with those between the single and two bar configuration. Apparently, the reinforcement responds to the excitation, in a similar way, whether it neighbours with one or more reinforcing steel rebars, for any value of concrete resistivity, concrete cover or injected current.

V.3.4.4. Influence of probe's position on the current density distribution

Last but not least, as it in a previous paragraph mentioned, simulations were carried out for another position of the probe on the concrete specimen's surface. In the figure V.24, the current density distribution is plotted along the upper rebar of the two rebar configuration, for these two different positions of the probe: (§V.3.1)

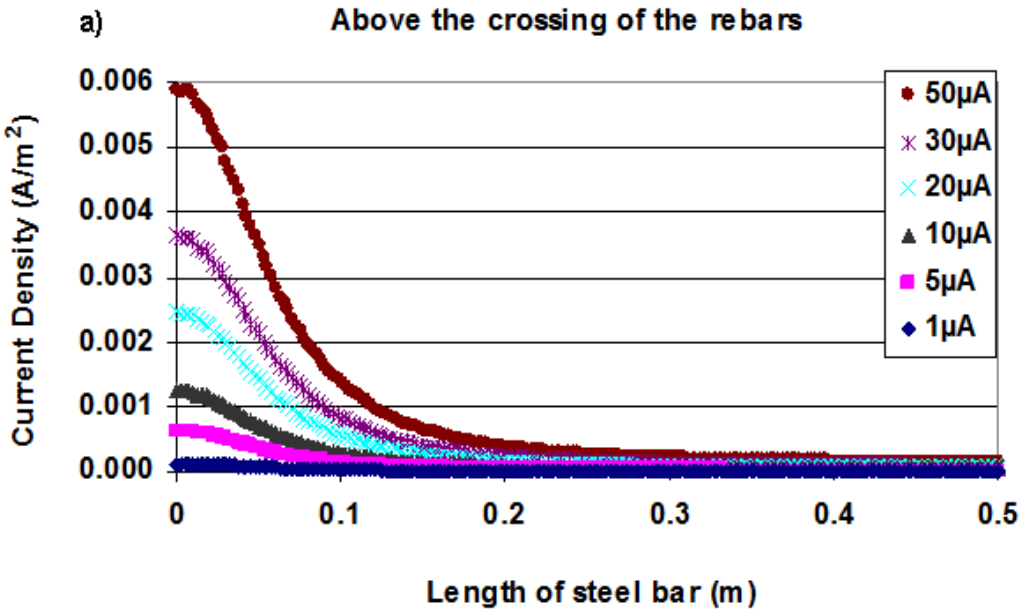

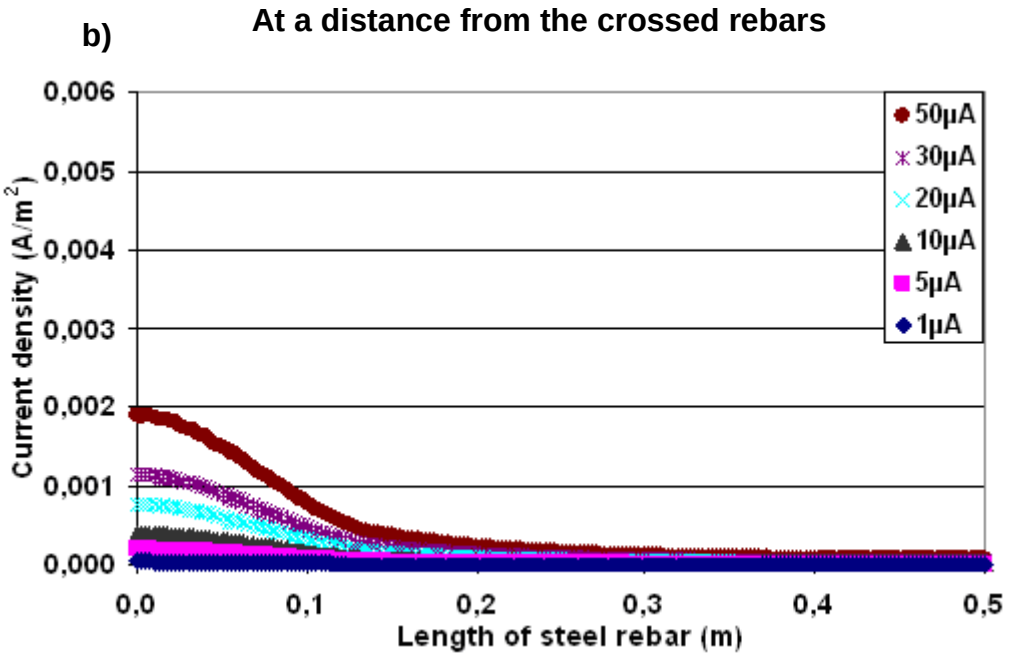

Figure V. 24: Current density distribution along the upper active steel bar for every value of injected current from the probe with ρ=2000 Ohm m and e=6 cm for the probe placed a) above the crossing of the rebars and b) at a distance from the crossed rebars.

As it can be observed from the above graphs, the position of the probe influences significantly the current density distribution, during the measurement, along the upper rebar of the two steel rebar configuration. Obviously, the information is more sensible when the probe is placed above the crossing of the rebars, since, according to the above graphs, the upper rebar receives more injected current for that position of the probe, rather than for a distance of 11.9cm from the axis of upper rebar and 9.4 cm from the axis of lower rebar.

V.3.5. Synthesis

In this paragraph the different numerical simulations of the novel probe proposed for the polarisation resistance measurement were presented. A description of the geometries under study, along with the equations and the applied conditions, was carried out. In addition, the polarisation phenomena of each reinforcement configuration during the numerical experiments of polarisation resistance measurements were studied under the influence of several physical and geometrical parameters. Firstly, it has been demonstrated that the point on the rebar right under the reference electrode exhibits the stronger polarisation. This observation comes into agreement with the results of S. Laurens (2010). Then, it has been stated that, this particular “point of interest” is more polarised, when the concrete resistivity,

the concrete cover and the injected current from the probe get higher. Furthermore, the different states of the reinforcement play no significant role to the way the current signal's attenuation along the rebar takes place, however, the polarisation for an active rebar is less stronger than for a passive rebar. Still a primary validation of the linearity of the proposed model was effectuated. In the following paragraph, the influence of each Butler-Volmer parameter describing the electrochemical state of the steel rebar is more thoroughly examined while in chapter VI the linear aspect is more thoroughly discussed. In addition, the influence of different reinforcement configurations was studied. Apparently, the presence of a reinforcement network around the measurement point affects the current density distribution along the rebar which is under test and diminishes its polarisation as a function of concrete resistivity, concrete cover (or concrete cover to size of CE ratio) and injected current from the probe. Finally, the influence of the position of the probe was tested, affirming that the probe should be positioned right above the steel rebar, in order to obtain precise information about the rebar's reaction to any perturbation. Table V.3 summarizes the influence of each physical and geometrical parameter on the polarisation of the "point of interest" according to the proposed measurement model:

Table V- 3: Influence of physical ad geometrical parameters on the polarisation of the "point of interest" according to the proposed measurement model

Parameters	**Polarisation of the "point of interest"**
Increase in:	
Concrete resistivity	**+***
Concrete cover (or concrete cover/size of CE)	**+**
Injected current	**+**
State of the reinforcement	
Active	**-**
Passive	+
Reinforcement configuration	
Two steel rebar vs. single bar	**-** (for small concrete cover and low resistivity) **-** (for big concrete cover and high resistivity)
Four steel rebar vs. single bar	**-** (for small concrete cover and low resistivity)

	- (for big concrete cover and high resistivity)
Probe's position	
Above the steel rebar	+
At a distance from the steel rebar	-

*+: increase in, -:decrease in

V.4. SENSITIVITY OF THE POLARISATION RESISTANCE MEASUREMENT TO ITS INFLUENCING PARAMETERS VIA NUMERICAL APPROACH: DESIGN OF EXPERIMENTS (DOE)

The main objective of Design of Experiments is to obtain the maximum of information out of a minimum of experiments. In other words, very often, there are problems which demand the simultaneous variation of all the examined parameters (factors), in order to obtain a maximum of information with a minimum of tests. In this particular study, these tests consist of factorial experiments. They are efficient at evaluating the effects and possible interactions of several factors (independent variables). Analysis of experiment design is built on the foundation of the analysis of variance, a collection of models that partition the observed variance into components, according to what factors the experiment must estimate or test. These experiments are carried out within the experiment domain, as it is defined by certain levels of the different factors.

In the following paragraphs an experimental design is developed for the proposed polarisation resistance measurement carried out on an active steel rebar, for the single-bar configuration. A response surface methodology (RSM) will be followed, in order to explore the relationships between several explanatory variables and one or more response variables. The statistical model suggested to use in RSM is a second-degree polynomial model. This model is only a primary approximation, and its use lies into the easiness of its application and estimation (W.Tinsson, 2010).

V.4.1. Experiment design for the estimation of the potential, E_{ar}, on the active steel rebar right under the measurement point

The obtained response, Ea (V), depends mainly on the following six factors:

- Resistivity, ρ, (Ohm m)
- Concrete cover, *e*, (cm)
- Injected current from the probe, I_{CE}, (μA) and
- The corrosion parameters of Butler-Volmer equation (eq.16 and eq.17):

  -Corrosion current, j_{corr},(A/m^2)

  -Tafel constants, β_{aa} (V/dec) and β_{ac} (V/dec)

The various possible ranges of values that could be used for these factors are summarised in the V.4 table. The limits for ρ, e and I_{CE} are the same used for the parametric study of the polarisation resistace measurement model (§V.3.2.) The limits for $\beta_{\alpha\alpha}$, $\beta_{\alpha c}$ and j_{corr} are in accordance with those found in literature (J.Ge,2007), (C.Kim, 2008), (J.Osbolt, 2011), (S.Soleimani, 2010).

TableV- 4 : Ranges of values for the factors influencing the potential response, Ea, (V), on the active steel rebar for the single bar configuration

Factors	Min	Max
ρ (Ohm m)	50	2000
e (cm),	1	6
I_{CE} (μA)	1	50
β_{aa} (V/dec).	0.09	0.3
β_{ac} (V/dec)	0.07	0.125
j_{corr} (A/m^2)	0.0003	0.008

Since an RSM was followed, a second-degree polynomial model was used, taking into account possible interactions between the factors in couple and quadratic effects of each factor. For that reason a D matrix **C**entral subs**C**ribed **C**omposite (CCC) design was implemented to estimate the polynomial model.

The CCC design uses only a fraction of the complete design. In this particular case, a fractional design of resolution V, was applied (Appendix A). Three experiments in the centre of the experimental domain were also carried out, in order to improve the quality and the adjustment analysis of the model. The values were normalised within the interval [-2,2]. The transition from an initial value x to a value within [α,b] is given via: $x^* = 2\left[\frac{2x-(\alpha+b)}{(b-\alpha)}\right]$. This allows the suggestion of the experimental protocol, which consists of the number of

experiments that should be carried out, expressed in their initial unities. For this study, the experimental protocol indicated the realisation of 47 experiments (Appendix A).

According to the method of linear regression, an analysis of variance was carried out (Appendix A).

The obtained elevated coefficient of determination (R2=0.96) shows a sufficient global adjustment of the statistic model (the model that passes from **all** the experimental points has R^2=1). More particularly, the second degree polynomial model, used in this study:

$$Y_1(x)=a_o+a_1x_1+a_2x_2+a_3x_3+a_4x_4+a_5x_5+a_1x_6+a_{12}x_1x_2+a_{13}x_1x_3+a_{14}x_1x_4+a_{15}x_1x_5+a_{16}x_1x_6+a_{23}x_2x_3+a_{24}x_2x_4+a_{25}x_2x_5+a_{26}x_2x_6+a_{34}x_3x_4+a_{35}x_3x_5+a_{36}x_3x_6+a_{45}x_4x_5+a_{46}x_4x_6+a_{56}x_5x_6+a_{11}x_1^2+a_{22}x_2^2+a_{33}x_3^2+a_{44}x_4^2+a_{55}x_5^2+a_{66}x_6^2$$

Where: a_o: the general average effect

a_1,a_2 etc: the linear effect of each factor

a_{11},a_{22} etc: the quadratic effect of each factor

a_{12},a_{13} etc: the effect of interaction between the factors x_1 and x_2, x_1 and x_3 etc

These parameters of the model are estimated as follows:

Table V- 5: Estimators, Standard deviation, t and p-values for each parameter.

Parameters	Estimators	Standard deviation	t (Student Test)	p-value
a_0	-0.407	0.2150	-2.1710	0.0428
a_1	0.000055	0.00006	0.9232	0.3675
a_2	0.0043	0.0241	0.1804	0.8588
a_3	0.0031	0.0024	1.3184	0.2031
a_4	0.3274	0.6040	0.5421	0.5940
a_5	0.8327	2.9297	0.2842	0.7793
a_6	-26.59	15.1076	-1.7602	0.0945
a_{12}	-0.0000076	0.00000491	-1.5397	0.1401
a_{13}	0.00000078	0.0000005	1.5587	0.1356
a_{14}	0.000128	0.00012	1.0971	0.2863
$a_{1\,5}$	0.000057	0.00045	0.1257	0.9013
a_{16}	-0.0048	0.0032	-1.5142	0.1464
a_{23}	-0.000613	0.000195	-3.1387	0.0054
a_{24}	-0.0559	0.0455	-1.2279	0.2345
a_{25}	-0.0268	0.1774	-0.1513	0.8813
a_{26}	1.8176	1.2419	1.4635	0.1597
a_{34}	0.0074	0.0046	1.5836	0.1298
a_{35}	0.0027	0.0181	0.1484	0.8836
a_{36}	-0.271	0.1267	-2.1393	0.0456
a_{45}	-0.108	4.2159	-0.0256	0.9798

$\mathbf{a_{46}}$	-17.67	29.59	-0.5970	0.5576
$\mathbf{a_{56}}$	-21.28	114.98	-0.1851	0.8551
$\mathbf{a_{11}}$	-0.000000017	0.00000001	-1.5589	0.1355
$\mathbf{a_{22}}$	0.0012	0.0016	0.7373	0.4699
$\mathbf{a_{33}}$	-0.00000495	0.000017	0.2890	0.7757
$\mathbf{a_{44}}$	-0.6026	0.9324	-0.6463	0.5258
$\mathbf{a_{55}}$	-3.4157	13.6124	-0.2509	0.8046
$\mathbf{a_{66}}$	3263.8	693.54	4.7061	0.0001538

At the knowledge of these parameters, the potential E_{ar} may be predicted (least squares method), via the following model:

$$\mathring{Y}_1(x)=-0.407+0.000055x_1+0.0043x_2+0.0031x_3+0.3274x_4+0.8327x_5-26.59x_6+0.00000756x_1x_2+0.00000078x_1x_3+0.000128x_1x_4+0.0000572x_1x_5-0.0048x_1x_6-0.000613x_2x_3-0.0559x_2x_4-0.0268x_2x_5+1.8176x_2x_6+0.0074x_3x_4+0.0027x_3x_5-0.2711x_3x_6-0.1080x_4x_5-17.6674x_4x_6-21.2793x_5x_6-0.000000017x_1^2+0.0012x_2^2-0.00000495x_3^2-0.6026x_4^2-3.4157x_5^2+3263.8x_6^2$$

In figure V.25, the potential response, E_{ar}, of each numerical experiment is traced versus the potential values, $\mathring{E}_{ar}$, predicted from the previous model:

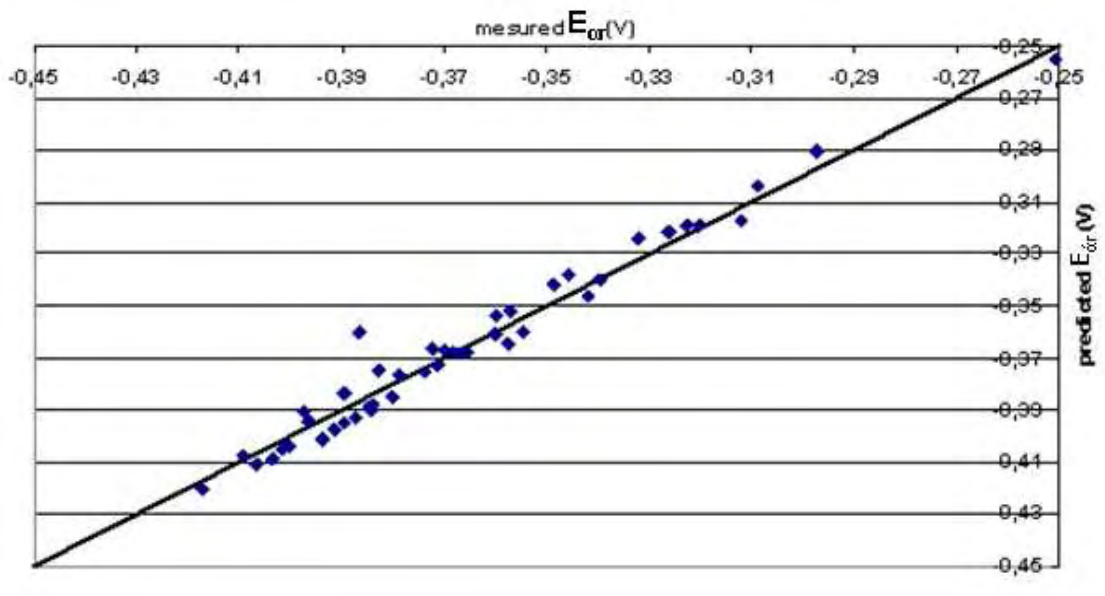

Figure V. 25: Potential response, E_{ar}, (V) of each numerical experiment vs. potential $\mathring{E}_{ar}$ (V) predicted from the statistical model.

Often, the use of a simpler model is desirable. In that case, it could be possible to eliminate those parameters that are less significant. The significance of the parameters is determined according to the student test (third column of table V.5). W. Tinsson has determined a threshold of *t= 5(%)*; those parameters whose t- value is a lot less than the threshold, can be

omitted from the statistical model. In this specific study, a_1, a_2, a_4, a_5, a_{15}, a_{25}, a_{35}, a_{45}, a_{46}, a_{56}, a_{22}, a_{33}, a_{44}, and a_{55} can be discarded.

On the other hand, the strongest influence on the potential response is observed for the parameter of the corrosion current density; it's linear (a_6) and quadratic (a_{66}) effects present a high t value. Then, the injected current (a_3) and resistivity (a_1) follow as the next most significant parameters; it is quite remarkable that all possible couples of the physical parameters-concrete cover included exhibit a strong influence on the potential response measured according to the proposed probe. For example, the effect of concrete cover (a_{23}) on the potential response changes significantly (t-value~-3.14) as a function of the current injected from the probe. That was clearly proven in figure V.23, where the geometric effect becomes quite intense for a small concrete cover and a high injected current (minus indicates that the effect becomes significant for an opposite tendency of the values of the parameters).

Furthermore, their t-values are, more or less, in the same order of magnitude. This could mean that an increase, for example of 20% in resistivity or concrete cover or injected current could move the potential response around 20% towards to more electropositive potential values.

In addition, it is clearly seen that the Tafel constants of the Butler Volmer equation do not play any important role on the potential response of the steel rebar.

Figure V.26 illustrates the potential response of the active steel rebar, predicted from the model, for the range of values of resistivity, injected current and corrosion current density of the steel rebar indicated in table V.4 .The parameters β_{aa} ; β_{ac}, and e are fixed at 0.2 V/dec, 0.1 V/dec and 3cm respectively. The black points correspond to the potential responses for the experimental domain, indicated by the CCC design.

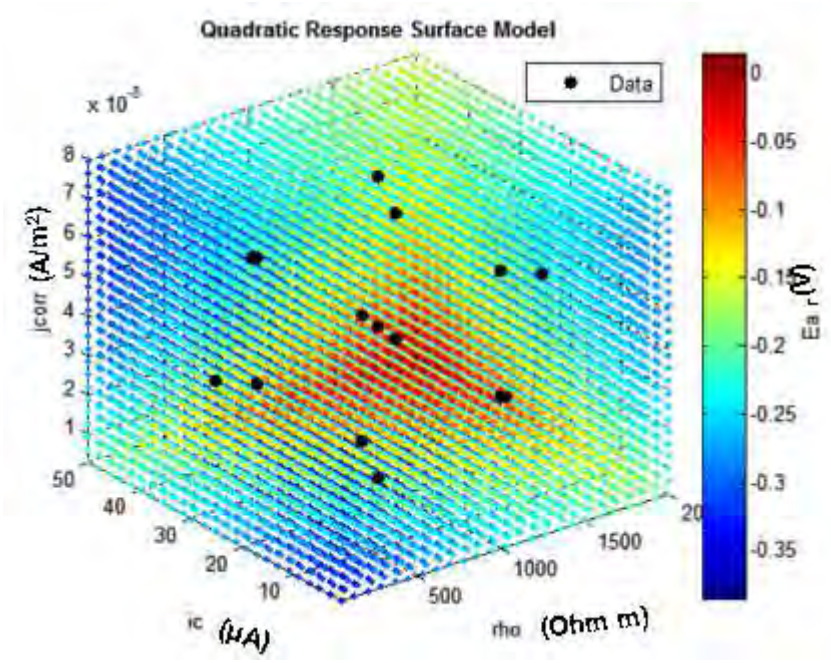

Figure V. 26: Quadratic surface model for the potential response, $\dot{E}_{ar}$ (V) as a function of resistivity, injected current and corrosions current density. β_{aa}; β_{ac}, and e are fixed at 0.2 V/dec, 0.1 V/dec and 3cm respectively. The black points correspond to the CCC design.

V.4.2. Experiment design for the estimation of the current density, j_{ar}, on the active steel rebar right under the measurement point

Similarly to the case of the potential response, E_{ar}, an RSM methodology was also followed for the estimation of the current density, j_{ar} on the steel rebar, right under the measurement point. A fractional CCC design of resolution V (Appendix A) was built for the same ranges of values, presented in table V.4. The experimental protocol and the current density values obtained after each numerical experiment and the results of the analysis of variance are given in the Appendix. For the current density response, the obtained coefficient of determination (R^2=0.988) shows a better global adjustment of the statistic model than for the case of the potential response.

The estimators for the parameters of the following statistic model are given in table V.6.

$$Y_2(x)=a_o+a_1x_1+a_2x_2+a_3x_3+a_4x_4+a_5x_5+a_1x_6+a_{12}x_1x_2+a_{13}x_1x_3+a_{14}x_1x_4+a_{15}x_1x_5+a_{16}x_1x_6+a_{23}x_2x_3+a_{24}x_2x_4+a_{25}x_2x_5+a_{26}x_2x_6+a_{34}x_3x_4+a_{35}x_3x_5+a_{36}x_3x_6+a_{45}x_4x_5+a_{46}x_4x_6+a_{56}x_5x_6+a_{11}x_1^2+a_{22}x_2^2+a_{33}x_3^2+a_{44}x_4^2+a_{55}x_5^2+a_{66}x_6^2$$

Table V- 6: Estimators, Standard deviation, t and p-values for each parameter.

Parameters	Estimators	Standard deviation	t (Student Test)	p-value
$\mathbf{a_0}$	-0.0092	0.0126	0.7346	0.4716
$\mathbf{a_1}$	0.0000068	0.0000035	1.9484	0.0663
$\mathbf{a_2}$	-0.0012	0.0014	-0.8306	0.4165
$\mathbf{a_3}$	0.00048	0.00014	3.4531	0.0027
$\mathbf{a_4}$	-0.0605	0.0353	-1.7163	0.1024
$\mathbf{a_5}$	-0.1644	0.1711	-0.9608	0.3487
$\mathbf{a_6}$	1.0535	0.8821	1.1943	0.2470
$\mathbf{a_{12}}$	-0.00000106	0.00000029	-3.6991	0.0015
$\mathbf{a_{13}}$	0.00000013	0.000000029	4.5018	0.00024
$\mathbf{a_{14}}$	-0.0000032	0.0000068	-0.4710	0.6430
$\mathbf{a_{1\,5}}$	-0.0000016	0.000027	-0.0598	0.9530
$\mathbf{a_{16}}$	-0.000092	0.000185	-0.4941	0.6269
$\mathbf{a_{23}}$	-0.000097	0.000011	-8.4854	0.000000069
$\mathbf{a_{24}}$	0.0057	0.0027	2.1602	0.0437
$\mathbf{a_{25}}$	-0.000415	0.0104	-0.0401	0.9685
$\mathbf{a_{26}}$	-0.1344	0.0725	-1.8533	0.0794
$\mathbf{a_{34}}$	-0.00073	0.00027	-2.6790	0.0148
$\mathbf{a_{35}}$	-0.000038	0.0011	-0.0355	0.9720
$\mathbf{a_{36}}$	0.0176	0.0074	2.3831	0.0278
$\mathbf{a_{45}}$	0.0913	0.2461	0.3709	.07148
$\mathbf{a_{46}}$	0.8948	1.7279	0.5178	0.6105
$\mathbf{a_{56}}$	-1.4326	6.7130	-0.2134	0.8333
$\mathbf{a_{11}}$	-0.0000000011	0.00000000063	-1.7469	0.0968
$\mathbf{a_{22}}$	0.0003	0.000096	3.1269	0.0056
$\mathbf{a_{33}}$	0.00000136	0.00000099	1.3583	0.1903
$\mathbf{a_{44}}$	0.0943	0.0544	1.7328	0.0993
$\mathbf{a_{55}}$	0.7836	0.7948	0.9860	0.3365
$\mathbf{a_{66}}$	-41.94	40.49	-1.0358	0.3133

At the knowledge of these parameters, the current density j_{ar} may be predicted (least squares method), via the following model:

$$\mathring{Y}_2(x)=-0.0092+0.0000068x_1-0.0012x_2+0.00048x_3-0.0605x_4-0.1644x_5+1.0535x_6-0.00000106x_1x_2+0.00000013x_1x_3-0.0000032x_1x_4-0.0000016x_1x_5-0.000092x_1x_6-0.000097x_2x_3+0.0057x_2x_4-0.000415x_2x_5-0.1344x_2x_6-0.00073x_3x_4-0.000038x_3x_5+0.0176x_3x_6+0.0913x_4x_5+0.8948x_4x_6-1.4326x_5x_6-0.0000000011x_1^2+0.0003x_2^2+0.00000136x_3^2+0.0943x_4^2+0.7836x_5^2-41.94x_6^2$$

In the figure V.27, the current density, j_{ar}, of each numerical experiment is plotted versus the current density values, $\hat{j}_{ar}$, predicted from the previous model:

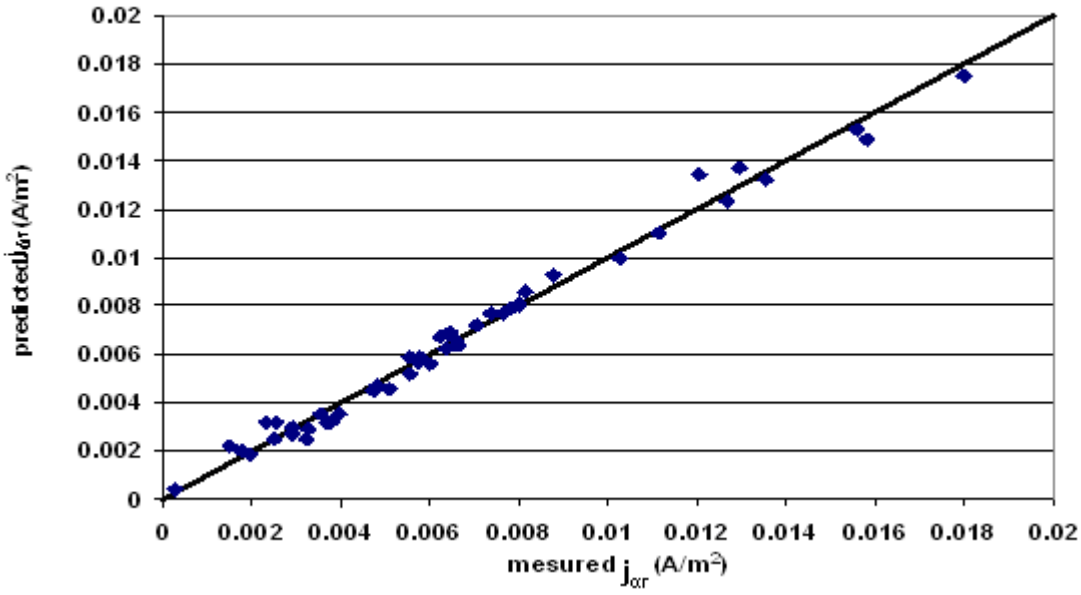

Figure V. 27: Current density response, j_{ar}, (A/m^2) of each numerical experiment vs. potential $\hat{j}_{ar}$ (A/m^2) predicted from the statistical model

As in the case of potential response, it could be also possible to eliminate those parameters less significant and simplify the statistic model for the current density response. Based on the student test (third column of table V.6) a_0, a_2, a_5, a_{14}, a_{15}, a_{16}, a_{25}, a_{35}, a_{45}, a_{46}, a_{56} et a_{55} could be eliminated, since their *t* is much less than the defined threshold.

On the other hand, current density response seems to be strongly influenced by the injected current from the probe. Furthermore, it is indicated that this factor influences strongly the effect of each other physical parameter on the current density response. For example, in figure V.13, it has been demonstrated that a high concrete resistivity leads to a strong polarisation of that "point of interest" on the steel rebar. The polarisation becomes even stronger for a high injected current. The high positive student test of the effect of resistivity coupled with the injected current confirms that behaviour. In addition, the interaction between the resistivity and the concrete exhibits a high t value, confirming that the strongest polarisation is achieved for a steel rebar embedded in concrete with low resistivity and high concrete cover. As far as the Butler-Volmer parameters are concerned, the linear and quadratic effects of β_{aa} and corrosion current density, j_{corr}, seem to be much stronger than the effect of β_{ac}. This could be expected, since an anodic polarisation is realised during the experiments (§I.2.2).

Last but not least, it can be noted that any change of 20% in the injected current or resistivity or anodic Tafel constant may lead to 100% change in the predicted value of current density response. Apparently, the statistical model predicting the current density distribution on the

active steel rebar exhibits a rather low tolerance to any possible changes of its influencing parameters. At the same, the potential response of the rebar is proportionally sensible to an increase or decrease of the different effects.

The graph (V.28) illustrates the current density on the "point of interest" on the active steel rebar surface, predicted from the model, for the range of values of resistivity, injected current and anodic Tafel constant of the active steel rebar indicated in table V.4. The parameters j_{corr}, β_{ac}, and e are fixed at 0.005A/m^2, 0.1 V/dec and 3cm respectively. The black points correspond to the potential responses for the experimental domain, indicated by the CCC design.

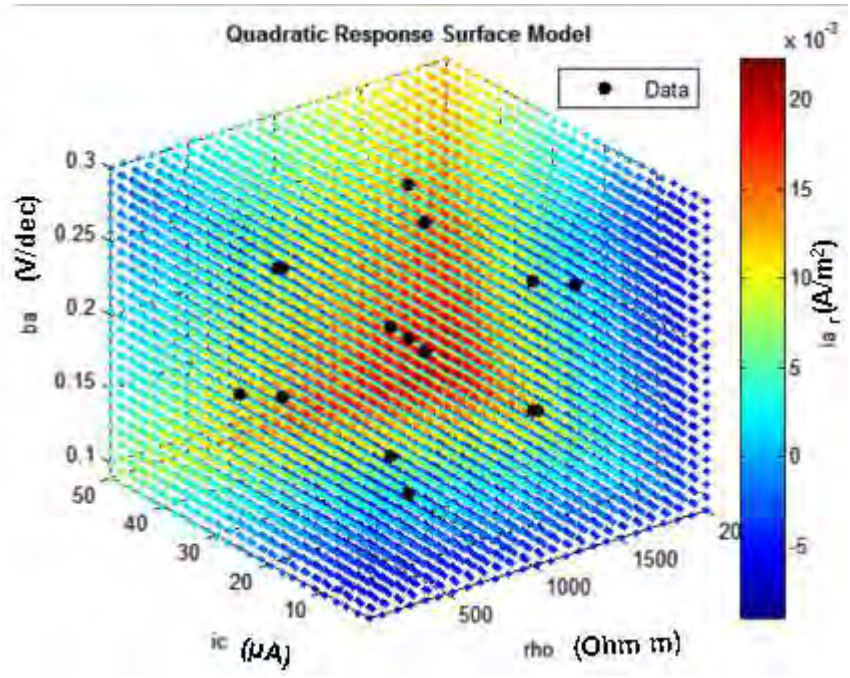

Figure V. 28: Quadratic surface model for the current density, $\hat{j}_{ar}$ (A/m^2) as a function of resistivity, injected current and anodic Tafel constant. j_{corr}, β_{ac}, and e are fixed at 0.005A/m^2, 0.1 V/dec and 3cm respectively. The black points correspond to the CCC design.

V.4.3 Synthesis

In this paragraph the sensibility of the proposed polarisation resistance measurement to several factors was examined via the method of experimental design. A RSM was followed and two second degree polynomial models were built to predict the potential response and the current density on an uniformly active steel rebar, right under the measurement point, in a single bar configuration, after the injection of current from the probe. The effects of the concrete resistivity, concrete cover, injected current, anodic and cathodic Tafel constants and the corrosion current density were examined. Possible effects from the interactions between

the factors, combined one by one, and quadratic effects of each factor were also taken into account. A fractional CCC design of resolution V was used to determine the different experiments. According to the analysis of variance, the statistic model was better adjusted for the current density estimation than for the potential response. According to the student test results, several effects were discarded in order to simplify the statistic model. **The potential response model seems to be sensitive to the effect of the corrosion current density, the injected current and resistivity**. The effects induced by the coupling of the physical influence are also remarkable. **In the case of the current density prediction model, the injected current affects the most the model's response**. Concrete resistivity and anodic Tafel constant influence also strongly the current density model. If a change of 20% is applied in one of the most influencing parameters, the potential model's response will by influenced proportionally, while the current density model's response will change by 100%. This observation is highly important when it comes to the development of a protocol for measuring the polarisation resistance under real conditions (chapter VI). The application of the proposed polarisation resistance measurement model requires the knowledge of resistivity, concrete cover and injected current. Thus, it was indicated that an error of less than 20% in the measurement of resistivity, estimation of concrete cover (chapter III) and the injection of the right current from the probe is considered as acceptable, in order to consequently evaluate as more correctly as possible the real values of potential and current density on the steel rebar. In addition, it is clearly demonstrated that the corrosion of the steel rebars (j_{corr}) also influences, in its turn, the measurement model. Finally, the predicted responses are traced as a function of their influencing parameters for all the range of their values.

Table V.7 provides with a list of the 4 most significant parameters (in descending order), on which according to DOE, the responses E_{ar} and j_{ar} depend:

Table V- 7: The 4 most significant parameters influencing the responses E_{ar} and j_{ar} respectively

Significant parameters in descending order / **Responses:**	**Potential, E_{ar} (V)**	**Current density, j_{ar} (A/m^2)°**
1	j_{corr}^2	e-I_{CE}
2	e-I_{CE}	ρ-I_{CE}
3	I_{CE}-j_{corr}	I_{CE}
4	j_{corr}	e^2

V.5. CALCULATION OF POLARISATION RESISTANCE ON THE SURFACE OF STEEL REBAR REINFORCEMENT AND CONSTRUCTION OF ABACUSES

The polarisation resistance is calculated according to the equation:

$$Rp = \frac{\Delta E_p}{j_{ar}} = \frac{E_{ar} - Ecorr}{j_{ar}} \qquad \text{(eq. 45)}$$

Where:

- ΔE_p (polarisation) is equal to the difference between E_{ar} at the "point of interest" on the reinforcement's surface and E_{corr} of the reinforcement,
- j_{ar} is equal to the current density at the "point of interest" on the surface of the steel rebar.

Via the numerical simulations, it is possible to establish those relationships, allowing to pass from measurement point on the concrete surface to the steel bar surface while abacuses and correction laws can be built up, involving rebar's concrete cover, concrete cover resistivity and injected current from the probe. The new established relationships will provide all the real information-of the reinforcement's reaction to the polarization- necessary for the calculation of the polarization resistance.

In the following paragraphs, the creation of these new relationships and the built up of the abacuses are presented for a polarization resistance measurement taking place above the middle of a single active or passive rebar and above the crossing of two crossed active steel rebars.

V.5.1. Correction laws and abacuses for a single active rebar

As it was previously shown, the potential response on the steel rebar is quite affected by an interaction between the resistivity and injected current (t=1.5587). Thus, the ohmic drop, ΔE_Ω, can be traced as a function of concrete resistivity, for every injected current and for each concrete cover. The ohmic drop ΔE_Ω (V) corresponds to the difference between the potential response measured by the reference electrode on the concrete surface and the real potential response on the steel rebar after the polarization:

$$\Delta E_\Omega = E_{RE} - E_{ar} \quad \text{(eq. 46)}$$

Where: E_{RE} (V) the potential response measured by the reference electrode on the concrete surface after polarisation

E_{ar} (V) the real potential response on the steel rebar after polarisation.

Figure V.29 depicts two graphs, where the ohmic drop is plotted versus the concrete resistivity and for every injected current, for a single active reinforcing rebar with a concrete cover of 1 and 6 cm:

a)

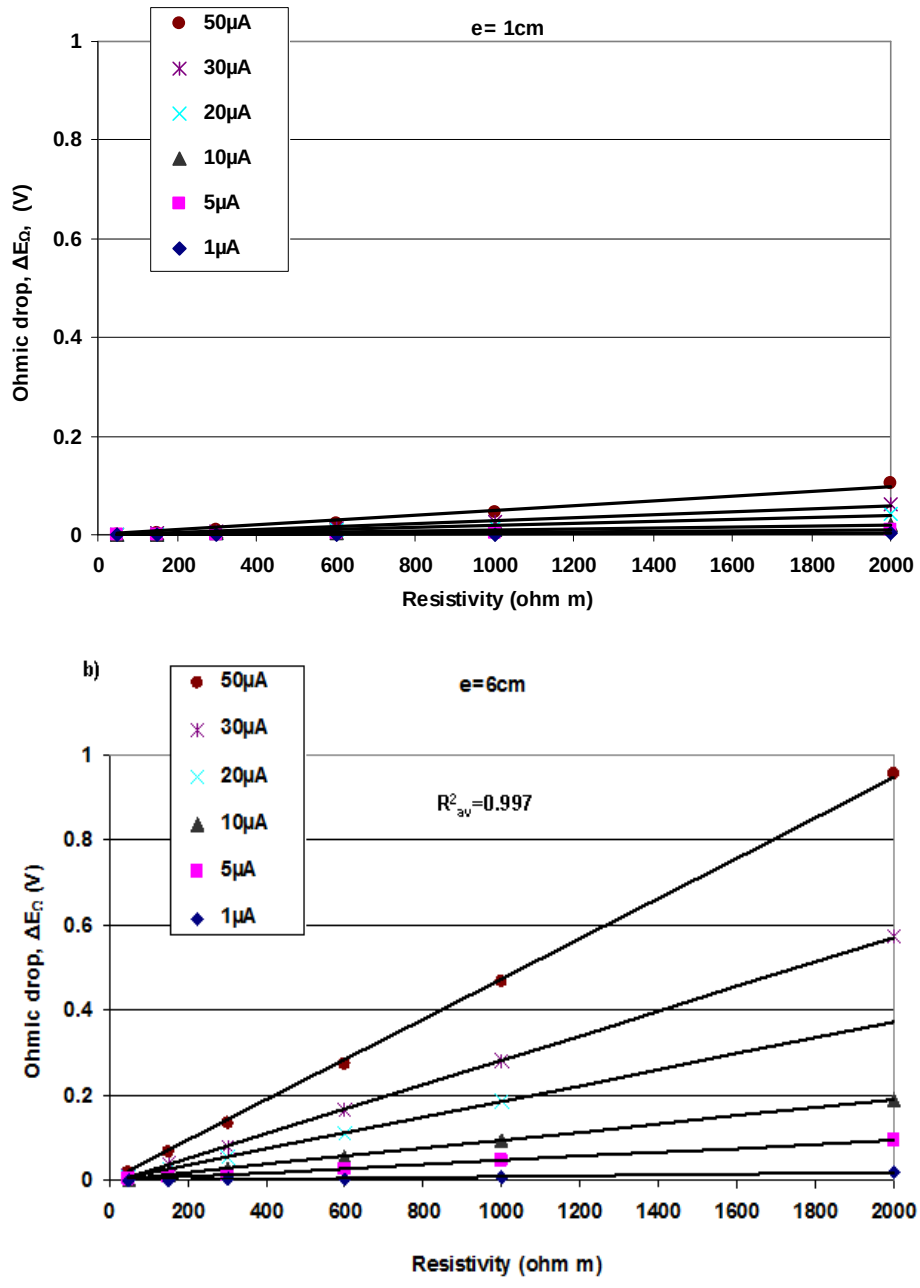

Figure V. 29: Ohmic drop versus resistivity for every injected current from the probe towards a single active steel rebar, embedded at a) 1cm and b) 6 cm, with the probe above the middle of the single bar.

According to figure V.29, the ohmic drop increases as the concrete resistivity and injected current increase too. As it can be seen, for every injected current, linear relationships can be plotted with a positive slope. These linear regressions are characterised by a very elevated coefficient of determination R^2 and thus they can be described by the following equation:

$$\Delta E_{\Omega} = E_{RE} - E_{ar} = k \cdot \rho \qquad \text{(eq. 47) or } E_{ar} = E_{RE} - k \cdot \rho \quad \text{(eq.48)}$$

The equation 48, leads from the measured potential value on the concrete surface to the real value of potential on the steel rebar. From the graphs of figure 54, abacuses can be built up, which will provide with the value of the coefficient *k*. More particularly, the slope *k* of each curve is plotted versus the concrete cover, for each injected current. Figure 86 depicts the abacus of $k=f(e,I_{CE})$ for one active single bar:

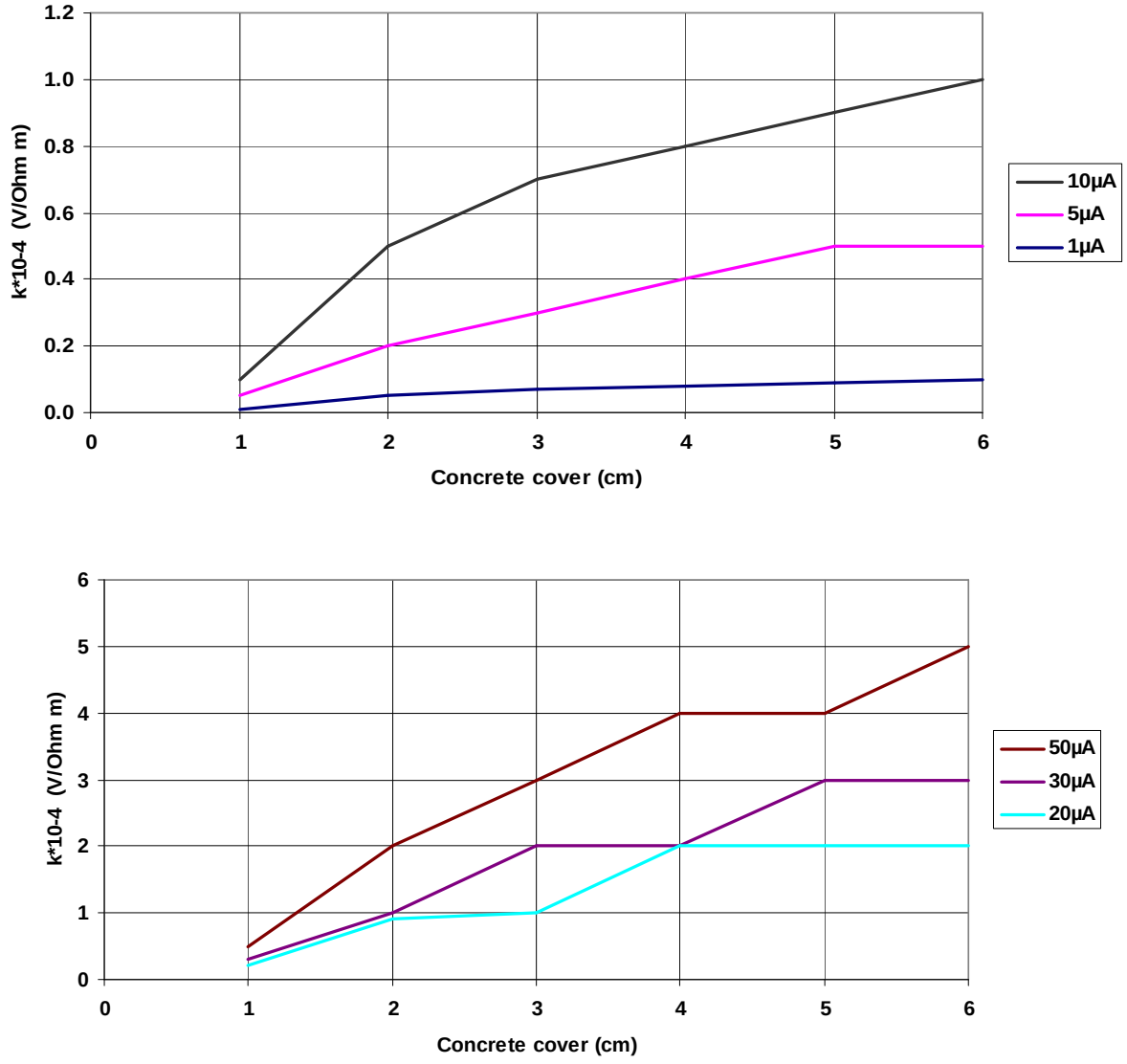

Figure V. 30: Abacus of coefficient k as a function of concrete cover for a) 1-5-10 μA and b) 20-30-50μA of the injected current from the probe towards a single active steel rebar. Region with reduced efficiency of the abacus is noted in red.

A similar procedure is followed in order to obtain the real current density on that "point of interest" on the steel rebar. The experimental design has demonstrated a rather strong effect of the interactions of resistivity with the injected current (t=4.5018) and resistivity with the concrete cover (t=-3.6991). The following graphs depict the curves plotted, for the $\ln(j_{ar}/i_{CE})$ versus the concrete cover, for each concrete resistivity and for 1 and 50 μA injected. At this stage it is important to precise that i_{CE} corresponds to the density of the injected current, calculated according to:

$$i_{CE} = \frac{I_{CE}}{S_{CE}} \qquad \text{(eq. 49)},$$

Where: S_{CE} is the surface of the counter electrode (m^2):

a)

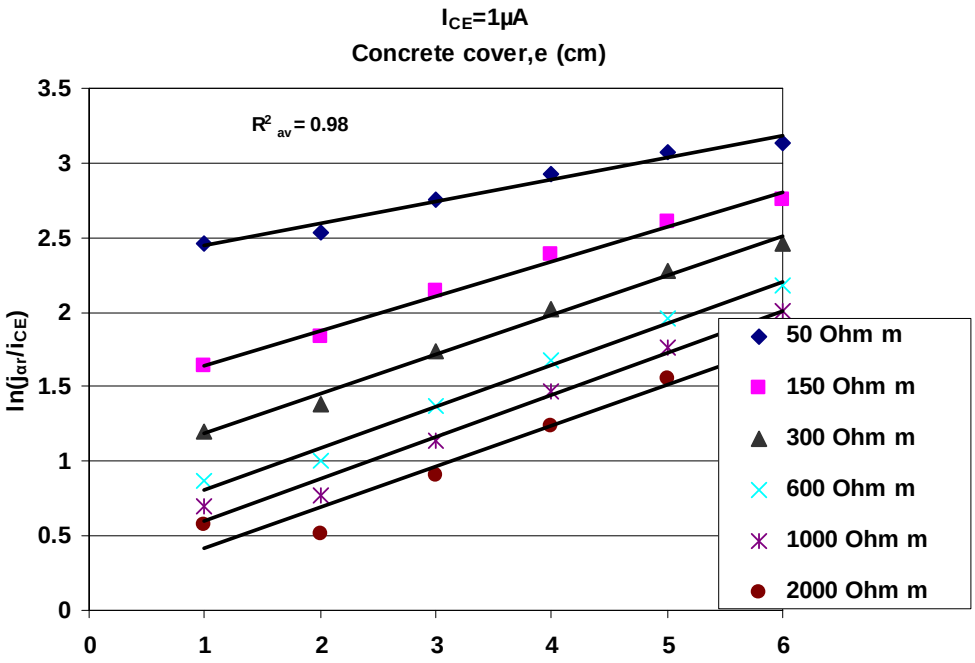

b)

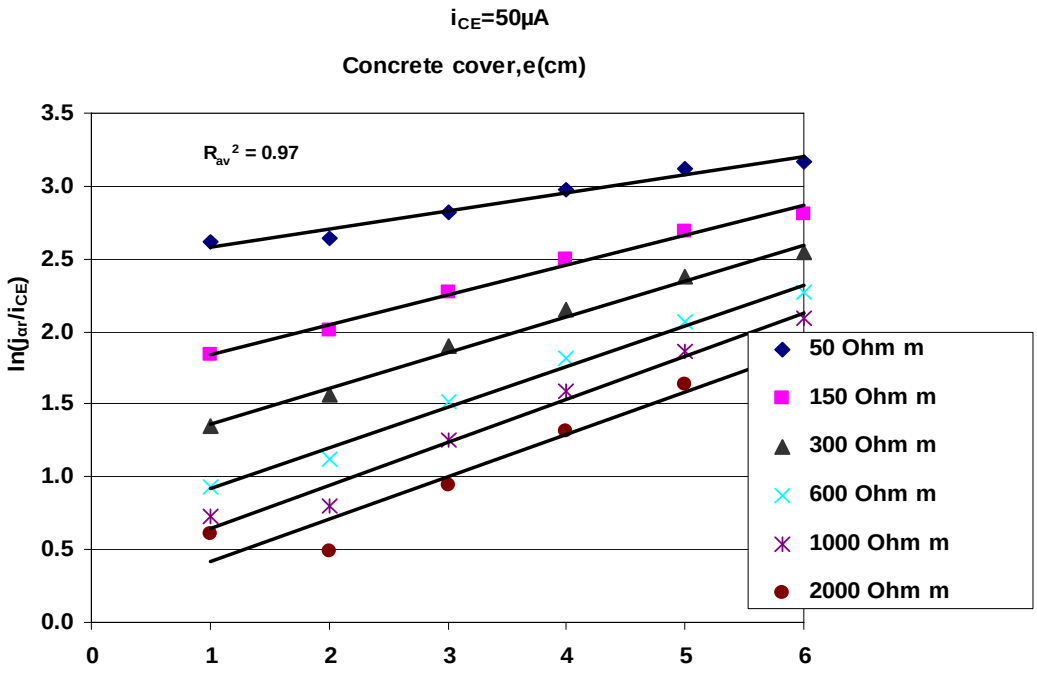

Figure V. 31: Ln(j_{ar}r/i_{CE}) versus concrete cover for each concrete resistivity and for an injected current of a)1 and b) 50μA, towards the single active steel rebar, with the probe above the middle of the single bar.

According to figure V.31, it seems that a linear tendency exists between the ln(j_{ar}/i_{CE}) and concrete cover, for each value of the resistivity since the coefficient of determination R^2 is quite elevated; the current density ratio augments as the resistivity increases and the concrete cover diminishes. The deviation from this tendency, observed for 1cm, is attributed to the geometric effect, which becomes more intense as resistivity reaches high values, such as $\rho \geq$ 800 Ohm m (see also §V.3.4.1). That signifies that there will be difficulties in the application of the model in the case of concrete resistivity higher than 800 Ohm m. Therefore, the equation that can be derived from the curves of figure V.31 and can lead to the evaluation of the current density on the steel rebar surface, right under the measurement point, is eq.50:

$$\ln\left(\frac{j_{ar}}{i_{CE}}\right) = A + B \cdot e \qquad \text{(eq. 50)}.$$

Based on the previous plots, abacuses were created in order to provide the constants A and B, so as to be integrated in the equation 50. The abacuses were built as a function of resistivity:

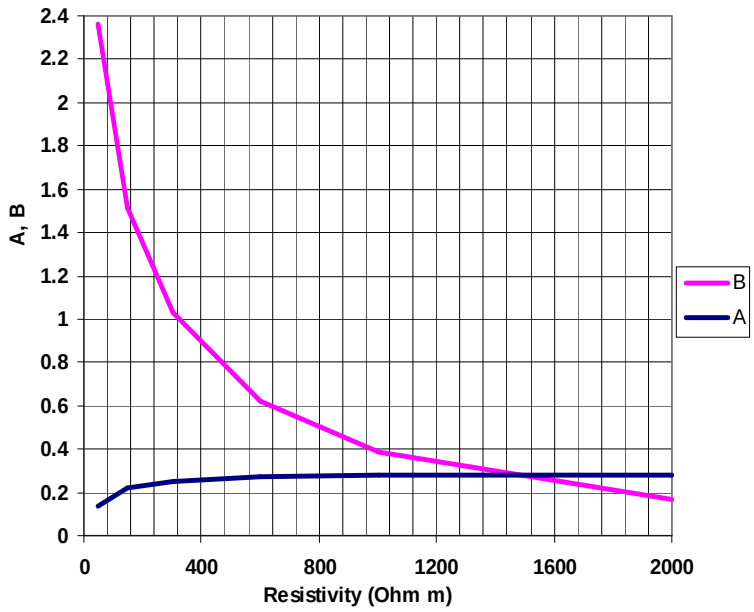

Figure V. 32: Abacus of coefficients A and B as a function of concrete resistivity, for a single active steel rebar.

As it is obvious, since the model used a certain range of the parameters concrete resistivity, concrete cover and injected current , the abacuses of k, A and B are built for the same ranges. In other words, **the abacuses should be used only when concrete resistivity is $50 \leq \rho \leq 2000$ Ohm m,, concrete cover $1 \leq e \leq 6$cm and injected current $1 \leq I_{CE} \leq 50\mu A$**. The same applies for the abacuses built in §IV.5.2 and §IV.5.3.

V.5.2. Correction laws and abacuses for a single passive rebar

As for the case of the active bar, the same procedure was followed in order to establish correction laws and abacuses for a single passive rebar. In the following graph, the ohmic drop is plotted against resistivity for each injected current and for a concrete cover of 6cm. The same kind of graphs was traced for all concrete covers:

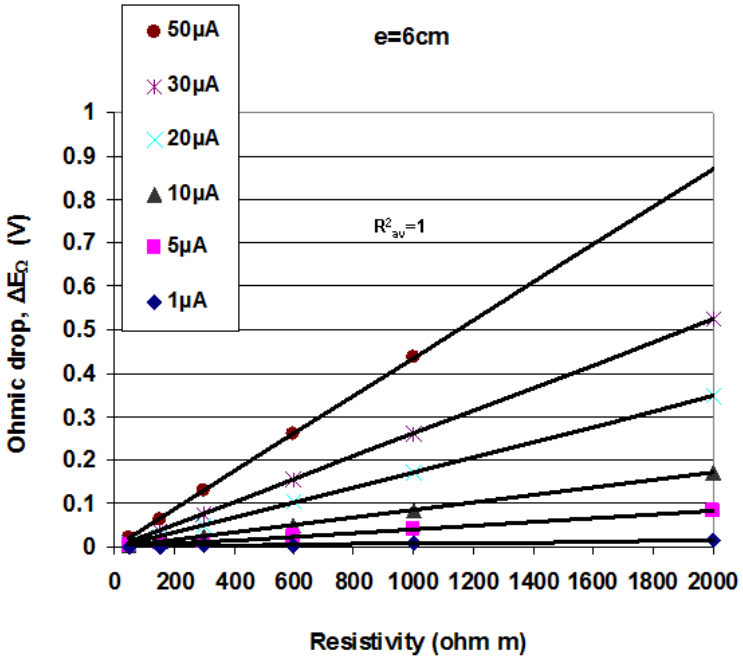

Figure V. 33: Ohmic drop versus resistivity for every injected current from the probe towards a single passive steel rebar, embedded at 6 cm with the probe above the middle of the single bar.

As it can be seen, the graph in figure V.33 exhibits the same (linear) tendency with that of the active steel rebar with again a perfect coefficient of determination (R^2=1). As a result, equation 32 can also be used in the case of a passive steel rebar. Then the abacus of the coefficient k is constructed:

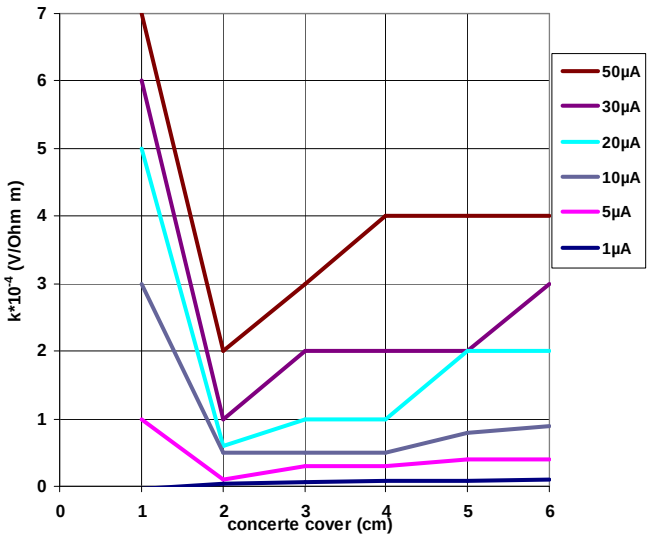

Figure V. 34: Abacus of coefficient k as a function of concrete cover for each injected current from the probe towards a single passive steel rebar.
Region with reduced efficiency of the abacus is noted in red.

According to the figure V.34, contrary to the active bar, it seems that coefficient k gets smaller values for the passive bar. In addition, a deviation from the general tendency is depicted for concrete covers between 1 and 2cm (1<e<2cm).

In the figure V.35, the ratio $\frac{j_{ar}}{i_{CE}}$ is plotted as a function of concrete cover for each resistivity for an injected current of 50 μA. The same graphs were created for all values of injected current:

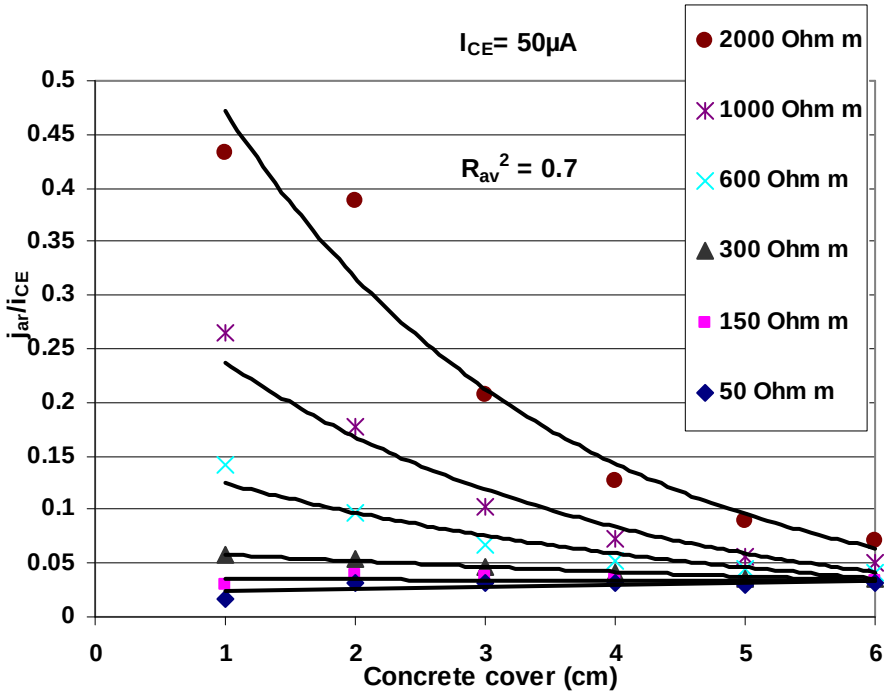

Figure V. 35: j_{ar}/i_{CE} versus concrete cover for each concrete resistivity and for an injected current of 50μA towards the single passive steel rebar, with the probe above the middle of the single bar.

The above obtained curves can be characterised by the equation:

$$\frac{j_{ar}}{i_{CE}} = a \cdot e^{b} \qquad \text{(eq. 51)}$$

It has to be stated that, according to figure V.35, the equation 51 adjusts less in the case of resistivity lower than 300 Ohm m, since coefficients of determination R^2 obtains values lower than 0.5. Thus, this could lead to a **less effective application of the model for passive steel rebars embedded in concrete with resistivity ρ<300 Ohm m**.

Abacuses of the constants a and b are then constructed for every concrete resistivity and injected current (figures V.36 and V.37):

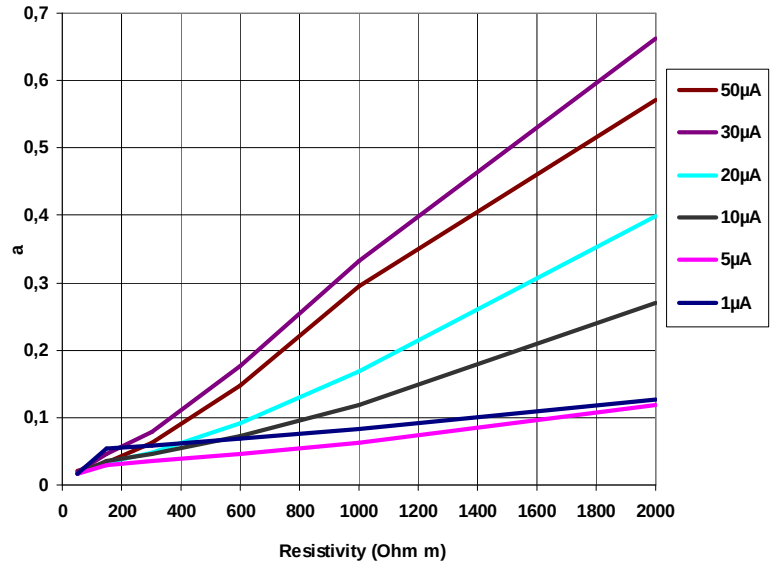

Figure V. 36: Abacus of coefficient a as a function of concrete resistivity, for a single passive steel rebar

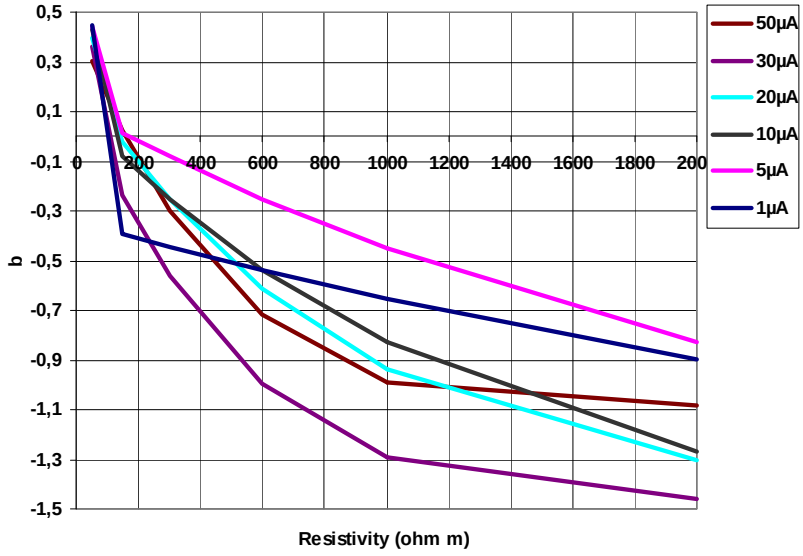

Figure V. 37: Abacus of coefficient b as a function of concrete resistivity, for a single passive steel rebar.

V.5.3. Correction laws and abacuses for the two crossed-rebar configuration.

As it has been already shown, in the case of the two crossed rebars configuration, and as far as the probe's position is concerned, the polarisation seems to be more effective when the electrode assembly is placed right above the crossing of the two rebars. However, compared to the single bar polarisation, some current losses are inevitable, since the lower steel rebar

attracts and receives a part of the injected current. For that reason, correction laws and abacuses are established for the two crossed rebar configuration.

Following the procedure, as described in the two previous paragraphs, it has been noted that the estimation of the real potential value and real current density, necessary for the calculation of polarisation resistance, according to equation 45, can also be realised according to the equations 48 and 50. Abacuses were then constructed for the constants of the equations k, A and B. Now, if these abacuses are compared with those for the single active rebar, very small differences can be noted between them (figures V.38, V.39). This could signify the possible use of the abacuses of a single rebar in the case of a polarisation resistance measurement above the crossing of two crossed rebars. Or simply, the crossing points of the rebars forming a network, could be avoided and since uniform conditions are assumed, the polarisation resistance measurement can be realised above any point along the rebars.

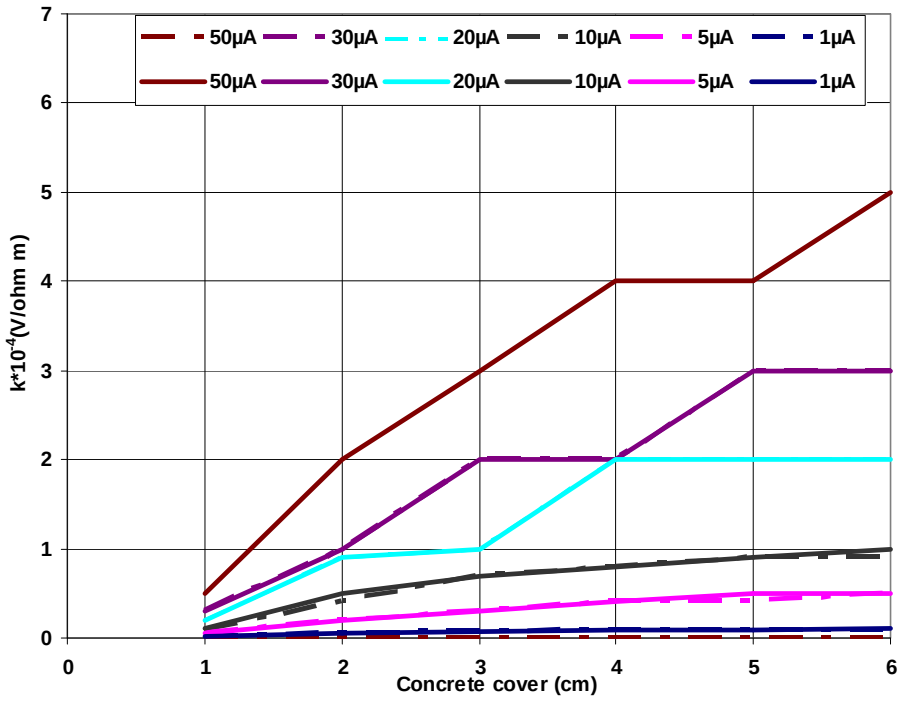

Figure V. 38: Abacus of coefficient k as a function of concrete cover for each injected current from the probe towards one single active rebar (full line) and two crossed active steel rebars (doted line).

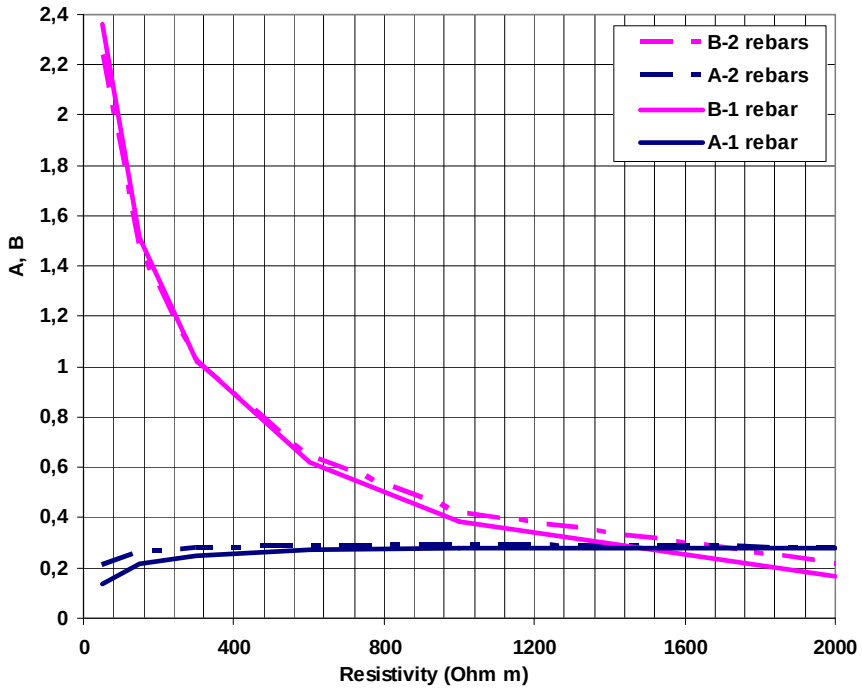

Figure V. 39: Abacus of coefficients A and B as a function of concrete resistivity, for one single active rebar (full line) and two crossed active steel rebars (doted line).

V.5.4. Synthesis

In the previous paragraphs, relationships, correction laws and abacuses were established in order to be able to evaluate the real potential and current density values, during polarisation, on the steel rebar, right under the measurement point on the concrete surfaces. Via these relationships and abacuses, the real value of polarisation resistance will be calculated for an active or a passive rebar. The procedure of calculating polarisation resistance is clearly depicted in figure V.40:

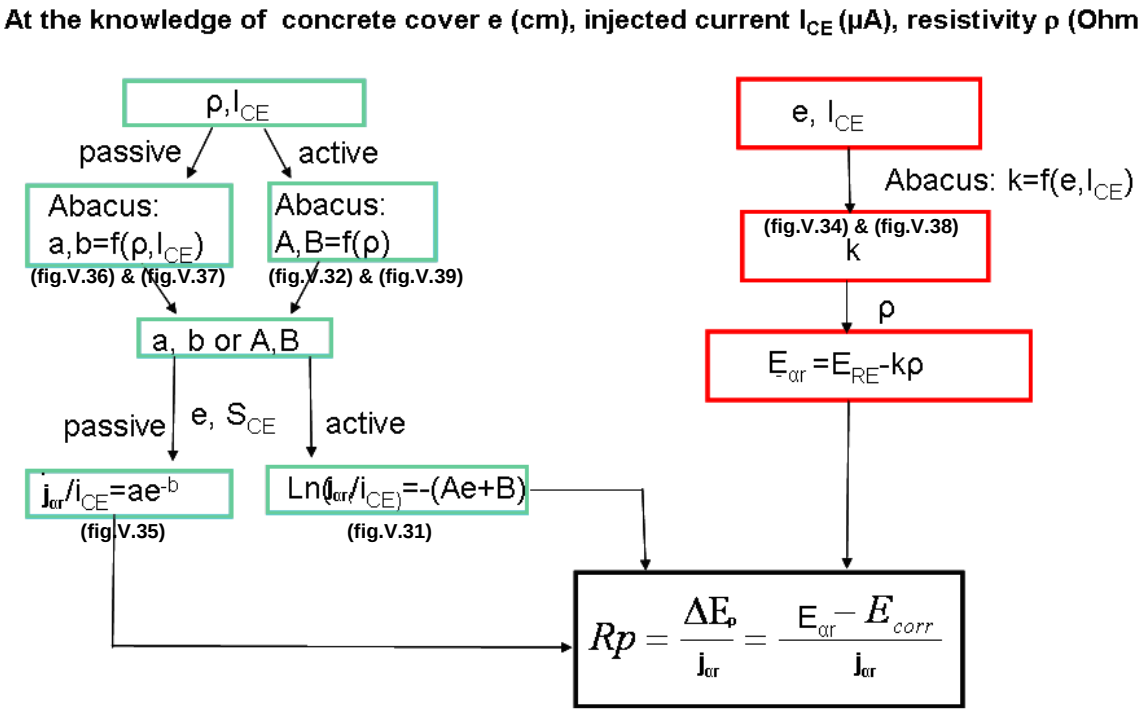

Figure V. 40: Schematic illustration of the procedure, calculating the real value of polarisation resistance for an active or passive rebar.

V.6. CONCLUSION

This chapter described an original operative measurement mode of polarisation resistance proposed for a more reliable characterization of the corrosion state of zones of the cooling towers potentially affected by corrosion, due to carbonation.

It has been demonstrated that the existing electrochemical techniques for characterising corrosion of reinforcing steel suffer from a reliability deficiency leading to a misleading estimation of the state of corrosion of reinforced concrete.

Therefore, an original operative measurement mode of resistance of polarisation, *Rp*, was proposed, adapted for cooling towers submitted to uniform corrosion. Its main advantage lies into its simplicity since a better and a more precise evaluation of the current distribution on the reinforcement can be carried out. In addition, this methodology proposed an original procedure in order to gather the real information about the polarization phenomena taking place on an active or passive steel bar's surface and so to calculate the real value of polarization resistance.

As a result, numerical simulations were launched in order to study the different phenomena occurring during this novel polarisation measurement for different geometries and taking into

account the influencing physical and geometrical parameters. With the aid of experimental design and analysis of variance, the influence of resistivity, concrete cover and injected current from the probe has been quantified. Apart from that, the effect of the parameters, characterising the state of corrosion of the reinforcement is given while a primary validation of the necessary linear condition of the proposed model is demonstrated. Last but not least, it has been underlined the importance of carrying out the polarisation measurement exactly right above the reinforcement.

Finally, via these different numerical experiments, relationships were established between the measurements performed at the surface of the concrete above the reinforcement and the actual values of potential and current density on the reinforcing steel which are really of concern for the diagnosis of the structure. Abacuses and correction laws are built involving the different parameters which influence the measurement and a procedure was developed for the correct evaluation of the polarisation resistance. **These abacuses and correction laws are valid only for: $50 \leq \rho \leq 2000$ Ohm m,, concrete cover $1 \leq e \leq 6$cm and injected current $1 \leq I_{CE} \leq 50\mu A$**.

The following chapter describes the application and experimental validation of the proposed measurement mode of polarisation resistance on lab scale. More specifically, the simulated conditions will be reproduced in a laboratory environment, having as main objectives the demonstration of the proposed procedure for calculating Rp and the development of a complete protocol of measurement and interpretation of Rp on site. Finally, the feasibility of applying this protocol on site will be also put under test.

VI. Experimental validation of the proposed measurement mode of polarisation resistance

VI.1. INTRODUCTION

As it has been already discussed, there is a high need for a measurement model of polarisation resistance, reliable and effective, which will provide with the correct information for the accurate evaluation of the state of reinforced structures. Chapter V presented an original operative measurement mode of polarisation resistance, adapted for cooling towers, submitted to uniform corrosion. Once the new procedure for calculating the real value of polarisation resistance is established, its efficient and effective applicability on real site conditions should be fortified. As a result, the experimental validation of the proposed measurement mode is required.

In this chapter, the lab scale demonstration and application of this new methodology is described. Firstly, the complete experimental program is given, including the several series of polarisation resistance measurements. The preparation and the conditioning of the concrete specimens and the results of the different materials' characterisation techniques are presented in the Appendix B. Finally, a thorough discussion of the results obtained from these measurements follows, leading to the primary development of a measurement protocol and interpretation of polarisation resistance on site.

VI.2. EXPERIMENTAL PROGRAM

In order to validate the new proposed model of polarisation resistance measurement, it was necessary to reproduce the simulated geometries in the laboratory, approaching as much as possible the real site conditions. The following paragraphs present, the concrete specimen's preparation, the experimental set up and the series of measurements carried out. The specimen's fabrication and conditioning are described in the Appendix B.

VI.2.1. Specimens' preparation

In order to realise the polarisation resistance measurements, the simulated geometries of the single and two crossed rebars were reproduced in lab scale conditions. Four concrete slabs of 1100x300x150 mm were casted, two with four single steel bars, (280mm long and ø=12 mm) (Type I), embedded at 20, 30, 40 and 50mm and two with four pairs of steel rebars, crossed

one (280mm long and ø=12mm) by one (150mm long and ø=12mm) at a single point of contact (Type II), also embedded at 20, 30, 40 and 50cmm. No electrical connection exists between the reinforcement embedded at the different depths for both types of slabs. One slab for each type of reinforcement geometry was intended for being at active (corrosive) state and the other one for being at passive state. All steel bars are smooth and round. The reinforced concrete specimens are illustrated in the figure VI.1.

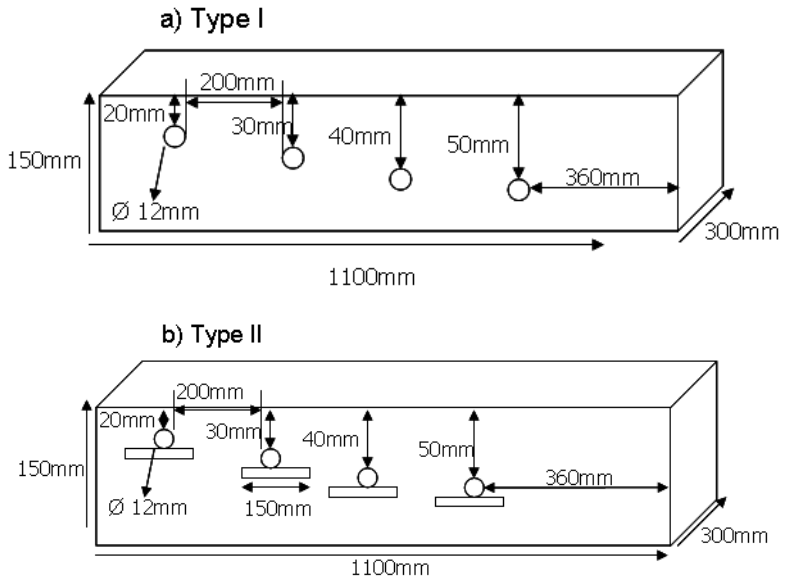

Figure VI. 1: Schematic illustration of concrete slabs of a) single bar configuration (Type I) and b) two crossed rebar configuration (Type II).

In order to eliminate any possible contact of the steel rebar with the external environment, which could alternate the desirable state of the reinforcement (i.e. additional corrosive activity), PVC hooves were used to cover the edges of the steel rebars (figure VI.2). In the case of the two crossed rebars configuration, the hooves were used only for the upper rebar.

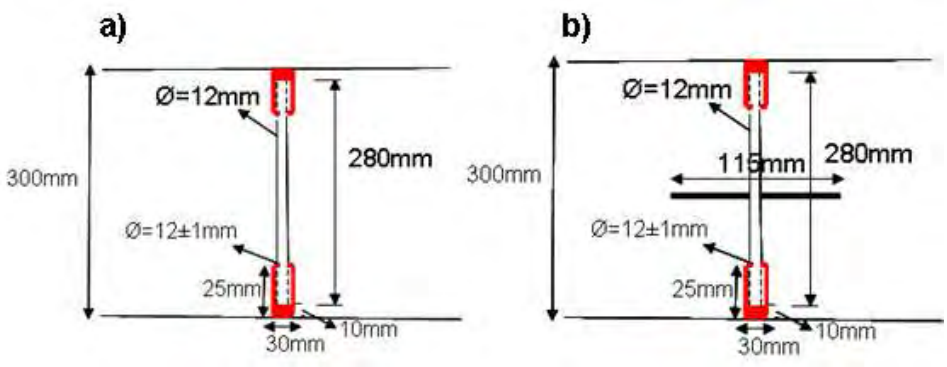

Figure VI. 2: Schematic illustration of the top view of the concrete slabs of a) single bar configuration (Type I) and b) two crossed rebar configuration (Type II). PVC hooves are marked with red colour.

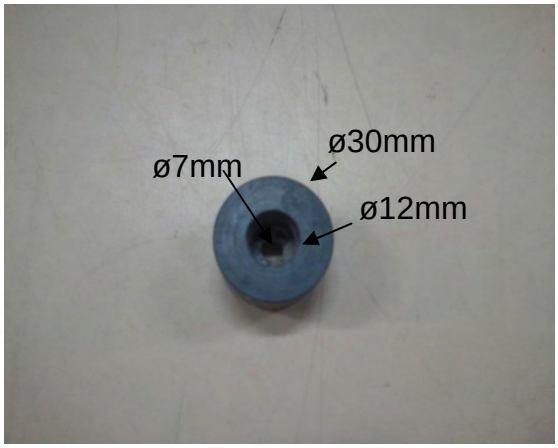

Figure VI. 3: PVC hooves used for eliminating any possible undesirable influence of the environment on the state of the reinforcement.

In addition, as it can also be observed in figure VI.2, the edges of the steel rebars (and so the PVC hooves) were drilled in order to achieve, via metallic screws (45 x 7mm), the electrical connexion, that is required, between the steel rebars and the polarisation resistance measurement system (figure VI.4):

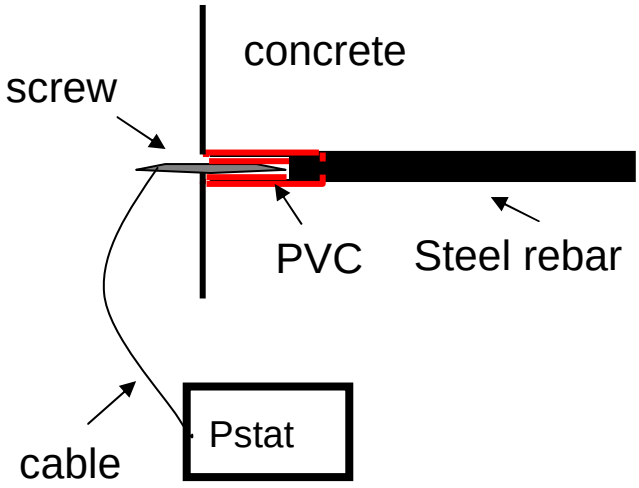

Figure VI. 4: Schematic illustration of the electrical connection between the steel rebars and the polarisation resistance measurement system.

For each type and state of concrete slab, cylindrical concrete specimens (110x220mm) were casted, intended for material characterisation via the measurements of:

- Compressive strength (Rc) at 28 days
- Accessible porosity to water
- Permeability to oxygen and Hg porosity.

Similarly, reinforced concrete cylinders were also fabricated in order to estimate the Tafel coefficients for each type and state of slab. Smooth rounded steel rebars, having a length of 170mm and a diameter of 12mm were embedded in cylindrical concrete specimens

(100x140mm). Concrete cover was fixed at 4cm for the embedded rebar. The configuration of the moulds used for casting the samples is schematically illustrated in figure VI.5. The steel rebar was adjusted in the middle of the mould via the aid of a PVC spacer with a hole:

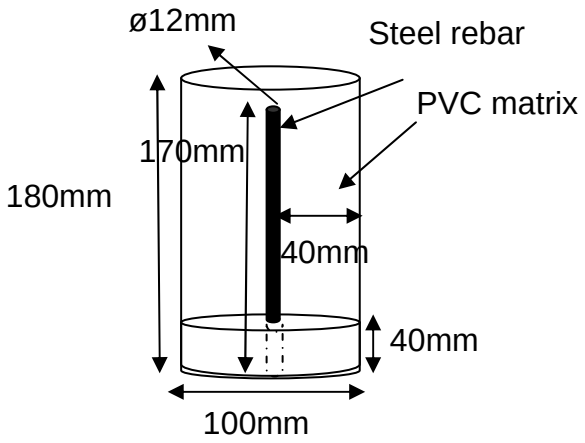

Figure VI. 5: Schematic illustration of the matrix used for the reinforced concrete specimen, intended for measuring Tafel constants.

Finally, it has to be noted that the active state of the slabs was achieved by storing the concrete specimens in a chamber of accelerated carbonation (50%CO_2, 60%HR). In order to check that the carbonation of the slab is fully achieved a certain number of cylindrical concrete specimens of the same height as the concrete slabs (110x150mm) were fabricated, to be able to control the evolution of carbonation.

VI.2.2. Materials' composition

The main objective, in this part of the study, was to fabricate concrete, whose composition, would approach, as much as possible, that of the concrete of EDF's cooling towers. For that reason, an EDF's document on the technical characteristics of cooling towers was used as guidance. For the fabrication of concrete, cement with 30% limestone filler (CEM II 32.5R) was used along with locally available aggregates (Carrières du Boulonnais), characterised by a low tendency of water absorption: sand (0/4mm), gravel (4/12mm) and coarse aggregates (12/20mm). In addition, it has been indicated a water to cement ratio (w/c) of 0.48. In order to improve the consistency of the concrete a super plasticiser was added (GLENIUM 27) at 0.5% of the mass of cement. Concrete formulation is summarised in table VI.1, while table VI.2 demonstrates the water absorption (%) of the aggregates, obtained according to the European standards NF EN 1097-6.

Table VI- 1: Concrete formulation

Composite	Content (kg/m^3)
Cement CEM II 32.5R	350
Water	167.5
Sand (0/4mm)	703
Gravel (4/12mm)	169
Coarse aggregate (12/20mm)	996
Super plasticiser GLENIUM 27	0.5% of the mass of cement
Theoretical W/C	0.48

Table VI- 2: Water absorption by the aggregates (NF EN 1097-6)

Type of aggregates	Water absorption (%)
Gravel (4/12mm)	0.7
Coarse aggregate (12/20mm)	0.6

Before embedding rebars into concrete, they were thoroughly cleaned with acetone and then with ethanol, in order to remove the remains of grease, due to the fabrication. In order to approach the real state of reinforcement on structures, no mechanical treatment was carried out. Thus, the natural protective oxide layer was preserved along the surface of the steel rebars. Figure VI.6 depicts the steel rebar before embedding it into the concrete:

Figure VI. 6: Steel rebar after cleaning it with acetone and ethanol to remove the grease and before embedding it into the concrete. No mechanical treatment was carried out.

The specimen's fabrication and conditioning is described in Appendix B;

VI.2.3. Synthesis

The tables VI.3, VI.4 and the figure VI.7, summarize the experimental program, followed in this study:

Table VI- 3: Details about the characterisation of concrete's mechanical and physical properties and the number of concrete specimen (SP), for each technique, for each type and state of concrete. C: carbonated, NC: non-carbonated. In parenthesis the diameter of the sample is given. The results of these techniques are given in the Appendix B.

Experimental methods	**Type I (one rebar configuration) Casting date:16/02/2012**		**Type II (two crossed rebars configuration) Casting date:10/01/2012**	
Resistance to compression strength (28 days) (EN-12390/3)	3SP(110x220mm)		3SP(110x220mm)	
	I-C	**I-NC**	**II-C**	**II-NC**
Accessible porosity to water (NF P18-459)	1SP(110x220mm)	1SP(110x220mm)	1SP(110x220mm)	1SP(110x220mm)
Gas Permeability (Cembureau method	1SP(110x220mm) + Hg porosimetry (ISO 15901-1:2005**)**	1SP(110x220mm) + Hg porosimetry (ISO 15901-1:2005)	1SP(110x220mm)	1SP(110x220mm)
Carbonation depth control	3SP(110x150mm)	3SP(110x150mm)	3SP(110x150mm)	3SP(110x150mm)

Table VI- 4: Experimental techniques for electrochemical characterisation and number of concrete slabs (SL) and specimens (SP), for each type and state of concrete.

Experimental methods	**Type I –(1 rebar configuration) Casting date: 16/02/2012**		**Type II –(2 crossed rebars configuration) Casting date: 10/01/2012**	
	I-C	**I-NC**	**II-C**	**II-NC**
Determination of corrosion current density				
Electrical resistivity (Wenner method)	1 SL(ø12mm)	1SL(ø12mm)	1 SL(ø12mm)	1 SL(ø12mm)
Corrosion Potential and Polarisation resistance	1 SL(ø12mm)	1SL(ø12mm)	1 SL(ø12mm)	1 SL(ø12mm)
Determination of weight losses due to corrosion				
Polarisation resistance vs. Gravimetric (destructive) technique	1 SL(ø12mm)			
Determination of Butler Volmer parameters				
Tafel Constants measurement	3SP(100x140mm,ø12mm)	3SP(100x140mm,ø12mm)		

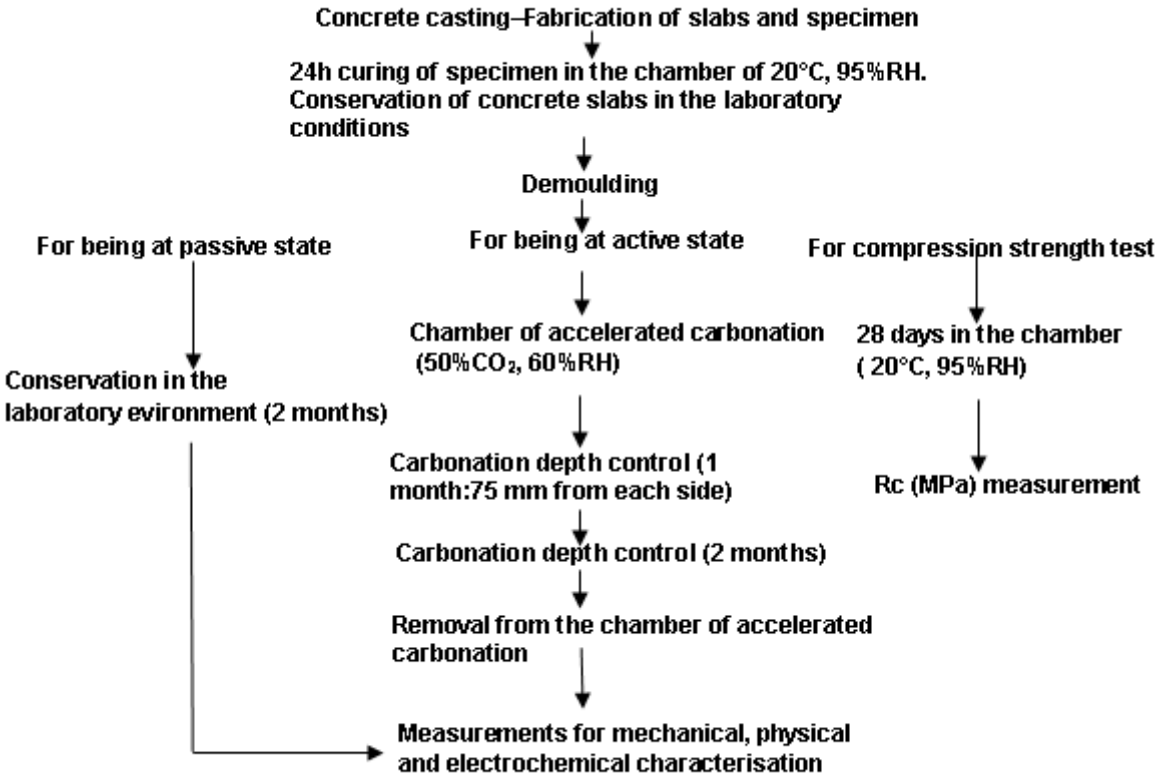

Figure VI. 7: Preparation and storage conditions chart flow of the concrete slabs and specimens, followed for both types of concrete.

VI.3. DETERMINATION OF ELECTROCHEMICAL PARAMETERS

In order to characterize the electrochemical parameters, Tafel constants measurements were carried out. The experimental procedure and set up are firstly presented and then the steps that are followed for estimating correctly the **Butler-Volmer parameters** are fully described.

VI.3.1. Experimental procedure and set up

In order to carry out these particular measurements, reinforced concrete specimen were fabricated and stored according to the procedures described in Appendix B . Figure VI.8 shows some of these reinforced cylinders, during their preparation for entering the chamber of accelerated carbonation. Resin was also used in the interface between the reinforcement exposed to the atmosphere and the concrete, as depicted in the same figure, in order to

eliminate all possible interactions (likely leading to undesirable corrosion) with the external environment:

Figure VI. 8: Cylindrical reinforced concrete specimen, used for the Tafel constant measurements

In order to realise the measurement, the specimens were immersed in a basin with water. A part of the concrete specimens was kept out of the water, so that they are continuously provided with free oxygen. The Tafel slope measurement is a 3 electrodes set-up, requiring an electrical connexion of the measurement system to the reinforcement: a titanium (Ti) grid was placed around the specimen consisting the counter electrode (CE), the reinforcement acts as the working electrode (WE), while as reference electrode (RE), a Saturated Calomel Electrode (E_{SCE}=+0.244V vs. SHE) immersed in water, is used. The measurement takes place via a channel mobile GAMRY Potentiostat/Galvanostat/ZRA (Reference 600). The experimental set up is illustrated in figure VI.9:

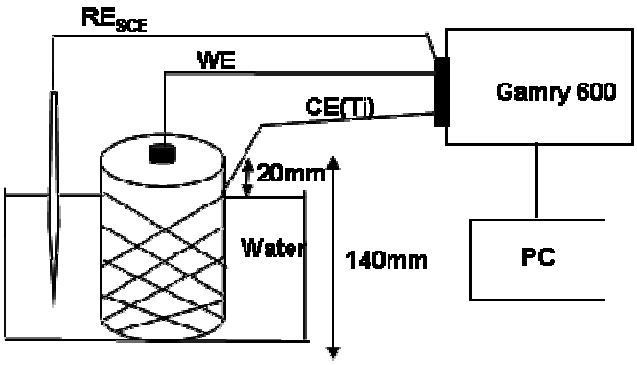

Figure VI. 9: Schematic illustration and picture of the experimental set up for the Constant Tafel measurements.

These measurements were performed for six concrete specimens of concrete type I : three specimens for active (carbonated) state and three for passive (non carbonated) state. From the relevant software (*Gamry Instruments Framework*), the *Tafel* measurement tab is chosen. The measurement consists of the following steps: firstly, the open circuit (OC) or corrosion potential, E_{corr}, is measured. Next, a *cathodic polarisation* of *-200mV* with respect to $E_{corr,,}$ is directly applied. Then, potential returns to equilibrium (corrosion) potential, E_{corr} and finally, an *anodic polarisation* of E_{corr}*+200mV* follows. The scan rate for this sweep polarisation was fixed at 0.5mV/sec. It has to be noted that after cathodic polarisation, often, the potential doesn't return to its OC initial value; still, a new equilibrium is established before anodic polarisation takes place. The figure VI.10 shows an example of curve plotted during the measurement for an active (carbonated) reinforced specimen:

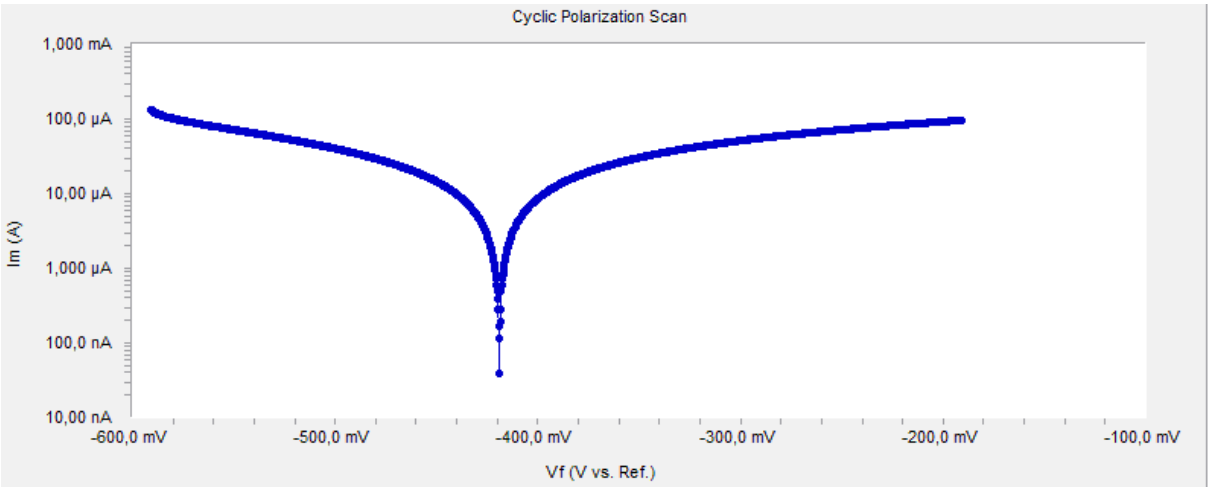

Figure VI. 10: Sweep polarisation curve plotted during the Tafel measurement for an active (carbonated) concrete specimen

VI.3.2. J_oR_Ω Correction

In order to evaluate properly the Butler-Volmer parameters, the ohmic drop due to the resistance of concrete, $R_{\Omega,}$ should be taken into account. For that reason, before the *Tafel* measurement, for each concrete specimen, the resistance of concrete was estimated, via the technique of galvanostatic pulse. As, it was demonstrated in paragraph II.2.3.2, this specific technique is based on Randles model (figure II.9). Via the equation (eq. 29), for $t_{polarisation}$*=0 sec*, the ohmic resistance of concrete, R_Ω, can be calculated.

More particularly, the measurement is realised for the same experimental configuration. Firstly, the OC or corrosion potential is measured till its stabilisation. Once the corrosion

potential stabilised, a current of 10µA is injected. The potential response, of an active specimen to this perturbation is recorded as a function of time (Figure VI.11):

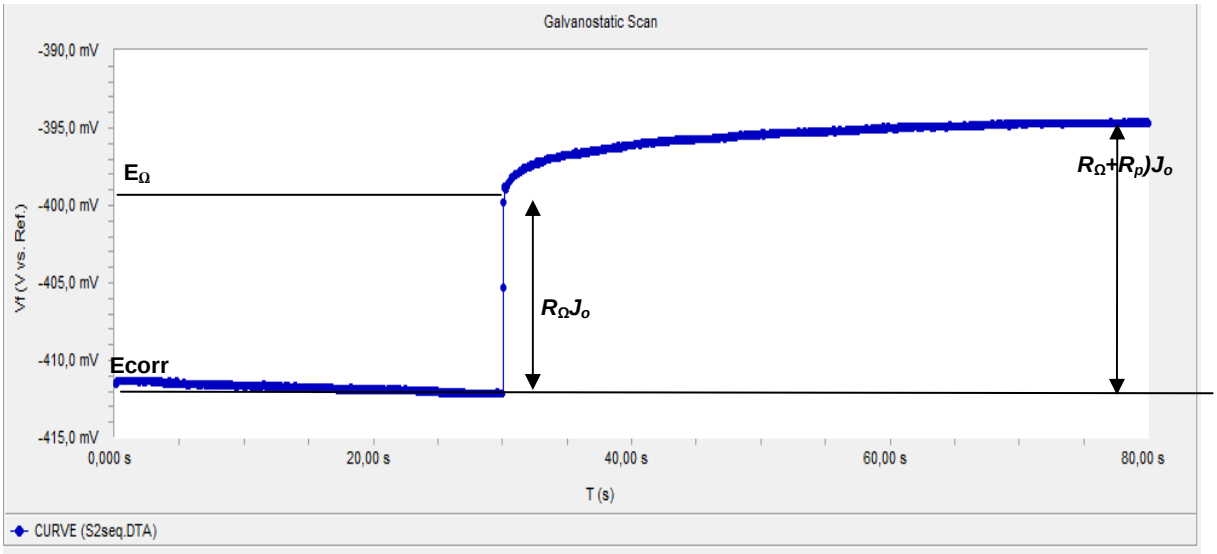

Figure VI. 11: Potential response of an active system to a short galvanostatic pulse of 10µA.The OC or corrosion potential is firstly measured till stabilisation. E_Ω(V) is the instantaneous response of the system, due to the ohmic resistance of concrete, according to Randles model see figure II.9).

Similar procedure was followed for the passive concrete specimen. The average values of resistance for carbonated and non carbonated specimen are shown in table VI.5:

Table VI- 5: Average values of the ohmic resistance, R_Ω (Ohm) of the carbonated (C) and non carbonated (NC) type II concrete specimens

	Type II	
	C	**NC**
R_Ω(Ohm)	1400 (min:1300; max:1500)	333 (min:300, max:400)

As it is expected, the carbonated concrete exhibits a higher resistance than the non carbonated concrete. These values were integrated into the same software and were used for the automatic correction of the Tafel curves. In the following figure the Tafel curves are depicted for an active concrete specimen, before and after J_oR_Ω correction

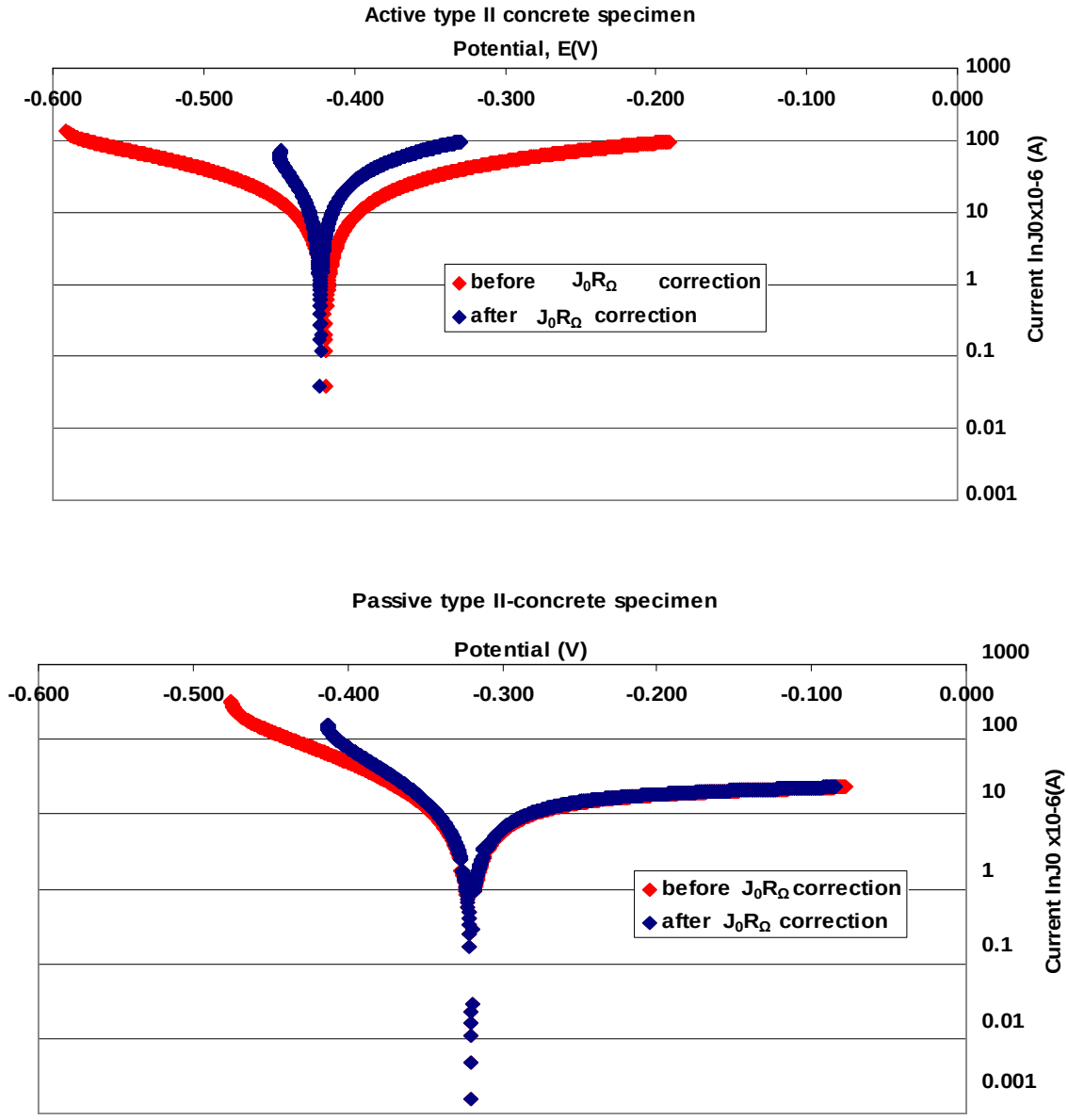

Figure VI. 12: Tafel curves for a) an active (carbonated) and b) passive (carbonated) type II concrete specimen before and after J_oR_Ω correction.

From figure VI.12, it can be clearly seen that the ohmic drop J_oR_Ω is more significant in the case of an active reinforced concrete specimen than for a passive specimen. This can be explained by the high resistance R_Ω and the high current values, J_o the carbonated concrete exhibited. On the other hand, the J_oR_Ω effect seems to influence much less (almost negligible for the anodic part of the curve) on the Tafel curve for passive specimen, since the resistance, R_Ω, of a non carbonated concrete was much lower than that of the carbonated concrete.

VI.3.3 Evaluation of parameters of Butler Volmer equation

Once the curves were corrected as described above, for all active and passive specimens, the Butler-Volmer equation (eq.16 and eq.17) was fitted-in automatically by the same software in order to estimate precisely the corrosion parameter values. The figure VI.13 demonstrates the experimentally measured Tafel curve along with the Butler-Volmer fitted-in curve, for an active concrete specimen:

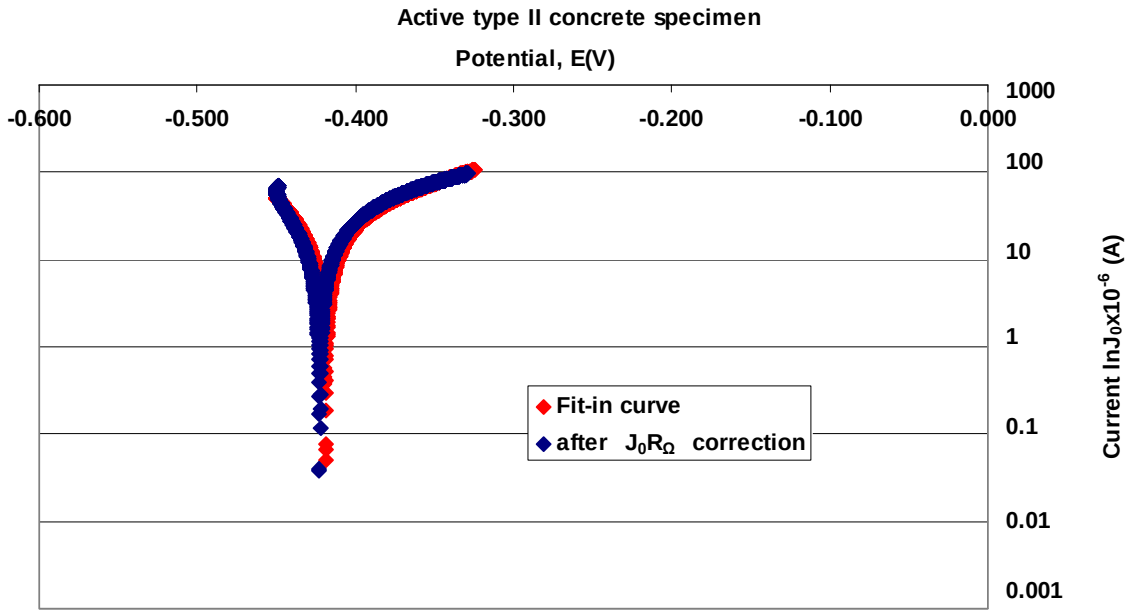

Figure VI. 13: Experimental Tafel and fitted-in curve for an active (carbonated) specimen. The slopes of the tangents for the cathodic (left) and anodic (rigt) parts of the curves represent the cathodic Tafel β_c and anodic Tafel β_a slopes respectively. The intersection of the tangents indicates the corrosion potential, Ecorr, and current, J_{corr}.

Table VI.6 summarises the Butler-Volmer parameters used during the simulations of the proposed polarisation resistance model (§V.3.2) and the average measured values for active (carbonated) and passive (non carbonated) reinforced concrete specimen, as they were estimated following the procedure explained previously:

Table VI- 6: Butler Volmer parameters used during the simulations of the proposed polarisation resistance model(§V.3.2)and average measured values for the carbonated (C) and non carbonated (NC) concrete(type II) specimens. The corrosion current density was calculated according to:j_{corr}/s_a, where s_a is the steel rebar's surface.

	C		**NC**	
	Values used in numerical simulations	**Experimental values**	**Values used in numerical simulations**	**Experimental values**
β_a **(V/dec)**	0.3	0.151 (min:0.115, max:0.192)	0.4	0.782 (min:0.571,max:1.184)
β_c **(V/dec)**	0.125	0.081 (min:0.073,max:0.094)	0.125	0.083 (min:0.077,max:0.09)
E_{corr} **(V)**	-0.419	-0.433 (min:-0.419,max:-0.440)	-0.102	-0.296(min:-0.281,max:-0.131)
j_{corr} **($\mu A/cm^2$)**	0.0050	0.0054 (min: 0.0028, max:0.0073)	0.0004	0.0009 (min: 0.0002, max:0.002)

As it can be seen above, **the Butler Volmer parameters used in simulations and those experimentally evaluated are in the same order of magnitude**. More specifically, the anodic Tafel slope β_a **is of high interest** in this study, since, as it was already presented in chapter IV, the polarisation resistance model proposes an anodic polarisation. So, in the case of the (active) carbonated reinforced concrete, a high value of β_a was used in the numerical model. The also relatively high value assessed via real experiments, confirmed the wise use of such an elevated value of β_a in simulations, and that corrosion due to carbonation, is a slower electrochemical process, evolving in time, contrary to corrosion induced by more aggressive environments, (J. Ge, O.B. Isgor,2007), (C.Y. Kim, 2008), (S. Soleimani, 2010), (M.Sohail, 2013).

In other words, **the steel rebar, corroded due to carbonation, can be considered as "less active" than the steel rebar corroded by chloride ions**. This behaviour will be also validated by the results of polarisation resistance measurement, presented and discussed in the following paragraph.

As far as β_c is concerned, the **experimental** values, although slightly lower than those used in the simulations, they are **the same for both states of the reinforcement**. The same value of

β_c was also used for the **numerical** experiments for active and passive steel rebar. Finally, the differences between numerical values of corrosion potential and current density and the ones estimated after real experiments are small.

The measured electrochemical parameters presented in table VI.6, **are representative only for the specimens fabricated in the frame of the current study**. This signifies that they correspond only to the steel rebars embedded in the specific casted concrete, whose formulation and storage conditions are described in Appendix B. They **cannot be considered as universal values** and must be validated before using them for other types of reinforced concrete or other storage/environmental conditions..

VI.3.4. Synthesis

This paragraph presented the, measurements that were carried out for the determination of the electrochemical parameters of the carbonated and non carbonated reinforced concrete specimens. The experimental procedure consisted plotting the Tafel curves. In order to estimate the real values of the Butler Volmer parameters, the Tafel curves were then corrected with the ohmic drop due to the resistance of concrete, which was determined in its turn via a galvanostatic measurement. Once the curves corrected, the Butler-Volmer model was fitted-in and the corrosion characteristics (E_{corr}, j_{corr}, β_a *and* β_c for active and passive steel rebar) were determined. These values were found to be in the same order of magnitude or quite close with the ones used for the numerical simulations (Chapter V) and indicated that **corrosion due to carbonation, is not a so fast nor quite intense neither highly aggressive procedure (compared to other aggressive environments) and its effects are more remarkable along term scale**.

VI.4. DETERMINATION OF THE CORROSION CURRENT DENSITY OF THE STEEL REBARS

In this chapter, the results of the electrochemical measurements carried out on the corroded and non corroded concrete slabs and specimens are presented. More particularly the results of polarisation resistance measurement carried out on the concrete slabs, according to the model presented in Chapter V, are fully described. Via several series of measurements, the linearity, feasibility, repeatability and spatial variability of the proposed technique is put under test. In addition, its reliability is checked with the aid of Faraday's law, allowing the development of a measurement protocol for the on site evaluation of corrosion rate.

In this paragraph, the application of the proposed polarisation resistance measurement mode will be demonstrated. Via series of measurements, carried out on the four concrete slabs (carbonated and non carbonated), several aspects of the technique (linearity, repeatability, spatial variability) were put into the test and the robustness of the procedure of calculating polarisation resistance was examined. Firstly, the establishment of the polarisation criteria and the development of the measurement procedure are thoroughly described. Then, the results of this lab scale application of the proposed polarisation resistance model for all series of measurements will be presented and discussed. The lab scale validation of the proposed polarisation resistance measurement allows the redaction of a primary protocol for measuring and interpreting the polarisation resistance on site, which is attached in the appendix C of this dissertation.

VI.4.1. Experimental procedure and set up

As it was already mentioned in Chapter V, the proposed polarisation resistance model requires the knowledge of important physical parameters, such as the resistivity, the concrete cover and the injected current. In this particular study, the concrete cover is already known (during the specimen's preparation) and the injected current will be defined according the polarisation criteria, as it will be explained later on this paragraph. As far as resistivity is concerned, it is measured via the method of Wenner (see§ II.2.1.). Thus, the first step of the experimental procedure of polarisation is measuring the concrete resistivity. The figure VI.14 illustrates schematically the successive positions of the Wenner probe on the concrete slabs for the two different configurations:

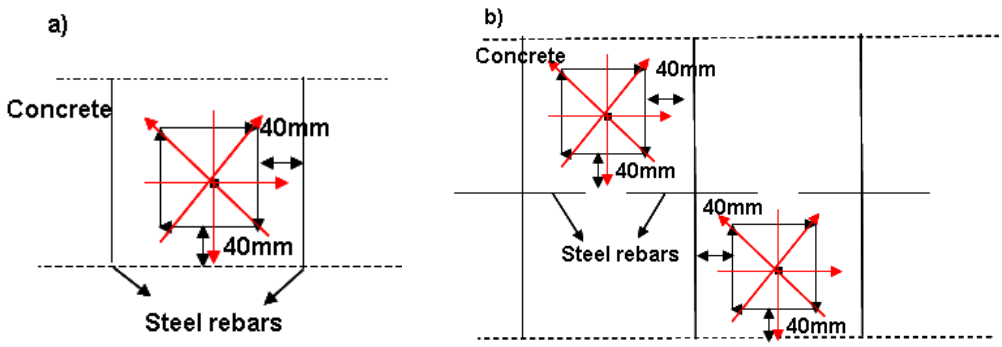

Figure VI. 14: Successive positions of Wenner probe for measuring concrete resistivity, indicated by the black and red arrows on the concrete slabs with a) the single rebar (type I) and b) the two crossed rebars (type II) configuration, for being at active (carbonated) and passive (non carbonated) state.

As it can be seen in the figure VI.14, the resistivity measurement takes place on the surface of the slabs free from the reinforcement in order to limit as much as possible the influence of the steel rebars on the measurement. They are carried out forming successively a rectangle and around a fixed point in the middle of the rectangle. The electrode spacing is 40mm. At each position of the rectangle, the probe is placed at a distance of 40mm from the reinforcement. Before the measurement takes place, the surface of the concrete slab is slightly humidified in order to facilitate the contact between the electrodes and the concrete surface (figure VI.15):

Figure VI. 15: Measurement of concrete resistivity on the slabs via the technique of Wenner. A slight humidification of the concrete surface is required in order to eliminate problems of resistance of contact.

As it was described in § II.2.1, every value of resistance, R_Ω, obtained is transformed into resistivity via the equation (21). Then the average resistivity is calculated out of all these values and it is integrated in the procedure of calculating polarisation resistance, Rp, as it was illustrated in figure V.40. It has to be noted, that this study is interested in measuring only the resistivity of concrete cover and not the bulk resistivity of the concrete slab. For that reason,

the Wenner probe was chosen, with an electrode spacing close to the concrete cover of the reinforcing steel rebars.

The next step in the polarisation resistance measurement consists of measuring the corrosion potential and the polarisation resistance. As it has been already indicated in §V.3.1, the proposed measurement consists of three electrodes (figure V.2). A stainless steel ring was fabricated and served as the counter electrode. Stainless steel was chosen due to its high resistance to corrosion. As it is already known, it consists of a single point measurement. The figure VI.16 depicts the experimental set up of the corrosion potential and polarisation resistance measurement, on one single point, on the surface of the reinforced concrete slab, right above the steel rebar:

Figure VI. 16: Experimental set up of the3 electrode polarisation resistance measurement, on one single point on the concrete surface of the slab, placed, right above the steel rebar: the stainless steel counter electrode (CE), the SCE reference electrode (RE) placed in the middle of the counter electrode and the steel rebar as the working electrode (WE) (connection of the measurement instrument to the steel rebar). A saturated wet sponge is used to facilitate the contact between the electrodes' configuration and the concrete's slab surface. The measurement takes place in the aid of the Gamry (Ref. 600) potentiostat.

As it has been already described in Chapter V, a current is injected from the counter electrode and the response of the system is measured in potential. In addition, the measurement has to **fulfil the criteria of linearity** (§V.2). In the current study, **a target-linear polarisation on the surface of the steel rebar was fixed at 20mV**. This value comes into agreement with the

polarisation **proposed by RILEM recommendation TC 154 EMC 3** (C. Andrade, C. Alonso, 2004).

Gamry (Ref. 600) potentiostat gave the possibility to "build" automatic sequences of measurements (*Sequences Wizard*); once these sequences were launched, they did not require any other interference from the experimenter. The first measurement is a measurement of OC or corrosion potential. Potential is traced as a function of time. The measurements lasts in total 200 sec, but if the potential value stays stable for 10 sec (*Stability:0.01mV/sec*) the measurement is interrupted (figure VI.17). Automatically, the galvanostatic measurement (*Galvanostatic scan*) starts. A current of 1μA is set and injected for 200 sec and the change in potential (from potential corrosion) is plotted versus time. Once more in case of potential stabilisation for 10 sec, (*Stability:0.01mV/sec*) the measurement is interrupted. Then, an OC potential measurement is carried out. During this period of de-polarisation (600sec), potential is traced as a function of time. Once potential returns to its initial equilibrium value and becomes stable (10 sec), then there are two options: in case of an achieved linear polarisation of 20mV on the steel rebar, the measurement is interrupted permanently and the procedure of calculating polarisation resistance, R_p, (figure V.40) takes place. Otherwise, another polarisation measurement is carried out, by increasing the injecting current at 5μA. The same procedure described above, is followed for all the other values of injected current, presented during the numerical simulations (Chapter V), 10, 20, 30 and 50μA, till a polarisation of 20mV is achieved in the surface of the steel rebar. Figure VI.18 demonstrates the polarisation curve plotted for an injected current of 30μA.

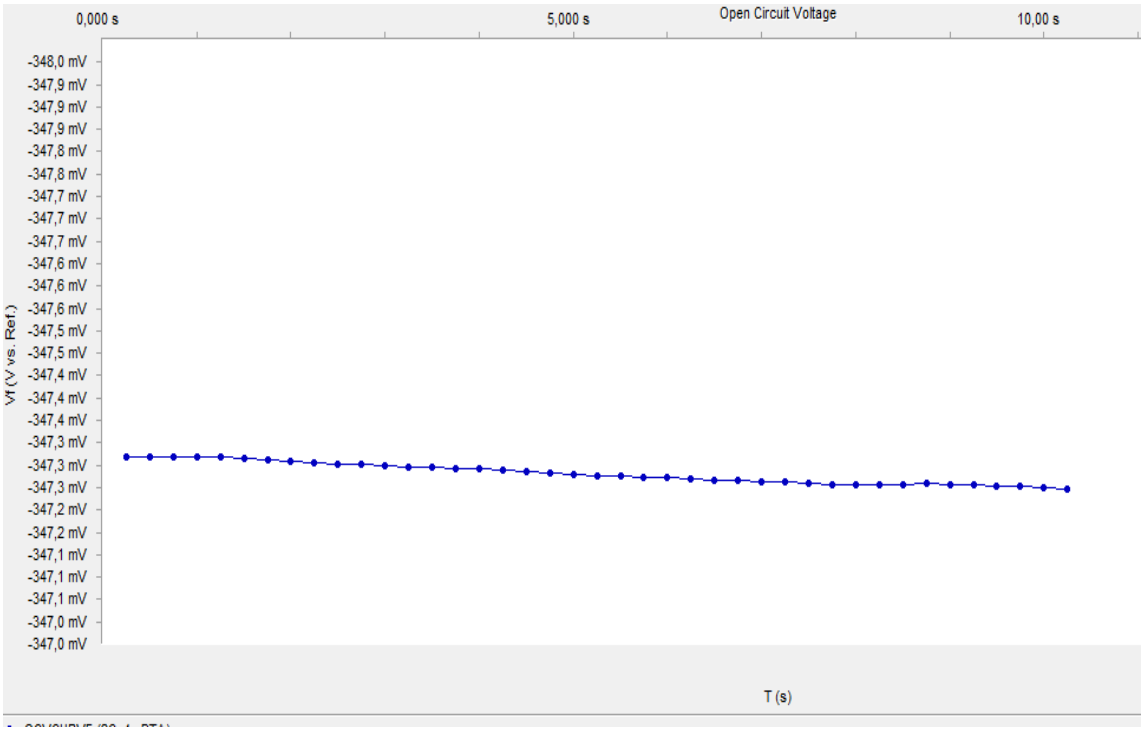

Figure VI. 17: OC or corrosion potential measurement taking place above the crossing of the two rebars at an active state, with a concrete cover of 2cm (type II carbonated (C)). The potential curve is plotted versus time, E=f(t). After 10 sec it was stabilised at 347.3mV.

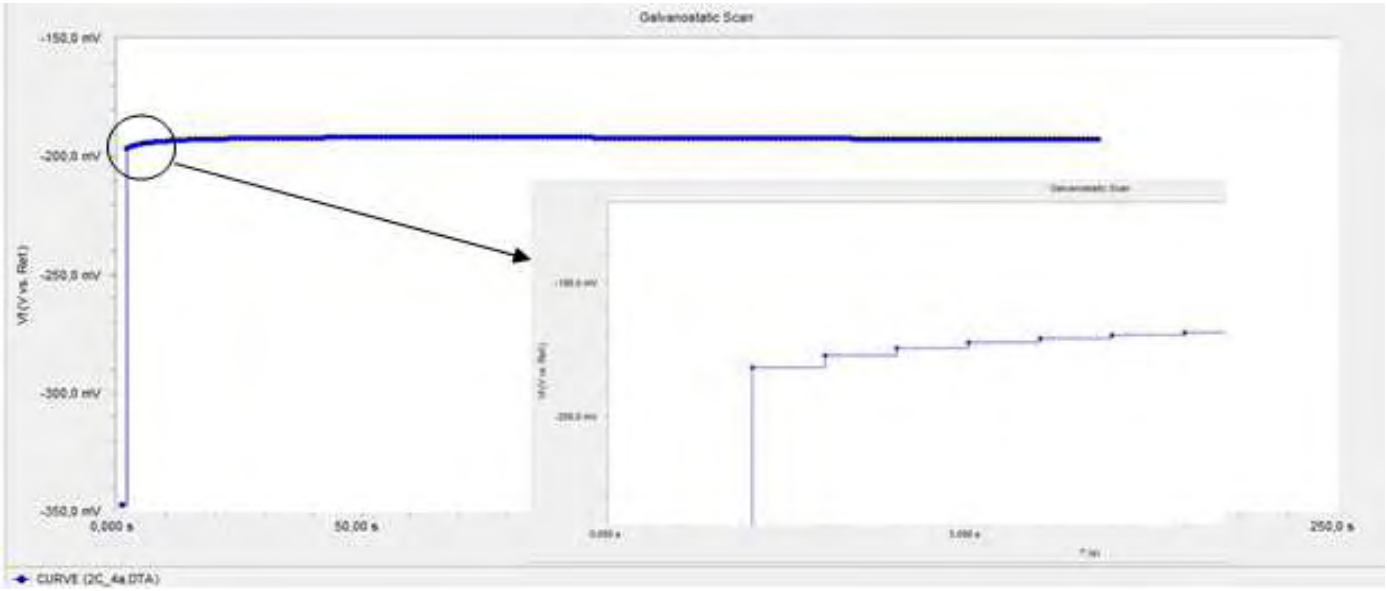

Figure VI. 18: Polarisation measurement taking place above the crossing of the two rebars at an active state, with a concrete cover of 2cm (type II carbonated (C)). A current is injected during 200 sec. This leads to reinforcement's polarisation. The potential curve is plotted against time (E=f(t)). The first point of the curve corresponds at t=0sec, where I_{CE}=0μA and E=Ecorr (V). In the zoomed zone of the curve the differed response can be observed. Then the potential curve becomes stable.

The whole measurement (on a single point) may last maximum 30 minutes. The figure VI.19 summarizes the procedure of measuring corrosion potential and polarisation:

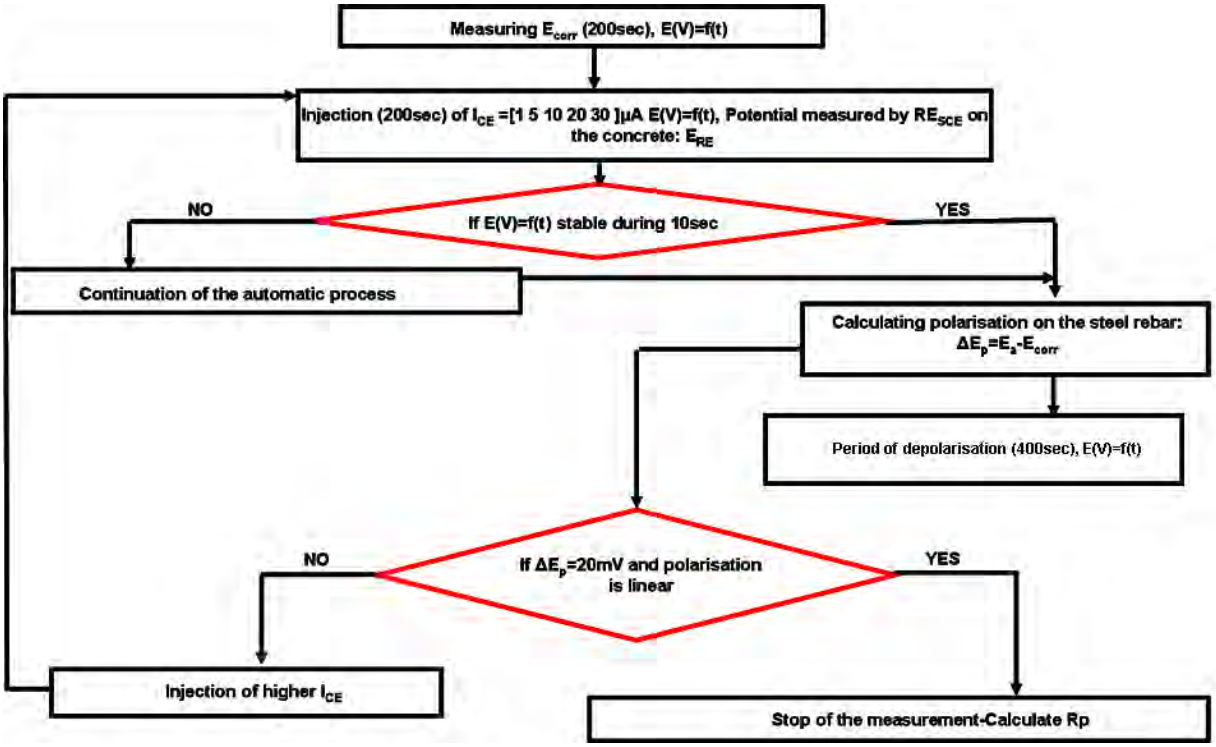

Figure VI. 19: Procedure of corrosion potential and polarisation measurement

The whole procedure is described with all details in the "Protocol of Polarisation Resistance measurement and interpretation on Reinforced Structures", in appendix C.

As it has been already mentioned, a series of polarisation resistance measurement were launched in order to validate the feasibility of the new proposed technique, and to examine several aspects of it: linearity, repeatability and spatial variability. In the following paragraphs, the results of these measurements are presented. In addition, this model has been used to perform a monitoring of the evolution of corrosion state in time of the active (carbonated) reinforced concrete slabs. Finally, weight loss measurements (Destructive gravimetric technique) were carried out and they were compared with those calculated via the Faraday's law.

VI.4.2. Demonstration of the proposed polarisation resistance measurement model: Validation of the feasibility of the technique

In order to check that this novel probe polarizes effectively and that the proposed procedure of measuring and interpreting polarisation resistance provides with reliable and correct information on the corrosion state of the reinforced concrete, measurements were carried out on the four reinforced concrete slabs (type I and II, carbonated and non carbonated), following the steps described in the previous paragraph. Thus, measurements were realised:

- For the type I (one single steel rebar) reinforced concrete slabs, carbonated and non carbonated, the probe was placed right above, in the middle of the steel rebar (similarly to the numerical Rp measurements) (figure VI.20, point "a").
- For the type II (two crossed steel rebars) reinforced concrete slabs, carbonated and non carbonated, the probe was placed right above the crossing of the rebars (as in the case of the numerical simulations). A series of measurement was also realised on a point, above the upper steel rebar, between the crossing and one of its edges (figure VI.20, point "b").

It has also to be mentioned, that before the polarisation measurement takes place, the desirable uniform state of the reinforcement, active or passive, was controlled, by carrying out OC potential measurements on several points along the steel rebar for type I and the upper steel rebar for type II. The figure VI.20 illustrates schematically the location of measurements carried out for validating the proposed technique:

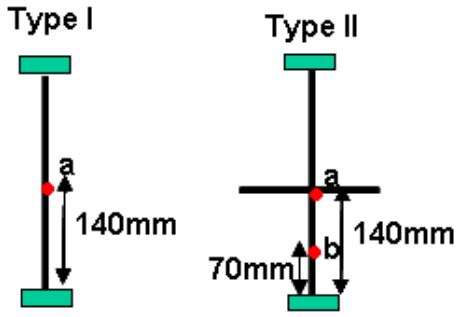

Figure VI. 20: Polarisation measurements above the middle of the single steel rebar (type I), the crossing and a point between the crossing and one of the edges of the upper steel rebar (type II).

Once the reinforced concrete slabs were removed from the chamber of accelerated carbonation, they were placed in the laboratory environment, along with the non carbonated slabs. All aluminium (Al) foils were removed from both carbonated and non carbonated slab. This series of measurement started 24 hours after removing the carbonated slabs from the chamber. This time of 24 hours served for the adaptation of the concrete slabs to their new storage environment.

In the following paragraph, a step by step demonstration of measuring and calculating polarisation resistance is carried out, in order to evaluate the corrosion state of the single bar embedded at 2cm, being at active state due to uniform carbonation, right after the removal of the concrete slab from the chamber of accelerated carbonation.

VI.4.2.1 Evaluation of the potential and current density on the steel rebar surface after polarisation

Firstly, the resistivity of the type I carbonated (I-C) concrete slab was measured according to the procedure previously described. Its average value was calculated and found 584 Ohm m, which can be considered reasonable since the slab was submitted to carbonation process and so carbonation products filled the concrete pores (see also §VI.3.1). **Secondly, the uniformity of corrosion potential** (and so of the state) along the steel rebar was confirmed; its values are ranged between -0.447 and -0.445 V. Obviously, according to the **ASTM standards** (table 2, §II.2.2) these values indicate the risk of a severe corrosion of the reinforcement.

Then, the sequence **of successive and alternate measurements of corrosion potential and polarisation is launched on point "a"** as depicted in figure VI.20. Once the first corrosion potential measurement is carried out (E_{corr}=-0.447 V), the probe injects 1μA and potential shift measured by the reference electrode reaches -0.442V. In order to confirm that the 20mV of polarisation was achieved on the surface of the reinforcement**, the real value of potential on that point of the steel rebar,** right under the reference electrode ("point of interest"), due to this current perturbation **has to be calculated**.

As it has been demonstrated in chapter V, this can be accomplished in the aid of abacus of **coefficient k** (figure V.30, § V.5.1) and the use of eq.48. So for concrete cover of 2 cm and an injected current of 1 μA coefficient k is found 0.00005. Now, for a measured potential value of -0.442 V, a resistivity of 584 Ohm m and via eq.48, the potential on the steel rebar, $\mathbf{E_{ar}}$, is equal to -0.445V. The figure VI.21 demonstrates the estimation of E_{ar}:

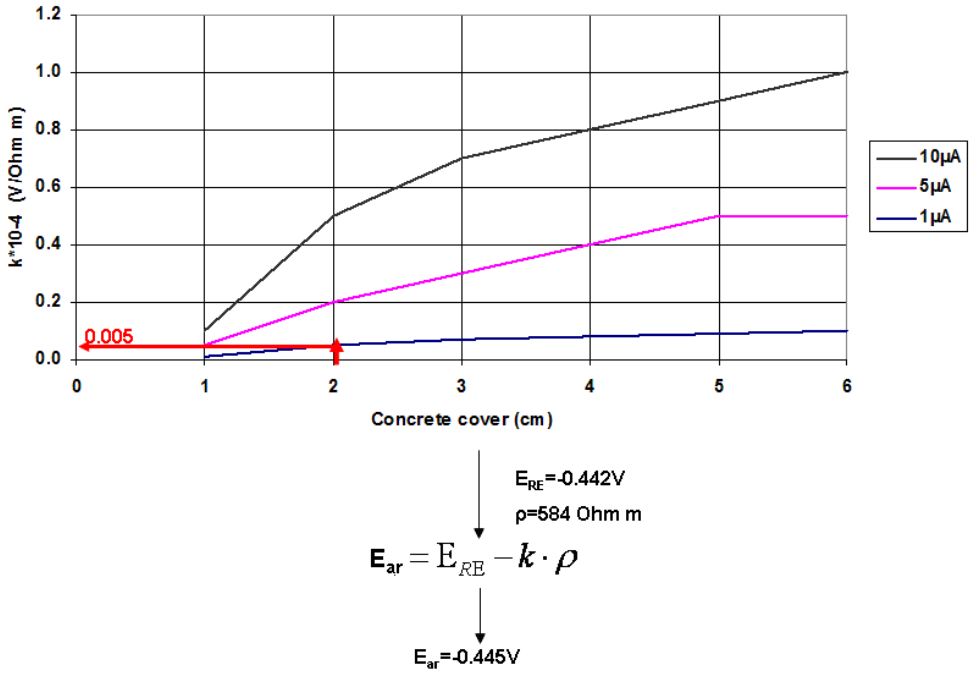

Figure VI. 21: Calculating E_{ar} (V) according to procedure described in §V.5.1 after injecting a current of 1µA.

Thus, the real potential shift on the rebar's surface can be estimated by this relation $\Delta Ep = E_{ar} - E_{corr} = 0.002V$ .As far as the value of current density, j_{ar}, is concerned, its calculation is realised as following: for the concrete resistivity of 584 Ohm m and via the abacus of **A, B** (figure V.32), the values of A and B are obtained. These values of the coefficients were integrated along with the value of concrete cover of 2cm and the injected current of 1µA in eq. 34 and so the current density, $\boldsymbol{j_{ar}}$, right under the measurement point is calculated at 0.001A/m^2. Figure VI.22 indicates schematically the procedure of calculating j_{ar}:

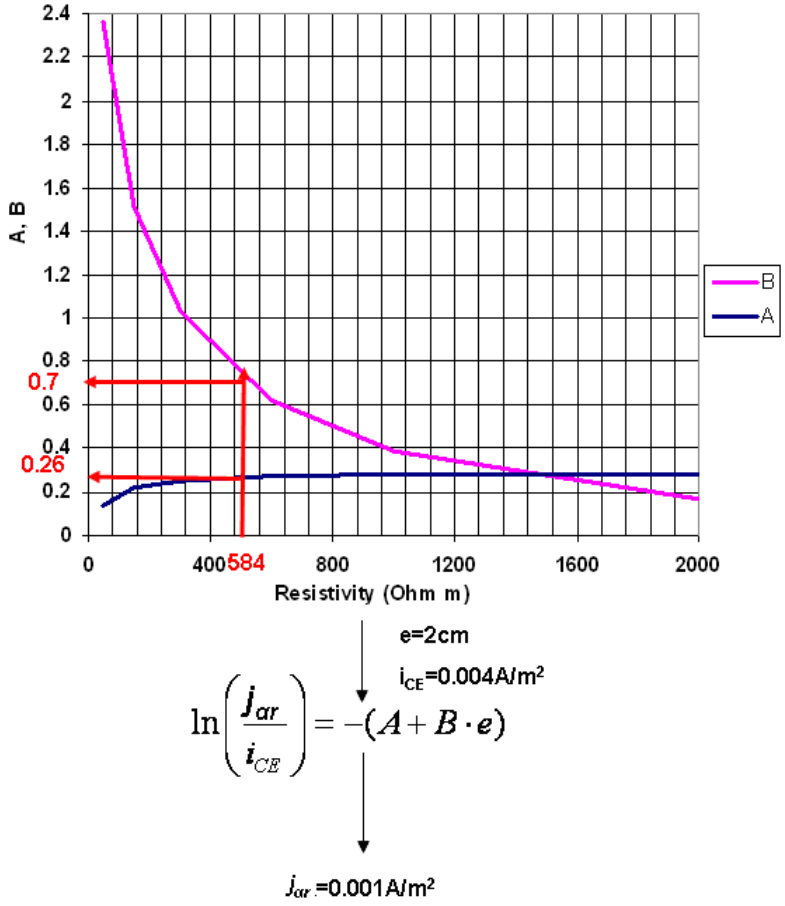

Figure VI. 22: Calculating j_{ar} (A/m^2) according to procedure described in §V.5.1 after injecting 50µA.

As it can be seen, the realised polarisation seems to be **much less than the targeted one of 20mV**. For that reason, according to figure VI.19, **a higher** value of current is injected. Following the same procedure, it has been stated that an injection of 20µA leads to a polarisation of 21mV. It has to be noted that after each current injection, the system didn't always return to its initial thermodynamic equilibrium, but during the de-polarisation period, it was establishing a new stable one. For every injected current till the achievement of the desirable polarisation, the potential, E_{ar}, (V) and j_{ar}(A/m^2) values were estimated according to the procedures depicted in figure VI.21 and VI.22.

VI.4.2.2. Calculation of polarization resistance and corrosion current density values

As it is already known, the polarisation resistance is defined as the slope of the linear part of the polarisation curve at E_{corr} (figure II.4.). So, **in order to estimate the value of polarisation resistance, the real polarisation *ΔEp* ($=E_{ar}-E_{corr}$) (V) was traced as a function of the current density, j_{ar} (A/m^2) for each injected current, (till 20mV of polarisation on the rebar's surface was achieved),** as following:

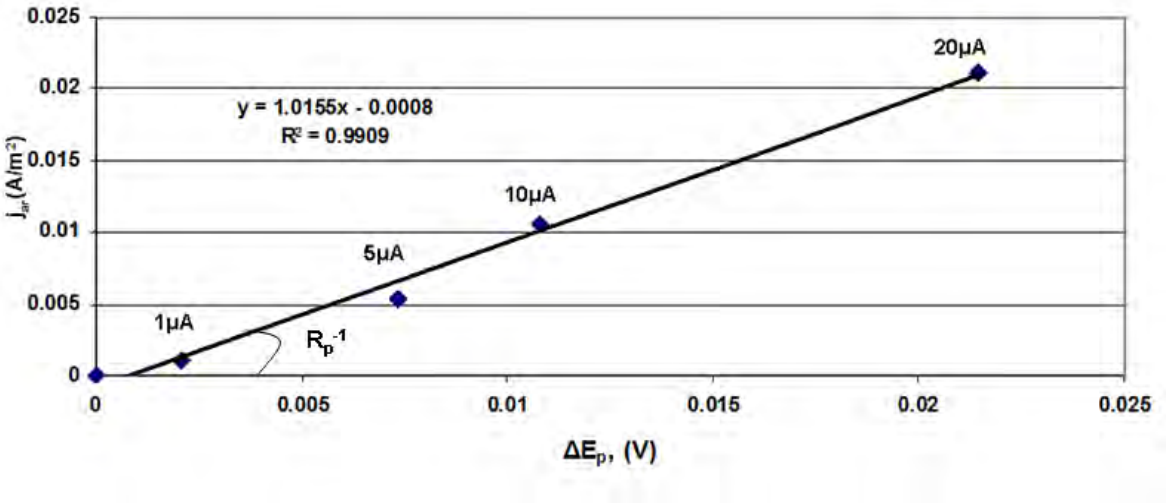

Figure VI. 23: Polarisation (ΔEp(V) vs. jar (A/m2)) curve at E_{corr} for polarisation resistance measurement on the active steel rebar embedded at 2cm.
The slope of this curve represents the Rp value ($Ohm.m^2$) of the steel rebar.

As it can be seen, in the above graph, the basic linear condition of the R_p measurement is quite respected. As it has been already mentioned, after each polarisation the system obtained a new equilibrium. The fit in of the curve is almost perfect, since the coefficient of determination is R^2=0.99. **As a criterion, R^2>0.85 was considered as acceptable, in order to confirm the linearity of the measurement and calculate the polarisation resistance value.**

Still, the **proposed model of measuring polarisation resistance can be considered quite reliable: a linear polarisation of 20mV (with a tolerance of ΔV= ±3mV) is achieved and so the main criteria of the polarisation measurement are full filled**. R_p is then calculated by the slope of the straight line and is found $1Ohm.m^2$.

In order to be able to estimate quantitatively the state of corrosion of the reinforcement, it is necessary to transform the polarisation resistance into corrosion current density. As it has been shown in §II.2.3.1, Stern and Geary (1951) presented eq.24 in order to calculate the

corrosion current density. In this particular study, the corrosion rate estimation is based on the same equation, undergoing two alterations:

- The term B is theoretically calculated via the equation $B = \frac{\beta_a \cdot \beta_c}{\ln(10) \cdot (\beta_\alpha \beta_c)}$ (eq. 52), where β_a and β_c the Tafel coefficients, that were used, in order to characterise the state (active or passive) of the concrete-reinforcement interface, (eq. 16 and 17), in the numerical simulations.
- As it is already clear, the proposed polarisation resistance measurement model doesn't confine the injected current within a specific area of the steel rebar. The units of the estimated polarisation resistance are A.m^2.

Thus, via eq. 52, by considering the values of Tafel slopes measured used in the simulations, B was found equal to 0.038 V contrary to the value of 0.026V proposed by Stern and Geary (1951) and RILEM recommendations (C. Andrade, C. Alonso, 2004). The corrosion current density can be then calculated as: $j_{corr} = \frac{B}{Rp}$ (eq. 53). In the example presented above, it has been estimated 2.5μA/cm^2. According to corrosion criteria, presented in table 4 (§II.2.3.2) (RILEM recommendations (C. Andrade, C. Alonso, 2004)), the corrosion is classified as high. This comes into agreement with the risk of corrosion indicated by the measurement of corrosion potential.

Similar procedure has been followed for the measurements carried out on the passive (non carbonated) reinforced concrete slabs. In order to calculate the real potential shift on the "point of interest" on steel rebar's surface, the abacus of *k* (figure V.34) and (eq. 48) are used. Similarly, the abacuses of a and b (figure V.36 and V.37) are used along with (eq. 51), in order to evaluate the real current density on that "point of interest". R_p is then calculated as it was demonstrated in figure V.40, and eq. 53 serves for estimating the corrosion current density. The constant *B* in this case is then calculated on the basis of β_a and β_c used in the simulations of passive steel rebars and is found equal to 0.041V. This value is lower than 0.052V, which is proposed by RILEM committee.

Figure VI.24 exhibits an example of calculating polarisation resistance and so estimating corrosion rate for the single steel rebar embedded at 2cm, being at passive state (I-NC):

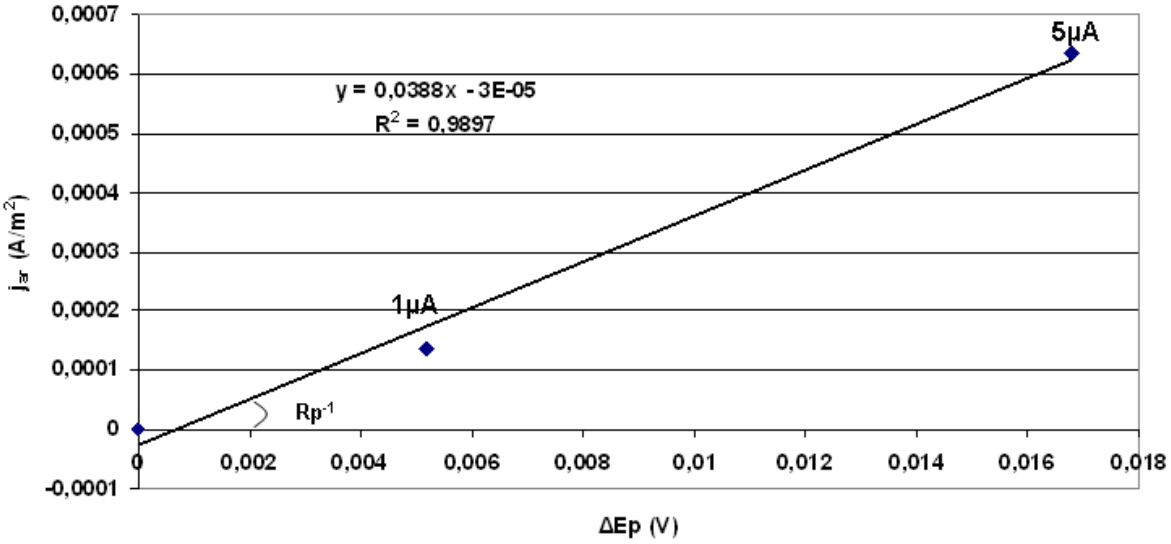

Figure VI. 24: Polarisation (ΔE_p(V) vs. j_{ar} (A/m^2)) Curve at E_{corr} for polarisation resistance measurement on the passive steel rebar embedded at 2cm. The slope of this curve represents the R_p value (Ohm m^2) of the steel rebar

In the figure VI.24, the linear polarisation of 20mV, is perfectly achieved (R^2=0.99). The polarisation resistance is equal to 25.8 Ohm.m^2. This graph confirms what it was demonstrated in §V.3.4.2 for measuring polarisation on passive rebars; 5µA of injected current were enough to induce a potential drift of 20mV on the steel rebar. Then, via eq.37, the corrosion current density is found 0.1µA/cm^2, classifying the corrosion according to table II.4 (RILEM recommendations (C. Andrade, C. Alonso, 2004)), as negligible. This behaviour can be expected, since the OC potential value of (-0.03V) has already indicated a very low risk of corrosion.

VI.4.2.3. Anodic aspect of the polarization resistance measurement

In this paragraph, a closer look at the "anodic aspect" of the polarisation resistance measurement is taken. The current dissertation proposed a polarisation resistance measurement model (chapter V) that injects a current, in the aim of **inducing anodic polarisation**. The establishment of relationships and the built-up of correction laws and abacuses were based on numerical **simulations of anodic polarisation**. Figure VI.24, apart from the linearity of the proposed technique, also confirmed the condition of anodic polarisation on the steel rebar surface, on that particular "point of interest".

However, it has been observed for concrete cover higher than 3cm that despite the anodic polarisation measured by the reference electrode on the concrete surface, the proposed

procedure gave potential values on the steel rebar, E_{ar} (V), more electropositive than the corrosion potential values.

Table VI.7 presents the polarisation data for the measurement taking place on the single steel rebar, embedded at 5cm, being at active state (same series of measurements as for 2cm, so ρ=584 Ohm.m).

Table VI- 7: Data obtained after induced polarisation for each injected current on the single bar embedded at 5cm, being at active state (I-C): E_{corr} (V), E_{RE} (V) measured by the RE_{SCE}, E_{ar} (V) calculated according to the proposed procedure of the new Rp model

E_{corr} (V)	I_{CE} (µA)	E_{RE}(V)	E_{ar} (V)
-0.475	1	-0.468	-0.473
-0.475	5	-0.446	-0.473
-0.471	10	-0.422	-0.470
-0.468	**20**	-0.376	**-0.482**
-0.466	**30**	-0.333	**-0.493**
-0.465	50	-0.248	-0.462

In the table VI.7, it can be clearly noticed that for the steel rebar embedded at 5cm, for none of the injected currents the model is well adapted ; the application of the correction laws and abacuses did not show the desirable polarisation of 20mV **(a polarisation of 20±3mV is considered as acceptable)** on the steel rebar. Especially, in the case of an injected current of 20 or 30µA, the corrections proposed by the model on the values measured by the reference electrode, are so strong indicating a false cathodic polarisation on the steel rebar, despite the anodic polarisation measured on the concrete surface. In this case, it is impossible to evaluate the corrosion rate of the reinforcement. This behaviour was even more intense when the resistivity increases (ρ≥800 Ohm m).

Thus, the **effectiveness and validity of the current proposed polarisation resistance model may be limited for certain ranges of concrete cover (e≤4cm) and resistivity (ρ≤800 Ohm m)**. It is also important to mention that this was mainly observed for measurements carried out on both types of configurations (I and II) for the active state of the reinforcement (C). As a result, according to what it has been already mentioned, figure V.40 may be completed (Figure VI.25):

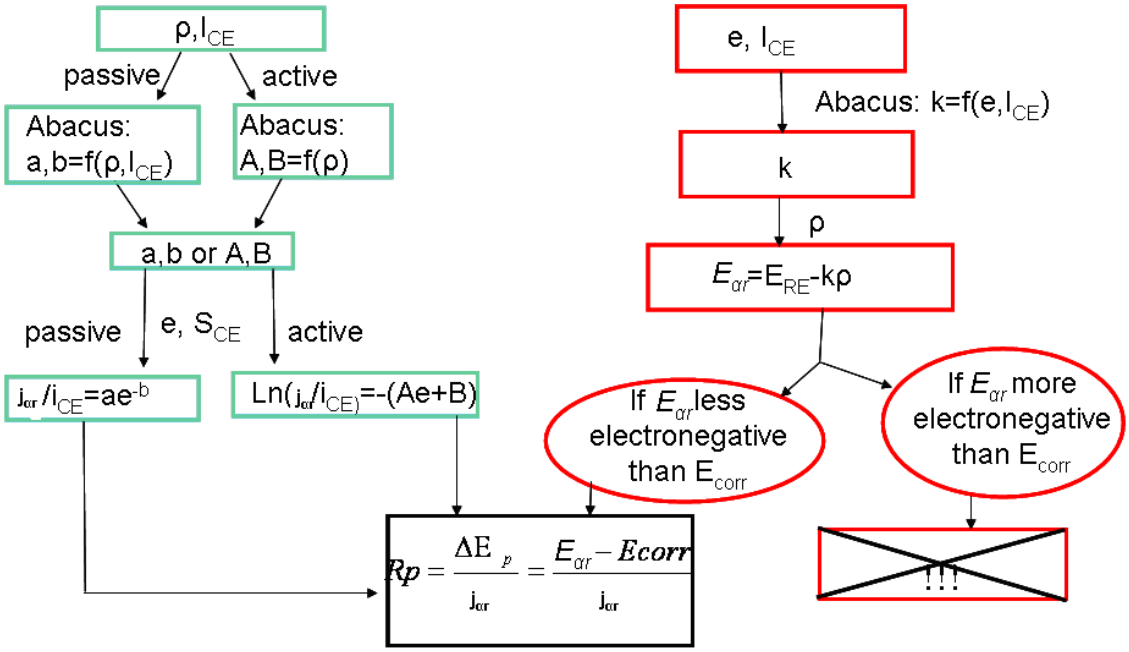

Figure VI. 25: Schematic illustration of the procedure, calculating the real value of polarisation resistance for an active or passive rebar

V.4.2.4 The aspect of time in polarization resistance measurement: Polarization and De-polarization duration

As it was described in earlier paragraphs, the duration of polarisation has been fixed to last **maximum 200 sec** (Galvapulse 20sec, Gecor 100sec). Both these time values were defined according to the **experience** obtained, after the realisation of several (>20) polarisation resistance measurements. It has been noticed that this duration (200sec) was long enough to assure that the potential shift due to the current injection evolves till it achieves and it certainly stabilises at its maximum value. In that way a smooth, effective and efficient polarisation is carried out for all steel rebars embedded with low (i.e. 2cm) and high (i.e. 5cm) concrete covers. This also comes into agreement with Luping's (2002) remarks concerning the influence of polarisation duration on the quality of the results obtained (§ IV.2).

As far as the depolarisation duration is concerned, contrary to the other existing techniques, the novel proposed methodology takes into account and needs to control the de-polarisation of the reinforcement after the end of the current injection. Once more, the depolarisation duration has been **experimentally** set at maximum 600sec. After several polarisation-depolarisation tests on concrete specimen of the laboratory, using different de polarisation durations, it has been noticed that 10min were sufficient for the system to return to its initial

equilibrium or obtain a new one after polarisation measurement, so as to be able to disturb again the steel rebar. For low values of injected current (i.e. 1-10μA), the system finds a thermodynamic equilibrium in much less time than 600sec.

Obviously, it consists of an apparent temporary equilibrium and the system obtains its real steady state, about 24 hours after the last polarisation. The data obtained after a continuous monitoring (the measurements have been realised every two days over a certain period of time) of the corrosion state of the carbonated slab, have been enlightening on this phenomenon. These data will be presented later on this chapter.

Generally, for all measurements, the OC potential difference, was diminished and limited to only 10mV.

VI.4.2.4 Synthesis

In the previous paragraphs, a demonstration of the polarisation resistance measurement model, proposed in this study, was carried out. The simulated geometries (and so the technical characteristics of the reinforced concrete cooling towers) were reproduced on real lab scale conditions, and thus concrete slabs, carbonated (active conditions) and non carbonated (passive conditions), with the single rebar and the two crossing rebars configuration were fabricated. A measurement procedure was developed, consisting two steps: a resistivity measurement and successive corrosion potential-galvanostatic measurements, till **a linear anodic polarisation of 20±3mV** was achieved. In addition, it was demonstrated step by step, the procedure of estimating polarisation resistance and proposed a new one for calculating corrosion current density. This paragraph confirmed **that the probe functions effectively, proved its feasibility (making rather possible its utilisation on the real site cooling towers) and validated the proposed interpretation technique, since both theoretical anodic and linear criteria are respected**. Still, the factors that could limit its effectiveness and efficiency (**efficient for e≤4cm, ρ≤800 Ohm m)** should not be neglected. Then, a reference to the aspect of **time** was made, clarifying that, for the moment, it is **experimentally** determined; however a more thorough investigation (i.e. numerical testing) on its influence on the system's response to the measurement could be recommended. Table V.1 (§V.1.1) is finally enriched with the technical characteristics of the polarisation resistance measurement method proposed in the current study and a new table (Table VI.8) can be proposed:

Table VI- 8: Technical Characteristics of GECOR 6, Galvapulse and LMDC model

	GECOR6	**Galvapulse**	**LMDC model**
Reference electrode	$Cu/CuSO_4$ (+0.199mV vs. E_{SHE})	Ag/AgCl (+0.318mV vs. E_{SHE})	SCE (+0.241mV vs. E_{SHE})
Contact between electrodes' configuration/concrete	Saturated wet sponge	Saturated wet sponge	Saturated wet sponge
Electrical continuity between instrument/reinforcement	Access and electrical connexion to the steel rebar	Access and electrical connexion to the steel bar	Access and electrical connexion to the steel rebar
Type of confinement of polarisation	Guard ring electrode (¢180mm) + 2 auxiliary reference electrodes	Guard ring electrode (¢99mm)	No
Injected current from the counter electrode ,I_{CE} (µA)	10	20-100	1,5,10,20,30,50 µA till linear anodic polarization of 20mV on the steel rebar
Injected current from the guard ring electrode, I_{GE} (µA)	Controlled by the potential difference between the 2 auxiliary reference electrodes: $\Delta E_{aux.ref}=0$.	Controlled by the potential of the counter electrode, E_{CE}	No
Polarisation duration (sec)	100	10	200sec
De polarisation duration (sec)	No	No	600 sec after each polarisation
Reinforcement length	105	70	No

assumed to be polarised (mm)			

VI.4.3. Application of the proposed polarisation resistance measurement model: Estimation of the corrosion current density of the reinforcement

The following paragraphs describe the results obtained for the series of the experimental measurements depicted in figure VI.20. Only the results for the steel rebars with the extreme values of concrete cover, for both types of configuration (I and II) and concrete state (C and NC) will be presented and discussed.

VI.4.3.1. Results obtained with slab I-C

In Figure VI.26, the average resistivity of the I-C slab and the corrosion potential values for the bars at 2 and 5cm are given for two measurements, the one realised in July 2012 and the other one in November 2012:

a)

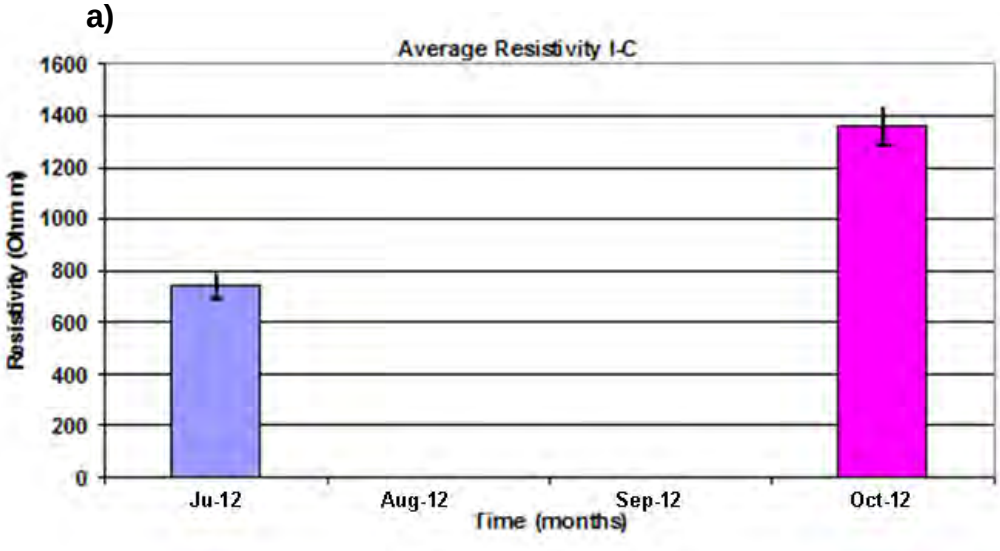

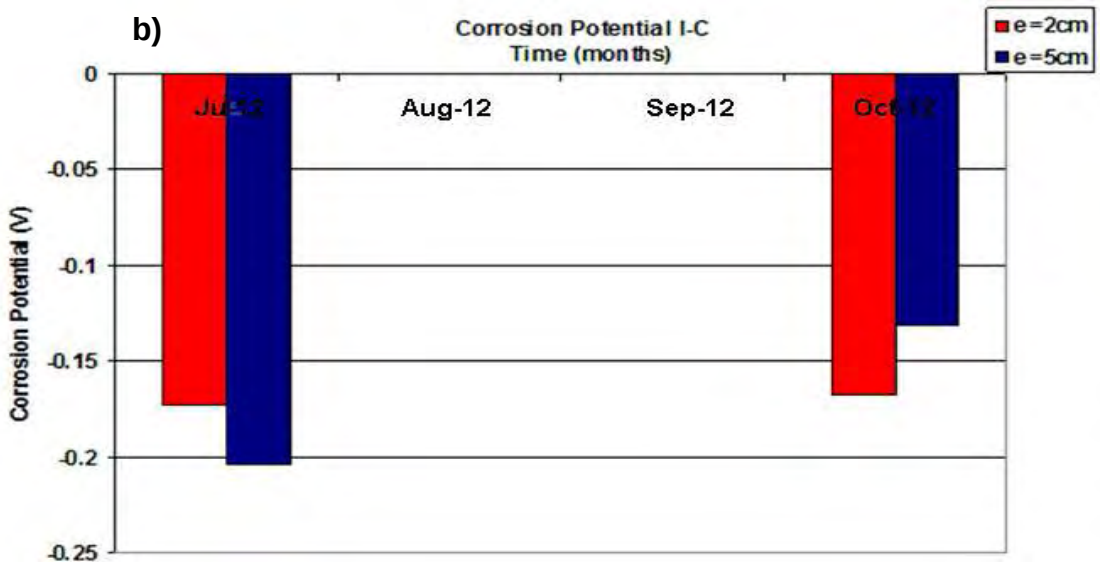

Figure VI. 26: Average concrete resistivity for I-C slab in July and October 2012 (a), corrosion potential values (before any polarisation) (b) for the steel rebar at 2 and 5cm. The slab had already been removed from the carbonation in June 2012, and from July till October, it was preserved in the laboratory ambiance.

As it can be seen from the figure VI.26, during July the concrete slab exhibited a relatively high but reasonable value of resistivity, since it was fully carbonated. For the same month, corrosion potential values show that both steel rebars exhibit an intermediate risk of corrosion (table II.2, §II.2.2.). However, the steel rebar at 5cm exhibited a more electronegative corrosion potential value than the steel rebar at 2cm. This could be considered as reasonable since the rebar at 2cm is closer to the concrete surface of the slab. Thus, the upper layers of the concrete slab may dry faster than the lower ones and this may be reflected in the value of the corrosion potential. Still, it could be said, that within this range of potential, it is impossible to obtain a clear image and define the risk of corrosion for the reinforcement.

Between July and October, where the concrete slab was maintained in the laboratory environment, concrete resistivity has augmented by 616 Ohm.m. Since resistivity is highly related to the water content of the concrete slab, the elevated value obtained in October, is the result of a strong decrease in the moisture content of the slab. Furthermore, corrosion potential stayed more or less stable for the steel rebar at 2cm (5mV of difference) while the increase of resistivity had a greater effect for the steel rebar at 5cm, since a corrosion potential decrease of 73mV was noticed. Still, for both steel rebars, their potential value indicated an intermediate risk of corrosion according to table II. 2, §II.2.2.

In addition, taking into account the values of resistivity, it could be implied that the concrete slab has started being dried out since its removal from the chamber of accelerated carbonation, inducing the slowing down of corrosion kinetics. In other words, **once the**

conditions that favour the evolution of corrosion in time were stopped (high water content in the ambiance), the corrosion mechanism could be eventually "blocked". In addition to that, the **dry warm period of summer** between the two measurements, could contribute to this "blockage" even more, **making the already once corroded steel rebars to act as "passives" in time**.

The values of polarisation resistance and corrosion current density presented in the table VI.9 and Figures VI.27 and VI.28, should provide with more accurate information for corrosive state of these two steel rebars. In addition, since the figure VI.26 **indicated a severe slowing down of the corrosion kinetics of the corroded rebars, the steel rebars were also treated as being "passive**", using the abacuses and correction laws that were developed for passive rebars.

Table VI- 9: Polarisation resistance measurement results for the embedded bars at 2 and 5cm, considered to be at active and passive state.

	Active state				**"Passive" state**	
Bar embedded at:	2		5		2	5
Measurement in:	**July 2012**	**October 2012**	**July 2012**	**October 2012**	**October 2012**	**October 2012**
Concrete resistivity	740	1383	740	1383	1383	1383
E_{corr} (V)	-0.173	-0.168	-0.204	-0.131	-0.168	-0.131
I_{CE} (µA) at which the polarization of 20mV was achieved	1	5	10	1	5	1
Rp (Ohm m2)	5.85	3.13	2.5	41	38	208
j_{corr} (µA/cm^2)	0.6	1.2	1.5	0.09	0.1	0.02

Via table VI.9, the following were noticed:

- In the case of the rebar embedded at **2cm**, it can be noticed that though the corrosion potential remained almost stable, it required much more current to polarise (20mV±3mV) the steel rebar on October. This can be attributed to the **big increase in concrete**

resistivity during the months between the two measurements and it confirms the influence of resistivity on the proposed model as it was presented in chapter V.

- On the contrary, in the case of **5cm**, it can be seen that along with the increase in resistivity, the **slowing down of the kinetics of corrosion of the rebar**, has led to the injection of a small current, being sufficient to achieve the desirable polarisation. This also comes into agreement with what has been stated for the influence of state of the reinforcement on the proposed model, thoroughly discussed in §V.3.4.2.
- Finally, when it comes to the influence of concrete cover on the proposed model, as it is expected (see also § V.3.4.1), for concrete cover of 5cm, more injected current was needed in order to polarise it effectively (20mV±3mV) than in the case of concrete cover 2cm. Still, the geometric effect (§V.3.4.1) shouldn't be neglected; for the measurement realised on October 2012, apart from the apparent change in the state of the rebar embedded at 5cm, the injection of a so low current value, compared to the one for the polarisation of the rebar at 2cm, can be also attributed partially to the geometric effect.

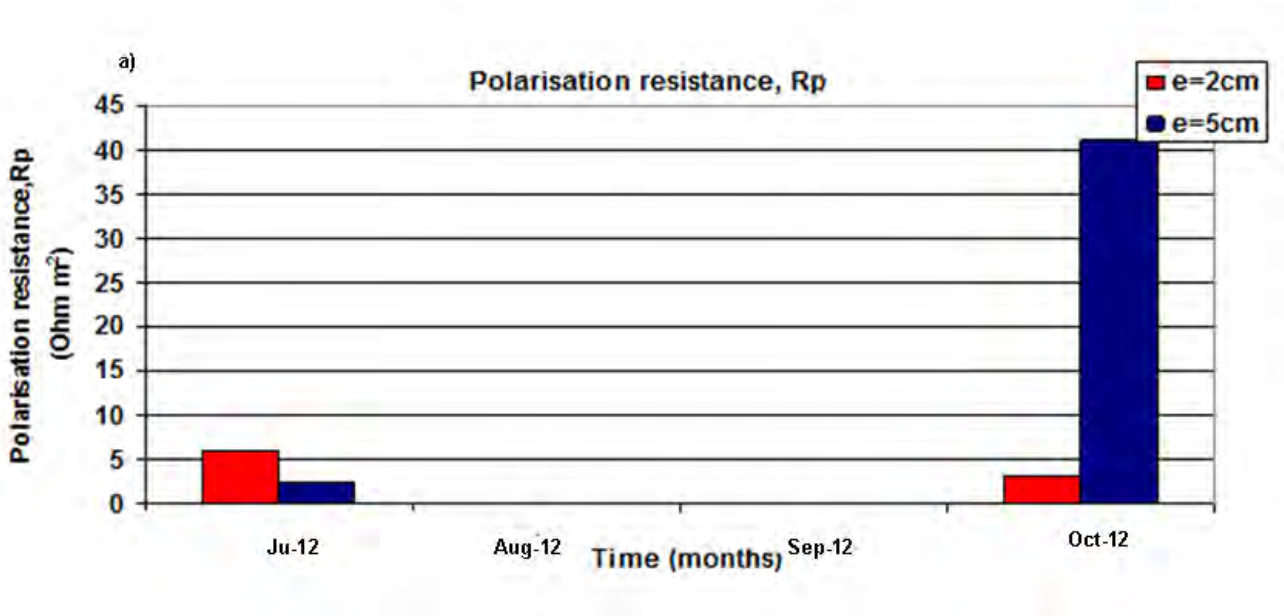

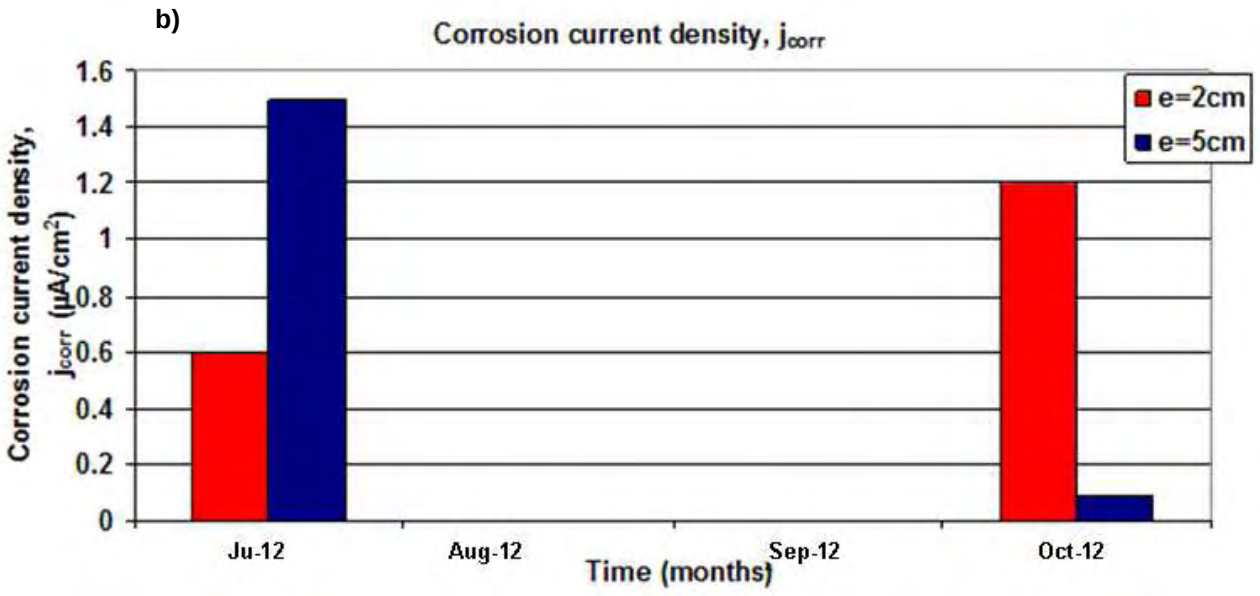

Figure VI. 27: a) Polarisation resistance and b) corrosion current density values for the active steel rebars embedded at 2 and 5cm, measured at two different periods (July and October 2012).

Now, according to the polarisation resistance and corrosion current density values of figure VI.27:

- In the case of the steel rebar at 2cm, the evaluation of corrosion current density indicates a severe corrosion. This may lead to confusion, since the steel rebar is presented rather active, while the opposite behaviour could be expected, considering the measured resistivity, corrosion potential and the value of current used for polarisation. Perhaps, in this particular case, due to the re humidification of the concrete surface during the resistivity measurement and the use of the saturated wet sponge, the state of the steel rebar embedded close to the concrete surface may have been influenced.
- As far as the rebar with a concrete cover of 5cm is concerned, in July it presents an elevated risk of corrosion, while 3 months later, in October, the rebar exhibits a very low value of corrosion current density, implying a very low risk of corrosion. This seems to be coherent with the values of measured resistivity, corrosion potential and the value of the current injected in order to polarise by 20±3mV the steel rebar. As a result, the slowing down of the corrosion kinetics of the steel rebar is confirmed.

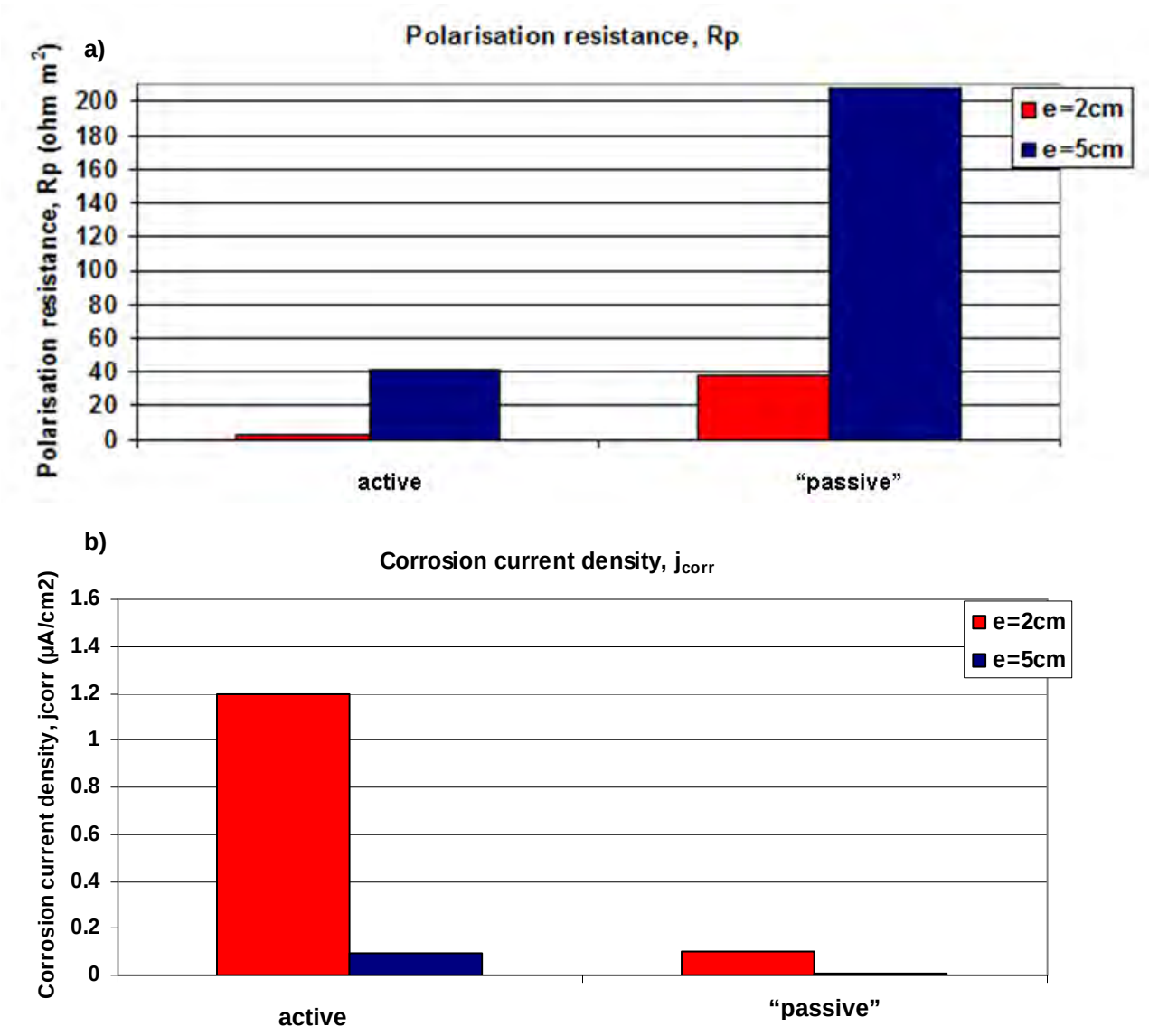

Figure VI. 28: a) Polarisation resistance and b) corrosion current density values for the embedded rebars at 2 and 5cm, measured at the same period (October 2012), treated as active and apparent "passive" rebars).

Now,as far as the results depicted in figure VI.28, it can be stated that:

- When the rebars for the measurement of October are treated as passive, the use of correction laws and abacuses give values of corrosion current density within the range of very low risk of corrosion. Still, the value for the rebar at 2cm is greater than that of the rebar at 5cm by a factor of 10. In addition, whether the rebar at 5cm is treated as passive or active, the risk of corrosion remains very low; on the other hand, in the case of the rebar with a concrete cover of 2cm, the use of correction laws for active conditions indicate a quite active rebar, while in the case of correction laws for passive rebars, the rebar acts as passive.

As it is understood by now, it seems that atmospheric carbonation is a less aggressive process against reinforced concrete, compared to corrosion induced by chlorides. This was also underlined by the measurement of Tafel constants, (§VI.3.2.) which exhibited high values, contrary to the ones found in literature for more aggressive environments.

Furthermore, these measurements showed how important role concrete resistivity plays on the evolution of corrosion and so, on the proposed polarisation resistance model. This also comes into agreement with the results given by the experimental design (DOE) in §V.4. Thus, the presence of high humidity in the ambiance (so high water content in the concrete slab) favours the corrosive activity while its absence may slow down or stop corrosion.

For that reason, after the end of these measurements, the I-C concrete slab was stored for 45 days, in the chamber of fixed temperature (20^{o}C) and humidity (95%RH), in order to re-activate the corrosion activity and evaluate again the corrosion state of the steel rebars. Once the corrosive state of the armatures was ensured, the concrete slab was transferred again in the laboratory environment and two days later new polarisation resistance measurements were launched.

VI.4.3.2. Results obtained with slab I-C: Reactivation of corrosion

The figures VI.29, VI.30 and VI.31 show the evolution of resistivity, corrosion potential and polarisation resistance.

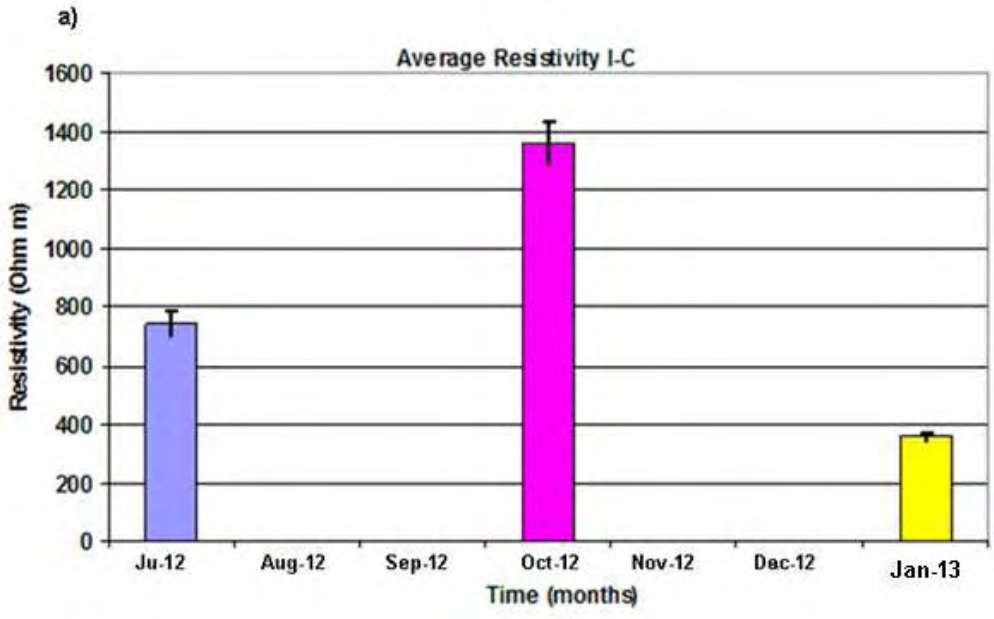

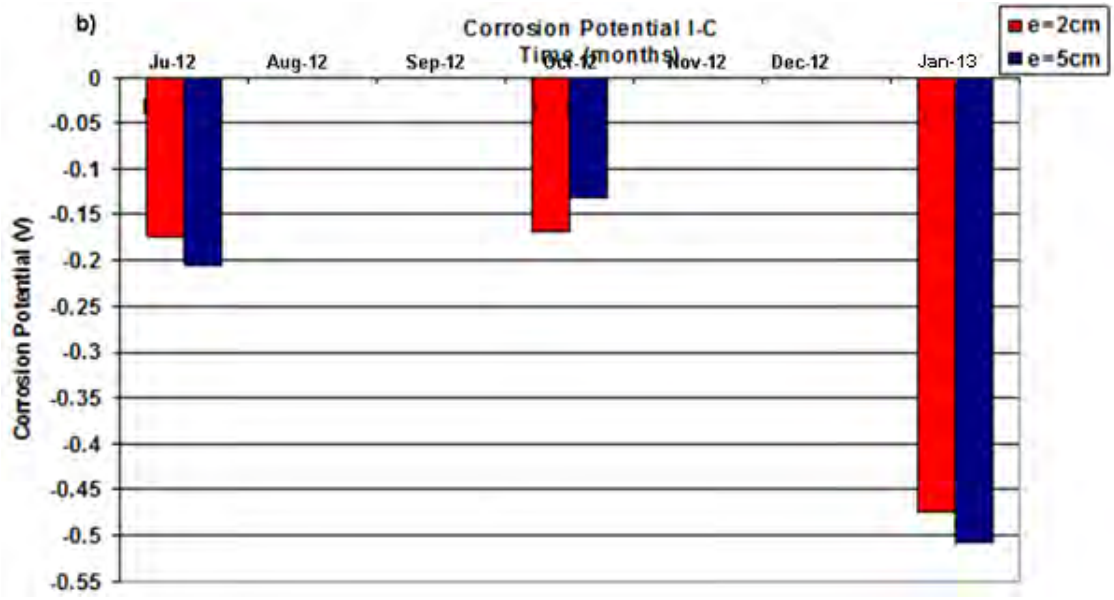

Figure VI. 29: a) Average concrete resistivity for I-C slab in July, October 2012 and January 2013, b) corrosion potential values (before any polarisation) for the steel rebar at 2 and 5cm. The slab was already removed from the carbonation chamber in June 2012, and from July till October 2012, it was preserved in the laboratory ambiance. In the end of November 2012, the slab was stored for 45 days in the chamber of fixed temperature (20°C) and humidity (95%).

Figure VI.29 clearly demonstrates that after the resistivity measured, after the slab being stored in the highly humid chamber, was 1000 Ohm .m lower than that measured in October. This decrease in resistivity is accompanied by the quite electronegative measured potential values of the steel rebars at 2 and 5cm, indicating an elevated risk of corrosion and confirming the restart of the corrosive activity. Despite some differences between the corrosion potential of the rebar at 2cm and that of the rebar at 5cm, the initial hypothesis of uniformity is still sufficiently applied.

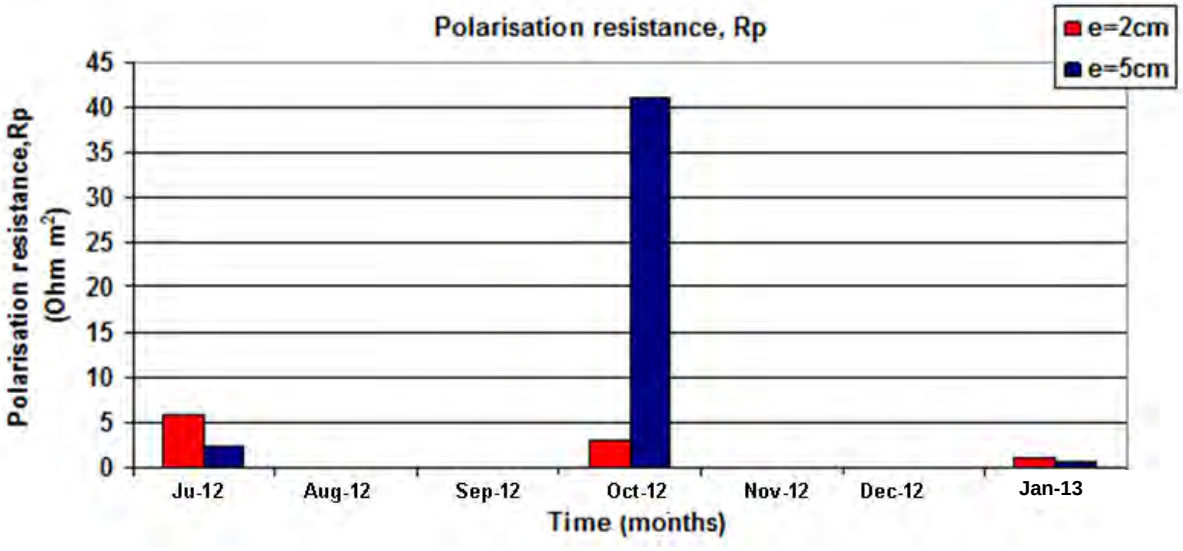

Figure VI. 30: Polarisation resistance values for the embedded rebars at 2 and 5cm, measured on July, October 2012 and January 2013.

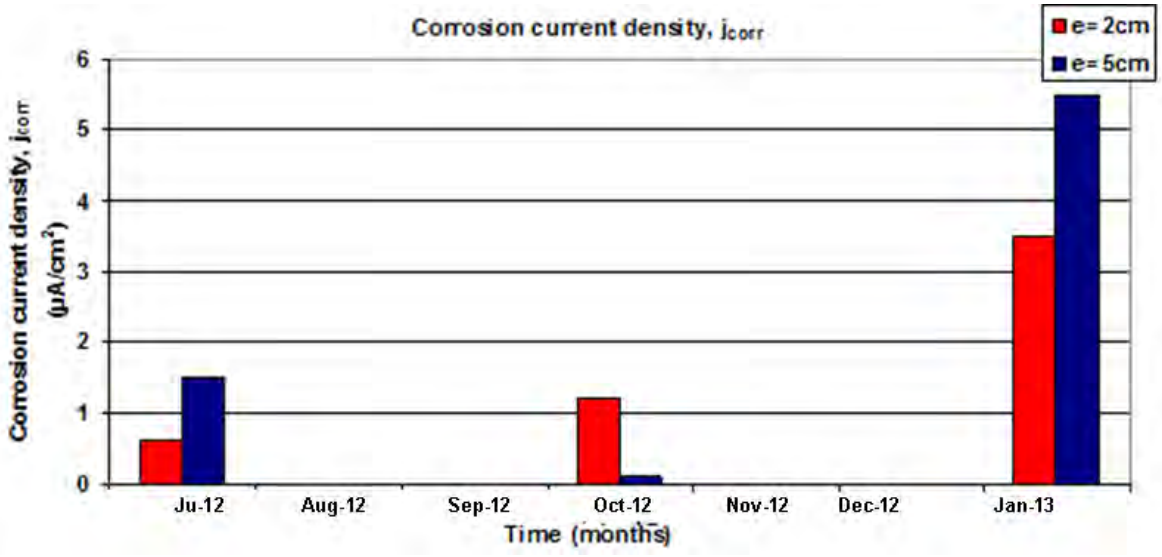

Figure VI. 31: Corrosion current density values for the embedded rebars at 2 and 5cm, measured in July, October 2012 and January 2013.

Next, figures VI.30 and VI.31 demonstrate that in January 2013, polarisation resistance has significantly decreased and so corrosion current density has proportionally increased compared to the values measured 3 months earlier. These new values suggested a sever corrosion and were in coherence with what was indicated by the concrete resistivity and corrosion potential measurement. Apparently, these results confirm that the moisture condition of the concrete is the major "catalyser" of the corrosion process.

Finally, in the figures VI.30 and VI.31, despite the more or less uniform conditions achieved, someone should notice significant differences between the polarisation resistance and corrosion current density values measured for the rebar at 2cm and those measured for the rebar at 5cm.

VI.4.3.3. Relation between polarization resistance-resistivity and polarization resistance-corrosion potential

As it can be seen by so far, the evolution of polarization resistance is indicated more or less by the evolution of resistivity and corrosion potential. Based on the results obtained and presented in the previous paragraphs, in figures VI.32 and VI.33 polarization resistance values are plotted against resistivity and corrosion potential values.

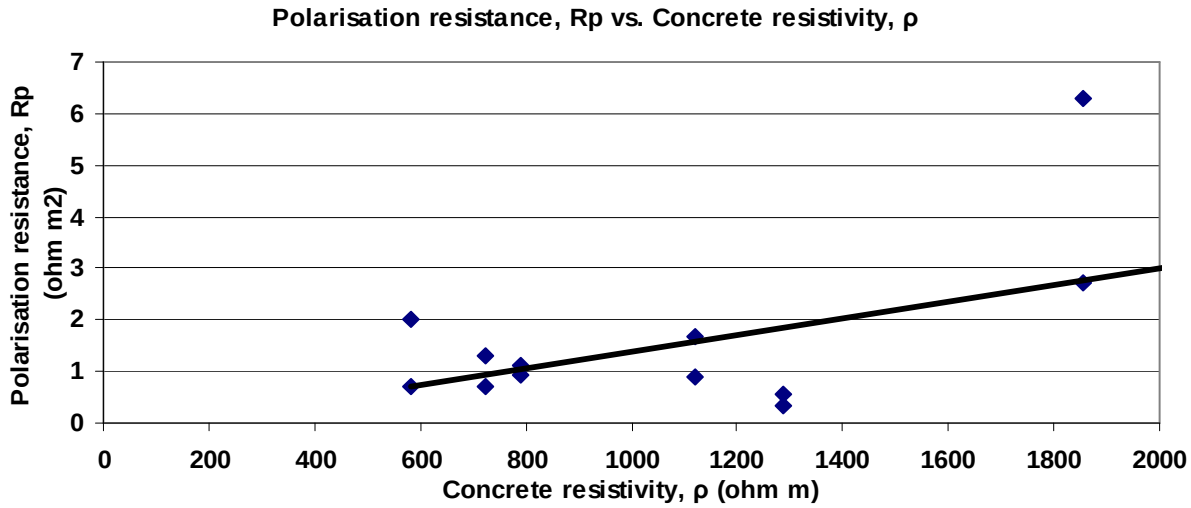

Figure VI. 32: Polarisation resistance Rp, plotted vs. Concrete resistivity, ρ.

As it can be seen, according to the figure VI.32, an augmentative tendency is observed between the polarization resistance and concrete resistivity. Especially, when concrete resistivity obtains really high values the augmentation in polarisation resistance becomes steeper. Same tendency is observed, in the figure VI.33, where polarization resistance is plotted against corrosion potential values. Obviously, the more the corrosion potential moves towards to less electronegative values the more the polarization resistance increases.

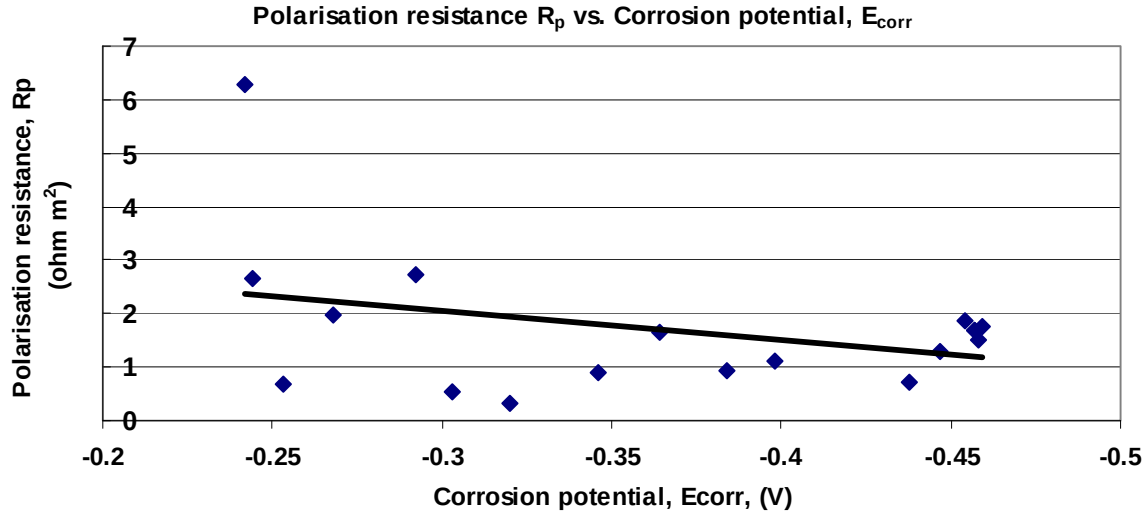

FigureVI. 33 : Polarisation resistance Rp, plotted vs. Corrosion potential, E_{corr}

VI.4.3.4. Results obtained with slab I-NC

The following paragraphs present the results obtained for the measurements of October 2012 carried out on the I-NC reinforced concrete slab and they are compared with those for the I-C slab, being realised at the same period. Firstly, figure VI.34 depicts the average measured concrete resistivity for these two concrete slabs and the corrosion potential values of the steel rebars embedded at 2 and 5 cm:

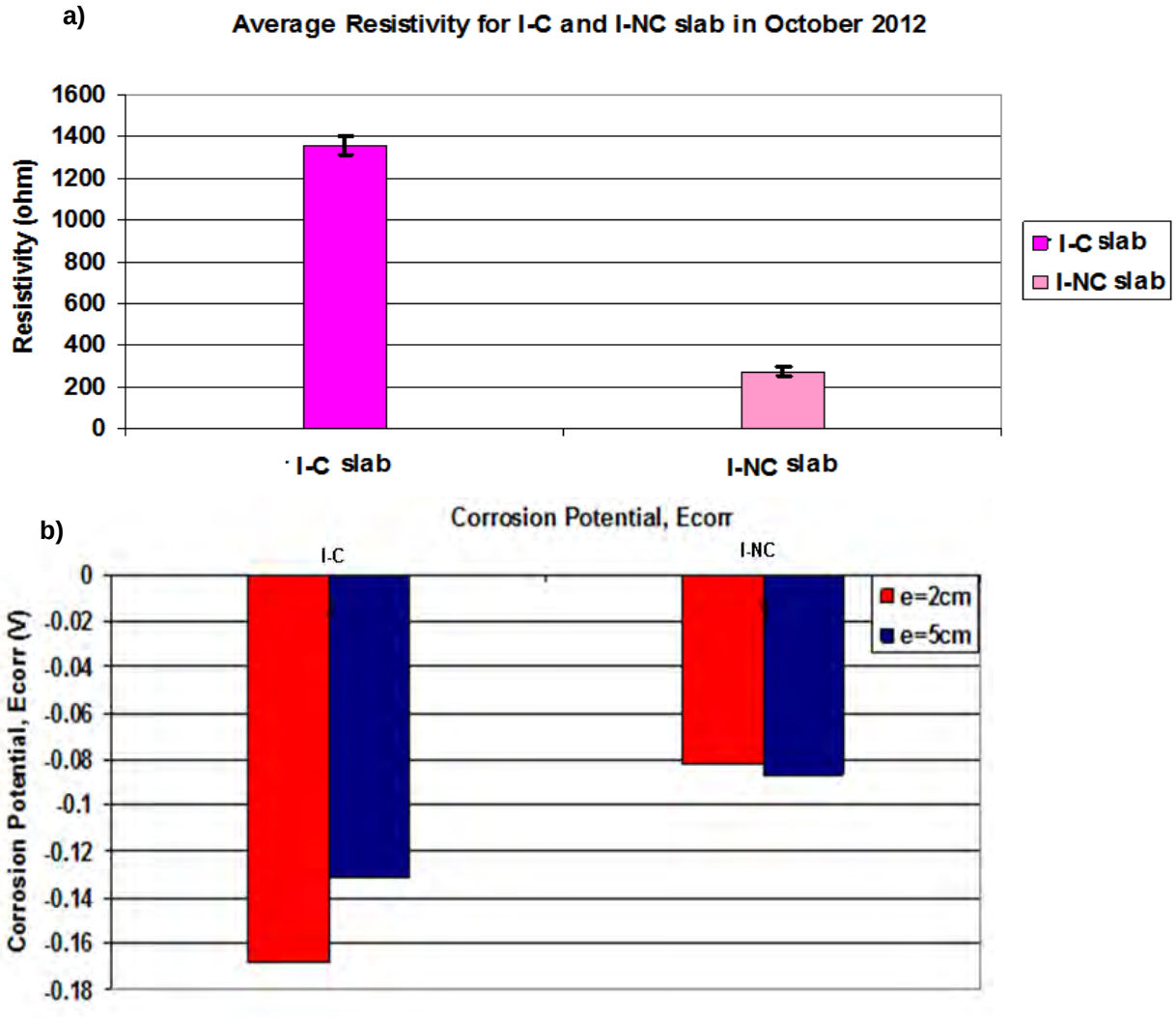

Figure VI. 34: a) Average concrete resistivity for the I-C and I-NC concrete slab and b) corrosion potential values for the embedded rebars at 2 and 5cm (b), measured in October 2012.

As it can be seen from figure VI.34 the concrete resistivity for the non carbonated (NC) slab is much lower than that for the carbonated (C) slab. This is considered to be expected, since carbonated concrete is much more compact than the non carbonated one. Furthermore, the potential values of the steel rebars in the NC slab are more electropositive than those in the case of the steel rebars in the C slab, indicating clearly a very low risk of corrosion and thus

confirming their passive state. The fact that the values between the steel rebar at 2cm and the one at 5cm differ only by 5mV suggests the establishment of uniform conditions.

The polarisation resistance and corrosion current densities values for the steel rebars are depicted in figure VI.35:

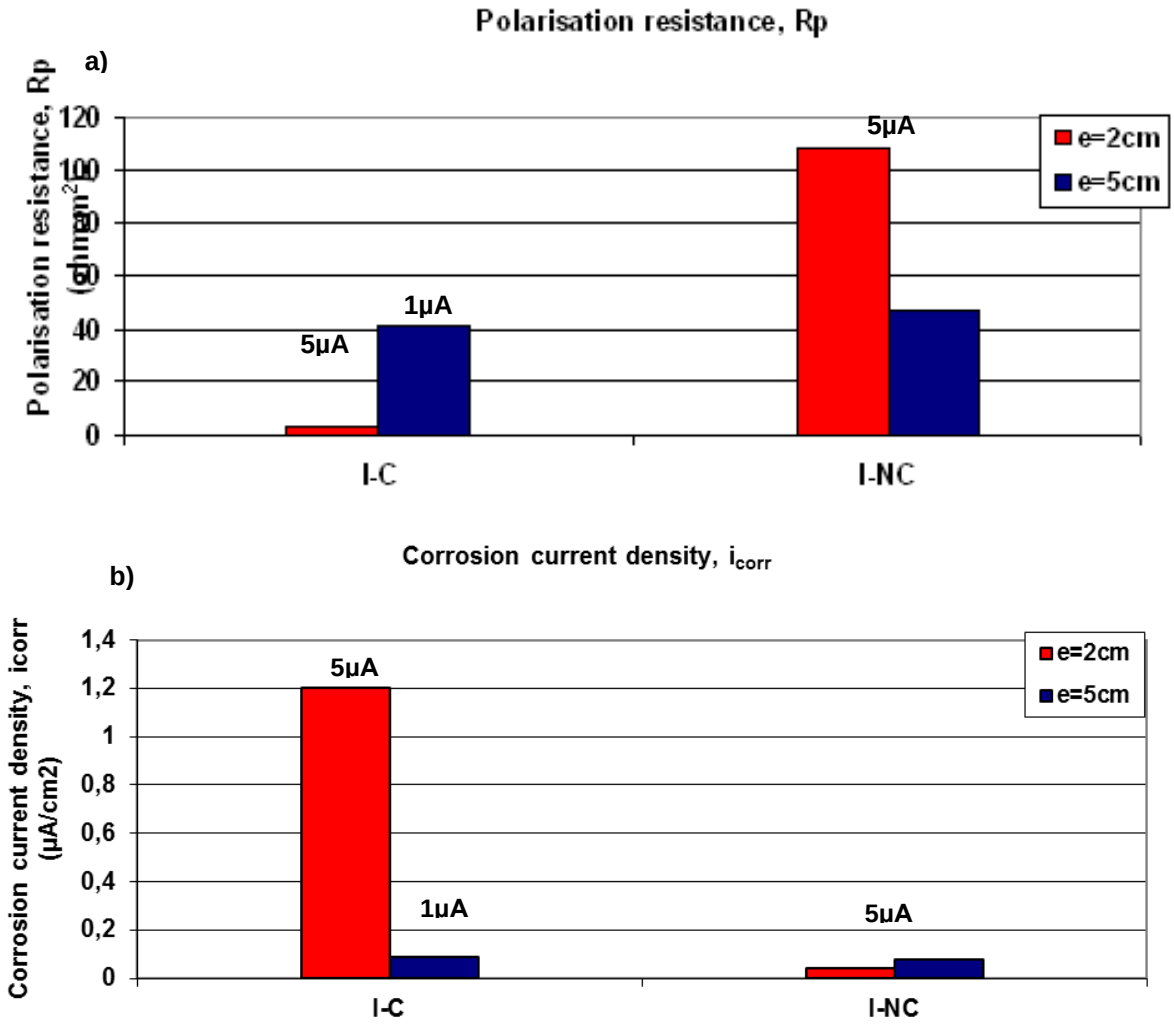

Figure VI. 35: Polarisation resistance, Rp, (a) and corrosion current density, j_{corr}, (b) values for the embedded rebars at 2 and 5cm, in the C and NC slabs, measured in October 2012. The value of injected current for which the polarisation-target of 20mV±3mV was achieved is also given for each measurement.

According to figure VI.35, the values obtained for the steel rebars in the NC slab indicate clearly that the reinforcement remains in a passive state, coming into agreement with the low risk of corrosion indicated by the corrosion potential values. In addition, the use of very small injected current (5µA) in order to polarize sufficiently the steel rebars confirms what it was discussed in §V.3.4.2 concerning the behavior of the passive steel rebars towards polarization. Furthermore, the current corrosion density estimated for the rebar embedded at 2cm is very close to that of the rebar embedded at 5cm, contrary to the case of the steel rebars embedded

in the C slab. Apparently, the passive steel rebars behave as it is expected to the imposed excitation. Apart from that, it could be reasonable to think that **in the case that resistivity and corrosion potential measurement indicate a strong passive state of the reinforcement, there would be no necessary reason to continue any further the investigation of the state of corrosion, by applying a polarization resistance measurement**. For that reason, in the following paragraph, where behavior of the configuration of two crossed rebars will be examined, only the results obtained for the carbonated concrete slab will be presented and discussed.

VI.4.3.5. Results obtained with slab II-C

In the case of the II-C slabs, polarization resistance measurements were carried out as they were indicated in the figure VI.20. The Figures VI.36 and VI.37, present the corrosion potential, polarisation resistance and corrosion current density values measured on October 2012 for points a and b, on the upper rebar of the two crossed rebar configuration, embedded at and 5cm respectively. The average resistivity of the II-C slab during that period was 726 Ohm m:

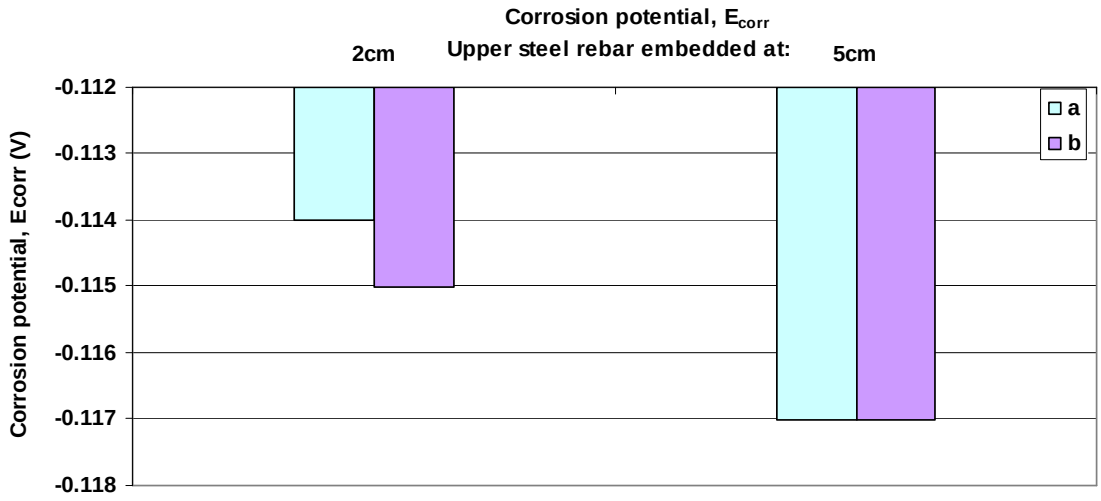

Figure VI. 36: Corrosion potential values for two different points (a and b) of measurement on the upper steel rebar embedded at 2 and 5cm.

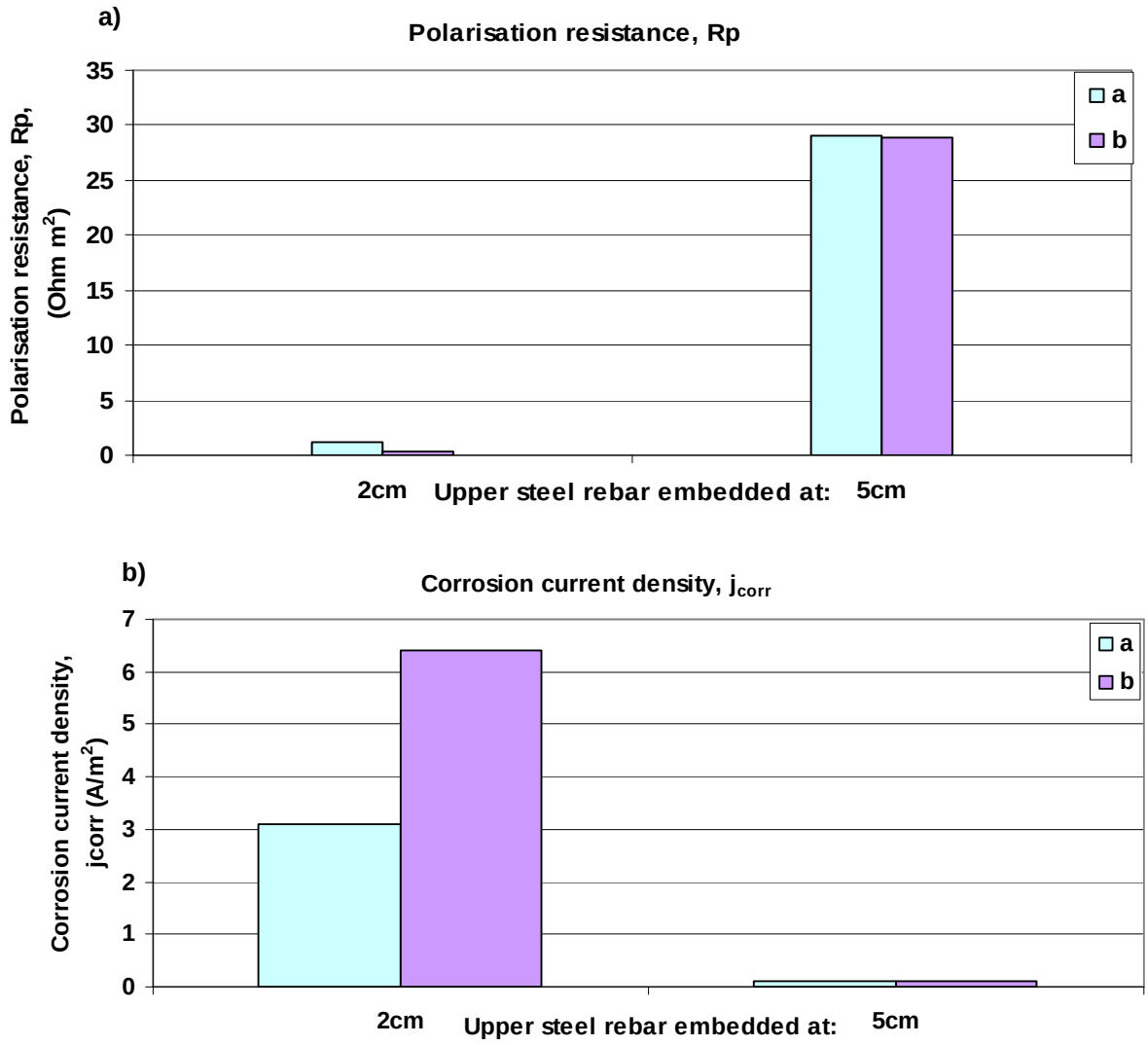

Figure VI. 37 : a) Polarisation resistance and b) corrosion current density values for two different points (a and b) of measurement on the upper steel rebar embedded at 2 and 5cm

Once more, the results of figure VI.36, suggest that uniform conditions have been well established and maintained along each rebar but also through the whole slab, since the corrosion potential values between the two rebars are very close to each other.

As it has been already mentioned in chapter V, the polarisation resistance values on point a were calculated according to the abacuses and correction laws developed for the measurement carried out above the crossing of the two rebars while on point b the abacuses and the correction laws established for the single bar configuration were used.

So, for figure VI.37.a it can be clearly observed, that in the case of a high concrete cover (e=5cm), the values are identical while in the case of a small concrete value (e=2cm), the corrosion current density estimated above the single bar is the double compared to the one measured right above the crossing of the two rebars. As it has been described in §V.3.4.3, this

difference in corrosion current density for the steel rebar at 2cm, can be related to the current that is lost when the measurement takes place above the crossing of the two rebars configuration. When the concrete cover becomes higher, the current losses become less for a high concrete resistivity.

Thus, it is confirmed that the geometrical effect, observed for the small values of concrete cover, combined with a quite resistive concrete, contribute to a larger dispersion of the injected current from the probe into the concrete. Finally, the concrete slab exhibits the same behaviour as the I-C slab (see §.VI.4.3.1), since both were stored under the same conditions.

VI.4.3.6. Synthesis

As it has been already presented in this paragraph, the proposed polarisation resistance measurement model was applied in all casted reinforced concrete slabs in order to evaluate the corrosion state of the reinforcement. The obtained results permitted to **confirm the role of the influencing parameters (resistivity, concrete cover, reinforcement configuration, state of the steel rebars) on the polarisation resistance measurement model**, as it was already discussed in chapter V. It showed that the evolution of corrosion is largely influenced by concrete moisture. In other words, **the water content in concrete expressed via the measurement of resistivity, greatly influences the corrosion process**. Thus, the absence of high humidity combined with the slow corrosive process in carbonated concrete, stops the corrosion of the steel rebars. This phenomenon became more remarkable for the steel rebars at high concrete covers. In addition, via the measurements carried out on the two crossed rebars configuration, it was concluded that **when the measurement is carried above the crossing of the rebars, embedded at small concrete cover, the results may be quite biased.**

VI.4.4. Uncertainty of the proposed polarisation resistance measurement model: tests of repeatability and spatial variability

As all measurements, the proposed method for measuring polarisation resistance of reinforced concrete is also subjected to variability. Its outcome may depend on the measuring system, the measurement procedure, the skill of the operator, the environment and other effects. Due to these influences, a dispersion of the measured may be observed, indicating how well the measurement is made. In order to identify the source of the errors leading to measurement

discrepancy, tests of repeatability and spatial variability were carried out. In the following paragraphs, the results of these tests will be presented and discussed.

VI.4.4.1. Repeatability test

Repeatability tests of the polarisation resistance measurement were carried out for type I of reinforcement configuration for the carbonated concrete slabs, in January 2013 (after the curing of the I-C and II-C slabs for 45 days in the chamber of fixed temperature (20^{o}C) and relative humidity (95%). The polarisation resistance measurement was repeated 10 times, on point "a" (figure VI.20). After and before each repetition, the electrode's configuration was disassembled and reassembled respectively. Table VI.10 presents **the results of the measurements that fulfilled the criteria of anodic linear polarisation,** for the repeatability test on the single bar (I-C) embedded at 2 cm:

Table VI- 10: Repeatability test results for the single bar (I-C) with concrete cover 2cm.

N^{o} of measurements	**E_{corr} (V)**	**I_{CE} (µA) for which $\Delta E_{p,max}$ was attained**	**E_{RE} (V)**	**ΔEp (=$E_{\alpha r}$-E_{corr}) (V)**	**$j_{\alpha r}$(A/m^2)**	**R_p (Ohm m^2)**	**j_{corr} (µA/cm^2)**
1	-0.459	10	-0.426	15.1	0.0088	1.77	2.1
2	-0.458	10	-0.427	12.5	0.0088	1.51	2.5
3	-0.454	10	-0.42	17.2	0.0088	1.88	2
4	-0.457	10	-0.424	22.0	0.0088	1.70	2.2
5	-0.456	10	-0.424	15.1	0.0088	1.68	2.2
6	-0.456	10	-0.424	14.1	0.0088	1.68	2.2
7	-0.456	10	-0.425	13.1	0.0088	1.68	2.2
Mean value	***-0.457***		***-0.425***	***15.6***	***0.0088***	***1.7***	***2.2***
Standard deviation	***0.0016***		***0.0022***	***3.21***	***-***	***0.11***	***0.15***
Coefficient of variation (%)	***0.35***		***0.52***	***20.62***	***-***	***6.55***	***6.04***

As it can be seen from the above table, for steel rebars with low concrete cover, the proposed measurement model exhibits a sufficient repeatability. The variation as far as corrosion potential and the potential response measured by the reference electrode on concrete's surface is quite low while polarisation resistance and corrosion current density exhibit an almost moderate variation. **This suggests that the measurement itself is repeatable but some improvement in the processing of the measured values by this novel model (abacuses and correction laws) could be proposed**. This can also be understood by the coefficient of variation in the case of the maximum polarisation on the steel rebar which is rather high. It seems for the same injected current, each time a different value-but still in the same order of magnitude- of ΔE_p is attained after the use of abacuses and correction laws. In addition, only for two measurements the targeted polarisation of 20mV±3mV was achieved, suggesting that the accuracy in estimating the values of polarisation resistance may be influenced. At the same time, j_{ar} didn't exhibit any variation, since at it is expected its calculation is based on quantities (i_{CE}, e, a and b) which remain fixed during all measurements. Hence, the variation in R_p is linked to the variation in ΔE_p. However, it has to be noted that polarization resistance values exhibited a moderate variation, lower than the one observed for ΔE_p.

Now, when it comes to the steel rebar at 5cm, the repeatability test was quite problematic, since after the first measurement, the proposed model couldn't approach the desirable ΔE_p. This also confirms that for the moment the proposed model is more efficient and effective for e≤4cm and ρ≤800 Ohm m, as it was already mentioned in previous paragraphs. However, the table VI.11 demonstrates, once more, that the experimental procedure is repeatable:

Table VI- 11: Repeatability test results for the single bar (I-C) with concrete cover 5cm.

N° of measurements	**E_{corr} (V)**	**E_{RE} (V)**	**I_{CE} (μA) for which E_{RE} was measured**
1	-0.450	-0.408	10
2	-0.447	-0.410	10
3	-0.446	-0.411	10
4	-0.445	-0.413	10
5	-0.443	-0.414	10
6	-0.442	-0.412	10
7	-0.442	-0.412	10

8	-0.442	-0.409	10
9	-0.441	-0.409	10
10	-0.441	-0.407	10
Mean value	***-0.444***	***-0.411***	
Standard deviation	***0.0031***	***0.0020***	
Coefficient de variation (%)	***0.70***	***0.49***	

VI.4.4.2. Spatial variability test

The spatial variability test was carried out for four positions regarding the initial position of the probe (point a on figure VI.20) on the steel rebars of I-C concrete slab, embedded at 2 and 5cm. Figure VI.38 illustrates the measurements carried out on the rebars, in October 2012, before the re activation of the corrosion process:

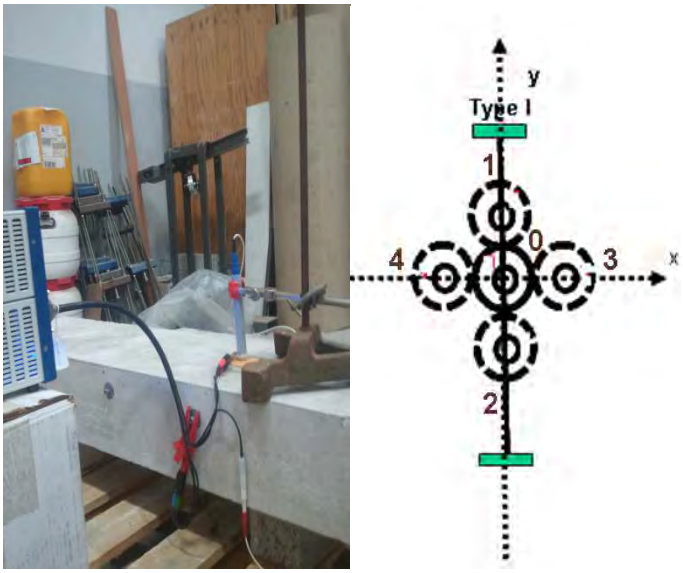

Figure VI. 38: Spatial variability test on the rebars embedded at 2 and 5cm of the I-C concrete slab in October 2012. Tests carried out on four successive positions (1,2,3,4) of the probe regarding its initial position (0) The centre of the probe is displaced by 2cm from its initial postion (0).. Positions 1 and 2: uncertainty regarding the positioning of the probe along the y axis (axis of the rebar). Positions 3 and 4: uncertainty regarding the positioning of the probe along the x-axis. After and before each measurement the electrodes' configuration was dissembled and reassembled.

The tables VI.12 and VI.13 summarize the results for this test realised on the single rebars at 2 and 5cm:

Table VI- 12: Results of spatial variability test on the rebar embedded at 2cm in the I-C concrete slab.

Positions of the probe	***0***	***1***	***2***	***3***	***4***	***Mean value***	***Standard deviation***	***Coefficient of variation (%)***
E_{corr} (V)	-0.173	-0.176	-0.183	-0.2	-0.216	***-0.19***	***0.016***	***8.5***
E_{RE} (V)	-0.121	-0.131	-0.145	-0.167	-0.185	***-0.15***	***0.023***	***15.6***
Rp (ohm m^2)	3.08	2.3	1.3	0.68	0.43	***1.56***	***0.1***	***64.0***
j_{corr} ($\mu A/cm^2$)	1.2	1.6	2.9	5.5	8.8	***4***	***2.83***	***70.8***
I_{CE} for which $\Delta Ep_{max}(\mu A)$	5	5	5	5	5			
ΔEp_{max}(V)	24	17.3	10.3	5.3	3.3	***12.06***	***7.67***	***63.6***

According to table VI.12, it seems that for small concrete covers, cautiousness is required as far as the positioning of the probe on the concrete surface is concerned. While variation for displacement of the probe along the y-axis can be attributed to the intrinsic error of the nature of the measurement or due to the operator, the variation becomes much more important when the probe moves along the x-axis. Apparently, for small concrete covers, when the probe is placed at some distance from the reinforcement, the polarisation is not effective and this leads to an imprecise and less reliable estimation of the polarisation resistance and corrosion current density. For that reason, in the case of steel rebars embedded at small concrete bars, the positioning of the probe right above the steel rebar must be ensured (see also §VI.3.4.4).

Table VI- 13: Results of spatial variability test on the rebar embedded at 5cm in the I-C concrete slab.

Positions of the probe	***0***	***1***	***2***	***3***	***4***	***Mean value***	***Standard deviation***	***Coefficient of variation (%)***
E_{corr} (V)	-0.131	-0.131	-0.131	-0.131	-0.131	***-0.131***	***0***	***0***

E_{RE} (V)	-0.096	-0.098	-0.096	-0.094	-0.097	***-0.096***	***0.0013***	***1.38***
Rp (ohm m^2)	41	37.4	27.4	29.4	28.3	***32.7***	***5.46***	***16.7***
j_{corr} ($\mu A/cm^2$)	0.09	0.10	0.14	0.13	0.13	***0.12***	***0.019***	***16.4***
I_{CE} for which $\Delta Ep_{max}(\mu A)$	1	1	1	1	1			
$\Delta Ep_{max}(V)$	27	24.7	26.7	25.7	24.7	***25.8***	***0.097***	***3.75***

As far as the results depicted in table VI.13 are concerned, the variation regarding the positioning of the probe, on a steel rebar embedded at 5cm is much less important than for the case of the steel rebar embedded at 2cm. Apparently, when the concrete cover is high, displacing the probe along or far from the steel rebar doesn't influence significantly the measurement and any variation observed is due to intrinsic errors of the measurement or errors of the operator.

The Figures VI.39 illustrate the dispersion of the data on the steel rebar with a concrete cover of 2cm and 5cm, confirming that the dispersion is highly significant in the case of small concrete covers:

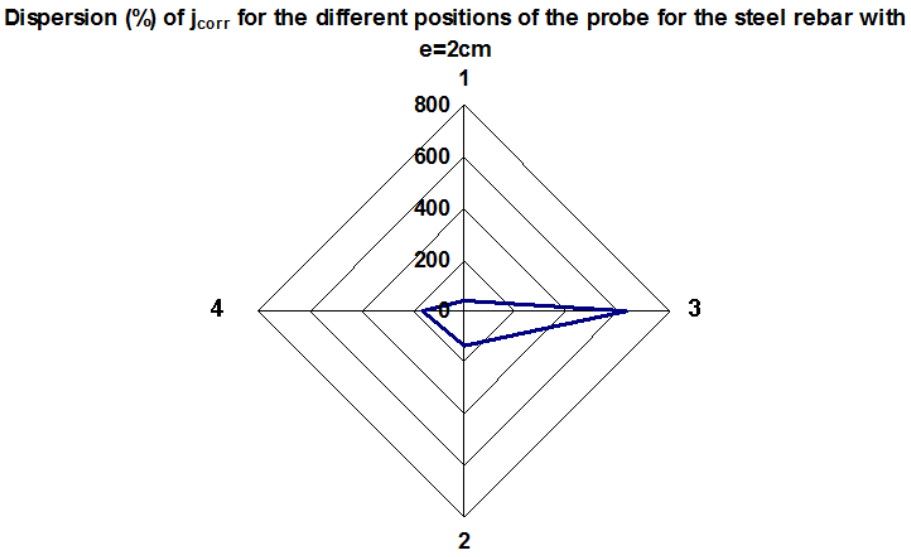

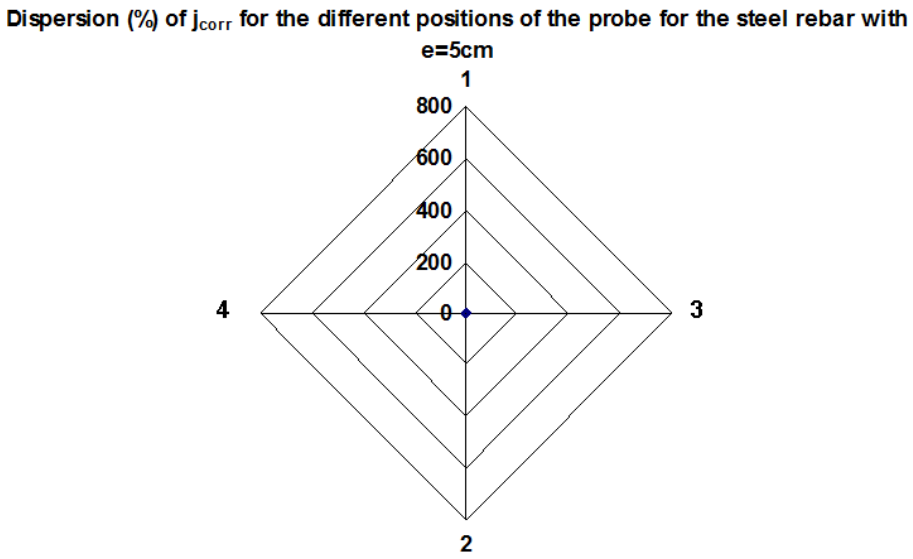

Figure VI. 39: Variation (%) of j_{corr} regarding position 0 of the probe for the steel rebar embedded at a) e=2cm and b) e=5cm in I-C concrete slab.

VI.4.4.3. Synthesis

In the current paragraph, the aspects of uncertainty of the measurement were examined for the carbonated concrete slab with single bar reinforcement configuration. **Repeatability** tests (10 repetitions) indicated a quite acceptable **(moderate) dispersion**, with potential for amelioration, in results for the steel rebar at **2cm**. On the contrary, the repeatability test was rather **problematic** in the case of **5cm**, implying, once again, that there are some difficulties in the adaptation of the model in the case of high concrete covers. As far as the position of the probe is concerned, **when the probe is displaced along the steel rebar**, whether the concrete cover is high whether is low, any dispersion observed can be **related to random errors,** such as the intrinsic error of the measurement or the errors due to the operator. However, when the probe is displaced even two centimetres **away from the steel rebar**, in the case **of small concrete covers,** the dispersion becomes quite significant, underlying **the importance of placing the probe right above the steel rebar**. On the contrary, for **high concrete covers**, a short displacement (within 2-4cm away from the steel rebar) **doesn't induce any strong deviations in the results**. The table VI.14 summarizes the repeatability and spatial variability test results (for more precision see Appedix 3, §5)

Table VI- 14: Overview on the dispersion of the results related to uncertainties of the measurement

Variability for::	**Concrete cover (cm)**	
	2	***5***
Repetitions on the same point of measurement	~	++
Displacement of the probe along the steel rebar (2-4cm away from the initial point of measurement)	~	~
Displacement away from the steel rebar (2-4cm)	++	-

, ++:very strong +:strong, , ~:moderate, -:insignificant

VI.4.5. Determination of weight losses due to corrosion and calculation of corrosion current density by Faraday law

In the following paragraphs the determination of corrosion rate of the steel rebars is carried out, expressed in terms of mass loss. The I-NC concrete slab is submitted to accelerated carbonation, and the evolution of corrosion current density, under controllable conditions (air conditioning chamber with θ=18°C, HR(%)=45), is monitored at regular intervals. More specifically, the measurement at regular intervals, of the concrete resistivity, corrosion potential, polarisation resistance and corrosion current density will allow to obtain a better view and improve the interpretation of the polarisation resistance. The measurements start two days after the exit of the slab from the chamber of accelerated carbonation. Those two days of "rest" serve for the adaptation of the slab to the new environmental conditions.

After a certain period of measurements, the slab is destructed and the steel rebars are weighed. Faraday's law is also applied and its results are compared with those of the destructive gravimetric technique. For the series of measurement the I-NC is noted as I-C2, where C: carbonated.

VI.4.5.1. Weight loss of steel rebars calculated according to Faraday's law

Faraday's law (see also §II.2.3.1) expresses the corrosion rate by relating the corrosion current to the weight loss of the steel, via the following equation:

$$m = \left(\frac{Q}{F}\right)\left(\frac{M}{z}\right) \qquad \text{(eq.54)}$$

Where m is the mass of the steel rebar lost due to corrosion process

Q us the total electric charge passed through the steel rebar ($Q = \int_0^{t_f} J_{corr} \cdot dt$)

F is the Faraday's constant (96485 C/mol)

M is the molar mass of the steel (55.85g/mol)

z is the number of free electrons (2 pour Fe)

In order to be able to estimate the total mass loss of the steel rebars via the above equation, a continuous monitoring of the evolution of corrosion is required. For that reason, the I-NC concrete slab was submitted to accelerated carbonation (50%CO_2, 60%HR); uniform carbonation was achieved one month later. Then, the I-C2 slab was placed in an air conditioning room where resistivity, corrosion potential and polarisation resistance measurements were carried out at regular intervals (every 3-4 days). The monitoring started 24 hours after the placement of the slab (in April 2013) in the air conditioning room and lasted 61 days (ended in June 2013).

In the figure VI.40, the evolution over time of the resistivity and corrosion potential for the steel rebars embedded at 2 and 5cm are illustrated:

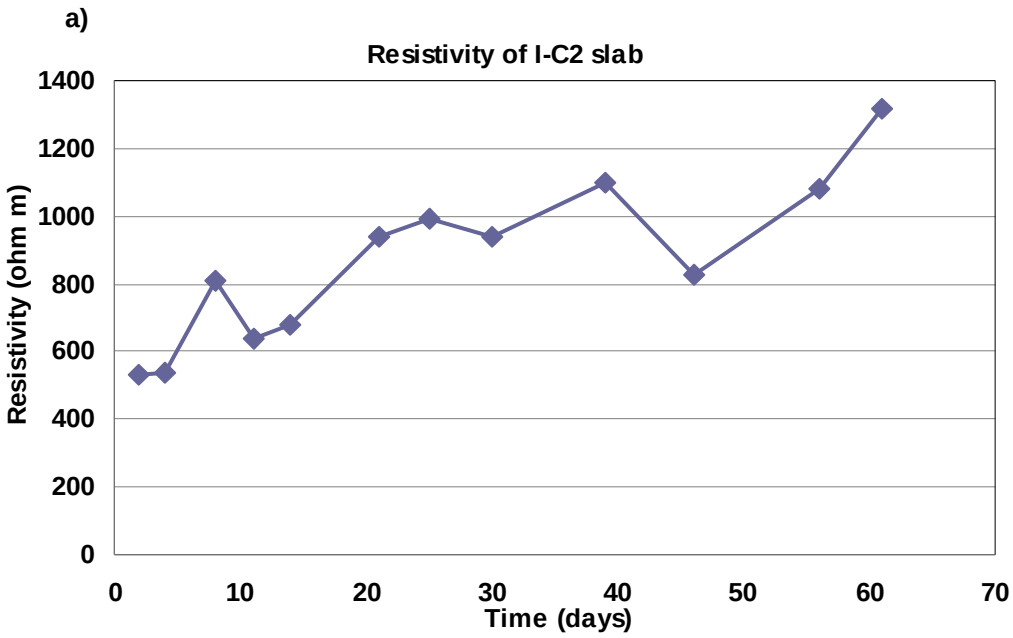

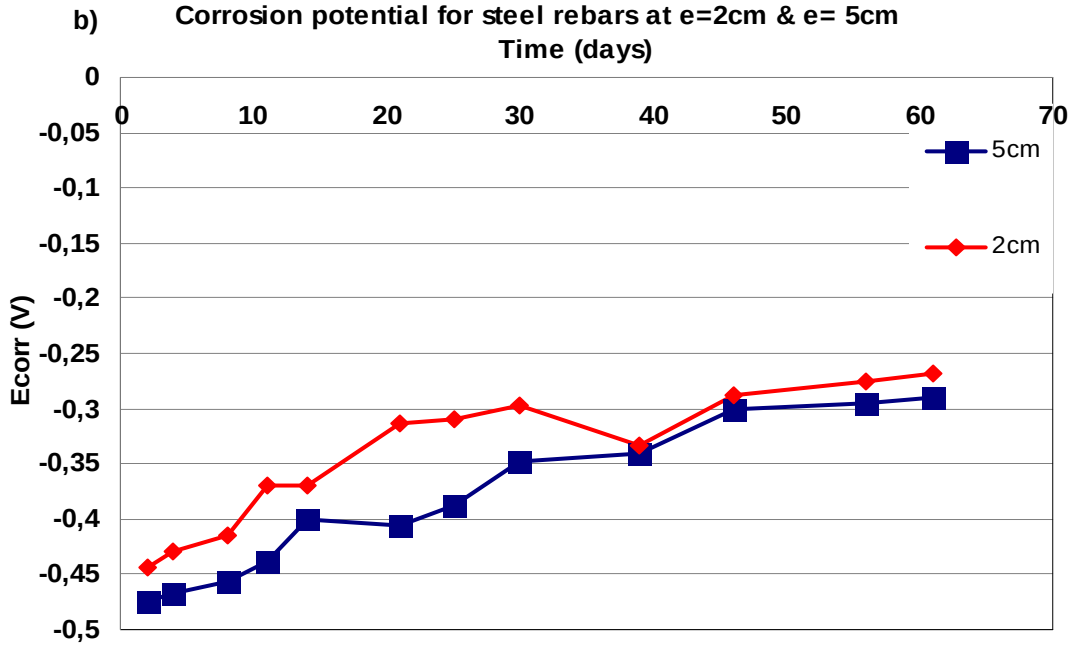

Figure VI. 40: Monitoring of the a) concrete resistivity of the slab and b) corrosion potential for the rebars embedded at 2 and 5cm. The measurement lasted 61 days.

According to figure VI.40a,. the resistivity remained stable during the first two measurements, while a generally smooth, relatively slow augmentation followed as a function of time, with some fluctuations the 11th, 30th and 46th day of measurement. One day after the removal of the slab from the chamber of accelerated carbonation, concrete resistivity was estimated at 534 Ω.m while after 61 days of storage in the air conditioned room it reached the values of 1320 Ω.m.

At the same time, corrosion potential (figure VI.40.b) for these two rebars evolved as it was expected; very electronegative values were noticed at the beginning of the measurement period, which, as time passed, moved towards to values less negative. Throughout the whole period of measurements the corrosion potential values confirmed that the bars were at an active corrosion state. Generally, the corrosion potential of 2cm was a bit less electronegative compared to that of 5cm (only a small fluctuation was observed on the 39th day). This can be attributed to the fact that the "front" of the drying process of concrete "arrives" firstly (reasonably) at the rebar embedded close to the concrete surface and then to the rebars embedded with higher concrete covers; The potential seemed to stabilize for both steel rebars in the last three measurements.

In Figures VI.41 the evolution of polarization resistance and corrosion current, J_{corr}, is depicted as a function of time. Corrosion current is calculated as

$$J_{corr} = j_{corr} * s_r \qquad \text{(eq. 55)},$$

where s_r is the surface of the steel rebar (s_r=0.011m^2).

Corrosion current will permit to estimate the quantity Q which is necessary for the calculation of the mass loss according to Faraday's law.

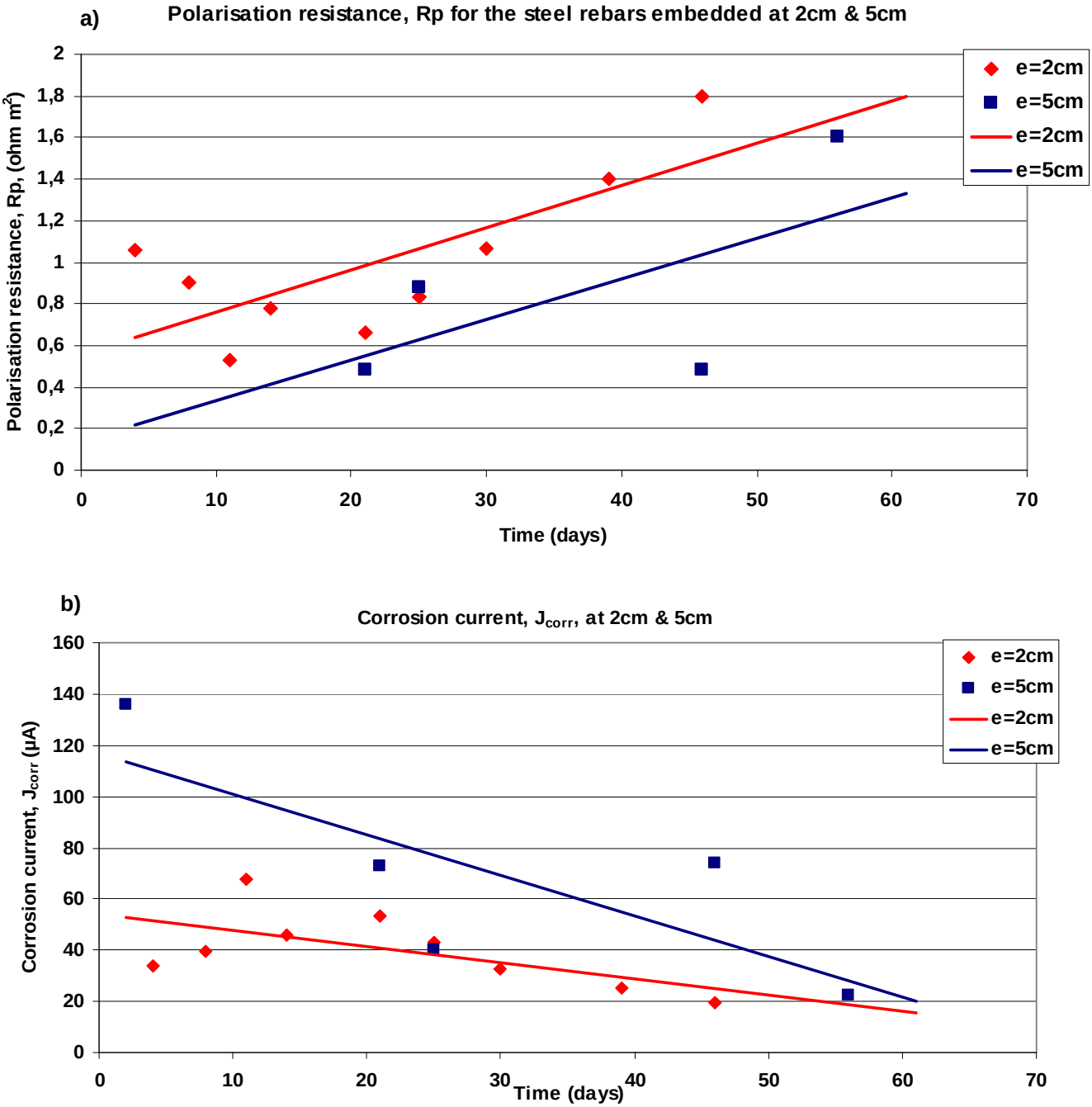

Figure VI. 41: Monitoring of a) polarisation resistance b) and corrosion current density for the rebars embedded at 2 and 5cm. The measurement lasted 61 days.

As it can be seen, from the figure VI.41, polarization resistance values exhibited an increasing tendency for both steel rebars while the corrosion current a decreasing one. Furthermore, the rebar embedded at 5cm exhibited stronger corrosion currents than the rebar at 2cm.

This evolution of corrosion current in time for the two rebars, comes into agreement with what was indicated from the evolution of corrosion potential. In addition, the fact that the polarisation resistance model is limited for low concrete cover and low resistivity is once more confirmed, since in the case of 5cm, the model couldn't be applied for all measurements.

It has to be noted that for the measurements carried out on the rebar embedded at 5cm, the adaptation of the proposed model of measuring polarisation resistance was quite problematic. More specifically, the application of the correction laws and abacuses indicated very weak polarisation, far from the target of 20±3mV anodic linear polarisation on the steel rebar, affecting in that way the precision of the estimated polarisation resistance. This confirms what has been stated previously in this chapter about **the limits of the application of the current polarisation resistance measurement model as far as the concrete cover and resistivity are concerned (limited for e≤4cm and ρ≤800 Ohm m)**

Now, the quantity Q can be calculated as $Q = \int_0^{t_f} Jcorr \cdot dt$ where t=0sec, the moment the slab is removed from the chamber of the accelerated carbonation and t_f=61days, the whole measurement period. This value was then integrated in (eq. 55) and the mass loss calculated for the rebars at 2 and 5cm is depicted in the figure VI.42:

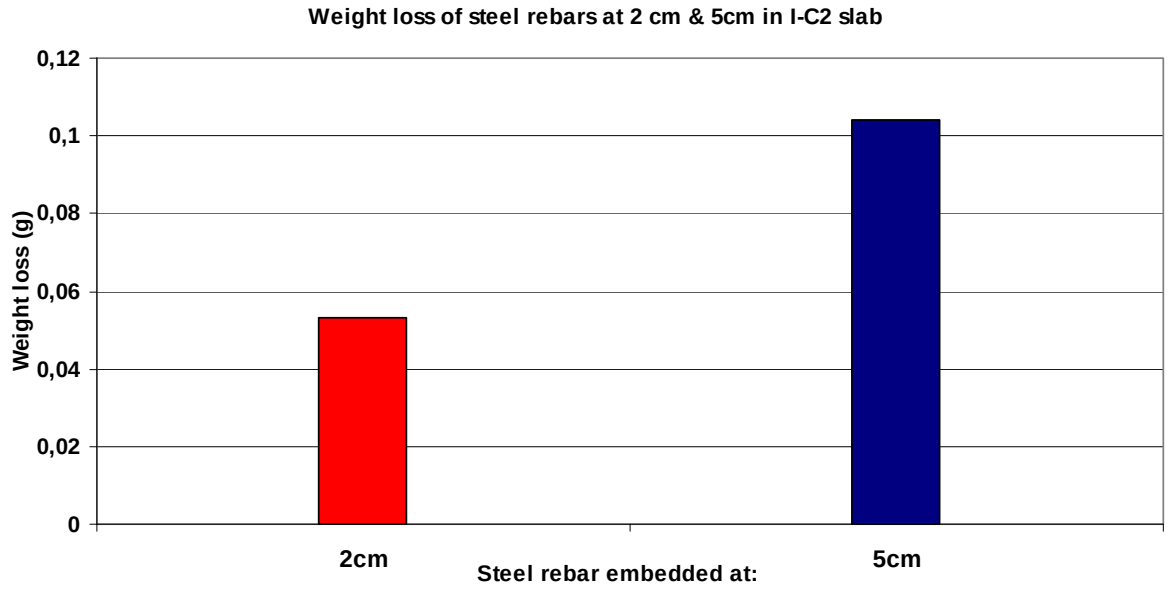

Figure VI. 42: Weight loss of steel rebars at 2cm and 5 cm in the I-C2 concrete slab, calculated according to Faraday's law after a monitoring of the corrosion current during 61 days.

According to the figure VI.42, the weight loss is greater for the rebar embedded at 5cm than for the rebar at 2cm. This can be regarded as quite expected, since corrosion current is higher for the rebar at 5 cm than for the rebar 2cm. However, the mass losses estimated via Faraday's law cannot be considered as highly significant, confirming that carbonation is not a very aggressive and intense phenomena progress, but its effects are more remarkable over long term periods (M.Sohail, 2013).

VI.4.5.2. Weight loss of steel rebars measured via a gravimetric technique vs. weight loss estimated via Faraday's law

In the previous paragraph, the mass loss of the rebars with concrete covers at 2 and 5cm were estimated via the use of Faraday's law, after a monitoring of the I-C2 slab for 61 days. The values obtained will be now compared with those measured after the destruction of the concrete slab.

Hence, after 61 days, the I-C2 slab was autopsied. In order to measure the real weight of the steel rebars, the corrosion products should be removed. The figure VI.45 shows a steel rebar, right after being removed from the concrete slab and the same steel rebar, right after the removal of the corrosion products from its surface, according to the European Standards ISO 8407:2009:

a)

b)

Figure VI. 43: Steel rebar right after its recovery from the I-C2 slab, where corrosion products are a) still on and b) right after the removal of these products, according to the instruction of the European Standards ISO 8407:2009.

According to the figure VI.43, the corrosion products were formed more or less uniformly along the steel rebar, as a result of the uniform carbonation. Once the steel rebars are cleaned, their weight is measured. The weight of the steel rebars at 2 and 5cm, measured before embedding them in the concrete slab (initial weight) and after their recovery from the slab and the removal of the corrosion products from their surface (final weight), is given, in table VI.15:

Table VI- 15: Weight measurement for the rebars at 2 and 5cm in the IC-2 concrete slab.

Concrete cover of the steel rebar (cm)	Initial weight (g)	Final weight (g)	Mass loss due to corrosion (g)
2	239.77	239.64	0.13
5	238.28	237.67	0.61

In figure VI.44 a comparison between the mass loss estimated via Faraday's law and the mass loss measured after the destruction of the slab is realised.

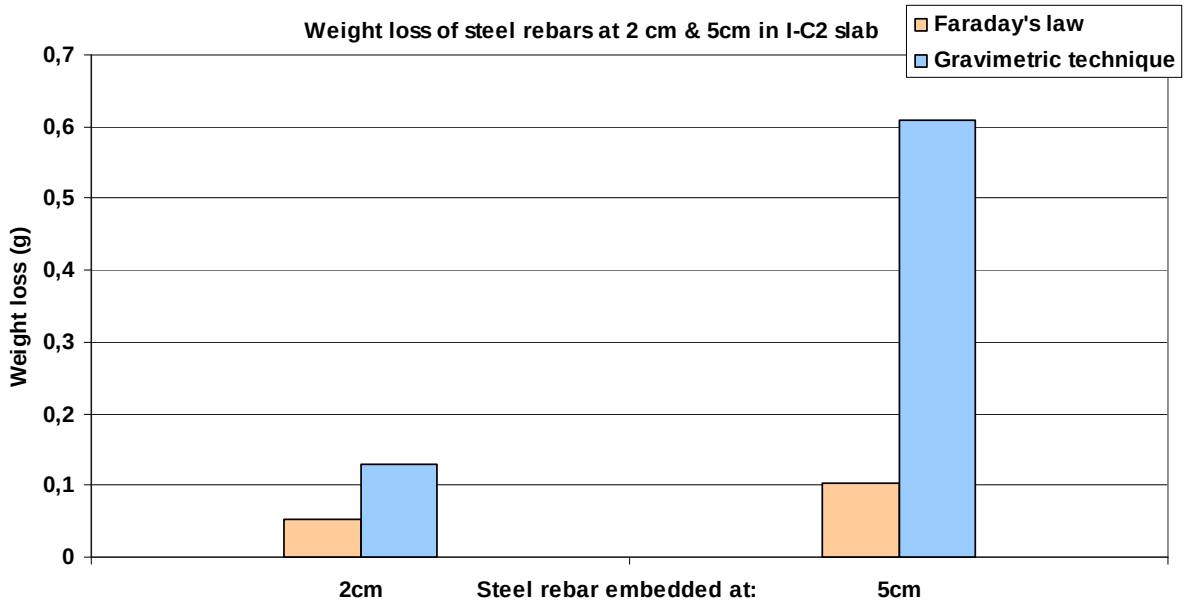

Figure VI. 44: Weight loss of the steel rebars embedded at 2 and 5cm for the I-C2 concrete slab estimated via Faraday's law and measured after being recovered from the concrete slab.

As it can be seen from the figure VI.44, both Faraday's law and the destructive technique indicate similar tendencies for the weight losses of the steel rebars at 2cm and 5cm. However, Faraday's law underestimated the mass loss, 50% for the steel rebar embedded at 2cm and 90% for the steel rebar embedded at 5cm.. However, this could also signify that the proposed

polarisation resistance model underestimates the polarisation resistance and thus the calculated corrosion current; this underestimation is more remarkable in the case of the rebar embedded at 5cm. As it has been already mentioned, the model, exhibits problems of adaptation for the case of high concrete cover and high resistivity. This affects directly the measurement of the polarisation resistance and the precision in the estimation of corrosion current, and thus the evaluation of the corrosion rate of the steel rebars. Now, adding any random errors (i.e. intrinsic error of the nature of the measurement, errors due to the operator), the combination of all the above may lead to the differences in weight loss (thus, corrosion rate) observed in the figure VI.44. Hence, as it is understood, ameliorations are required as far as the adaptation of the proposed polarisation resistance model is concerned, in order to estimate with higher precision the polarisation resistance and thus obtain the correct information on the corrosion state of the reinforcement.

VI.4.5.3. Synthesis

The paragraphs above, firstly described the results obtained after the realisation of resistivity and polarisation measurements at regular time intervals (every 3 or 4 days). It was signified that in the case of a **real reinforced concrete structure**, in order to evaluate correctly the corrosion to which the structure (i.e. cooling towers) is submitted, **it is highly recommended the continuous monitoring of ambient conditions (temperature, humidity) and the realisation of polarisation resistance measurement at frequent intervals**. Obviously, one single measurement at one single point and single time cannot provide with those information on the evolution of corrosion and the state of the structure. This is of crucial importance, when decisions will have to be taken for a reliable and effective act on the maintenance or reparation of the structure.

Then, the estimation of the corrosion rate of the single active steel rebars in the carbonated concrete slab was carried out. It was expressed in terms of **mass loss**, via a destructive technique and the Faraday's law. Differences were noticed, since **Faraday's law underestimated the mass loss of the steel rebars, compared to the ones measured after the rebars were removed and cleaned to vanish the corrosion products.** This could signify in its turn that the proposed model may overestimate the polarisation resistance and thus

underestimate the corrosion current density. This becomes once more quite remarkable in the case of the high concrete covers. **Thus, improvements are imperative, as far as the fit in of the model is concerned, in order to improve its efficiency and effectiveness**. . Last but not least, via all these results and particularly **via the test of monitoring, it was proven that the evolution of polarisation resistance (thus corrosion current density) was more or less suggested by the way the corrosion potential and concrete resistivity evolved**. Thus, this could suggest that **when it comes to real structures conditions, a monitoring of these two quantities at regular intervals, could be indicative whether polarisation resistance measurement should be measured or not**.

VI.5. CONCLUSION

This chapter presented the lab scale experimental application of the proposed polarisation resistance measurement methodology. The experimental program that was developed by reproducing the simulated geometries of Chapter V was aiming at approach as much as possible the real structures conditions and characteristics. Then, a several series of measurements was launched, having as main objective the validation of the feasibility, efficiency and effectiveness of this new technique on the evaluation of the corrosion state of the reinforcement.

Firstly, as it was presented, the reinforced concrete specimen and slabs, carbonated (for active conditions) and non carbonated (for passive conditions) were submitted to tests for the characterisation of the mechanical (Appendix B) and physical properties of concrete. **These tests indicated that the evolution of corrosion is directly related to the nature of concrete**.

Then, a certain series of electrochemical measurements were launched for the estimation of the corrosion state of the reinforcement. In the frame of these tests, **the efficiency of the novel probe and the feasibility of proposed polarisation resistance measurement technique were confirmed. In addition, its basic theoretical principles were validated and the limits of its effectiveness were also indicated and taken into consideration during the procedure of calculating polarisation resistance and thus corrosion current density**.

Throughout the results obtained from all these measurements, the effect of the influencing parameters as it was described in chapter V was also confirmed. It was clearly demonstrated **that atmospheric carbonation is a slow long term process, greatly favoured by the**

presence of humidity. Thus, it was underlined that the evolution of **polarisation resistance is directly linked and indicated by the corrosion potential and resistivity measurements**.

Furthermore, it was proven that as all experimental methods, the proposed model is also subjected to some uncertainties, which are quite sensible to the concrete cover of the reinforcement. **More specifically, in the case of a small concrete cover, uncertainties become highly significant when the probe is not placed right above the steel rebar. Other uncertainties are linked to random errors** (i.e. intrinsic error of the measurements, errors of the operator).

Last but not least, the effectiveness of the proposed technique was put under test, via the measurements of weight loss of the steel rebars. It was clearly suggested that **ameliorations as far as the adaptation of the model should be carried out in order to improve its precision** and efficiency.

To conclude, this chapter clearly proved that **the polarisation resistance measurement model, proposed in this study, can be applied for the on site estimation of corrosion state of reinforcement on cooling towers**. The concept of a universal technique of measuring polarisation resistance applied in any case and under any conditions was clearly put into question. On the contrary the current study proved that each case (or structure) should be investigated as an isolated one, taking into consideration those factors that directly influence her. **The methodology that was developed in this dissertation corresponds specifically for the case-problem posed by EDF: cooling towers submitted to uniform conditions of corrosion (carbonation).**

Certainly, there is still work to be done, as far as the efficient and effective adaptation of the model is concerned, i.e. for all cases of concrete cover. Practical aspects of the measurement can also be improved (i.e. aspect of time, procedure of humidification before resistivity measurement).The figure VI.45 proposes schematically a first version of a complete protocol of measuring polarisation resistance on a single point on site, according to the proposed technique.

Finally, this experimental validation of the proposed polarisation resistance measurement model proved that a single on site measurement at a specific moment cannot provide with all the necessary information for the evolution of the corrosion state of the reinforcement. On the contrary, **via a continuous monitoring of the ambient conditions (i.e. via humidity and temperature sensors) and the realisation of measurements at short regular intervals, a better view can be obtained on the real state and thus the durability of the structure**.

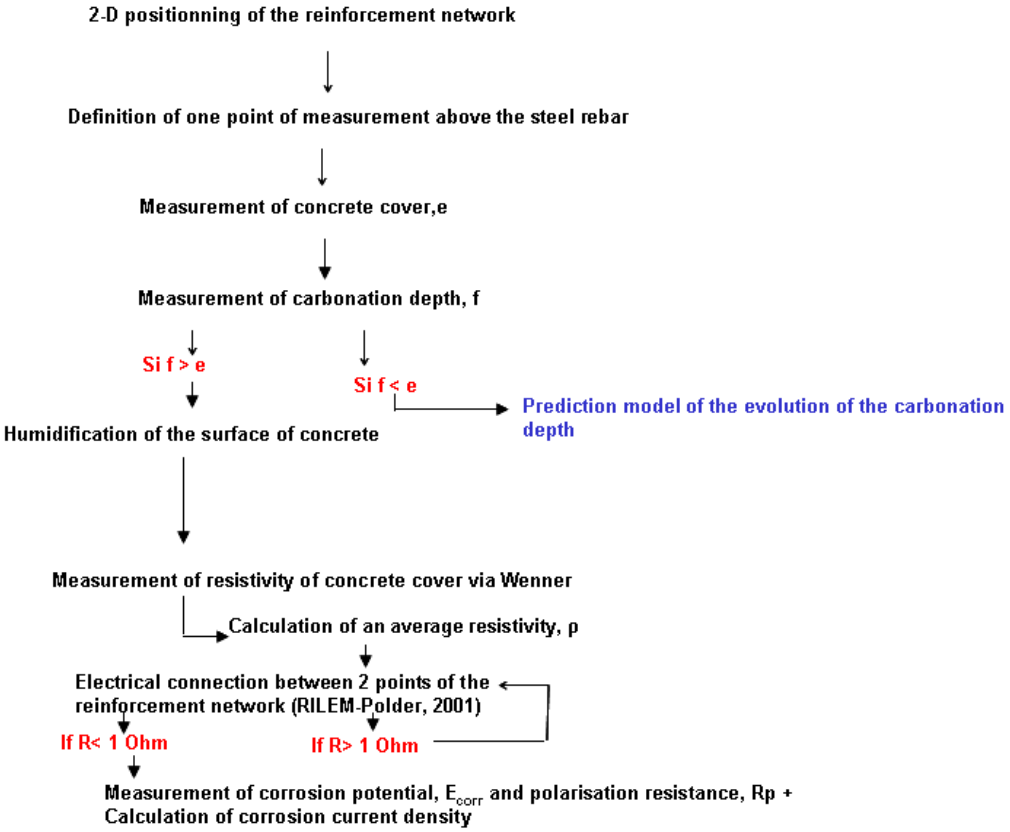

Figure VI. 45: A first version of a complete protocol of measuring polarisation resistance on a single point on reinforced concrete cooling towers of energy production sites

CONCLUSIONS AND PERSPECTIVES

The current study had as a main objective the detection of corrosion of EDF's reinforced concrete cooling towers which are submitted to uniform conditions of corrosion, due to atmospheric carbonation, based on a double approach:

- The use of a dynamic, non destructive tool, such as Ground Penetrating Radar (GPR) for
    - the delimitation of those zones (contrasts of permittivity-peak to peak amplitude mapping) on cooling towers which exhibit a potential risk of corrosion.
    - the localization of the steel rebars and the exact estimation of their concrete cover thickness
- The use of a local electrochemical technique, for those areas indicated by the radar as an elevated risk corrosion zones. It consists of the operative use of the technique of linear polarization for the assessment of cooling towers' corrosion, by:
    - Proposing an alternative measurement mode and interpretation protocol for the correct and real evaluation of the corrosion kinetics, in the aid of numerical simulations.
    - Validating the robustness of the proposed technique on lab scale.

Now, the principal conclusions of the work presented in this thesis are enlisted below:

- Use of Ground Penetrating Radar
    1. **Peak to peak amplitude mapping** of real structures surfaces is **feasible**. Due to logistics and time schedule difficulties, it was impossible to carry out radar profiles and thus to obtain a peak to peak amplitude mapping on a cooling tower surface.
    2. The precise estimation of **concrete cover thickness** is of major importance, since it consists one of the main entries in the proposed polarization resistance measurement mode. Difficulties for its precise evaluation are presented, due to the registration of mixed (direct wave- reflection) signals. These are induced by the low concrete cover thickness of the steel rebar reinforcement ($e \leq 3cm$) in real site structures (thus cooling towers). Among the techniques presented in this study, **SVD** (EDF R&D) and **Subtraction of the direct signal** (LMDC) were more efficient in signals' separation.

- Use of an alternative polarization resistance measurement mode,

Here, the conclusions can be divided into categories: those which consist of scientific/ academic interest and those of an industrial interest.

In the first category the following were stated:

1. **A new simple probe and an alternative procedure of estimation of polarization resistance** were developed via numerical simulations. Relationships and abacuses laws lead to the collection **of real information** about the state of the reinforcement.
2. The experimental lab scale application of the proposed model was considered as effective and efficient. **The anodic and linear conditions of the measurement are confirmed**. The model can be applied on real conditions on corroded cooling towers.
3. The established relationships and abacuses were developed only for concrete cover **thickness $1 \leq e \leq 6$cm and concrete resistivity, $50 \leq \rho \leq 2000$ Ohm m**.
4. The determination of the electrochemical parameters, indicated that **carbonation is a slow long term process** and that corrosion is linked to the nature of concrete. Resistivity and corrosion potential indicate the evolution of polarization resistance and corrosion current density. When these two first quantities indicate **passive conditions** (according to ASTM and RILEM classification), there **is no need to proceed**.

Now, the conclusions that follow, concern mainly the operator-EDF of this methodology:

5. The proposed measurement and interpretation mode can **be adapted only in the case of cooling towers suffering from carbonation (uniform corrosion).** The physical (concrete cover thickness, resistivity) and geometrical (injected current, position of the probe) influencing parameters on this application are now mastered**: A tolerance of <15% in the estimation of concrete cover and resistivity** is allowed. An elevated **precision in the injected current and the position of the probe** right above the steel rebar is required
6. A first **proposal of an operative protocol for a real site measurement on a single point** was made. A first lab scale estimation of the measurement uncertainties is given but without taking into account any uncertainties of the model.

7. Isolated single point measurements, carried out with a very low frequency on cooling towers, do not allow with any reliable information on the evolution of corrosion and thus the real state of the structures. **A continuous monitoring** of the conditions (temperature and relative humidity sensors) that favor (or not) the evolution of corrosion and the realization of measurements (resistivity, corrosion potential and polarization) at regular short intervals is required. The frequency of the measurements should be determined by the structure managers, taking into account the role and the functionality of the cooling towers in the energy production installations and according with economical aspects.

As far as the work that still has to be done, some **perspectives** of the current thesis are given on the:

- Ground Penetrating Radar:
  - **Carrying out radar profiles** on cooling towers' surfaces is regarded as the major next step for this part of the thesis. This would permit to put under test the efficiency of the procedure of delimitating those zones with a potential risk of corrosion. The resistivity and polarization resistance measurement that would follow, could also confirm the potential of the technique.
  - In order to overcome the obstacle of the mixture of signals, it is absolutely necessary to achieve a successful separation of the mixed signals by using the appropriate signal processing tools. The main objective would be **to limit the error on the precision of concrete cover thickness estimation <5%**, which would in its turn influence and increase the precision of the proposed polarization resistance measurement response.

- Alternative polarization resistance measurement mode:
  - One very important perspective of the current work is the transition from the laboratory environment to the real conditions. In other words, this signifies the **application of the proposed methodology on cooling towers**, which would permit to validate the robustness of the approach on site.
  - In the frame of the current work, difficulties came about when the methodology was tested for concrete cover thickness, e>4cm. Further work should be carried out in order to precise the problem origin (i.e. nature of concrete). Thus, in the

aim of ameliorating the precision and the efficiency **for all the ranges of concrete cover thickness**, **the adaptation** of the proposed polarization resistance measurement model should be **further improved**.

- **As far as the uncertainties of the proposed technique are concerned, it is imperative, that further investigation should be carried out on the definition of all the uncertainties**. That also requires the integration of the errors of the numerical model. Once defined, it is important that they are validated after real site testing and the protocol being up dated.
- Furthermore, practical aspects of the polarization resistance measurement procedure (i.e. **aspect of time**) should be improved. A possible integration of these aspects in the numerical simulations of the model could enlighten on their influence on the model's effectiveness. As far as the concrete resistivity measurement is concerned, since it proceeds of the polarization measurement, a procedure protocol should be established A basic requirement should be that the **resistivity protocol** shouldn't induce any changes in the corrosive conditions on the reinforcement. This mainly concerns the **procedure of humidification of the concrete surface, which could modify the electrochemical state of the rebars**. In such a case, the polarization resistance results could give erroneous information about the real condition of the reinforced structure.
- Apart from carbonation phenomenon, the presence of **more aggressive environments for the cooling towers** (i.e. algues, chloride and sulphate ions), could definitely induce more severe corrosion conditions and thus a great damage. In addition, carbonation depth testing on cooling towers have shown that, in some cases the carbonation front has barely arrived on the steel reinforcement at the moment of its measurement. That would provide with **conditions of galvanic corrosion** (passive/active interface of the steel rebars). All the previously mentioned, consist part of the reality, taking into account the role and location of cooling towers. As a result, another perspective of the current thesis would be the **evolution of the proposed model by adapting it into more realistic conditions.** Tests of the model under these conditions should be carried out in a numerical and then a laboratory environment.
- As it can be understood, the knowledge of the electrochemical parameters can be hardly attained when it comes to reinforcing steel rebars on the real structure. This can be due to practical difficulties (i.e. obtaining a part of the reinforcement

from the structure is impossible). For that reason, this thesis suggests as a future outlook, the **achievement of an efficient *a priori* evaluation of the electrochemical (Butler-Volmer) parameters of steel reinforcement corrosion** of the structure, before the application of the polarization resistance measurement technique. This would provide with an important feedback on the evolution of model, which for the moment is developed on fixed values of the Butler Volmer parameters. In that way, the model would become more flexible in its adaptation.

- Finally, the current thesis was focused only on an example of real structures, on the way towards a more reliable and precise on site estimation of the corrosion. However, it can be considered as the base and research can be carried on, in order that the **proposed procedure is developed and applied on other reinforced concrete structures** (i.e. reactor buildings) that, in its turn would signify as a next step, the **evolution and expansion of the current recommendations** as far as the domain of their efficient application is concerned.

BIBLIOGRAPHY

S. Ahmad, (2003), *Reinforcement corrosion in concrete structures, its monitoring and service life prediction-a review*, Cement & Concrete Composites 27, 459-471

A. Alani (2013), *Applications of ground penetrating radar (GPR) in bridge deck monitoring and assessment*, Journal of Applied Geophysics xxx (2013) xxx–xxx

C. Andrade,(1995), *The importance of geometrical considerations in the measurement of steel corrosion in concrete by means of ac impedance*, Corrosion Science 37, No 12, pp 2013-2025

C. Andrade (1995), *Galvanic Corrosion of steel in Concrete*, Materials Science Forum 192-194, pp 899-906

C. Andrade, (2004), *Test methods for on site corrosion rate measurement of steel reinforcement in concrete by means of the polarization resistance method*, Materials and Structures 37: 623-642

C. Andrade, (2010), *Numerical modelling of current lines of on site corrosion rate meters used in concrete*,

R. Arndt (2009), *NDE for corrosion detection in reinforced concrete structures-a bechmark approach*, NDTCE'09, Non-Destructive Testing in Civil Engineering Nantes, France, June 30th – July 3rd, 2009

J.P Balayssac (2006), *Evaluation non destructive du béton d'enrobage. Approche multi-technique*, REGC 10-2, pp913-932

J.P. Balayssac, (2007) *Evaluation non destructive des ouvrages en béton armé*, Annales du bâtiment et des travaux publics no 4**,** pp.20-40

J.P.Balayssac (2005), *Cover concrete evaluation: The contribution of GPR technique-Experimental studies ad flied measurements***,** 6th It.Congress: Global Construction: Ultimate Concrete Opportunities, Dundee, Ecosse

P.C. Bamu, (2005) *Damage, deterioration and the long-term structural performance of cooling tower shells: A survey of developments over the past 50 years*, Engineering Structures 27 1794-1800

Z. Bazant, (1979) *Physical model for steel corrosion in concrete sea structures-theory & application*, J Structural Division, Am Soc Civ Eng, Vol. 105, pp.154-166

L. Bertolini (1997) *Concrete resistivity and reinforcement corrosion rate as a function of temperature and humidity of the environment*, TNO report 97-BT-R0574, 85.

D.Breysse (2012), *Non-Destructive Assessment of concrete structures: Reliability ad Limits of Single and Combined Techniques*, RILEM, Springer, pp.85-97

J.P. Broomfield (1997), *Corrosion of steel in concrete*, E&FN SPON, p.p. 33-36, 40-53, 63-73

BS EN 583-2:2001, *Non destructive testing, Ultrasonic examination. Sensitivity and Range Settings*

BS EN 12390/3 (2002) *Testing hardened concrete-Compressive strength of test specimens*

C.W. Chang, (2009) *Measurement radius of reinforcing steel bar in concrete using digital image GPR*, Construction and Building Materials 23 1057-1063

X. Chen, (2010)**,** *Exploitation des résultats d'essais (Eiffage,2009)de Cattenom 1,* EDF CEIDRE/TEGG/SGC

X. Chen, (2010)**,** *Avis Technique,* EDTGC 1000146, EDF-CEIDRE

A. Clément, (2012) *Numerical study of the linear polarisation resistance technique applied to reinforced concrete for corrosion assessment*, EJECE, 16:3-4, 491-504

B.E. Conway, (1999) *Modern aspects of electrochemistry* no.32, 143-156

Committee on the safety of nuclear installations, (2002) *Technical note: Electrochemical Techniques to detect corrosion in concrete structures in nuclear installations***,** NEA/CSNI/R(2002)21

F. Coppel, (2009), *Estimation de l'enrobage des armatures des coques d'aéroréfrigérants, Note technique*, EDTGC 080304, EDF-CEIDRE

Cox, (1997) *Corrosion and Protection of Metals in Contact with Concrete*, COST 509 Final Report, EUR 17608 EN, European Commission, DG XII Science, Research and Development, Brussels

L. Dao et al, (2010) *Modeling Steel Corrosion in Concrete Structures (Part 1 & Part 2)* Int. J, Electrochem.Sci., Vol. 5

X. Dérobert,, (2001), *Localisation des armatures des ouvrages d'art en béton armé ou précontraint par les techniques de radar*, Bulletin des Laboratoires des ponts et chaussées 230, 57-65

W.P.S Dias(2000), *Reduction of concrete sorptivity with age through carbonation*, Cem. Concr. Res. 30 (2000), 1255-1261

Document Scientifique (2010) du projet *ANR- EvaDéos,* Programme VILLES DURABLES

R.L. Du Plooy (2013), *The development ad combination of electromagnetic non destructive evaluation techniques for the assessment of cover concrete condition prior to corrosion*, Thèse de Doctorat, en génie Civil, Nantes

B. Elsener, (2002), *Macrocell Corrosion of steel in concrete*, Cement & Concrete Composites 24, 65-72

Féderation internationale du béton,(2003), *Monitoring and safety evaluation of existing concrete structures*, p.147

S. Feliu, (1985), *The determination of the corrosion rate of steel in concrete by a non-stationary method*, Corrosion Science 25, No. 917

E. Fisher, (1992), *Examples of reverse time migration of single channel, ground penetrating radar profiles*, Geophysics 57, 577-586

L.W. Galagedara, (2005), *Field studies of the GPR ground wave method for estimating soil water content during irrigation and drainage*, Journal of Hydrology 301, 182-197

L.W. Galagedara, (2003) *An analysis of the ground – penetrating radar direct ground*

J. Ge, (2007) *Effects of Tafel slope, exchange current density and electrode wave method for soil water content measuremen²t*, Hydrological Processes 17, 3615-3628

Gulikers, (2005) *Theoretical considerations on the supposed linear relationship between concrete resistivity and corrosion rate of steel reinforcement*, Materials and Corrosion 56, No.6

R. Hamrouche (2011), *Reconnaissance Géométrique des structures en maçonnerie ou en béton par imagerie radar multi récepteurs: approche numérique et expérimentale*, Thèse de doctorat en génie civil, Toulouse

Y. He (1996), *Experimental Study of Reinforced Concrete Beams Using Acoustic Surface Waveguides*, Building an International Community of Structural Engineers, Proceedings of the Structures Congress XIV Conference, ASCE, pp.869-875, Chicago, April 1996.

G. Ji, (2006) *On the numerical solution of Laplace's equation with nonlinear boundary conditions for corrosion of steel in concrete*, Joint international on Computing and Decision Making in Civil and Building Engineering 3667-3676

ISO 8407 (2009) *Corrosion of metals and alloys - Removal of corrosion products from corrosion test specimen*

D.E. John, (1981), *Uses of AC impedance technique in studies of steel in concrete in immersed conditions*, Corrosion Journal 16, No 102

V. K. Karastathis (2002), *Geophysical methods contributing to the testing of concrete dams. Application at the Marathon Dam*, Journal of Applied Geophysics, 50- 3, pp: 247–260

C.-Y. Kim, (2008), *Numerical analysis of localized steel corrosion in concrete*, Construction and Building Materials 22, 1129-1136

G. Klysz (2004), *Spectral analysis of radar surface waves for non-destructive evaluation of cover concrete* NDT & E International 37, 221-227

G. Klysz, (2007), *Determination of volumetric water content of concrete using ground-penetrating radar*, Cement and Concrete Research 37, 1164-1171

F-N Kong, (1998) actes 7e Cong. Int. GPR Lawrence (Etats-Unis)

J. Kropp, (1995) *Relations between transport characteristics and durability in Kropp, J., Hilsdorf,* H.K. (Eds.), Performance Criteria for Concrete Durability. RILEM Report 12, E and FN Spon Editions, pp. 97–137

A. Lamber (1994)**,** *Les Contrôles non destructifs-Généralités,* CETIM, p.17

C. Larsen (2007), *Technology report on Electrical Resistivity as an Indicator and Cracking Tendency in hardening concrete,* Norwegian Public Roads Administration.

J.F. Lataste (2003), *Electrical resistivity measurement applied to cracking assessment on reinforced concrete structures in civil engineering*, NDT&E International 36 (2003) 383–394

S. Laurens (2001), *Aptitude de la technique radar à la caractérisation du béton d'enrobage-Aide au diagnostic de la corrosion des armatures*, Thèse de doctorat en sciences appliquées, Toulouse

S. Laurens, (2010), *Simulation numérique de la mesure de résistance de polarisation linéaire des armatures du béton,* Applet L3-3/2

D.W. Law (2004), *Measurement of loss of steel from reinforcing bars in concrete using linear polarisation resistance measurements*, NDT&E International, 37- 5, pp.381-388

Y. Le Pape (2010), *Influence de la corrosion des aciers sur le comportement des structures en béton armé-Etat de l'art et propositions d'orientation du programme de R&D 2011-14*, EDF R&D, MMC

Luping, (2002), *Calibration of the Electrochemical Methods for the Corrosion Rate Measurement of steel in Concrete*, Nordtest project No 1531-01

D. Macdonald, (2009), *Why electrochemical Impedance Spectroscopy is the Ultimate Tool in Mechanistic Analysis*, ECS Transactions 19 (20), 55-79

D.D. MacDonald, (1987) NACE Corrosion '87, Vol 120, San Fransisco, California

C. Maierhofer, (1996), *Application and Optimization of Impulse Radar for Non Destructive Testing in Civil Engineering*, actes 5e Cong. Int. GPR, Sendai (Japon), 663-672

S. Malagodi, (1996), *Approaches to increase resolution of radar signal*, actes 5e Cong. Int. GPR, Sendai (Japon), 283-288

S. Malagodi (1996): *Location of archaeological structures using GPR method: Three-dimensional data acquisition and radar signal processing*, Archaeological Prospection, vol. 3, pp. 13-23

J-L. Mari (2001) *Traitement du signal pour géologues et géophysiciens, Techniques de base*, Vol.2

J. Mars (2011), B.E.#03 FILTRAGE MULTIDIMENSIONNEL, GIPLSA Lab, Grenoble

M.E. Mitzithra, (2008), *Corrosion of limestone mortars in a solution of chloride ions combined with sulphate ions at low temperatures*, Diploma Thesis, National Technical University of Athens, Greece

A. Nasser, (2010) *Influence of steel-concrete interface condition on galvanic corrosion currents in carbonated concrete*, Corrosion Science 52 2878-2890

NF EN 1097-6 (2001) *Essais pour déterminer les caractéristiques mécaniques et physiques des granulats. Détermination de la masse volumique réelle et du coefficient d'absorption d'eau*

NF P18-353 (1985): *Concrete, mortar and grout admixtures. Measurement of the percentage of entrained air in fresh concrete using an air meter*.

NF P18-451 (1981) *Concrete. Slump test*.

NF P18-459 (2010)**:** *Concrete –Testing hardened concrete-Testing porosity and density*

Nygaard, (2009), *Corrosion rate of steel in concrete: evaluation of confinement techniques for on-site corrosion rate measurements*, Materials and Structures 42:1059-1076

J. Ozbolt, (2011) *3D Numerical modelling of steel corrosion in concrete structures*, Corrosion Science 53 4166-4177

I. Petre-Lazar (2007), *Bilan du projet DURO_GC-Durabilité et reparation des ouvrages de genie civil en béton*, EDF R&D

R. Polder, (2000), *Test Methods for on site meausurement of resistivity of concrete, Materials and Structures*, Vol.33, 603-611

A.E. Poursaee (2007), *An Analysis of the factors influencing electrochemical measurements of the condition of reinforcing steel in concrete structures*, University of Waterloo, Waterloo Ontario, Canada

A. Poursaee (2011), *Corrosion measurement techniques in steel reinforced concrete*, Journal of ASTM International, 8(5):1–15

A. A. Ramezanianpour (2011), *Practical evaluation of relationship between concrete resistivity, water penetration, rapid chloride penetration and compressive strength,* Construction and Building Materials 25 (2011) 2472–2479

R. Revie, (2011), Uhlig's Corrosion Handbook,Wiley, 3rd Edition, p.153

T. Roure, (2009), *Bilan du groupe de travail sur l'étude des modes de ruine des aéroréfrigérants*, Note d'étude EGSSC090304, EDF SEPTEN

A. Steffens, (2002) *Modeling carbonation for corrosion risk prediction of concrete structures*, Cement and Concrete Research 32 935-941

S. Soleimani, (2010) *Modelling the kinetics of corrosion in concrete patch repairs and identification of governing parameter*, Cement & Concrete Composites 32 360-368

A.Saetta, (2004), *Experimental investigation and numerical modelling of carbonation process in reinforced concrete structures***,** Cement and Concrete Research 34 (2004) 571–579

A. Saetta, (2004), *Experimental investigation and numerical modelling of carbonation process in reinforced concrete structures Part II. Practical Applications***,** Cement and Concrete Research 34 (2004) 571–579

A.A. Sagues, (1990) NACE Corrosion '90, Vol. 132, Las Vegas, Nevada

M.J. Sansalone, (1998)**,** *The Impact echo method***,** NDTnet, Vol.3, No.2

Z.M. Sbartaï, (2007), *Using radar direct wave for concrete condition assessment: Correlation with electrical resistivity*, Journal of Applied Geophysics 62 361-374

Z.M. Sbartaï, (2009), *Non-destructive evaluation of concrete physical condition using radar and artificial neural networks*, Construction and Building Materials 23, 837-845

M. Sohail (2013), *Corrosion of Steel in Concrete:developmet of an Accelerated Test by Carbonation and Galvanic coupling***,** Thèse de Doctorat en genie civil, Toulouse

G. Song (1998)**,** *Corrosion of steel in concrete: causes, detection and precision*, Review Report 4, arrb Transport Research

Soutsos, (2001), *Dielectric properties of concrete and their influence on radar testing*, NDT & E International, 34, 419-425

M. Stern, A.L. Geary (1957), *Electrochemical Polarization I. A Theoretical Analysis of the Shape of Polarization Curves*, Journal of the Electrochemical Society 104-1, pp.56-63

W. Telford (1990), *Applied Geophysics*,2nd edition, Cambridge University Press

W. Tinsson (2010), *Plans d'expérience: constructions et analyses statistiques*, Mathématiques & Applications 67, Springer

C. Toulemonde (2010)**,** *Proposition de méthodologie d'étude des coques du parc des aéroréfrigérants en vue de leur classement***,** EDF R&D

F. Toutlemonde (2008) F*ield experience of UHPFRC durability in an air cooling tower*

G. Turner, (1994), *Subsurface radar propagation deconvolution*, Geophysics 59, 215-223

K. Viriyametanont, (2008), *Radar survey of concrete elements: Effect of concrete properties on propagation velocity and time zero*, NDTE & E International 41, 198-207

J.Wall (2009), *Concrete Civil Infrastructure in U.S. Commercial Nuclear Power Plants***,** Internal Report, Electric Power Research Institute

J. Warkus, (2006), *Modelling of reinforcement corrosion-Corrosion with extensive cathodes*, Materials and Corrosion, 57, No 12

R. Weydert (1999) E*lectrolytic Resistivity of Cover Concrete: Relevance*, Measurement and Interpretation. Eighth Int. Conf. on Durability of Materials and Components. Vancouver, Canada, May 30 June 3, 1999

R.Witasse (2000), *Contribution à ;la comprehénsion du comportement d'une coque d'aéroréfrigérant vielli: définition d'un état inital, influence des effets différés sous sollicitations hydro-mécaniques***,** Thèse de doctorat en génie civil, Lyon

H. Wojtas, (2004), *Determination of corrosion rate of reinforcement with a modulated guard ring electrode; analysis of errors due to lateral current distribution*, Corrosion Science 46 1621-1632

W. Yeih, (1998) *A study on the multiple reciprocity and complex-valued formulation for the Helmholtz equation*, Adv. Eng. Softw. 29, 7–12.

APPENDIX A

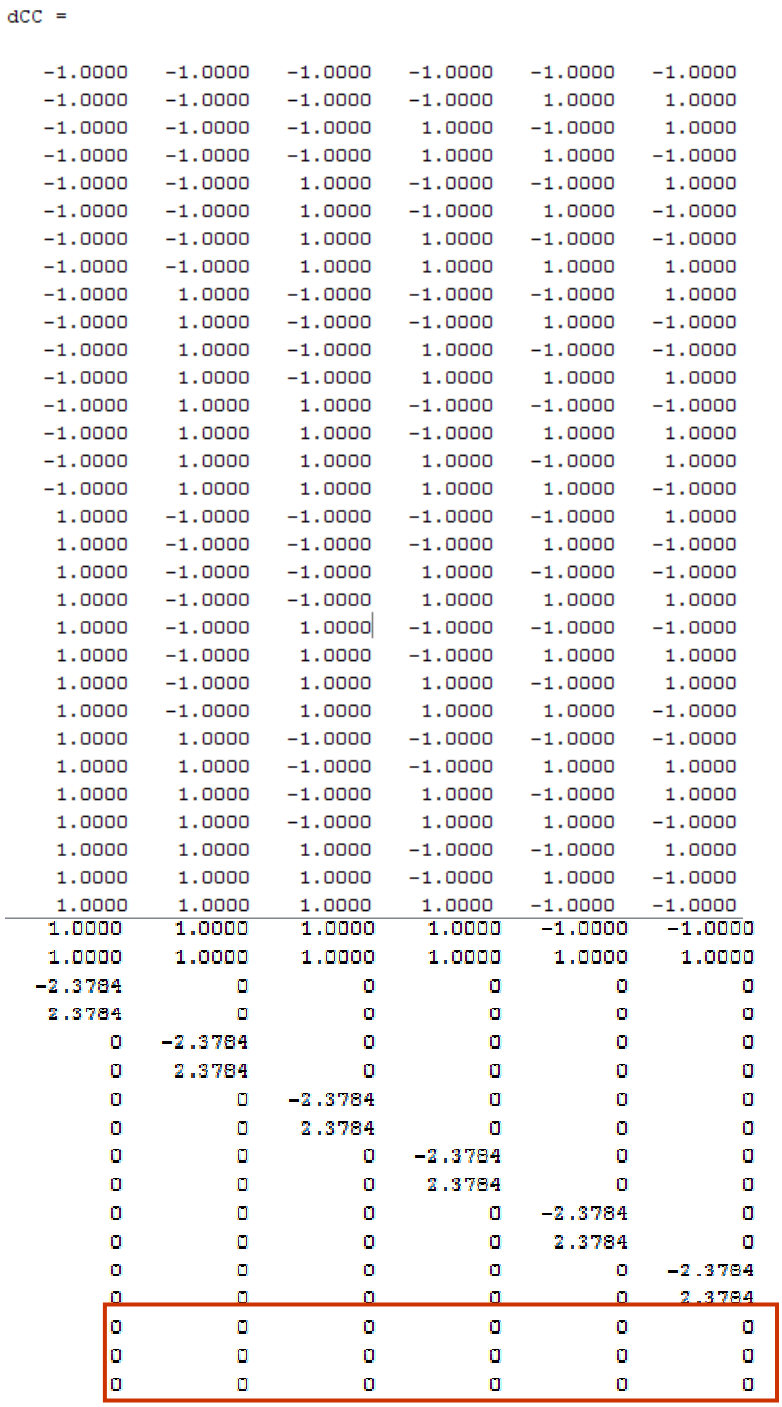

dCC =

-1.0000	-1.0000	-1.0000	-1.0000	-1.0000	-1.0000
-1.0000	-1.0000	-1.0000	-1.0000	1.0000	1.0000
-1.0000	-1.0000	-1.0000	1.0000	-1.0000	1.0000
-1.0000	-1.0000	-1.0000	1.0000	1.0000	-1.0000
-1.0000	-1.0000	1.0000	-1.0000	-1.0000	1.0000
-1.0000	-1.0000	1.0000	-1.0000	1.0000	-1.0000
-1.0000	-1.0000	1.0000	1.0000	-1.0000	-1.0000
-1.0000	-1.0000	1.0000	1.0000	1.0000	1.0000
-1.0000	1.0000	-1.0000	-1.0000	-1.0000	1.0000
-1.0000	1.0000	-1.0000	-1.0000	1.0000	-1.0000
-1.0000	1.0000	-1.0000	1.0000	-1.0000	-1.0000
-1.0000	1.0000	-1.0000	1.0000	1.0000	1.0000
-1.0000	1.0000	1.0000	-1.0000	-1.0000	-1.0000
-1.0000	1.0000	1.0000	-1.0000	1.0000	1.0000
-1.0000	1.0000	1.0000	1.0000	-1.0000	1.0000
-1.0000	1.0000	1.0000	1.0000	1.0000	-1.0000
1.0000	-1.0000	-1.0000	-1.0000	-1.0000	1.0000
1.0000	-1.0000	-1.0000	-1.0000	1.0000	-1.0000
1.0000	-1.0000	-1.0000	1.0000	-1.0000	-1.0000
1.0000	-1.0000	-1.0000	1.0000	1.0000	1.0000
1.0000	-1.0000	1.0000	-1.0000	-1.0000	-1.0000
1.0000	-1.0000	1.0000	-1.0000	1.0000	1.0000
1.0000	-1.0000	1.0000	1.0000	-1.0000	1.0000
1.0000	-1.0000	1.0000	1.0000	1.0000	-1.0000
1.0000	1.0000	-1.0000	-1.0000	-1.0000	-1.0000
1.0000	1.0000	-1.0000	-1.0000	1.0000	1.0000
1.0000	1.0000	-1.0000	1.0000	-1.0000	1.0000
1.0000	1.0000	-1.0000	1.0000	1.0000	-1.0000
1.0000	1.0000	1.0000	-1.0000	-1.0000	1.0000
1.0000	1.0000	1.0000	-1.0000	1.0000	-1.0000
1.0000	1.0000	1.0000	1.0000	-1.0000	-1.0000
1.0000	1.0000	1.0000	1.0000	1.0000	1.0000
-2.3784	0	0	0	0	0
2.3784	0	0	0	0	0
0	-2.3784	0	0	0	0
0	2.3784	0	0	0	0
0	0	-2.3784	0	0	0
0	0	2.3784	0	0	0
0	0	0	-2.3784	0	0
0	0	0	2.3784	0	0
0	0	0	0	-2.3784	0
0	0	0	0	2.3784	0
0	0	0	0	0	-2.3784
0	0	0	0	0	2.3784
0	0	0	0	0	0
0	0	0	0	0	0
0	0	0	0	0	0

Figure A. 1: Fractional CCC design of resolution V for 6 factors. The last three lines (in red) correspond to experiments that are realised in the centre of the experimental domain. Each number corresponds to the normalised value of the real value of the factors (the factors take their values in the common interval [-2,2]). The value 1 corresponds to the maximum level of the factor and the value -1 to the minimum. 0 corresponds to an intermediate level. Each line corresponds to a possible combination of the factors and defined according to DOE's theory (W. Tinsson, 2010).

TableA- 1: Experimental protocol with the combinations of the values of the factors, as determined by the experimental design. For each experiment the potential response, E_{ar}, (V) is given.

Exp.	***ρ(Ohmm)= x_1***	***e(cm)= x_2***	***I_{CE}(μA)= x_3***	***β_{aa}(V/dec)= x_4***	***β_{ac}(V/dec)= x_5***	***j_{corr} (A/cm^2)= x_6***	***Ea(V)= Y_1***
1	615.5	2.45	15.21	0.1509	0.0859	0.0025	-0.3787
2	615.5	2.45	15.21	0.1509	0.1090	0.0057	-0.3915
3	615.5	2.45	15.21	0.2391	0.0859	0.0057	-0.3893
4	615.5	2.45	15.21	0.2391	0.1090	0.0025	-0.3721
5	615.5	2.45	35.79	0.1509	0.0859	0.0057	-0.3575
6	615.5	2.45	35.79	0.1509	0.1090	0.0025	-0.3260
7	615.5	2.45	35.79	0.2391	0.0859	0.0025	-0.3087
8	615.5	2.45	35.79	0.2391	0.1090	0.0057	-0.3416
9	615.5	4.55	15.21	0.1509	0.0859	0.0057	-0.4065
10	615.5	4.55	15.21	0.1509	0.1090	0.0025	-0.3973
11	615.5	4.55	15.21	0.2391	0.0859	0.0025	-0.3963
12	615.5	4.55	15.21	0.2391	0.1090	0.0057	-0.4037
13	615.5	4.55	35.79	0.1509	0.0859	0.0025	-0.3700
14	615.5	4.55	35.79	0.1509	0.1090	0.0057	-0.3872
15	615.5	4.55	35.79	0.2391	0.0859	0.0057	-0.3839
16	615.5	4.55	35.79	0.2391	0.1090	0.0025	-0.3597
17	1434.5	2.45	15.21	0.1509	0.0859	0.0057	-0.3842
18	1434.5	2.45	15.21	0.1509	0.1090	0.0025	-0.3573
19	1434.5	2.45	15.21	0.2391	0.0859	0.0025	-0.3458
20	1434.5	2.45	15.21	0.2391	0.1090	0.0057	-0.3738
21	1434.5	2.45	35.79	0.1509	0.0859	0.0025	-0.2973
22	1434.5	2.45	35.79	0.1509	0.1090	0.0057	-0.3393
23	1434.5	2.45	35.79	0.2391	0.0859	0.0057	-0.3121
24	1434.5	2.45	35.79	0.2391	0.1090	0.0025	-0.2506

25	1434.5	4.55	15.21	0.1509	0.0859	0.0025	-0.3896
26	1434.5	4.55	15.21	0.1509	0.1090	0.0057	-0.4016
27	1434.5	4.55	15.21	0.2391	0.0859	0.0057	-0.4003
28	1434.5	4.55	15.21	0.2391	0.1090	0.0025	-0.3825
29	1434.5	4.55	35.79	0.1509	0.0859	0.0057	-0.3801
30	1434.5	4.55	35.79	0.1509	0.1090	0.0025	-0.3488
31	1434.5	4.55	35.79	0.2391	0.0859	0.0025	-0.33207
32	1434.5	4.55	35.79	0.2391	0.1090	0.0057	-0.3674
33	50	3.5	25.5	0.195	0.0975	0.0041	-0.4090
34	2000	3.5	25.5	0.195	0.0975	0.0041	-0.3545
35	1025	1	25.5	0.195	0.0975	0.0041	-0.3225
36	1025	6	25.5	0.195	0.0975	0.00415	-0.3938
37	1025	3.5	1	0.195	0.0975	0.00415	-0.4171
38	1025	3.5	50	0.195	0.0975	0.00415	-0.3203
39	1025	3.5	25.5	0.09	0.0975	0.00415	-0.3847
40	1025	3.5	25.5	0.3	0.0975	0.00415	-0.3600
41	1025	3.5	25.5	0.195	0.07	0.00415	-0.3712
42	1025	3.5	25.5	0.195	0.125	0.00415	-0.3657
43	1025	3.5	25.5	0.195	0.0975	0.0003	-0.2481
44	1025	3.5	25.5	0.195	0.0975	0.008	-0.3866
45	1025	3.5	25.5	0.195	0.0975	0.00415	-0.3681
46	1025	3.5	25.5	0.195	0.0975	0.00415	-0.3681
47	1025	3.5	25.5	0.195	0.0975	0.00415	-0.3681

Table A- 2: Results of the analysis of variance after the method of linear regression the potential response, E_{ar}, model)

Source	Degrees of freedom (ddl)	Sum of squares
Regression	27	0.0612
Error	19	0.0027
F-statistic vs. constant model	15.95	
p-value	1.75e-06	
Mean square error (MSE)	3.16e-08	
Coefficient of determination (R^2)	0.96	

Table A- 3.: Experimental protocol with the combinations of the values of the factors, as determined by the experimental design. For each experiment the current density value, j_{ar}. (A/m^2) is given

Exp.	$\rho(Ohmm)=x_1$	$e(cm)=x_2$	$I_{CE}(\mu A)=x_3$	$b_a(V/dec)=x_4$	$b_c(V/dec)=x_5$	$j_{corr}=x_6$ (A/m^2)	$j_a(A/m^2))=Y_2$
1	615.5	2.45	15.21	0.1509	0.0859	0.0025	0.0039
2	615.5	2.45	15.21	0.1509	0.1090	0.0057	0.0055
3	615.5	2.45	15.21	0.2391	0.0859	0.0057	0.0051
4	615.5	2.45	15.21	0.2391	0.1090	0.0025	0.0032
5	615.5	2.45	35.79	0.1509	0.0859	0.0057	0.0135
6	615.5	2.45	35.79	0.1509	0.1090	0.0025	0.0102
7	615.5	2.45	35.79	0.2391	0.0859	0.0025	0.0076
8	615.5	2.45	35.79	0.2391	0.1090	0.0057	0.0111
9	615.5	4.55	15.21	0.1509	0.0859	0.0057	0.0029
10	615.5	4.55	15.21	0.1509	0.1090	0.0025	0.0019
11	615.5	4.55	15.21	0.2391	0.0859	0.0025	0.0018
12	615.5	4.55	15.21	0.2391	0.1090	0.0057	0.0025
13	615.5	4.55	35.79	0.1509	0.0859	0.0025	0.0047
14	615.5	4.55	35.79	0.1509	0.1090	0.0057	0.0066
15	615.5	4.55	35.79	0.2391	0.0859	0.0057	0.0059

16	615.5	4.55	35.79	0.2391	0.1090	0.0025	0.0037
17	1434.5	2.45	15.21	0.1509	0.0859	0.0057	0.0073
18	1434.5	2.45	15.21	0.1509	0.1090	0.0025	0.0057
19	1434.5	2.45	15.21	0.2391	0.0859	0.0025	0.0048
20	1434.5	2.45	15.21	0.2391	0.1090	0.0057	0.0066
21	1434.5	2.45	35.79	0.1509	0.0859	0.0025	0.0158
22	1434.5	2.45	35.79	0.1509	0.1090	0.0057	0.0180
23	1434.5	2.45	35.79	0.2391	0.0859	0.0057	0.0155
24	1434.5	2.45	35.79	0.2391	0.1090	0.0025	0.0126
25	1434.5	4.55	15.21	0.1509	0.0859	0.0025	0.0028
26	1434.5	4.55	15.21	0.1509	0.1090	0.0057	0.0036
27	1434.5	4.55	15.21	0.2391	0.0859	0.0057	0.0035
28	1434.5	4.55	15.21	0.2391	0.1090	0.0025	0.0024
29	1434.5	4.55	35.79	0.1509	0.0859	0.0057	0.0087
30	1434.5	4.55	35.79	0.1509	0.1090	0.0025	0.0070
31	1434.5	4.55	35.79	0.2391	0.0859	0.0025	0.0057
32	1434.5	4.55	35.79	0.2391	0.1090	0.0057	0.0078
33	50	3.5	25.5	0.195	0.0975	0.0041	0.0014
34	2000	3.5	25.5	0.195	0.0975	0.0041	0.0079
35	1025	1	25.5	0.195	0.0975	0.0041	0.0120
36	1025	6	25.5	0.195	0.0975	0.0041	0.0032
37	1025	3.5	1	0.195	0.0975	0.0041	0.0026
38	1025	3.5	50	0.195	0.0975	0.0041	0.0129
39	1025	3.5	25.5	0.09	0.0975	0.0041	0.0081

40	1025	3.5	25.5	0.3	0.0975	0.0041	0.0055
41	1025	3.5	25.5	0.195	0.07	0.0041	0.0064
42	1025	3.5	25.5	0.195	0.125	0.0041	0.0062
43	1025	3.5	25.5	0.195	0.0975	0.0003	0.0023
44	1025	3.5	25.5	0.195	0.0975	0.008	0.0080
45	1025	3.5	25.5	0.195	0.0975	0.0041	0.0063
46	1025	3.5	25.5	0.195	0.0975	0.0041	0.0063
47	1025	3.5	25.5	0.195	0.0975	0.0041	0.0063

Table A- 4: Results of the analysis of variance after the method of linear regression the current density response, j_{ar}, model

Source	**Degrees of freedom (ddl)**	**Sum of squares**
Regression	27	7.48e-04
Error	19	9.21e-06
F-statistic vs. constant model	57.16	
p-value	3.24e-13	
Mean square error (MSE)	4.85e-07	
Coefficient of determination (R^2)	0.988	

APPENDIX B

B.1. Specimens' fabrication and conditioning

The two different types of concrete, having the same composition, were casted in two different dates (figure B.1). Table B.1. summarizes the characteristics of fresh concrete for these two different fabrications.

Figure B. 1: Casting of the reinforced concrete slabs and specimen

Table B- 1.: Fresh concrete characteristics

	Type I **Casting date:16/02/2012**	**Type II** **Casting date:10/01/2012**
(NF P 18-451) Concrete slump test(cm)	9	17.5
Real W/C	0.56	0.56
(NF P 18-353) Air(%)	2	2.3
Real density(kg/m^3)	2420	2334

The differences observed between the two concrete fabrications may be attributed to different casting conditions for those two dates (i.e. different state of the mixer, errors during the calculation of the real water content of the aggregates).

Once the concrete specimens were casted, the slabs were stored directly in the laboratory environment while the cylindrical specimens were cured in a chamber of fixed temperature (20°C) and relative humidity (95%) (figure B.2). 24h later all specimens were de moulded. The cylindrical specimens intended for mechanical testing at 28 days, were then preserved for

28 days in the chamber of fixed temperature and humidity while the remaining samples were maintained in the laboratory environment.

Every 15 days, the weight of the concrete slabs was controlled. Once their weight was stabilised (1 month after the first weight measurement), the slabs intended for being at active state, were placed in a chamber of accelerated carbonation (50%CO_2, 60% RH) (figure B.4.). In order to avoid the diffusion of CO_2 from the sides of the concrete slabs they were covered with self-adhesive aluminium (Al) paper. Similar procedure was followed for the cylindrical specimen, scheduled also to be carbonated.

Figure B. 2:24h curing of the concrete specimens in a chamber of fixed temperature (20°C) andrelative humidity (95°C).

a)

b)

Figure B. 3: a) Reinforced concrete slab) and b) cylindrical specimen before storing in the chamber of accelerated carbonation (50%CO_2, 60% RH). Their sides are covered with self-adhesive Al paper.

Figure B. 4: Chamber of accelerated carbonation (50%CO_2, 60%.RH)

On the other hand, the slabs intended to stay at passive state, were covered entirely with self adhesive aluminium paper, in order to avoid any undesirable corrosion from the environmental conditions (figure B.5) and they were preserved in the laboratory:

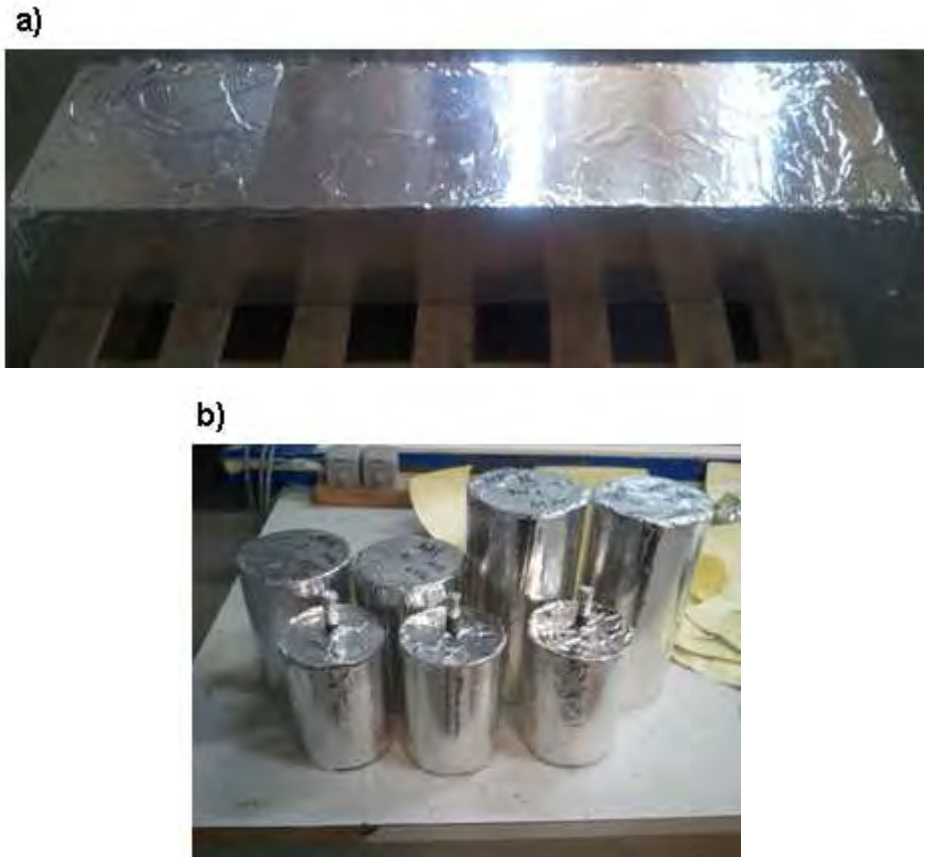

Figure B. 5: a) Reinforced concrete slab and b) cylindrical specimen entirely covered with auto adhesive Al paper, in order to avoid any undesirable corrosion from environmental conditions.

In the case of reinforced concrete specimens (either active or passive), used for the Tafel constants measurements, the part of the reinforcement remaining out from the specimen, was first covered with resin and then with Al paper, to isolate it from any possible contact with the external environment.

After two months of storage in the chamber of accelerated carbonation, the slab and the cylindrical specimen were uniformly carbonated. This was confirmed by spraying phenolphthalein on the broken face obtained after splitting a cylindrical sample.

Figure B. 6: Concrete specimen for control of carbonation. Controlling the ingress of carbonation with phenolphthalein after one month (right) and two months (left).

As it can be seen from the figure B.6, after one month in the chamber of accelerated carbonation, the specimens were fully uniformly carbonated, since the colour of the broken face didn't change. The concrete specimen stayed in the corrosive environment for one more month. Furthermore, the passive state of the non carbonated specimen was also confirmed by following the same procedure (figure B.7):

Figure B. 7: Concrete specimen for control of carbonation. Carbonation ingress tested with phenolphthalein after one month (right) and two months (left). Violet colour indicates that the specimen is not carbonated.

Finally, once the uniform carbonation was achieved, all concrete specimens were stored in the laboratory environment without the Al paper.

B.2. Mechanical and physical characteristics of casted concrete

In order to obtain information on the mechanical and physical properties of the casted concrete, compression strength, porosity and permeability tests were carried out. The results for both types of concrete, carbonated and non carbonated, are indicated in table B.2. As it is already known, the compressive strength testing was carried out on concrete specimen conserved for 28 days, after being de moulded, in the chamber of fixed temperature (20°C) and relative humidity (95%). The porosity and permeability tests were carried out right after the removal of the specimen from the chamber of accelerated carbonation. For the same period, the passive slabs and specimens were preserved in the laboratory environment.

Table B- 2: Mechanical and physical characteristics of casted concrete Type I and Type II, carbonated and non carbonated.

Mechanical and Physical Characteristics	**Type I Casting date:16/02/2012**		**Type II Casting date:10/01/2012**	
Compressive strength R_c (28 days) (MPa) (EN-12390/3)	25.4		27.2	
	I-C	**-NC**	**C**	**NC**
Accessible porosity to water (%) (NF P18-459)	14	17.8	14.4	16.2
Oxygen Permeability, k_{O2} ($10^{-15}m^2$) (Cembureau method)	1.85	3.32	1.71	3.31

As it can be seen on table B.2, the compressive strength is **not really high** for both types of concrete. This can be expected due to **the type of the cement** used (CEM II 32.5R) and the use of **coarse aggregates** (12/20mm) in the concrete casting, impoverishing the paste's cohesion. These low values of strength are also justified by the relatively high porosity, measured for the non-carbonated concrete. In addition, as it can be seen, **porosity diminishes**, for a **carbonated concrete**, which can be considered as reasonable, since the product of carbonation precipitates and fills the pores. Similar behaviour is exhibited for the gas permeability: the concrete becomes more **compact after carbonation**, and as a result, **less permeable to gases**. Furthermore, both types of concrete, whether at active or passive state, exhibit values in the same order of magnitude. Thus, a relatively porous and quite permeable

to gases concrete was casted for both cases, which can explain, at a certain level, the rapid ingress of carbonation within only 2 months.

Last but not least, the technique of mercury (Hg) porosimetry (ISO 15901-1:2005) was carried out for type I, in order to obtain information on the pore size distribution of the carbonated and non carbonated concrete. The results are illustrated in the figure B.8.

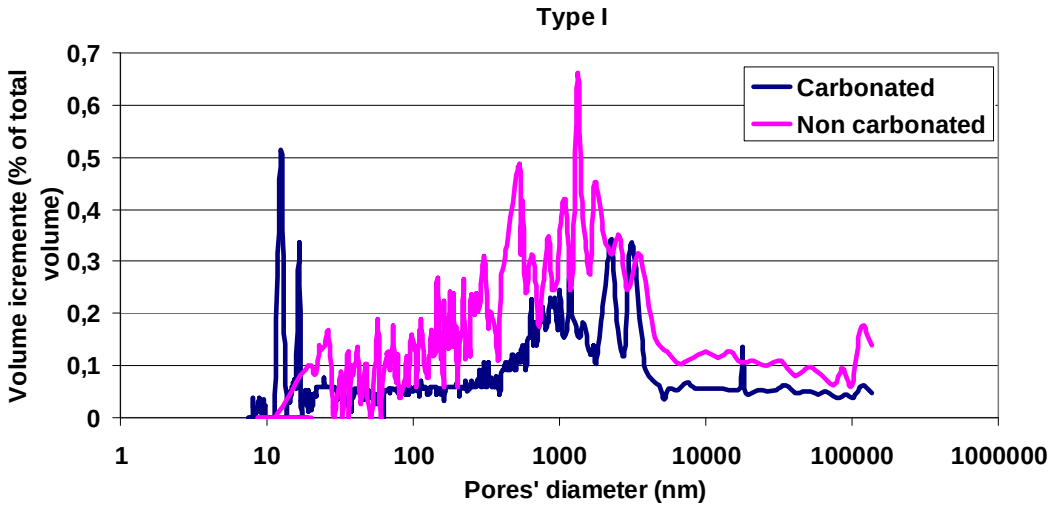

Figure B. 8: Pore size distribution according to Hg porosimetry for the concrete type I (1 single rebar configuration), carbonated (blue curve) and non carbonated (pink curve). The curves are highly disturbed due to the measurement's noise.

As it can be seen from figure B.8, pore size seems to be mostly distributed between 100 and 10000 nm. As far as carbonated concrete is concerned, for the carbonated concrete it seems that the carbonation products precipitate and fill the pores, leading to an expected decrease in porosity (blue curve) of concrete.

B.3. Synthesis

Firstly, in this paragraph, the results for compression strength, porosity and permeability testing were presented for both types of casted concrete, being at active and passive state. a relatively porous concrete was casted, with a pores' size distribution between 100-1000nm, exhibiting a relatively low compressive strength and not extremely high values of gas permeability. Both types of concrete exhibited values in the same order of magnitude. For the concrete specimen submitted to carbonation, porosity and oxygen permeability values decrease. Still, the differences between the values for active (carbonated) and passive (non carbonated) concrete specimen are not so significant.

APPENDIX C

Technique of polarisation resistance for one single point on site measurement
Determination of corrosion current density of the reinforcement

1. Objective of the technique

Measuring the polarisation resistance and estimate the corrosion current density of reinforcing steel in carbonated concrete.

Other measurements provided: concrete cover, e, concrete resistivity and corrosion potential.

2. Domain of application

All the measurements are realised on the concrete surface of the structure under the following conditions:

- Measurement of the carbonation depth (phenolophtaleine solution test). If carbonation depth is lower than the concrete cover of the first layer of steel rebars, the procedure must be stopped.
- The distance between the steel rebars must be superior or equal to 20cm.

3. Definitions of zones and points of measurement

3.1 3D positioning of the steel rebars and measurement of the concrete cover of steel rebars via the technique of Ground Penetrating Radar (See Protocol –C2D2-ACDC)

3.2. Measurement of resistivity of concrete cover of steel rebars

Square meshes are determined between the rebars of the measurement zone. The dimensions of these squares must be 12 x 12cm, and the distance between each side of the square and the neighbour steel rebar must be higher than 4cm. In total, 8 measurements of resistivity are carried out.

3.3. Measurement of corrosion potential and polarisation resistance of steel rebars

Definition of measurement points right above the single steel rebars.

4. Operative mode

The measurements are carried out in the following order:

4.1. Measurement of concrete cover

Value measured on site

Equipment: Ground Penetrating Radar, Pachometer.
Procedure of measurement as indicated by **(***Protocol Technique radar, Vitesse des ondes directes–C2D2-ACDC).* Determination of the dimensions of concrete cover.

4.2. Measurement of resistivity of concrete cover via the method of Wenner

Equipment:

- **Instrument (LMDC):** AVO: MEGGER DET5/4RF (or similar)**.**
- **Equipment**: Probe of four (4) electrodes, with a spacing of 4cm and a small piece of sponge integrated on the base of each electrode.
- **Additional equipment**: a sprayer with tap water and a tray

Before the measurement:

- Slight humidification of the concrete surface in order to avoid any problems of contact between the probe and the surface of structure.
- Humidification of the sponges of the electrodes.

Acquisition of the measurement:

- Placing and strong holding of the probe on the concrete surface
- Measurement of resistivity via several successive positions of the probe (figure 1). Retrieval of the Resistance (R) en K Ohm.

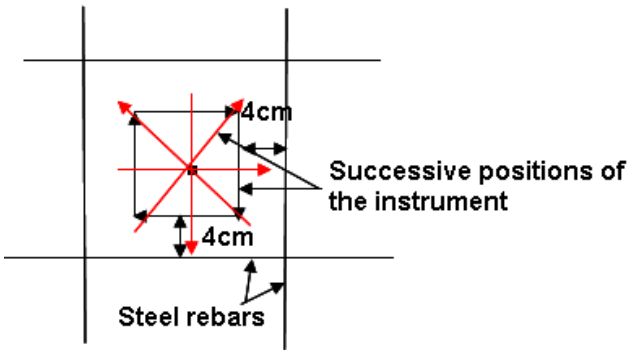

Figure C. 1: Successive positions of Wenner probe for measuring concrete resistivity, indicated by the black arrows of the formed square. A point is fixed in the middle of the square and the probe is placed as indicated by the red arrows.

Value after processing-on site

For every measured Resistance (R), the value of resistivity is calculated via the following equation:

$$\rho(Ohm \cdot m) = 2 \cdot \pi \cdot a \cdot R \quad \text{(eq. 1)}$$

Where:

α(m): the electrode spacing (=4cm)

R: the Resistance measured in K. Ohm

- Calculation of the mean value of resistivity, $\overline{\rho}$, of concrete cover. If $\overline{\rho} \geq 1500$ Ohm.m, the procedure must be stopped.

4.3. Corrosion potential and polarisation resistance measurement

Equipment:

- **Instrument (LMDC):** Potentiostat GAMRY Ref. 600 of 1 channel, equipped with a laptop for measurement settings and data processing or similar
- **Main equipment:**

  - Counter Electrode (CE): a stainless steel ring (d_{ex}=20mm, d_{in}=8mm, thickness?)
  - Reference Electrode (RE): Saturated Calomel Electrode (SCE:+0.244V vs. SHE, 25°C)
  - Working Electrode: Steel rebar
- **Additional equipment: a** compressed air jet, a sprayer with tap water, a sponge of 50x50mm, crocodile clips, wires.

Before the measurement:

- Confirmation of saturation conditions and absence of air for the reference electrode. Otherwise filling with KCl solution.
- Drilling of the concrete surface for accessing the reinforcement. Then, piercing the steel rebar, for the establishment of electrical connexion between the rebar and the instrument, in the aid of the self drilling screws. Piercing at least at two points of the measurement zone and confirm the electrical connection among the steel rebars of the network.
- Remove all the dust from and around the drilling area via the compressed air jet.

Experimental setup and procedure:

- The sponge is humidified (till saturation) and placed on the measurement point on the concrete surface, right above the reinforcement.
  It's a 3 electrodes' measurement: the ring (CE) is placed on the sponge. The reference electrode (RE) is placed in the middle of the counter electrode. The red cable of the potentiostat is connected via the crocodile clip to the CE and the white cable to the reference electrode. The green cable is connected via the crocodile clip to the steel rebar. The potentiostat is connected via another cable to the laptop where the measurement is set.

Acquisition:

A personal folder (Surname, Name) is created in *My Gamry Data*. All the measurement files will be saved in that folder. The software *Gamry Framework* is opened. If the indication *Device on* is lightened green, the potentiostat is well connected to the laptop and the

measurements can be effectuated. If the indication *Device On* is lightened red, the potentiostat is not connected to the laptop.

4.3.1. Test of electrical connection between the steel rebars of the measurement zone

Measuring the resistance between two points of the reinforcement network. The resistance :must be less than 1 Ohm (Reference: RILEM TC 154-EMC *Half ell potential measurements*).

4.3.2. Corrosion potential and polarisation resistance measurement.

4.3.2.1. Definition of sequences of measurements

Experiment→ Sequence Wizard. A sequence is defined *(Define Sequence)* by drugging the measurements –to- be- done from the list of measurements (*General→ Open Circuit Potential*, *DC 105→Galvanostatic*) on the left to the empty region on the right. Once the sequence is defined, it saved (*Save Sequence*) in the personal folder that have been created earlier in *My Gamry Data*. The created sequence is loaded via *Load Sequence* and launched via *Run Sequence*.

4.3.2.2. Creation of sequences of measurements

Via the creation of sequences of measurements energy and time is economised, since it allows the realisation of measurements consecutively with any intervention from the operator. The following sequence is created:

- Corrosion Potential measurement (*General→ Open Circuit Potential*)

Total time (s): 200
Sample Period (s): 0.5
Stability (mV/s): 0.01
Sample area (cm^2): 1

- Polarisation resistance measurement (*DC 105→Galvanostatic*)

Initial I (mA/cm^2): 0
Initial time (s): 1
Final I (mA/cm^2):.0.001 (injected current: 1µA)
Sample Period (s): 0.5
Sample area (cm^2): 1
Density (g/cm3): by default
Equiv. wt: by default

- Corrosion Potential measurement (*General→ Open Circuit Potential*)

Total time (s): 600
Sample Period (s): 0.5
Stability (mV/s): 0.01
Sample area (cm^2): 1

- Polarisation resistance measurement (*DC 105→Galvanostatic*)

Initial I (mA/cm^2): 0
Initial time (s): 1
Final I (mA/cm^2):.0.005 (injected current: 5μA)
Sample Period (s): 0.5
Sample area (cm^2): 1
Density (g/cm3): by default
Equiv. wt: by default
…….

The values of the injected current are shown in the following table:

Table C- 1: Values of the injected current integrated as Final I in the sequence:

Injected current, I_{CE} (μA)	*Final I (mA/cm^2)*
1	0.001
5	0.005
10	0.01
20	0.02
30	0.03
50	0.05

4.3.2.3. Launching of the Sequence

Run Sequence. During the first measurement of corrosion potential, potential is plotted as a function of time. The measurements last in total 200 sec, but if the potential value stays stable for 10 sec the measurement is interrupted. Automatically, the galvanostatic measurement starts. A current of 1μA is set and injected for 200 sec and the change in potential (from potential corrosion) is traced as a function of time. Once more in case of potential stabilisation for 10 sec, the measurement is interrupted. Then, another OC potential measurement is carried out. During this period of de-polarisation (600sec), potential is traced as a function of time. Once potential returns to its initial equilibrium value and becomes stable (10 sec), then there are two options: in case of an achieved **linear polarisation, ΔE_p, of 20 ±3 mV** on the steel rebar, the measurement is interrupted permanently and the procedure of calculating polarisation resistance, R_p, takes place. Otherwise, another polarisation measurement is carried out, by augmenting the injecting current at 5μA. The same procedure described above, is followed for all the other values of injected current, presented in the table 1 till a

polarisation ΔE_p, of 20 ±3 mV is achieved in the surface of the steel rebar. The whole measurement (on a single point) may last, more or less, 30 minutes. The following figure summarizes the procedure of measuring corrosion potential and polarisation:

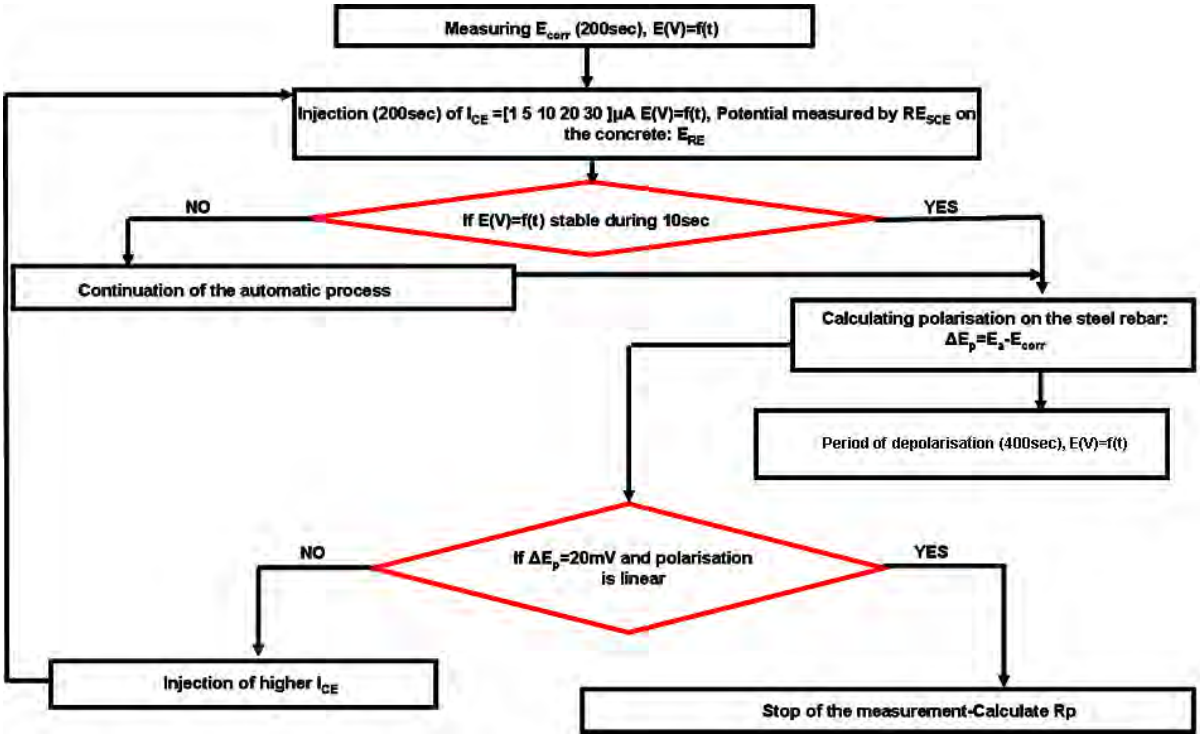

Figure C. 2: Procedure of corrosion potential and polarisation measurement

After each measurement, the corrosion potential, $E_{corr,}$ (V) and the potential measured by the reference electrode, E_{RE}, (V) are noted. E_{RE} (V) must always be more electropositive than E_{corr} (V) (anodic polarisation). If it is not the case, an injection of positive current, during the creation of the sequences, must be ensured. In order to calculate ΔE_p, the following procedure is followed:

a. Based on the following table, an indication as far as the state of the reinforcement is given:

Table C- 2: ASTM-C867 recommendations for corrosion potential (J.P.Broomfield, 1997)

Ecorr (vs. E_{SCE}) (V)	**Risk de corrosion**
>-0,126	Low (>10% risk of corrosion)
-0,276 - -0,126	Intermediate corrosion risk
<-0,276	High (<90% risk of corrosion)
<-0,426	Severe Corrosion

In case a low risk of corrosion is indicated, the procedure is stopped. In case a high risk or severe corrosion is indicated, then via the use of abacus k for active steel rebar and the relationship (2), the potential on the steel rebar, E_{ar}, (V) is calculated.

$$E_{ar} = E_{RE} - k \cdot \rho \qquad \text{(eq. 2).}$$

Now, in case, E_{ar}>E_{corr} the procedure is stopped. In case E_{ar}<$E_{corr,}$ then ΔE_p is calculated as following:

$$\Delta Ep\ (V) = E_{ar} - E_{corr} \qquad \text{(eq. 3).}$$

The whole experimental set up is depicted in the following pictures:

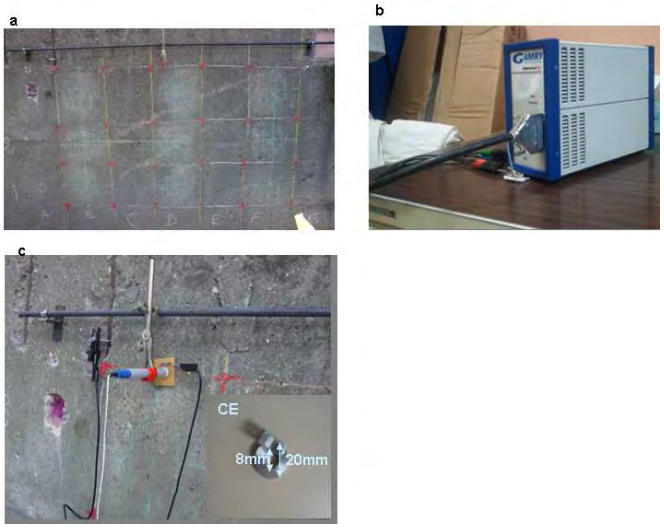

Figure C. 3: a) Definition of measurement zones . Formation of squares for the resistivity measurement and definition of points right above the steel rebars for the corrosion potential and polarisation resistance measurement. b). Potentiostat GAMRY Ref. 600 of 1 channel, equipped with a laptop for measurement settings and data processing. c). Experimental set up and electrodes' configuration during the polarisation resistance measurement.

4.3.2.4. End of the Sequence

Once the polarisation, **ΔE_p, of 20 ±3 mV** is achieved the measurement is stopped. The folder with the measurement files is retrieved. The devices are then switched off in the following order:

a. Potentiostat
b. Laptop for measurement settings.

5. Uncertainties.

*In this paragraph only a general idea on the uncertainties during the tests (repeatability, positioning of the probe) carried out in the **laboratory environment** are given. The uncertainties of the numerical model are not included.*

- **For concrete cover of steel rebars e ≤3cm:**

-Measurement repeatable for < 10 measurements.
-Acceptable displacement of the probe along the axis of the steel rebar: ±2-4cm
-Acceptable displacement of the probe at a distance from the axis of the steel rebar < 2cm,

- **For concrete cover of steel rebars e >3cm:**

-No repeatable measurement
-Acceptable displacement of the probe along the axis of the steel rebar: ±2-4cm
-Acceptable displacement of the probe at a distance from the axis of the steel rebar: 2cm

6. Results

Value after processing-on site

6.1 Calculation of polarisation resistance, R_p.

Apart from E_{ar} (V), the current density on the steel rebar j_{ar} (A/m^2) is also calculated for every value of injected current till **ΔE_p, of 20 ±3 mV** is achieved, in the aid of abacus of A,B (for active steel rebars) and the equation of:

$$\ln\left(\frac{j_{ar}}{i_{CE}}\right) = -(A + B \cdot e) \qquad \text{(eq. 4)}$$

The procedure is summarized in the following figure:

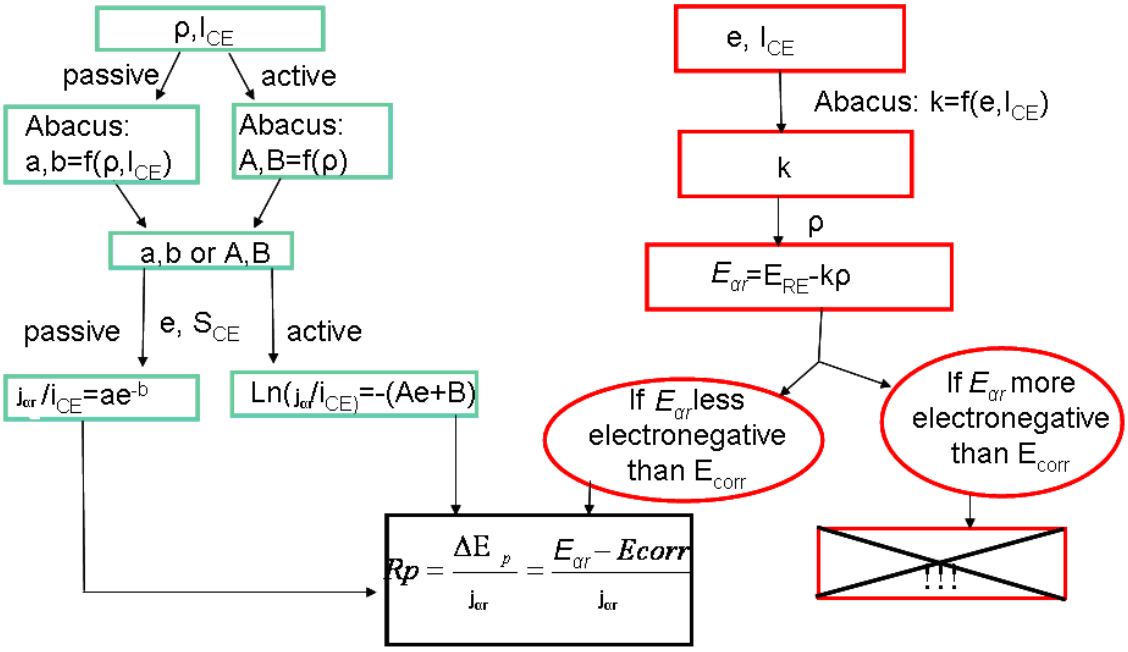

FigureC. 4 : Procedure of calculating, the potential, E_{ar} (V) and the current density; i_{ar} (A/m^2) on the steel rebar.

Finally, for all the values found, ΔE_{ar} (V) is plotted vs. j_{ar} (A/m^2). The coefficient of determination of the linear regression must be higher than **R^2>0.85**. Rp is then calculated. If R^2<0.85 the procedure is continued but the operator should take into consideration that the precision in the calculation of Rp is diminished. The slope of that corresponds to Rp^{-1} (Ohm m2)$^{-1}$. An example is given below:

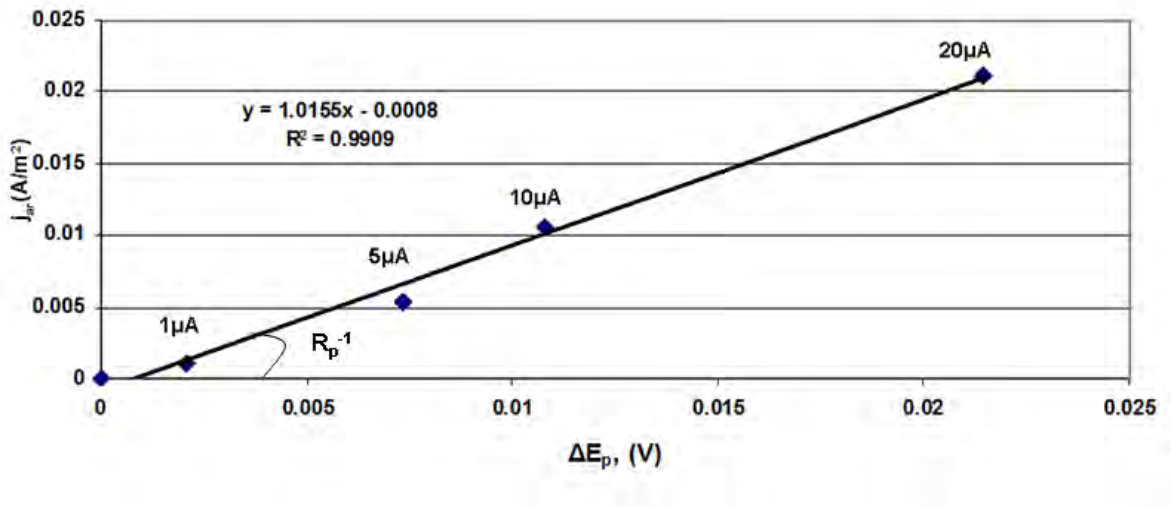

FigureC. 5: Polarisation (E_{ar}(V) vs. j_{ar} (A/m^2)) Curve at E_{corr} for polarisation resistance measurement on an active steel rebar. The slope of this curve represents the Rp value (Ohm m^2) of the steel rebar.

6.2 Calculation of corrosion current density, j_{corr} (µA/cm^2)

The corrosion current density is calculated according to the following equation:

$$j_{corr} = \frac{B}{Rp} \qquad \text{(eq. 5).}$$

Where constant B = 0.038V for the active steel rebar. Corrosion is classified according to table 3:

Table C- 3: Correlation between corrosion classification and corrosion current density (D.W. Law, 2004)

j_{corr}(µAcm^{-2})	Corrosion classification
0,1-0,2	Very low or passive
0,2-0,5	Low to moderate
0,5-1	Moderate to high
>1	High

Note: In case the corrosion potential measurement indicates an intermediate or undefined risk of corrosion, the previous procedure for the estimation of polarisation resistance and corrosion current density should be followed. Taking into consideration, the measured resistivity, the polarisation resistance results, the value of injected current at which ΔE_p, of 20 ±3 mV is

achieved, the whole procedure should be repeated at regular frequent intervals (a continuous monitoring of ambient conditions, resistivity, corrosion potential, polarisation resistance and corrosion current density), in order to confirm the evolution and the tendency of the reinforcement towards an active or a passive state.

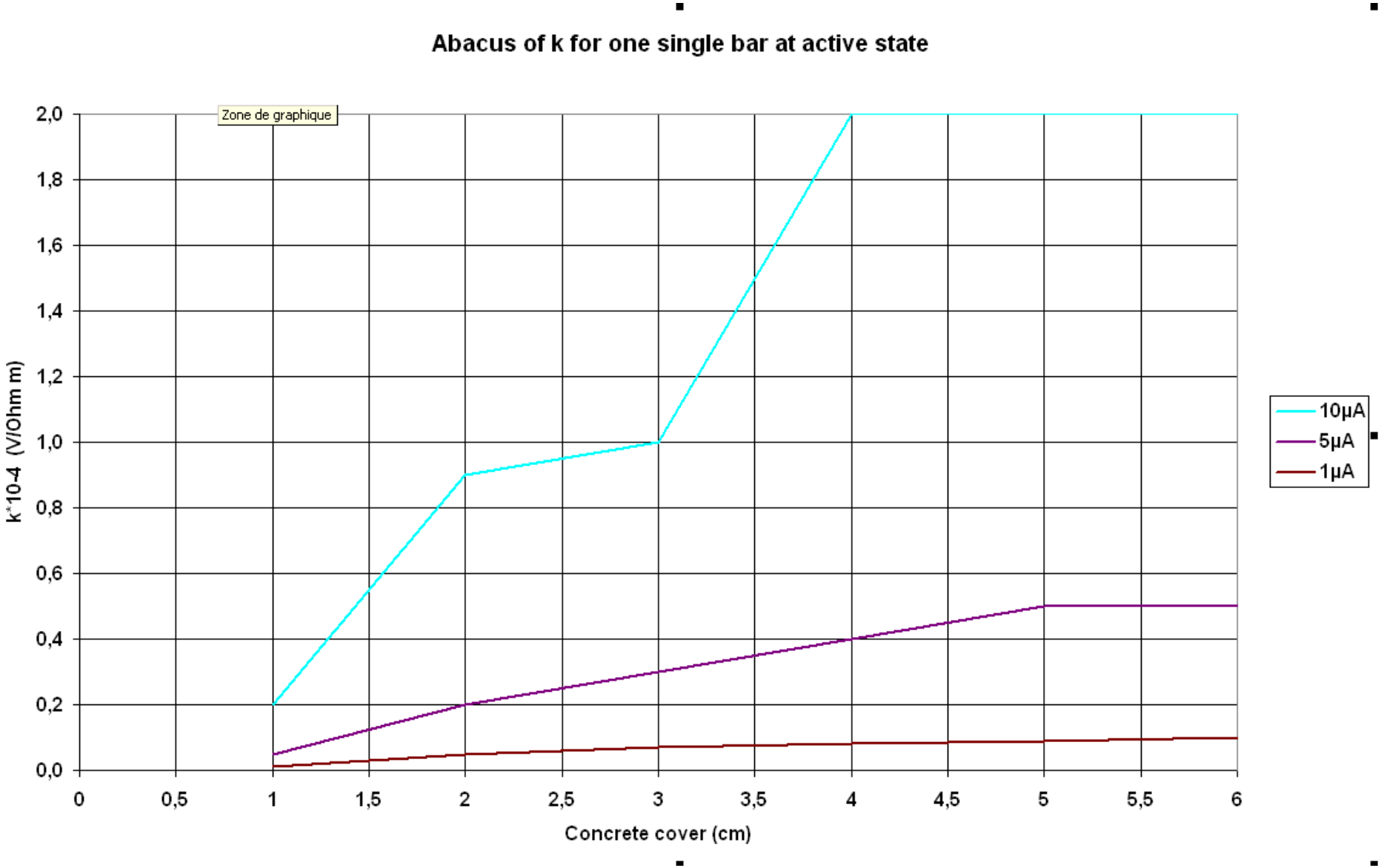
Abacus of k for one single bar at active state
Zone de graphique
k*10-4 (V/Ohm m)
2,0
1,8
1,6
1,4
1,2
1,0
0,8
0,6
0,4
0,2
0,0
0
0,5
1
1,5
2
2,5
3
3,5
4
4,5
5
5,5
6
Concrete cover (cm)
10µA
5µA
1µA

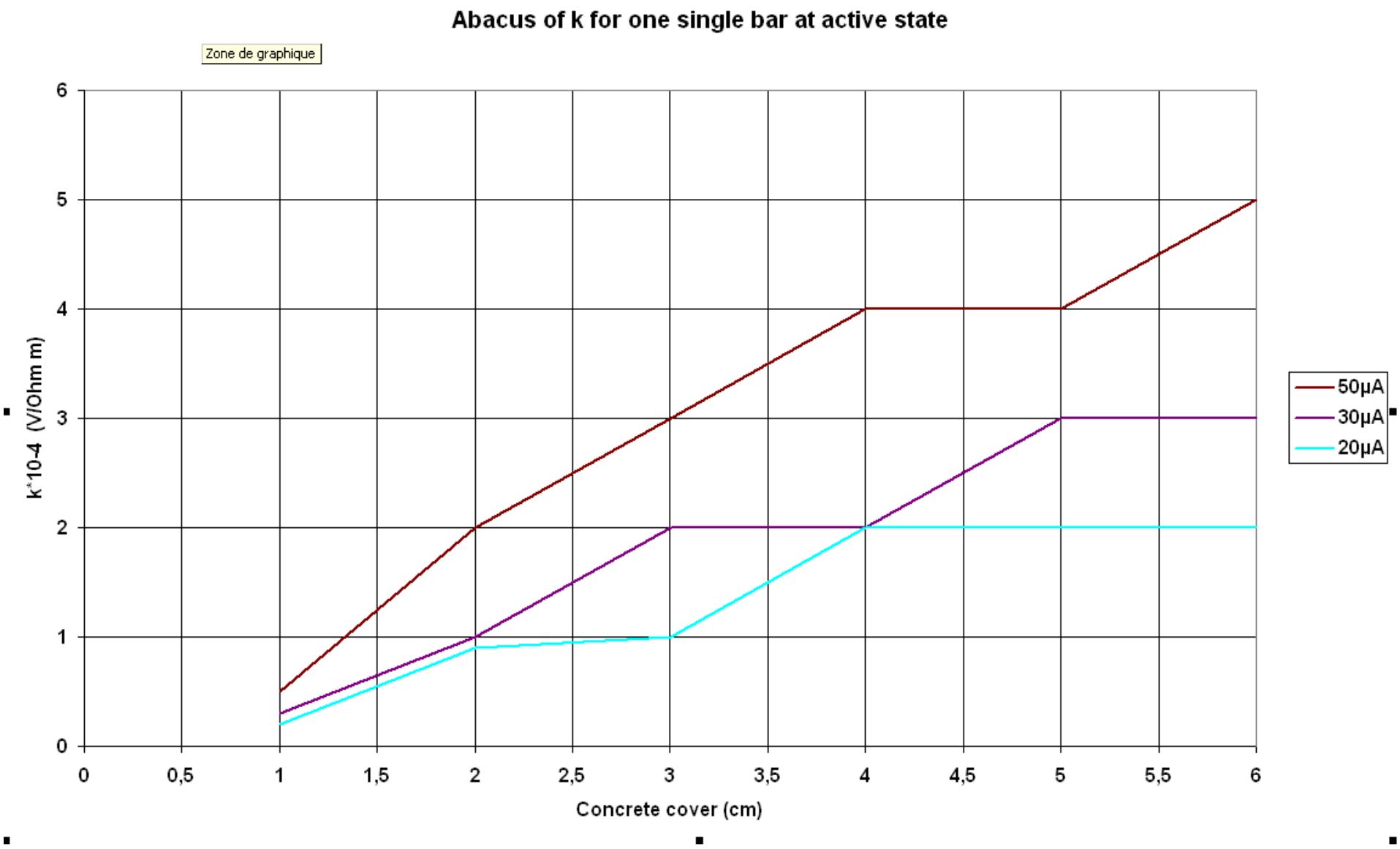
Abacus of k for one single bar at active state
Zone de graphique
k*10-4 (V/Ohm m)
Concrete cover (cm)
0
1
2
3
4
5
6
0
0,5
1
1,5
2
2,5
3
3,5
4
4,5
5
5,5
6
50µA
30µA
20µA

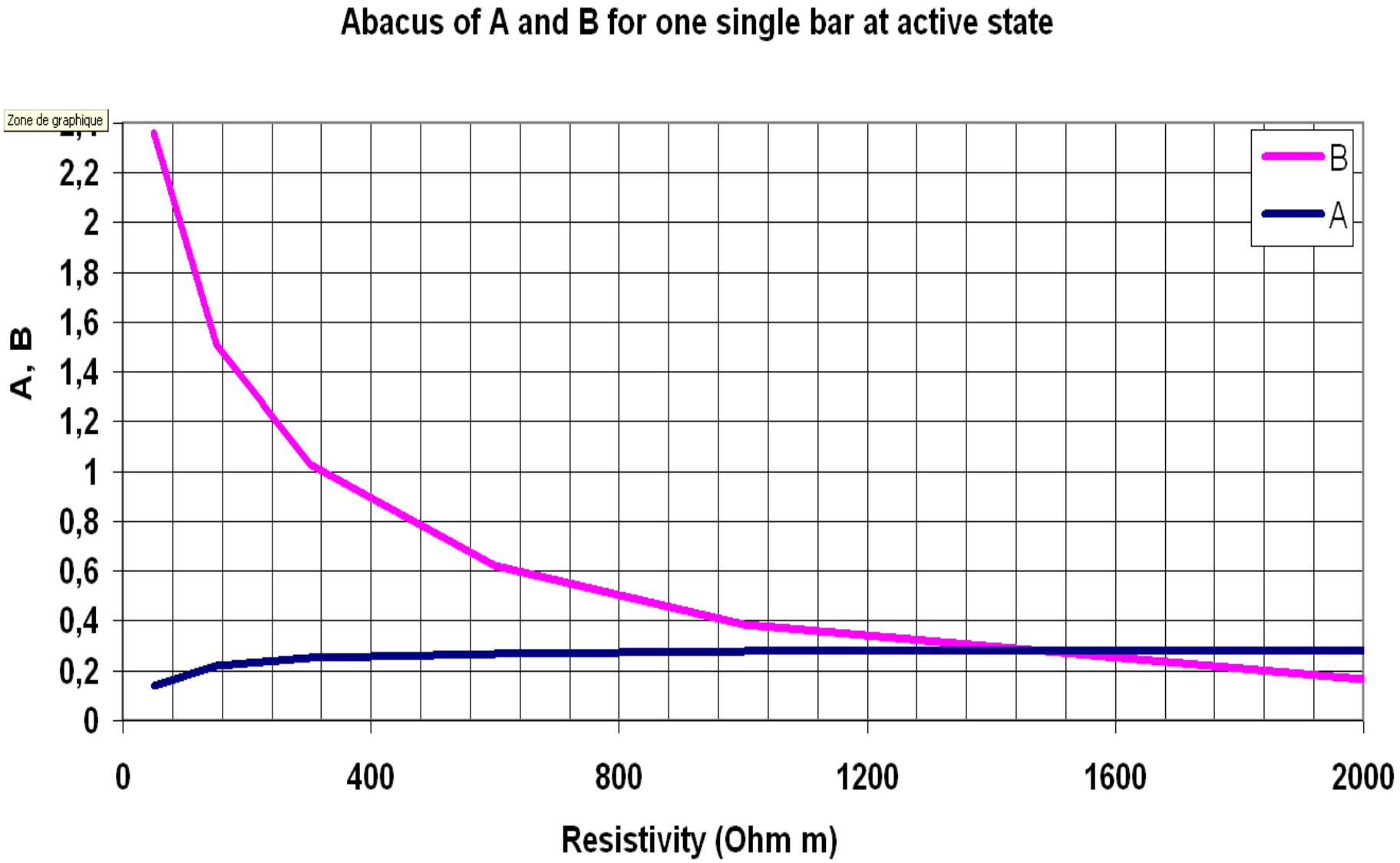
Abacus of A and B for one single bar at active state
Zone de graphique
A, B
2,2
2
1,8
1,6
1,4
1,2
1
0,8
0,6
0,4
0,2
0
0
400
800
1200
1600
2000
Resistivity (Ohm m)
B
A